



LUND UNIVERSITY

Limiting conditions for a sustained flame over condensed fuels

Analysis by experiments and stagnant layer theory

Vermina Plathner, Frida

2020

Document Version:

Publisher's PDF, also known as Version of record

[Link to publication](#)

Citation for published version (APA):

Vermina Plathner, F. (2020). *Limiting conditions for a sustained flame over condensed fuels: Analysis by experiments and stagnant layer theory*. Division of Fire Safety Engineering, Lund University.

Total number of authors:

1

General rights

Unless other specific re-use rights are stated the following general rights apply:

Copyright and moral rights for the publications made accessible in the public portal are retained by the authors and/or other copyright owners and it is a condition of accessing publications that users recognise and abide by the legal requirements associated with these rights.

- Users may download and print one copy of any publication from the public portal for the purpose of private study or research.
- You may not further distribute the material or use it for any profit-making activity or commercial gain
- You may freely distribute the URL identifying the publication in the public portal

Read more about Creative commons licenses: <https://creativecommons.org/licenses/>

Take down policy

If you believe that this document breaches copyright please contact us providing details, and we will remove access to the work immediately and investigate your claim.

LUND UNIVERSITY

PO Box 117
221 00 Lund
+46 46-222 00 00

Limiting conditions for a sustained flame over condensed fuels

Analysis by experiments and stagnant layer theory

FRIDA VERMINA PLATHNER | DIVISION OF FIRE SAFETY ENGINEERING | LUND UNIVERSITY



Limiting conditions for a sustained flame over condensed fuels

Analysis by experiments and stagnant layer theory

Frida Vermina Plathner



LUND
UNIVERSITY

DOCTORAL DISSERTATION

by due permission of the Faculty of Engineering, Lund University, Sweden.

To be defended on the 26th of February 2020.

Faculty opponent

Marc Janssens, Southwest Research Institute, USA

Organization LUND UNIVERSITY Division of Fire Safety Engineering, Faculty of Engineering Author Frida Vermina Plathner	Document name Doctoral dissertation	
	Date of issue 26th of February 2020	
	Sponsoring organization EU commission, RISE, NASA	
Title and subtitle Limiting conditions for a sustained flame over condensed fuels: Analysis by experiments and stagnant layer theory		
Abstract Ignition and extinction characteristics of a material determine whether a fire will be initiated and grow. In fire safety engineering, where modellers deal with a multitude of materials, simplified thresholds are commonly used to determine when ignition and extinction occur. Such a threshold is the critical mass flux, which describes when sufficient fuel vapour is produced to support sustained flaming. A related criterion is the critical heat release rate. This thesis is an investigation of how these two thresholds are correlated to environmental and fuel specific properties. This assessment is accomplished with small-scale experiments and stagnant layer theory. Experimental equipment were fine tuned to enable quantification of each investigated influence on the threshold criteria. A cone calorimeter sample set-up was modified so that the sample material could be exposed to a more uniform heat flux and the influence of external heating on the critical mass flux could be better quantified. Porous gas burners have been used previously to emulate burning of condensed fuels. In this thesis, such burners were used so that mass transport at the limiting points could be held at a constant rate. A set of burners with different diameters were used to provide insight on the influence of the convective heat transfer coefficient on the critical mass flux. Both the cone calorimeter test results and the gas burner results yielded information about the chemical heat of combustion of the fuels. It is shown that the critical mass flux, but not the critical heat release rate, is a function of the chemical heat of combustion. The thresholds are also dependent on the sample size, which is seen in the correlation for the convective heat transfer coefficient. Although the external heat flux influences the mass loss rate history it does not significantly change the amount of pyrolysates needed for sustained flaming. The findings are summarized in an engineering correlation that can be used to find approximate values for fire modelling.		
Key words Critical mass flux, diffusion flame, extinction, sustained ignition, chemical heat of combustion, convective heat transfer coefficient, external heat flux		
Classification system and/or index terms (if any) -		
Supplementary bibliographical information Report 1062 ISRN LUTVDG/TVBB—1062--SE		Language English
ISSN and key title 1402-3504		ISBN 978-91-7895-412-4 (print) 978-91-7895-413-1 (pdf)
Recipient's notes	Number of pages 188	Price
	Security classification Open	

I, the undersigned, being the copyright owner of the abstract of the above-mentioned dissertation, hereby grant to all reference sources permission to publish and disseminate the abstract of the above-mentioned dissertation.

Signature Frida Vermina Plathner Date 13th of January 2020

Limiting conditions for a sustained flame over condensed fuels

Analysis by experiments and stagnant layer theory

Frida Vermina Plathner



LUND
UNIVERSITY

Cover illustration based on a photo by Stefan Svensson

Copyright pp. 1-130 Frida Vermina Plathner, except:

Figure 4 © Society of Fire Protection Engineers

Figures 5, 10, 18, 27, 28, 31 and 32 © Elsevier

Figures 7 and 29 © Wiley

Figures 8 and 9 © International Association for Fire Safety Science

Figure A.5 © ASTM

Figure A.7 © Bal

Paper I © Wiley

Paper II © Wiley

Paper III © Elsevier

Paper IV © Elsevier

Faculty of Engineering
Division of Fire Safety Engineering

ISBN 978-91-7895-412-4 (print)

ISBN 978-91-7895-413-1 (pdf)

Printed in Sweden by Media-Tryck, Lund University
Lund 2020



Media-Tryck is a Nordic Swan Ecolabel certified provider of printed material. Read more about our environmental work at www.mediatryck.lu.se

MADE IN SWEDEN 

Acknowledgement

Throughout the work underlying this thesis, I have received a great deal of support from a lot of people. I would like to start by acknowledging my main supervisor Patrick van Hees at Lund University, who has helped me beyond what I could credit him for, and who provided me with a network in the field of fire science and engineering for which I am profoundly grateful. Also, other senior researchers at Lund University and RISE have given me invaluable feedback and guidance. Petra Andersson, Bjarne Husted, Daniel Nilsson, Francine Amon and Berit Andersson have provided me with comments on both the style and content of my writing, and this dissertation would not be possible without them.

My time at DBI gave me valuable insights into fire testing procedures. I am grateful to the firetools team for sweating alongside me with their own PhD studies, and also the laboratory staff for giving us practical advice and for letting us use their equipment.

I would like to thank Steve Grayson and his teams at FTT and Interscience Communications for taking care of new PhD students. I much appreciate the moral support I have received.

Finally, I constantly go back to the warm summer I spent at the University of Maryland, to the amazing people I met there, and to the long bike rides with Peter's Gitane. I would like to single out James Quintiere since, not only did he challenge and enrich my work, he also turned out to be great at hosting pool parties.

This thesis has been conducted mainly with funding from the European Union's Seventh Framework Programme. I would also like to acknowledge the support of RISE, that have given economical means for me to complete my work, and to DBI, Lund University, the University of Maryland and NASA, that enabled me to use vital equipment for my study.

And to my family – I love you.

Frida Vermina Plathner
Malmö, January 13, 2020

Populärvetenskaplig sammanfattning

Att bränder uppstår är ett relativt vanligt fenomen som kan orsaka både dödsfall och ekonomiska skador. I hemmiljön och inom industrin förekommer många olika typer av material som antingen kan vara första objektet att antändas, och dessa material kan antändas samtidigt, eller också antänds de till följd av att närliggande föremål brinner. Antändning är ett viktigt fenomen också eftersom flamspridning kan ses som en serie av antändningar.

När ett brännbart föremål eller vätska upphettas bildas brännbara gaser i närheten av bränslets yta. En diffusionsflamma kan bildas över materialet om det finns tillräckligt med brännbara gaser för en fortlöpande förbränning. En utgångspunkt för att bestämma när antändning av ett material sker kan därför vara att mäta massavbrinningen vid ögonblicket då en diffusionsflamma uppstår. Inom brandmodellering är detta dock ett relativt nytt begrepp, då antändning oftast beskrivits med en uppmätt yttemperatur på materialet – alternativt en kritisk värmestrålning.

En uppmätt kritisk massavbränning beror på uppmätbara och kontrollerbara miljöparametrar, såsom syremängd i omgivningen, vilken typ av material det är och om flammans drivs av lyftkraft på grund av temperaturskillnader eller om det finns ett påtvingat flöde.

De studier som existerar idag uppvisar därför en stor variation i uppmätta resultat. För att använda de uppmätta resultaten i egna modeller behöver man veta om ens objekt har samma typ av miljö/omgivning som de värden man hittar i tabeller. Denna avhandling syftar därför till att undersöka hur den kritiska massavbrinningen varierar med ett par av de mest betydelsefulla parametrarna, nämligen vilket material det är och hur stor dess bränslebädd är. Inverkan av infallande värmestrålning har också undersökts. Materialval representeras förenklat av den effektiva förbränningsentalpi och bränslebäddens storlek återfinns i ekvationer för den konvektiva värmeöverföringskoefficienten.

Resultaten visar att den kritiska massavbrinningen blir högre om de brännbara gaserna har lägre effektiv förbränningsentalpi. Ett nära relaterat gränsmått för antändning – den kritiska effektutvecklingen – är istället konstant för en stor mängd gaser. För de gaser som har en effektiv förbränningsentalpi under 10 kJ/g är dock förhållandet annorlunda och ett konstant värde kan inte antas. Också en mindre bränslebädd innebär en större kritisk massavbränning. Den infallande värmestrålningen däremot har försumbar betydelse för när kritiska förhållanden föreligger (den kritiska massavbrinningen).

Avhandlingen mynnar ut i en ingenjörsekvation som kan användas för att approximera vilket värde som ska användas vid modellering.

Summary

Ignition is one of the most important phenomena in unwanted combustion. In a fire several materials may ignite and burn simultaneously, and little is known about the combustion reaction kinetics of fuel gases that emerge upon heating. Simplified ignition thresholds have therefore traditionally been used in fire modelling to describe the ignition and extinction events. One of the thresholds that has been used by several researchers is the critical mass flux, which is the amount of fuel gases needed for sustained combustion. In fire safety engineering, this is a relatively new threshold, since ignition has commonly been described by a critical surface temperature or a critical heat flux upon the material.

The critical mass flux depends on measurable and controllable fuel and environmental properties, such as the oxygen mass fraction of the surrounding air, type of material, and flow field. The available experimental studies therefore provide varying results. To use these results in a model, knowledge is required about whether the modelled object is exposed to a similar environment as the tested specimen. This thesis therefore aims to investigate how the critical mass flux varies with a few key factors, namely its dependence on the type of material, the flow field, and the incident heat flux. Material type is represented in a simplified manner by the chemical heat of combustion and, by varying the fuel bed size, it is possible to correlate the critical mass flux to the convective heat transfer coefficient.

The results show that the critical mass flux is high for materials with low chemical heats of combustion, and vice versa. A closely related threshold for ignition – the critical heat release rate – is approximately constant for a large span of gas mixtures. For gases with a chemical heat of combustion below 10 kJ/g, however, a constant value cannot be assumed.

A smaller fuel bed infers a larger critical heat flux. The incident heat flux, however, has a negligible impact on the critical mass flux, despite its influence on the mass loss history.

The findings are summarized in an engineering correlation that can be used to approximate the critical mass flux value to use in modelling

Content

1	Introduction.....	15
1.1	Modelling of piloted ignition and extinction	16
1.2	Experiments on piloted ignition.....	19
1.3	Objectives	20
1.4	Publications	20
1.4.1	Appended publications	20
1.4.2	Related publications	21
1.5	Delimitations	22
1.6	Limitations.....	23
1.7	Thesis outline.....	24
2	Theory of sustained flaming.....	27
2.1	Pre-mixed flames.....	28
2.2	Diffusion flames	30
2.3	Critical mass flux.....	32
2.4	Ignition of solids.....	33
2.5	Extinction	35
2.5.1	Fire point theory	35
2.5.2	Stagnant layer theory.....	35
3	Review of experimental determination of the critical mass flux	41
3.1	Experimental influences on the critical mass flux	41
3.1.1	Operating definitions of ignition and extinction.....	41
3.1.2	Specific characteristics of the tested material and its pyrolysates.....	42
3.1.3	Environmental conditions.....	47
3.1.4	Test apparatus design	48
3.2	Experimental methods	50
3.2.1	Cone calorimeter	50
3.2.2	Fire propagation apparatus	54
3.2.3	Edinburgh University ignition apparatus.....	55
3.2.4	Forced ignition and flame spread test.....	55
3.2.5	Fire point apparatus	55
3.2.6	Emulating gas burners	57
3.2.7	Summary of apparatus evaluation	59
3.3	Measurements of the critical mass flux at ignition	60
3.4	Measurements of the critical mass flux at extinction.....	66
4	Selecting parameters based on a sensitivity analysis.....	69
4.1	Sensitivity analysis	69
4.2	Motivation for parameter selection.....	70

5	Selection and development of experimental methods	73
5.1	Cone calorimeter modification	73
5.2	Burning rate emulator (BRE).....	80
6	Correlating the critical mass flux to fuel and environmental factors.....	85
6.1	The influence of fuel.....	85
6.1.1	Chemical heat of combustion	85
6.2	The influence of the convective heat transfer coefficient	90
6.3	The influence of incident heat flux	92
6.4	Summary of influencing parameters.....	94
7	Discussion	95
7.1	Experimental instrumentation.....	95
7.1.1	Cone calorimeter modification	96
7.1.2	Burning rate emulator	96
7.2	Experimental results	98
7.2.1	Fuel dependence	98
7.2.2	The influence of the heat transfer coefficient and fuel bed size ..	99
7.2.3	The influence of incident heat flux	101
7.2.4	Scalability of small-scale data	101
7.3	The critical mass flux in fire modelling.....	102
8	Conclusions	103
9	Future work	107
	References	109
	Appendix A: The critical mass flux in ignition and flame spread modelling	119
A.1	Introduction	119
A.2	Method.....	120
A.2.1	Sensitivity model	120
A.2.2	Parameter data	121
A.3	Models	121
A.3.1	Ignition temperature	121
A.3.2	Critical heat flux	124
A.3.3	Time to ignition	125
A.3.4	Flame spread.....	129
A.4	Conclusions	130

List of figures

Figure 1. Sketch of the work flow	25
Figure 2. Arrhenius Equation: k vs T	28
Figure 3. Flammability limits, adapted from Zabetakis (1965) by permission	29
Figure 4. Flame zone in a diffusion flame, adapted from Rangwala, (2016) by permission	31
Figure 5. Flame temperature, reproduced from T'ien and Endo (2013) by permission.....	32
Figure 6. Heat balance at the surface	34
Figure 7. Stagnant layer model, reproduced from Quintiere (2006b) by permission.....	36
Figure 8. Sustained ignition of PMMA, from Kashiwagi, Inaba and Brown (1986) by permission	44
Figure 9. Radiation fraction for turbulent flames vs. laminar smoke point flame length, reproduced from de Ris (1989) by permission	46
Figure 10. Influence of distance between igniter and sample, reproduced from Jiakun <i>et al.</i> (2013) by permission	49
Figure 11. ISO 5660 Cone calorimeter (CC)	52
Figure 12. Cone calorimeter sample arrangement	53
Figure 13. Heat flux distributions in % for cone calorimeter sample surfaces, based on reported measurements in Janssens <i>et al.</i> (2008).....	54
Figure 14. ISO 12136 Fire propagation apparatus (FPA)	55
Figure 15. Edinburgh University ignition apparatus (EDUA)	56
Figure 16. Forced ignition and flame spread test (FIST).....	56
Figure 17. Fire point apparatus	57
Figure 18. Burner emulated flames compared to condensed phase fuels, from Zhang <i>et al.</i> (2015) by permission	59
Figure 19. Parameter sensitivity of Eq. (2.10) for black PMMA.....	71
Figure 20. Modelled geometry and mesh	75
Figure 21. View factor between the sample surface and the cone heater	76
Figure 22. Simulated incident heat radiation (in %) to a square or a circular sample (black lines) at 50 kW/m ² . The red dashed line marks the central 50 by 50 mm area.	77
Figure 23. Sample set-up in Paper II.....	78
Figure 24. Example of noisy output in the cone calorimeter. PMMA. Test start: $t=0$	79
Figure 25. Relation between the chemical heat of combustion and the laminar smoke point.....	81
Figure 26. BRE gas burner, set I.....	83
Figure 27. BRE gas burner, set II.....	84
Figure 28. Critical mass flux at ignition.....	86
Figure 29. Critical heat release rate at ignition, measured in the cone calorimeter	87
Figure 30. Critical mass flux: Influence of fuel bed size	91
Figure 31. Froude number for gas mixtures in burners of 25, 50 and 100 mm diameter	92
Figure 32. BRE burner flames.....	100
Figure 33. Evolution of the flame base diameter at ignition in the cone calorimeter for two different fuels.....	100

Nomenclature

A	Pre-exponential factor	s^{-1}
B	Spalding B number	-
c_p	Specific heat capacity	$J\ kg^{-1}\ K^{-1}$
C	Constants in Ra	-
d	Distance	m
D	Diameter	m
E_a	Activation energy	$J\ mol^{-1}$
f	Function	-
F	View factor	-
Fr	Froude number	-
g	Gravitational acceleration	$m\ s^{-2}$
h	Height	m
h_c	Convective heat transfer coefficient	$W\ m^{-2}\ K^{-1}$
ΔH_c	Chemical heat of combustion	$kJ\ g^{-1}$
ΔH_g	Heat of gasification	$kJ\ g^{-1}$
ΔH_{net}	Net heat of complete combustion	$kJ\ g^{-1}$
ΔH_{ox}	Heat of combustion per unit gram of oxygen consumed	$kJ\ g^{-1}\text{-}O_2$
HRP	Heat release parameter	-
k	Thermal conductivity	$W\ m^{-1}\ K^{-1}$
k	Rate constant for a first order chemical reaction	s^{-1}
L	Latent heat of vaporization	$J\ kg^{-1}$
L^*	Characteristic length	m
m	Reaction order	-
m	Mass	g
\dot{m}''_{cr}	Critical mass flux	$g\ m^{-2}\ s$
MW	Molecular mass	$g\ mol^{-1}$
n	Reaction order	-
Nu	Nusselt number	-
P	Pressure	Pa
$\dot{q}''_{f,c}$	Convective heat flux from flame	$kW\ m^{-2}$
\dot{q}''_{ext}	External heat from environment	$kW\ m^{-2}$
$\dot{q}''_{f,r}$	Absorbed heat radiation from flame	$kW\ m^{-2}$
$\dot{q}''_{f,r}$	Emitted heat radiation	$kW\ m^{-2}$
\dot{Q}_{tot}	Total heat flux	$kW\ m^{-2}$
\dot{Q}''_{cr}	Critical heat release rate	$kW\ m^{-2}$
R	Universal gas constant	$J\ mol^{-1}\ K^{-1}$
r	Radius	m

r	Stoichiometric oxygen to fuel mass ratio	-
Ra	Rayleigh number	-
S	Surface area	m ²
S	Rate of transfer of sensible heat	kW m ⁻²
t	Time	s
T	Temperature	K
u	Flow velocity	m ³ s ⁻¹
V	Volume	m ³
X _r	Radiative fraction	-
Y	Mass fraction	-
z	Height	m

Greek

α	Thermal diffusivity	m ² s ⁻¹
α_s	Absorptivity	-
ρ	Density	kg m ⁻³
δ	Thickness	m
ε	Emissivity	-
Φ	Maximum fraction of heat that the flame may lose to the surface	-
ν	Kinematic viscosity	m ² s ⁻¹
σ	Stefan-Boltzmann constant	W m ⁻² K ⁻⁴
μ	Mass fraction of char	-

Subscripts

a	Activation
abs	Absorbed
conv	Convective
cr	Critical
eff	Effective
emi	Emitted
ext	External
f	Flame
F	Fuel
F,0	Fuel at surface 0+
f,r	Flame radiation
g	Gas
ig	Ignition

inc	Incident
l	Loss
m	Mixture
ox	Oxygen
O ₂	Oxygen
prod	Products
r	Reactants
r	Radiation
rr	Re-radiation
ref	Reflected
s	Surface / Solid
p	Pressure
tot	Total
0	Initial
∞	Ambient

Superscripts

.	Per unit time
'	Per unit length
*	Dimensionless

Parameter values and definitions

Appropriate values for the physical constants are:

Gravitational acceleration	$g = 9.81 \text{ m s}^{-2}$
Universal gas constant	$R = 8.314 \text{ J K}^{-1} \text{ mol}^{-1}$
Stefan-Boltzmann constant	$\sigma = 5.67 \cdot 10^{-8} \text{ W m}^{-2} \text{ K}^{-4}$

Abbreviations

ABS	Acrylonitrile butadiene styrene
BRE	Burning rate emulator
CACC	Controlled atmosphere cone calorimeter
CC	Cone calorimeter
chl	Chlorinated
CLT	Cross laminated timber
EDUA	Edinburgh University ignition apparatus
FIST	Forced ignition and flame spread test
FPA	Fire propagation apparatus
FR	Fire retarded
H	Horizontal
HD-PE	High density polyethylene
HIPS	High impact polystyrene
HRP	Heat release parameter
HRR	Heat release rate
ISO	International Organization for Standardization
LOI	Limiting oxygen index
PA6	Polyamide 6
PE	Polyethylene
POM	Polyoxymethylene
POM-C	Polyoxymethylene (copolymer acetal)
PMMA	Polymethyl methacrylate
PS	Polystyrene
PP	Polypropylene
PP/GL	Polypropylene / fibre glass composite
PIR	Polyisocyanurate
PUR	Polyurethane
PVC	Polyvinyl chloride
Std	Standard deviation
V	Vertical

1 Introduction

Ignition is a process where a system undergoes a transition from a non-reactive to a reactive self-sustained state. It is a subject of investigation in a variety of fields, both from the viewpoint of wanted combustion (e.g. engines, power plants and turbines) and that of undesired combustion, such as uncontrolled fire (Atreya, 1998).

The consequences of unwanted combustion can be disastrous, which is evidenced by both national and international statistics. In Sweden, the fire rescue service responds to over 6 000 fire incidents in homes per year, which equals 0.6 incidents per 1 000 inhabitants per year (Johansson, 2012). In Europe over two million domestic fires are reported per year, and the same number for the US is half a million home fires (Kobes and Groenewegen, 2009; Evarts, 2018).

When it comes to a growing fire, ignition and extinction are important events. With no ignition there is no fire. But ignition is not only important for the initiation of fire; it also plays an important role in fire spread and growth (Atreya, 1998). Time to ignition (t_{ig}) is directly related to the flame spread rate. The time it takes for a material to ignite in a fire is also useful for exploring the sequence of events in a room fire (Quintiere, 2006b, p. 159). Questions regarding if a material will ignite upon a given heat exposure and, if so – when – are important considerations in fire safety engineering. Similarly, extinction characteristics of a material will give evidence for an ease-of-extinction threshold as a counterpart to a sustained ignition threshold. In flame spread, burn-out fronts are characterized by extinction parameters, which are also used for calculating the amount of suppressants needed to extinguish a fire.

While scientific advances in unwanted combustion have greatly benefited our society, both societal and economic losses are still high. More research is needed in several areas; one of those includes the understanding of fire in its development phase in order to e.g. improve fire safe building design. It is therefore important to better understand ignition and extinction, and improve the models in which these parameters are used, in order to make certain that modelling input is chosen on a proper basis.

Recently a study at the Imperial College compared pyrolysis and ignition modelling results based on the modelling of a material slab exposed to transient heat exposures, as is the case in a real fire scenario. Different modelling thresholds were used for when ignition was assumed to occur and it was concluded that the use of a critical rate of pyrolysates as an ignition threshold gave more accurate prediction results than other common limiting conditions at ignition (Vermesi *et al.*, 2016). However, there are limited

numbers of studies that quantify this threshold or studies that relate it to variations in the environmental setting, which makes it a topic worth more research.

1.1 Modelling of piloted ignition and extinction

In combustion physics, ignition and extinction limits are usually calculated with combustion reaction kinetics. This approach demands both a high level of knowledge of the fuel gases involved, and high computational times. In fire safety engineering, however, dealing with complex solid material combinations and liquids, there is a need for more practical, simple descriptions of the processes. Upon decomposition of solid materials, a complex mixture of fuel gases is emitted. Unlike the case in e.g. an engine, unwanted combustion occurs in materials which are not always known beforehand. As an example, a fire in a dwelling can involve furniture, linings, electrical equipment etc. Most of these items consist of a multitude of materials. It is not practical to model all combustion reactions of such a complex mixture, especially not at a larger scale, such as a room, where multiple objects containing various fuels are involved in the scenario. Therefore, fire researchers have proposed various simplified criteria for the ignition and extinction events that can be used as input in fire calculations without knowledge of the detailed chemistry. Criteria regarding both the solid phase and the gas phase have been proposed. The common denominator amongst the criteria is that all methods have utilized a limiting threshold of a measurable quantity. Ignition thresholds have different values for different types of ignition (flashing, sustained, auto-ignition etc.). The definition of ignition here is the initiation of sustained combustion, ignited with the aid of an external energy source (pilot). Summarized, common modelling criteria for piloted ignition are:

- Ignition temperature
The flammability of a liquid is assessed with an open or closed cup test (e.g. ISO 2592 Cleveland open cup test (International Organization for Standardization (ISO), 2000)). The flash and fire points of the liquid are defined as the lowest liquid bulk temperatures at which the vapours produce a flash or a sustained flame, respectively. The ignition of a solid material cannot be defined by a bulk temperature of the solid, since the solid has a temperature gradient. However, ignition of the solid is assumed to occur when its surface reaches a certain ignition temperature, T_{ig} (Drysdale, 2011, p. 249).
- Critical heat flux
The critical heat flux corresponds to ignition in infinite time. In other words, it is the heat flux below which not enough fuel vapours are produced to create a fuel/air mixture that may support a sustained flame (Delichatsios, 2005; Tewarson, 1994). Experimentally, this parameter is retrieved by plotting $1/\sqrt{t_{ig}}$ versus the incident heat flux \dot{q}''_{inc} , which in many cases produce a straight line,

where the critical heat flux is found in the intersection with the x-axis. In this method, heat losses are ignored, and the sample is considered semi-infinite. However, at long ignition times, corresponding to low heat fluxes, heat losses to the rear face of the sample may not be negligible. The semi-infinite assumption is not applicable for thin materials. Delichasios, Panagiotou and Kiley (1991) showed that a linear extrapolation of the critical heat flux would therefore likely provide a 70 % estimate of the 'true' value.

- Critical flame temperature
A common threshold for extinction is a minimum flame temperature where a sufficient reaction rate can be sustained (Williams, 1981). The specification of a maximum fraction of heat that a flame may lose to the material surface without being extinguished is a similar threshold to the flame temperature (Rasbash, 1986).
- Critical mass flux
The critical mass flux is described by a minimum flow rate of fuel volatiles that can support a sustained flame (Bamford, Crank and Malan, 1946). A related criterion - the critical heat release rate (\dot{Q}''_{cr}) - is defined as the critical mass flux multiplied by the chemical heat of combustion (Babrauskas, 2003; Lyon and Quintiere, 2007).

Other less commonly suggested thresholds also exist. Sauer (1956) tested thick slabs of wood and found that a minimum char depth was established before ignition could occur. Kashiwagi (1973) proposed a critical reaction rate of $10^{-5} \text{ g cm}^{-3} \text{ s}^{-1}$ for the gases in the boundary layer (just above the solid surface). Deverall and Lai (1969) conducted a theoretical study of ignition, in which they suggested that ignition occurred when the temperature gradient of the solid/gas interface was reversed.

Ignition has traditionally been associated with the solid phase in fire models despite the fact that ignition occurs in the gas phase (Fernandez-Pello, 2011). One simplified description of ignition used in fire research is the concept that all solid fuels have a unique ignition temperature at their surface, and that a material is ignited once it is heated to this temperature. Associating ignition to a material's surface temperature is a practical way of determining ignitability. In most cases the methodology is sufficiently precise, e.g. for comparative ignitability studies or in many predictive fire growth models. Despite its practicality, the traditional principle is not strictly applicable to other scales, geometries, materials or environments (Rich *et al.*, 2007) and an ignition temperature is not suitable when a material is exposed to a discontinuous heat flux (Drysdale, 2011, pp. 263-268). Martin (1965) and Weatherford and Sheppard (1965) provide evidence of the importance of the heating history and temperature gradient to the time to ignition (and surface temperature). More researchers have criticized the assumption of a constant, well-defined ignition surface temperature (Córdova *et al.*, 2001). Atreya and Abu-Zaid (1991) showed that for weakly reacting materials, low or fluctuating oxygen concentrations, or high flow

velocities, surface temperatures would exceed their expected ignition thresholds before the point that they would ignite under conditions more favourable for combustion. Roslon *et al.* (2000) provided examples where materials ignited before their ignition temperatures were reached, or below their critical heat flux. This occurred in oxidizer flows with a high oxygen content, or in low flow microgravity environments.

Instead of describing ignition with the ignition temperature, Bamford, Crank and Malan (1946) suggested that ignition (and extinction) may be described by a critical mass flux, i.e. the minimum fuel flow rate needed for combustion to initiate and continue. Researchers have experimentally studied critical mass flow rates of pyrolysis gases, showing the parameter to be affected by environmental conditions (Drysedale and Thomson, 1989; Rasbash *et al.*, 1986), such as flow velocity (Córdova and Fernandez-Pello, 2000), oxygen concentration (Delichatsios, 2005), pressure (Feres *et al.*, 2011) and water vapour (Atreya and Abu-Zaid, 1991). Rich *et al.* (2007) recently studied ignition of polymethyl methacrylate (PMMA) samples and found that the critical mass flux at the limiting points may be calculated as a function of fuel and environmental properties. The threshold may therefore be included in pyrolysis sub-models to calculate time to ignition, where the criticality is based on existing fuel and environmental properties within the model – hence no separate experiments are needed.

In line with the findings of Rich *et al.* (2007) a review of fire models indicates that modellers recently have moved from describing the ignition event with an ignition temperature towards a description of ignition with a critical mass flux (Vermina Lundström, van Hees and Guillaume, 2017). In Table 1, a few prediction models for compartment fires, developed between 1980 and 2019, have been categorized based on their ignition criteria. Many fire models were developed during this time period and not all are found or included in the table. Despite this, recent trends of ignition modelling can be observed. First, the review demonstrates that four criticalities have been most common for modelling ignition, namely (1) time to ignition (t_{ig}), (2) ignition (surface or pyrolysis) temperature (T_{ig}), (3) critical mass flux of pyrolysis gases (\dot{m}'_{cr}), and (4) critical heat flux (\dot{q}'_{cr}). The table suggests that the critical mass flux is a new modelling parameter. If this trend continues, it is also reasonable to assume that there will be an even wider use of the critical mass flux in a few years, in comparison to the other presented criteria. It is also suggested that the critical heat flux has not been frequently used in recent models. This is probably because most common pyrolysis models for fire engineering have ignition temperature and critical mass flux as their options of choice. It is not clear from the review how extinction is modelled. This is mainly because modellers seldom explicitly state how they model extinction or whether they model extinction at all (Grant and Drysdale, 1995).

Table 1. Ignition criteria used in modelling (Paper I / Vermina Lundström *et al.*, 2017)

Years	Number of prediction models	t_{ig} (%)	T_{ig} (%)	\dot{q}_{cr}'' (%)	\dot{m}_{cr}'' (%)
1980-1990	5	20	40	40	0
1990-2000	21	9	86	5	0
2000-2010	8	25	25	0	50
2010-2019	9	10	35	0	55

1.2 Experiments on piloted ignition

One of the reasons why ignition temperature has been a widely accepted ignition threshold in fire modelling, as shown in Table 1, is the difficulties associated with measurements of gas phase properties such as the critical mass flux (Lautenberger, Torero and Fernandez-Pello, 2006). The critical mass flux, despite being a gas phase parameter, is experimentally measured as a solid phase threshold (the mass loss rate of the solid sample at the point of ignition). Ignition and extinction are highly transient phenomena, and both solid and gas phase properties vary during the combustion process. Errors may be introduced in the measurements taken at the point in time where ignition or extinction occur. As an example of the transient behaviour: pyrolysis is almost negligible before ignition; however, at the moment a sustained flame appears, the mass loss from the sample increases rapidly. The same phenomenon, but reversed, is seen for the mass loss at extinction. The operator has only a short time interval to log the correct moment, and therefore precision of the experimental results can be questionable. In such experiments, both the resolution and accuracy of the weighing device, as well as the control of environmental parameters, are of importance to gain reasonable results. Ignition temperatures are also difficult to measure, since the thermocouple mounting at the surface is difficult (Janssens, 2006). However, the surface temperature just before and after ignition does not vary much and the results are therefore more robust.

Published experimental measurements of the critical mass flux range approximately between 1 and 10 g/m²-s for various materials at sustained ignition. Tewarson (2002) measured critical mass flux in a bench-scale equipment called the ISO 12136 fire propagation apparatus (FPA) (ISO, 2011) and obtained critical mass fluxes of 3-5 g/m²-s for common polymers. The same materials were later tested at the University of Edinburgh with a bench-scale arrangement similar to that of the ISO 5660 cone calorimeter (CC) (ISO, 2015). In these experiments, the results were lower by a factor of 2-5 (Thomson and Drysdale, 1989) compared to the results by Tewarson (found in (Tewarson, 2002)). Critical mass loss rates for extinction vary as well; this will be presented in Chapter 3.

1.3 Objectives

As introduced above, the critical mass flux at ignition and extinction for arbitrary fuels can be directly calculated as a function of fuel and environmental properties. Still, experimental values of the critical mass flux vary considerably. It is therefore of interest to investigate and quantify the properties that have an impact on the critical mass flux in order to explain the large range of experimental values of the threshold.

In order to do so, it is necessary first to investigate the characteristics of the experimental equipment used and their suitability for determining the critical mass flux. Next, identify possible improvements to the measurement and methods in order to achieve a more precise set of data.

Finally, since the critical mass flux is a gas phase phenomenon and its size depends on the surrounding environment, it is necessary to investigate influencing parameters through experiments and theory.

In this thesis, a threshold for sustained ignition and extinction - the critical mass flux - is studied. The objectives of this thesis are to:

- Evaluate and select experimental equipment for assessing the critical mass flux.
- Make suggestions for how the experimental equipment can be modified in order to increase the precision of the critical mass flux determination.
- Identify key parameters that influence the critical mass flux and assess their impact through a theoretical framework.

1.4 Publications

The research presented in this thesis is based on four appended papers. In addition to the appended papers, further research that the author has been involved in is listed as ‘related publications’. The papers and reports that are not included may provide the reader with additional information on the research topic.

1.4.1 Appended publications

All four papers in this thesis have been published in international scientific journals and therefore also been subject to peer review. Reference to each publication is listed below followed by a description of the author’s contribution to each paper.

Paper I Vermina Lundström, F., van Hees, P., & Guillaume, E. (2017).
A review on prediction models for full-scale fire behaviour of building products. *Fire and Materials*, 41(3), 225-244.

- Paper II Vermina Plathner, F., & van Hees, P. (2019). Experimental assessment of bench-scale ignitability parameters. *Fire and Materials*, 43(2), 123-130.
- Paper III Vermina Lundström, F., Sunderland, P.B., Quintiere, J.G., van Hees, P., & de Ris, J.L. (2017). Study of ignition and extinction of small-scale fires in experiments with an emulating gas burner. *Fire Safety Journal*, 87(1), 18-24.
- Paper IV Vermina Plathner, F., Quintiere, J.G., & van Hees, P. (2019). Analysis of extinction and sustained ignition. *Fire Safety Journal*, 105(4), 51-61.

In Paper I, no experiments were conducted. The review of prediction models for fire behaviour was conducted as part of a work package under the Firetools project, of which this thesis is a part of. Dr. Guillaume and Dr. van Hees reviewed the paper before publication.

In paper II the author was responsible for all steps and the outcome was reviewed by Dr. van Hees.

In paper III, the experimental device used was already designed for an ongoing project. However, fine tuning of experimental set-up and procedure, troubleshooting as well as executing the experiments were done by the author. Data analysis was conducted by the author and guided by Dr. Sunderland, Dr. Quintiere, and Dr. de Ris. Within this group, possible design improvements were also discussed. Dr. van Hees reviewed the paper before publication.

In paper IV the experimental equipment was designed already, although a few troubleshooting issues had to be resolved initially by the author. Data analysis was conducted by the author and guided by Dr. Quintiere. Dr. Quintiere and Dr. van Hees reviewed the paper before publication.

This thesis also provides an Appendix, in addition to the listed publications, where examples are given for how the critical mass flux is used in ignition and flame spread modelling.

1.4.2 Related publications

The following papers and reports have been published during this PhD, but are not included in the dissertation:

Vermina Lundström, F., & van Hees, P. (2016) Experimental Assessment of Bench-Scale Ignitability Parameters. *Interflam 2016: Proceedings of the 14th International Conference* (pp. 1369-1380). London, UK: Interscience Communication Ltd.

Bhargava, A., Livkiss, K., & Vermina Lundström, F. (2016). System Fire Behaviour of Building Products. Copenhagen, Denmark: Restricted technical report, EU.

Bhargava, A., Livkiss, K., & Vermina Lundström, F. (2016). Solid and Composite Material Fire Behaviour for Building Products. Copenhagen, Denmark: Restricted technical report, EU.

Quintiere, J. G., Markan, A., Sunderland, P. B., Baum, H. R., de Ris, J. L., Stocker, D. P., & Vermina Lundström, F. (2017, July). *A Gas Burner Emulator for Condensed-Phase Burning*. Paper presented at the 9th International Seminar on Flame Structure, Novosibirsk, Russia.

Vermina Lundström, F., Sunderland, P.B., Quintiere, J.G., van Hees, P., & de Ris, J.L. (2016). Using a Porous Bed Gas Burner for Studying Ignition and Extinction of Condensed-Phase Fuels. In Chao, J., Liu, N.A. et al. (Eds.), *Proceedings of the 8th International Seminar on Fire and Explosion Hazards* (pp. 507-516), Hefei, China: University of Science and Technology of China Press. doi: 10.20285/c.skfls.8thISFEH.051.

Vermina Lundström, F., & van Hees, P. (2015). Challenges in Determining Critical Mass Flux for Ignition. *Fire and Materials: Proceedings of the 14th International Conference* (pp. 198-209), London, UK: Interscience Communication Ltd.

Vermina Lundström, F. (2015). Evaluation and Development of Test Methods for Heat Transfer Properties at Elevated Temperatures. Copenhagen, Denmark: Restricted technical report, EU.

Andres, B., Bhargava, A., Livkiss, K., Vermina Lundström, F., & Wilkens, K. (2014). Review of Models Relevant for the FIRETOOLS Project. Copenhagen, Denmark: Restricted technical report, EU.

1.5 Delimitations

Ignition temperature and critical heat flux at ignition have been extensively studied in fire research and are therefore criticalities that have not been explored in this thesis. Additionally, the critical heat flux has not been employed extensively during the last decades (refer to Table 1). Although various types of ignition and extinction mechanisms exist, not all of them are investigated in this thesis.

- Flaming combustion
This thesis is limited to the onset and offset of combustion involving flames. The potential of smouldering, glowing ignition or extinction of such kind is not explored.
- Diffusion flames
The focus of this thesis is on diffusion flames. Ignition of pre-mixed fuel and oxidizer (e.g. flash point), which fills an important function, for instance in

opposed flow flame spread (Quintiere, 2006a), is touched upon in Paper III, but not included in the thesis summary.

- Natural laminar flow
The actively burning fuel area decreases when a material is about to extinguish, just like the burning area of a material in the ignition process increases. This thesis investigates sustained ignition and extinction through the use of small-scale tests. Radiation effects from the flames are neither measured nor theoretically explored, as it is assumed that the dominant heat transfer for small flames is convection. Also, the fuel bed sizes correspond to laminar, and to some extent transitional, but not turbulent, flow.
- Normal environment
The thesis will confine itself to burning in air, under normal pressure and gravity. Experiments in microgravity under the same project as Papers III and IV have been performed by Quintiere *et al.* (2017) and Markan (2018), for the interested reader.
- Piloted ignition
Auto-ignition of fuel gases is highly dependent on ambient conditions and geometry. Therefore, most ignitability tests make use of a pilot, which is a more conservative mode of ignition. Piloted ignition is also more likely in a compartment fire, where sparks or flames from a burning object act as an igniter to the next object (Lautenberger *et al.*, 2006). This thesis deals only with piloted ignition.

1.6 Limitations

Limitations consider weaknesses that decrease the generalizability of findings. The limitations of this study include:

- Using a stagnant layer theory
No numerical modelling nor other analytical approaches involving a critical mass flux were included to analyse the experimental findings. This infers that a sensitivity analysis could only be conducted upon the influences included in the theoretical expressions used. Other environmental and fuel specific characteristics exist that in some cases alter the results. One example is the oxidation rate of fuel gas, which is not included in the theoretical expression but is hypothesized to contribute to variation in results.
- Material selection
Only a few materials were tested in the thesis. Validation concerning both

charring materials and materials that produce considerable amounts of water vapour and/or inert species have not been explored.

- Solid fuels
Although the theoretical expressions used in this thesis can be applied to liquids, experiments have only been conducted on solid materials.
- Fuel gases and diluents
Four burner fuel gases and one diluent were selected to represent a set of hydrocarbon gases based on their smoke points. The burner fuel gases had (undiluted) laminar smoke points ranging between 50 and 300 mm. Fuels with smoke points outside this range are not represented by these burner gases. Similarly, the only diluent used was nitrogen. Other diluents, such as carbon dioxide, provide slightly different results.
- Influence of igniter
The influence of igniter type and position has not been assessed.

1.7 Thesis outline

This thesis consists of nine chapters, one appendix and four appended publications. The four appended papers form the basis of results presented in the thesis chapters. The chapters put the findings in context and provide an overview of the research process.

Chapters 1-3 and Appendix A constitute a summary of previous work. These chapters are supplementary material for Paper I, in which a broader review was conducted. In Chapter 1 (Introduction) the research objectives are formulated based on the present evolution of fire prediction models that were reviewed in Paper I. Chapter 2 (Theory of sustained flaming) introduces the relevant terms and models that have been used in Papers II-IV to analyse experimental data. Chapter 3 (Review of experimental determination of the critical mass flux) provides an overview of earlier research in the topic. This chapter is a supplement to Paper I in which the review is more generic. Experimental equipment previously used for measuring the critical mass flux are introduced and their advantages and disadvantages are subsequently discussed. Previously measured mass flux data are also reported to illustrate how the environment and type of fuel introduce variation in measured results.

Chapters 4-5 represent the method sections. Chapter 4 (Selecting parameters to study with a sensitivity analysis) illustrates the effect that variations in each influential parameter has on the critical mass flux, based on the theoretical expression in Chapter 2. Motivation of why certain parameters are selected for further investigation is thus found in Chapter 4. Chapter 5 (Selection and development of experimental methods) motivates the choice of experimental equipment used in the present research and illustrates how these devices are modified to provide improved data for the specific research tasks.

Chapters 6-9 outline the experimental findings, their limitations and their use. In Chapter 6 (Correlating the critical mass flux to fuel and environmental factors) the results from Papers II-IV are presented. Chapter 7 (Discussion) contains limitations of the experimental equipment used and the cases for which the results have not been validated. Chapter 8 (Conclusions) summarises the overall research findings. Chapter 9 (Future work) outlines suggestions for future studies related to the research topic.

The work flow and how each paper is linked with the thesis summary is presented in Figure 1.

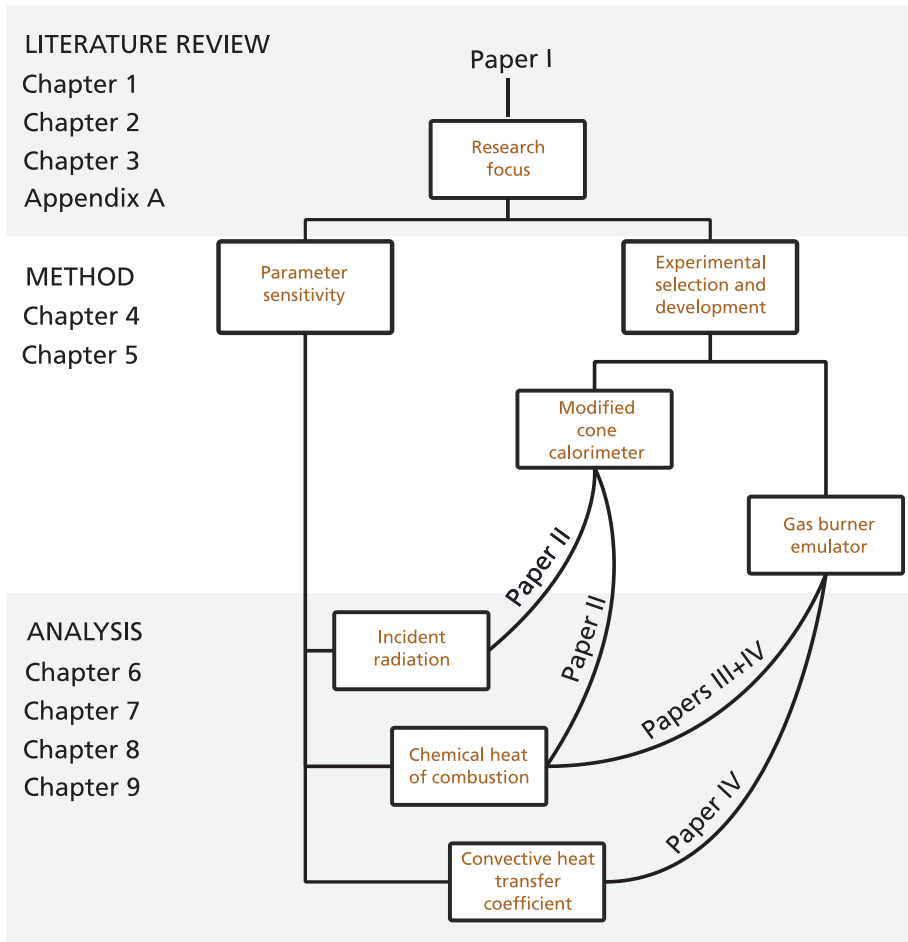


Figure 1. Sketch of the work flow

2 Theory of sustained flaming

Combustion is a complex process and involves a large number of chemical reactions. It can however be described as



in a simplified manner. That is, for combustion to take place, there needs to be both fuel volatiles and oxygen present. In complete combustion, carbon dioxide and water are produced. However, combustion is rarely fully complete, and carbon monoxide and hydrocarbons are commonly part of the gas product mixture. The rate at which combustion takes place is often expressed by an Arrhenius expression

$$\frac{d[\text{fuel}]}{dt} = k[\text{fuel}]^n[\text{oxygen}]^m \quad (2.2a)$$

$$k = Ae^{-E_a/(RT)} \quad (2.2b)$$

where $[\text{fuel}]$ and $[\text{oxygen}]$ are the molar concentration of combustible volatiles and oxygen respectively. In solid burning, the fuel is comprised of the volatile decomposition products emitted from the solid. The activation energy E_a is the threshold energy that reactants must acquire to initiate combustion, R is the universal gas constant, and T is the temperature. The sum of the exponentials, $(n + m)$, is the reaction order, and k is the rate constant. The pre-exponential factor A is a measure of the frequency of molecular collisions leading to combustion. An arbitrary reaction is plotted in Figure 2 showing the relation between k and T . The equation (and Figure 2) states that the warmer it is, the faster the combustion reaction proceeds (McAllister, Chen and Fernandez-Pello, 2011).

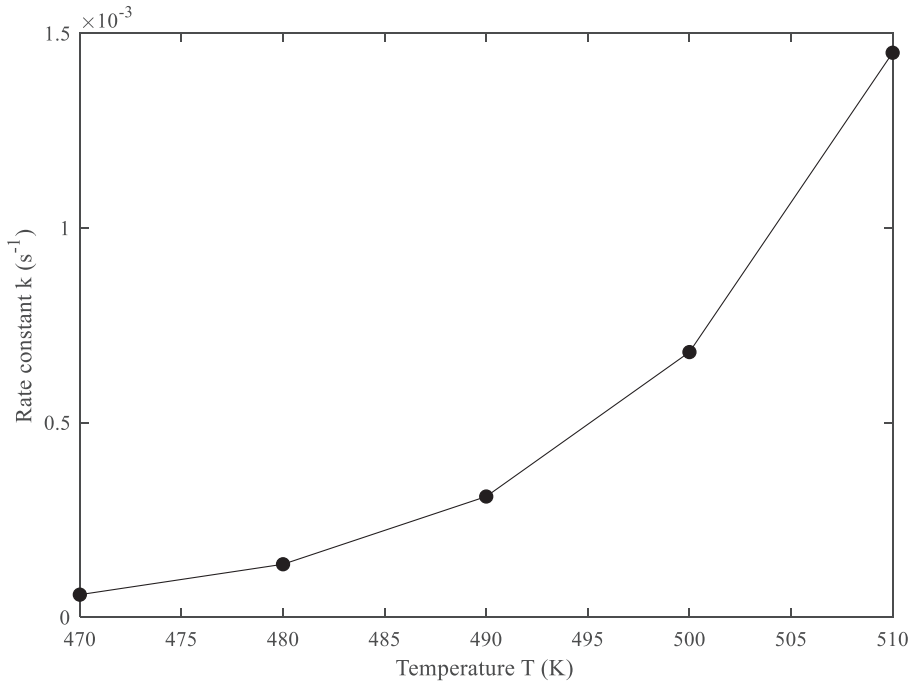


Figure 2. Arrhenius Equation: k vs T

2.1 Pre-mixed flames

The temperature of a flame is related to combustion kinetics. The adiabatic flame temperature is defined as the maximum temperature that can be achieved in combustion. This temperature, for a pre-mixed case, is dependent on possible diluents, that do not take part in combustion but are heated by the flame. An example diluent is nitrogen, when a fuel is burning in air. The adiabatic flame temperature T_f corresponding to complete combustion can be approximated by

$$T_f = T_\infty + \frac{\Delta H_{net}}{\sum(n_i c_{p,i})} \quad (2.3)$$

where n_i is the number of moles of each product species (i), ΔH_{net} is the net heat of complete combustion and $c_{p,i}$ is the specific heat of these species, taken at a film temperature.

The adiabatic temperature depends on the amount of fuel in the fuel/oxygen mixture (Dryer and Westbrook, 1981). A mixture is flammable within the lower and upper

flammability limits. In fire safety, the lower flammability limit (LFL) of vapours over a liquid or solid fuel is of special interest, since a flame will not propagate below this point even if ignition is achieved locally. Drysdale (2011, p. 33) lists calculated adiabatic flame temperatures at the LFL for a few hydrocarbon gases. These temperatures are 1600 ± 100 K.

The flammable range of a fuel/air mixture widens with increasing temperature of the mixture, as presented in Figure 3 (Zabetakis, 1965). A non-flammable mixture in room temperature may therefore become flammable if heated. This is exemplified by the two dashed lines, showing that whilst a given mixture is not flammable at T_1 , a temperature increase to T_2 will lead to a flammable mixture.

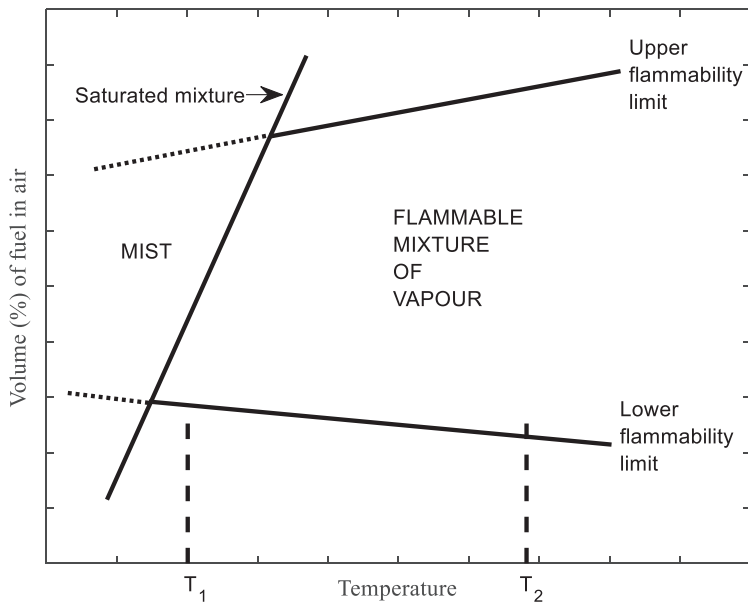


Figure 3. Flammability limits, adapted from Zabetakis (1965) by permission

Another approach for evaluating critical limits of flaming, developed by Rasbash (1976), is to define a maximum fraction of heat that a flame may lose to the surface ϕ . For a pre-mixed flame that is

$$\phi = 1 - Q_{prod}(T_f)/Q_{reac} \quad (2.4)$$

where Q_{prod} is the heat retained in the combustion products (which is a function of the flame temperature T_f) and Q_{reac} is the heat input from the reactants to the stoichiometric mixture.

2.2 Diffusion flames

Most combustion studies deal with gases that are mixed prior to combustion. However, in fire, the mixing of fuel and air is an integral part of the burning behaviour, and combustion occurs mostly as a diffusion flame. A diffusion flame is a flame where the reactants, usually fuel and air, are separate before they mix and combust. The fuel is initially in a liquid or solid state, so that phase change and / or decomposition is required for a combustion process in gas phase to occur. The fuel gas must then mix with oxygen so that a flammable mixture is formed. An early study by Burke and Schumann (1928) on laminar diffusion flames showed that combustion takes place in the zone where fuel and air mix. When this mixture is ignited it is referred to as the flame zone. The burning rate was shown to be controlled by the mixing rate of fuel and oxidizer, rather than by the rate of reaction. Figure 4 shows a sketch of a flame zone in a diffusion flame, reproduced from Rangwala (2016) and Kanury (1977).

The adiabatic flame temperature of a diffusion flame is not as easily calculated as that of a pre-mixed flame. Maček (1976) examined flame temperatures of both premixed and diffusion flames at their critical limits. In his work, pre-mixed flames were evaluated at their LFL and diffusion flame extinctions were evaluated at their limiting oxygen index (LOI), i.e. the minimum concentration of oxygen that can support combustion. He saw that the LOI experiments agreed with stoichiometric fuel concentrations, which gave slightly higher temperatures than the pre-mixed flames. He reasoned that extinction of a diffusion flame would occur somewhere between the two limits, and that the critical diffusion flame temperature would be similar to that of a pre-mixed flame, i.e. ~ 1600 K.

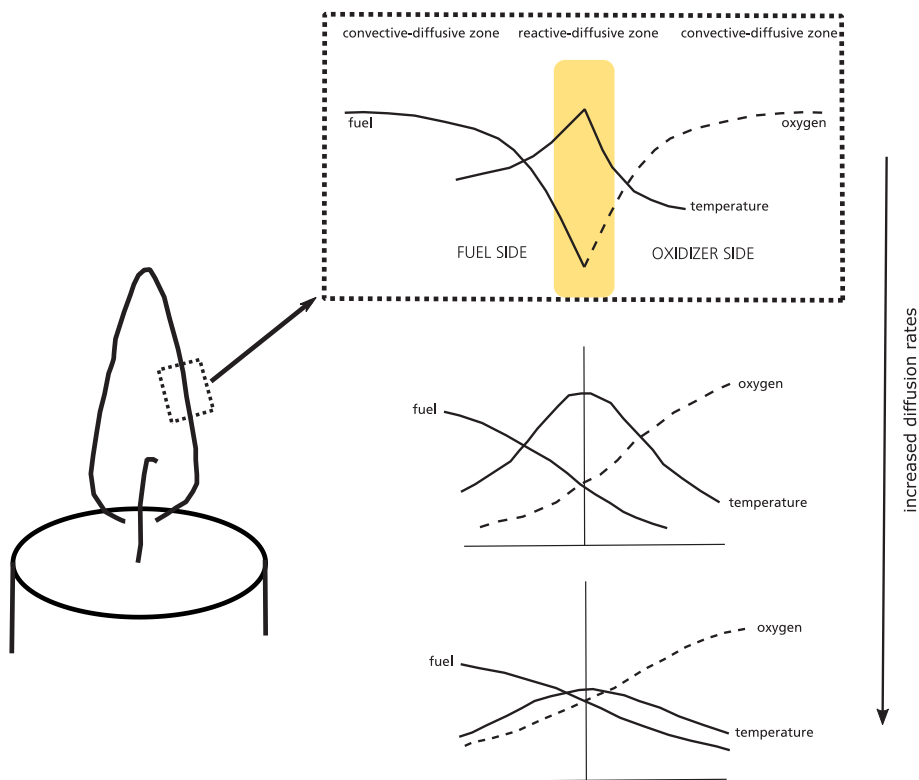


Figure 4. Flame zone in a diffusion flame, adapted from Rangwala, (2016) by permission

Williams (1981) showed that the adiabatic flame temperature at extinction of a diffusion flame varies slightly with the reactivity of the fuel and is roughly in the range 1700-2300 K for common hydrocarbon fuels. In reality the heat lost from the flame causes the actual flame temperature to drop. Williams therefore compared the calculated adiabatic flame temperatures to experimentally measured values. He reviewed values reported by Peters (1979) ranging between 1650 for methane to 1880 for iso-octane. Williams concluded that 1600 K would suffice as a conservative limiting temperature for modelling purposes.

This value is in line with experimental research studies. Amongst these studies are Melvin, Moss and Clarke (1971), Hirano, Noreikis and Waterman (1974) and Simmons and Wolfhard (1957), who measured values of 1500-1650 K for diffusion flames at the extinction limit.

The flame temperature at extinction of a diffusion flame is dependent on flow conditions (Williams, 1981). The flow velocity is related to the strain rate which makes the flame “stretch”. T’ien and Endo (2013) exemplifies how the flame temperature

changes with strain rate at critical conditions. When the flow velocity is low, heat loss from the flame is mainly by conduction to the surface. Extinction then occurs by quenching. If the flow velocity increases, the flame extinguishes due to blow-off of the flame, and the critical flame temperature increases.

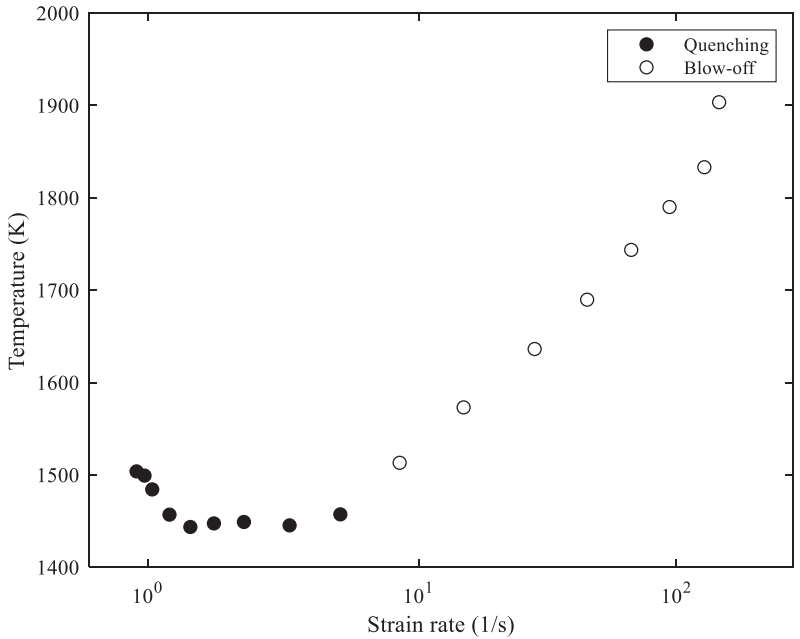


Figure 5. Flame temperature, reproduced from T'ien and Endo (2013) by permission

Fire researchers have validated (Delichatsios, 2005) and utilized (Quintiere and Rangwala, 2004) the theory that flame extinction and piloted ignition near surfaces are associated with low strain rates for flames in natural fire conditions. The critical flame temperature at low strain rates is approximately constant as seen in Figure 5.

2.3 Critical mass flux

The flow field can be held approximately constant during testing. Therefore, the mass loss rate of the liquid or solid fuel will be the defining parameter for the fuel/oxidizer mixture ratio and consequently also for the flame temperature of flames in close vicinity to the fuel surface. Bamford *et al.* (1946) were the first to suggest the critical mass flow

rate as a simplified and more practical surrogate to a fundamental description of flame ignition and extinction than the critical flame temperature. However, for theoretically calculating the critical mass flux, specifying the critical flame temperature is still required. Theory for the critical mass flux is further described in Section 2.5.

There is some evidence that the critical mass loss rate at sustained ignition and extinction are similar (Tewarson, 1982). However, making this measurement this requires a well-placed igniter that can ignite the gases as soon as they form a mixture that can support a sustained flame.

2.4 Ignition of solids

Several researchers have conducted reviews of research on ignition of solids. Amongst them are Babrauskas (2003), Fernandez-Pello (2011), Kashiwagi (1994), Atreya (1998) and Torero (2016). In this thesis, only general aspects of ignition that are related to the critical mass flux are presented. The reader is directed to these comprehensive works for further knowledge of ignition of solids, as it would not be possible to cover all aspects of ignition here.

When a solid material undergoes heating, fuel gases are produced. When gases leave the fuel surface, they mix with the surrounding air, as seen in Figure 6. With further heating, more volatiles are produced. The fuel/air mixture may be ignited when the mixture reaches its LFL in the proximity of an ignition source. A flame appears that propagates away from the source of ignition. This is visually observed in the form of a ‘flash’ of light over the fuel surface and is consequently called the flash point. If the generation rate of combustible volatiles and heat is sufficient to sustain a flame, a diffusion flame may anchor to the fuel surface. This point in the ignition process is defined as sustained ignition or the fire point and is close to stoichiometric burning (Torero, 2016). Upon further heating, the full fuel surface is involved in burning. This is the end point of the transient ignition process and the beginning of quasi-steady burning. In this thesis, the end point of ignition is called the ‘anchor point’ (Vermina Lundström, Sunderland, Quintiere, van Hees and de Ris, 2017).

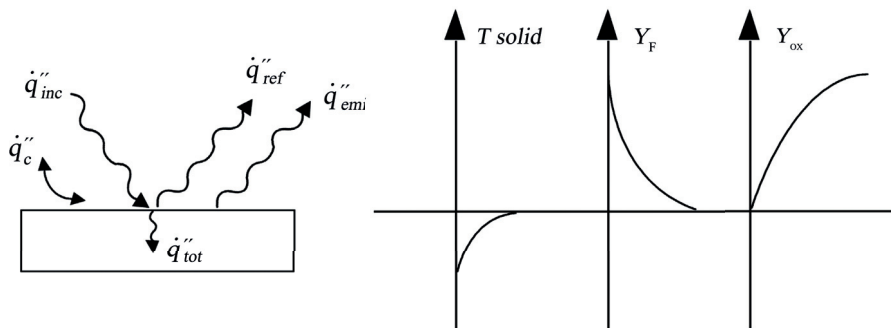


Figure 6. Heat balance at the surface

In the fire literature, piloted ignition of an irradiated solid material is commonly described by a time scale, with three time steps, namely the pyrolysis time, the mixing time and the combustion time. A stage of inert heating is also included in the pyrolysis time. The pyrolysis time is generally the largest contributor to the total ignition time (~ 100 s) and is primarily depicted by the thermal inertia of the solid (Quintiere, 2006b). Both in classical thermal theory and complex pyrolysis models, time to ignition has been shown to be most sensitive to the properties of thermal inertia (Bal, 2012).

The second time component is the mixing time. This is the time it takes for the fuel gases to mix with air in the control volume of interest and to build up a flammable mixture near an ignition source. The mixing time is generally dependent on flow (if the air is quiescent or in motion), geometry (i.e. motion direction of gases relative to the gravity vector) and to some extent also on the reactants involved (their molecular weight) (Kanury, 2002). The mixing time is on the order of a few seconds (Quintiere, 2006b).

Thirdly, the chemical time is characterized by the time it takes for a flammable mixture to react in the vicinity of an igniter. The chemical time can be described by Arrhenius components, which are fuel dependent, and gas phase conductivity. The chemical time is usually very short, on the order of $\sim 10^{-4}$ s (Quintiere, 2006b).

The statement that there is a critical mass flux for ignition of a flame is supported by both experimental and theoretical studies. The experimental studies are presented in section 3.1.1. Regarding theoretical work, Atreya and Wichman (1989) deduced a critical mass loss rate of $1.8 \text{ g}/(\text{m}^2\text{s})$. They came to this conclusion by using the near constant flame temperature for extinction. Tzeng, Atreya and Wichman (1990) modelled a heated thin “gaseous slab” with a stoichiometric fuel/air mixture, up to the critical flame temperature. They concluded that the conditions at sustained ignition are the same as those at extinction.

2.5 Extinction

Extinction of a diffusion flame can occur when either the solid surface or the gas phase (flame) is impacted, and these two mechanisms are often treated in a separate manner. Flame extinction (gas phase extinction) is commonly associated with a reduction in the flame temperature to the point where heat loss from the flame cannot be compensated by heat produced by combustion. Extinction may also occur due to cooling of the fuel surface (by e.g. water) or if the material burns out and releases no further volatile fuel to support a flame (Särdqvist, 2002). Flame extinction without adding a suppressant is often referred to as auto-extinction and is an important parameter when it comes to flame spread and sustained burning. Auto-extinction may come into play when a charring material is burning. The char layer creates a 'protective layer' between the flame and virgin material, reducing the rate of heat transfer. Therefore, with time, the virgin material produces less volatiles and finally extinguishes (Drysdale, 2011, p. 213).

2.5.1 Fire point theory

A theoretical description of extinction is found in the fire point equation by Rasbash (1976), described by an energy balance

$$S = (\phi\Delta H_c - L)\dot{m}''_{cr} + \dot{q}''_{abs} - \dot{q}''_{emi} \quad (2.5)$$

where S is rate of transfer of sensible heat, ϕ is the maximum fraction of heat that the flame may lose to the surface without being extinguished, ΔH_c is the chemical heat of combustion, \dot{m}''_{cr} is the critical mass flux, \dot{q}''_{abs} denotes the absorbed heat radiation from the flame and from other external heat sources, and \dot{q}''_{emi} is the emitted heat radiation from the surface. L is the latent heat of vaporization. Extinction occurs if $S < 0$. The critical condition may then be written at $S = 0$ as given by Rasbash (1986)

$$\dot{m}''_{cr} = (\dot{q}''_{emi} - \dot{q}''_{abs})/(\phi\Delta H_c - L) \quad (2.6)$$

2.5.2 Stagnant layer theory

Several researchers have utilized the stagnant layer model for diffusion flames, as derived by Spalding (1953). The theory is one-dimensional, and its configuration is shown in Figure 7. It is assumed that combustion and diffusional changes of mass, heat and momentum occur in the boundary layer (with thickness δ) over the surface, and that species concentrations only vary in y -direction.

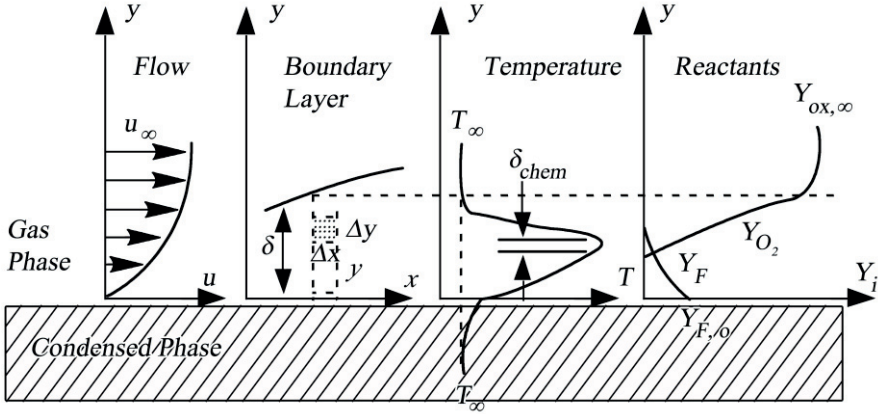


Figure 7. Stagnant layer model, reproduced from Quintiere (2006b) by permission

The burning rate in the control volume is

$$\dot{m}'' = \frac{k}{c_p \delta} \ln(1 + B) \quad (2.7)$$

where k and c_p denote the conductivity and specific heat of gas, respectively. For a convective boundary layer, the approximation $h_c = k/\delta$ is reasonable, where h_c is the convective heat transfer coefficient. B is the Spalding mass transfer number, given by

$$B = \frac{Y_{ox}(1-X_r)\Delta H_{ox} - c_p(T_s - T_\infty)}{L_m} \quad (2.8)$$

which is an expression of the ratio of chemical energy released to that required for pyrolysis. Note the resemblance to ϕ in the fire point theory. Y_{ox} and ΔH_{ox} are the oxygen mass fraction in air and the heat of combustion per gram of oxygen consumed. X_r is the flame radiation fraction. T_s and T_∞ are the surface and ambient temperatures respectively. $L_m = L - (\dot{q}''_{abs} + \dot{q}''_{c,f} - \dot{q}''_{emi} - \dot{q}''_{condensed})/\dot{m}''$ is a mathematical generalization of the heat of vaporization L , so that transient condensed phase terms such as charring, and effects of e.g. water interaction with the flame and surface may be accounted for (within the term $\dot{q}''_{condensed}$). These effects are further described by Quintiere and Rangwala (2004).

It can be shown that the time it takes for fuel gases to combust is much shorter than the time for transport of gases into the control volume in Figure 7. In other words, the thickness of the reaction region is thinner than the boundary layer thickness. The thickness of the reaction region can therefore be approximated by an infinitesimally thin

sheet – a flame sheet. The temperature of this sheet (the flame temperature T_f) is stated in Eq. (2.9)

$$c_p(T_f - T_\infty) = \frac{(1-X_r)\Delta H_c Y_{F,0} - L_m - c_p(T_s - T_\infty)}{1 + (\Delta H_c Y_{F,0}) / (\Delta H_{ox} Y_{ox})} \quad (2.9)$$

in which ΔH_c is the chemical heat of combustion and $Y_{F,0}$ is the fuel mass fraction at the fuel surface, which for a pure fuel is 1 (inert materials in the solid reduce the value). Combining Eqns. (2.7-2.9) results in an expression for the critical mass flux at extinction, where the remaining parameters are gas phase properties

$$\dot{m}''_{cr} = \left(\frac{h_c}{c_p} \right) \ln \left[1 + \frac{[Y_{ox}(1-X_r)\Delta H_{ox} - c_p(T_s - T_\infty)]}{\Delta H_c Y_{F,0}(1-X_r) + c_p(T_s - T_\infty) - c_p(T_f - T_\infty)} \frac{\Delta H_c Y_{F,0}}{(1 + \frac{\Delta H_c Y_{F,0}}{\Delta H_{ox} Y_{ox}})} \right] \quad (2.10)$$

Eq. (2.10) indicates that the convective heat transfer coefficient (h_c), and the specific heat of gas (c_p) should be influential on the result. The oxidizer constants for a flame burning in air are known; the oxygen mass fraction (Y_{ox}) in air is 0.233 and the ambient temperature (T_∞) is approximately 293 K. Thornton (1917) showed that, for many hydrocarbon fuels, the heat of combustion per gram of oxygen consumed (ΔH_{ox}) is approximately constant, as $\Delta H_{ox} = 13.1$ kJ/g-O₂. Small flames burning in sufficient air are dominated by convective heat transfer, whereas the flame radiation fraction (X_r) is small or neglected. The flame temperature (T_f) at extinction or ignition is commonly assumed to be 1500-1600 K, as described in Section 2.2. Surface temperatures (T_s) for many hydrocarbon fuels at ignition are approximately between 600 and 900 K (Lyon and Quintiere, 2007).

Inserting constant values for c_p , ΔH_{ox} , T_∞ , Y_{ox} , X_r , $Y_{F,0}$, T_s , and T_f , the critical mass flux (\dot{m}''_{cr}) is indicated to be a function of the chemical heat of combustion of the fuel gas (ΔH_c) and the convective heat transfer coefficient (h_c):

$$\dot{m}''_{cr} = f(\Delta H_c, h_c) \quad (2.11)$$

The convective heat transfer coefficient is calculated from the Nusselt number (Nu) as

$$Nu_D = \frac{h_c D}{k} \quad (2.12)$$

where D is the hydraulic diameter (e.g. the inner diameter of a pipe or the thickness of a candle wick) and k is the conductivity of gas. The Nusselt number is expressed by empirical correlations, based on dimension and geometry of the object that is heated or cooled. The characteristic length depends on the geometry of the object. For a hot plate facing up one empirical expression for Nu is

$$Nu_D = (C_0 + CRa_D^{1/4}) \quad (2.13)$$

where C and C_0 are empirically based constants (Gebhart, 1971, p. 372). The Rayleigh number (Ra) has importance for the convective flow and is defined as

$$Ra_D = (g(T_f - T_\infty)D^3)/(T_{film}\alpha\nu) \quad (2.14)$$

where g is gravitational acceleration, T_{film} denotes the mean of surface and flame temperature, α is thermal diffusivity and ν is kinematic viscosity.

So, if we again assume constant values, but this time for g , T_{film} , α and ν , the convective heat transfer coefficient – and thus also the critical mass loss rate – is a function of the fuel bed diameter D

$$\dot{m}''_{cr} = f(\Delta H_c, D) \quad (2.15)$$

Several assumptions are made in order to arrive at Eqns. (2.7)-(2.15), with the conclusions in Eq. (2.15); these assumptions are:

- 1 D transport processes
In the model it is assumed that all transport processes occur in the direction perpendicular to the solid or liquid layer, and that negligible transport occurs across the sample face.
- Gas phase properties are constant
Specific heat, conductivity, thermal diffusivity and kinematic viscosity of fuel and air are assumed to be constant (invariant of temperature) and equal for all reactants and inert gases involved.

In reality, these properties vary with temperature, and may be approximated by $c_p = .001+5 \cdot 10^{-10}T^{1.8}$ for the specific heat, $k = .000291T^{0.79}$ for conductivity, and $\nu = 1.1 \cdot 10^{-9}T^{1.68}$ for the kinematic viscosity of air (Wickström, 2016). This means, that if the temperature is raised from ambient to 1000 K, there is a two- and six-fold increase for conductivity and kinematic viscosity, respectively. Specific heat only differs by 10 %. However, at the moment of sustained ignition and extinction the gas temperature is assumed to be constant at 1600 K.

The fuel-to-air ratio in a flammable mixture is usually low, so air properties are assumed for all species.

- Heat and mass diffusion rates are equal
This means that the Lewis number is unity. This approximation has been deemed reasonable for combustion of common fuels in air (Quintiere, 2006b, p. 239; Law, 1984) but may introduce inaccuracies for exceptionally light or heavy molecules. One gas where this assumption is not applicable is hydrogen.

- Global, infinitely fast kinetics
It is assumed that chemical reactions occur in a very thin zone (commonly referred to as a flame sheet) and that reaction time therefore is approximately zero.
- Laminar flow
Laminar flow is assumed, flowing only in the direction perpendicular to the slab.
- Convective heat transfer
It is assumed that convective heat transfer dominates as the flame decreases in size before extinction. Radiative heat transfer is ignored in the model, except that a radiation fraction is included.
- The fuel mass fraction in the condensed phase is unity
The mass fraction of fuel within the condensed phase is assumed unity (small amounts of oxygen or nitrogen dissolved are neglected) (Kanury, 1977).
- Ignition and extinction have similar values for the critical mass flux.
Both the fire point theory provided by Rasbash (1975;1976) (as explained in Section 2.5.1) and experimental data by e.g. Heskestad (1980), Magee and Reitz (1975) and Tewarson (1982) provide evidence that the critical mass loss rate at sustained ignition and extinction are similar, given that the critical mass loss rate for ignition is measured at the time when the sustained flame is established (Tewarson, 1982) and the igniter is placed in a beneficial position with sufficient energy to ignite the flammable mixture.
- The burning rate equals the fuel mass loss rate
The fuel mass loss rate is in reality comprised of the mass rate of fuel consumed in combustion (the burning rate), the rate of inert gases released, and the combustible gases that are released but not combusted in the flame. For simplicity it is assumed that all gases are burned and that no inerts are released. However, the latter assumption is relaxed later in this thesis, since the fuel mass fraction at the surface is part of the theoretical expression.
- The heat of combustion is the chemical rate of energy released per unit fuel mass lost
This assumption is a consequence of the previous assumption.

It is clear from Eq. (2.10) that the critical mass flux varies with oxygen content (see Y_{ox} in Eq. (2.10)). This dependence has been investigated by several authors, e.g. Delichatsios (2005), Marquis, Guillaume and Camillo (2014), Quintiere and Rangwala (2004) and Rich *et al.* (2007), therefore a detailed study of this subject is redundant. This thesis instead investigates the influence of fuel bed size and chemical heat of combustion on the critical mass flux, as they are considered influential parameters in Eqns. (2.7)-(2.15).

3 Review of experimental determination of the critical mass flux

This chapter focuses on the evaluation of experimental equipment used for obtaining the critical mass flux at ignition and extinction. Measurements of critical mass flux vary due to material characteristics and differences in the features of the experimental equipment introduce variations in the measurements of the critical mass loss used. Babrauskas (2002) named four reasons for spread in flammability test results:

- Operating definition of events
- Specific characteristics of the tested material
- Environmental conditions
- Test apparatus design

These four points make up the basis for the choice of influencing parameters investigated in this thesis. A short summary of previous work on this subject is given in the following paragraph.

3.1 Experimental influences on the critical mass flux

From Eq. (2.10) it is clear that the critical mass flux is dependent on several factors. The effect that each parameter is expected to have on the critical mass flux may be quantified by a parameter sensitivity study, which is the focus of Chapter 4. This section is intended to give a broader introduction to possible dependencies and limitations related to experimental work.

3.1.1 Operating definitions of ignition and extinction

The definition of ignition and extinction may have an influence on the measured results; it also underlines the importance of clearly specified and controlled experimental work.

The definition of ignition is usually not specified in the reviewed papers, although a criterion for when the operator will log ignition is needed. It is assumed here that most studies record ignition at the point when a sustained flame is visible (for an arbitrary length of time).

There exist several definitions of ignition. Early studies (circa 1960) presented ignition results without regarding visual observations. The onset of flaming was instead determined by a set value or the slope plotted from thermocouple readings (Babrauskas, 2002). The general definition of ignition by ISO 13943 is that a flame is sustained on or over a test specimen for longer than a specified time (ISO, 2017a). In both the ISO 5660 cone calorimeter and the ISO 12136 fire propagation apparatus, ignition is said to occur when a flame is sustained on or above the sample surface for at least 10 s. The ISO 2592 Cleveland open cup test (for liquids) has a similar definition, but the defined time for a sustained flame is 5 s (ISO, 2017b). Drysdale and Thomson (1989) evaluated ignition at the moment a sustained flame appeared, without specifying a minimum length of flame sustainability. Khan and de Ris (2005) proposed that the onset of ignition could be evaluated from the peak of the second derivative of the mass vs. time curve.

Extinction is not defined by ISO 13943 (ISO, 2017a), but is commonly referred to as the end of combustion. Extinction is attributed to a reduction of flame temperature, i.e. it occurs when the energy losses are greater than the energy released. Extinguishing mechanisms are typically divided into extinguishing by gas phase effects or by surface impact (Särdqvist, 2002).

3.1.2 Specific characteristics of the tested material and its pyrolysates

Recalling Eq. (2.10), the tested material and its gas phase properties are characterized through the parameters:

- chemical heat of combustion, ΔH_c ;
- surface temperature, T_s ;
- flame temperature, T_f ;
- flame radiation fraction, X_r ; and
- fuel mass fraction at the surface, $Y_{F,0}$,

where each parameter and its impact on the critical mass flux is shortly described below.

3.1.2.1 Chemical heat of combustion

Different fuels have different critical mass flux values. Drysdale and Thomson (1989) found that oxygenated¹ materials require higher critical mass fluxes than non-oxygenated materials at ignition. Oxygenated materials generally have lower chemical heats of combustion than non-oxygenated materials; this leads to the hypothesis that the critical mass flux is a function of the chemical heat of combustion.

Tewarson (2002) introduced the critical heat release rate, in order to bypass the strong dependency on the chemical heat of combustion. The critical heat release rate (\dot{Q}''_{cr}) is the product of the critical mass flux and the chemical heat of combustion.

$$\dot{Q}''_{cr} = \dot{m}''_{cr} \Delta H_c \quad (3.1)$$

Tewarson concluded that \dot{Q}''_{cr} is only weakly dependent on the chemical nature of the material (represented by its chemical heat of combustion). Lyon and Quintiere (2007) calculated the critical heat release rates for several polymers, obtaining an average value of 66 ± 17 kW/m².

3.1.2.2 Surface temperature

The surface temperature of a material at piloted ignition is sometimes used as a threshold in modelling. The temperature of an irradiated material slab needs to be approximately 250 - 400°C before ignition can occur (Table 2) (Drysdale, 2011), but this value depends on external factors such as the flow conditions.

Table 2. Ignition surface temperatures, reproduced from data in Drysdale (2011, p. 260)

Material	T_{ig} (°C)
Wood	350
Western red cedar	354
Redwood	364
Radiata pine	349
Douglas fir	350
Victorian ash	311
PMMA	310
POM	281
PE	363
PP	334
PS	366

The surface temperature of a material increases upon heating, but it levels out before ignition occurs. The opposite is true for the critical mass loss rate, as seen in Figure 8,

¹ Oxygenated materials are materials that contain oxygen as part of the chemical structure. Examples include PMMA, POM and PA.

where the temperature and mass loss rate histories of black PMMA are presented. This behaviour provides an indication that, although the pyrolysis rate is dependent on the temperature profile within the specimen, the mass flux is only weakly dependent on the surface temperature. However, an increase in surface temperature at the limiting points indicates that the required mass flux for sustained flaming is slightly lowered.

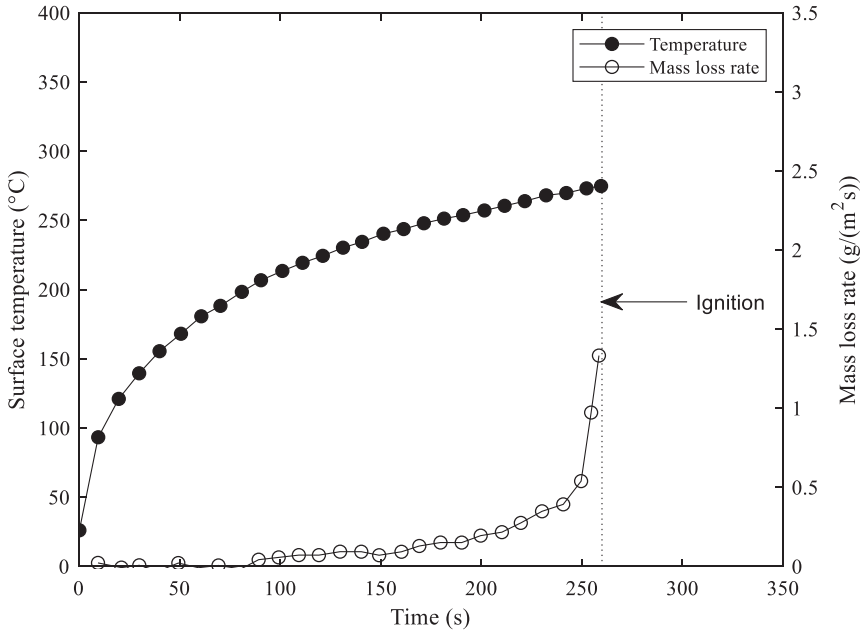


Figure 8. Sustained ignition of PMMA, from Kashiwagi, Inaba and Brown (1986) by permission

3.1.2.3 Flame temperature

Adiabatic flame temperatures for common hydrocarbons at the limiting conditions are somewhat fuel dependent, as shown by Peters (1979), who measured flame temperatures between 1650 K for methane to 1880 for iso-octane. Williams (1981) states that the flame temperatures at extinction are inversely related to the reactivity of fuels in combustion, where a low flame temperature at extinction corresponds to a reactive fuel. The reactivity of fuel gases is evident in measured Arrhenius combustion properties (A, E_a, n, m) and exemplified in Table 3. Chemically inhibited flames have a higher activation energy (Quintiere and Rangwala, 2004). A higher activation energy (and a higher flame temperature) indicates a lower rate of reaction in the flame (recall Eq. (2.1)). In turn, a lower reaction rate means that a higher mass flux is needed for a sustained flame.

Although variant, Williams (1981) concluded that 1600 K would suffice as a conservative limiting temperature for many fuel gases. An increase in the flame temperature (above the limiting temperature) increases the critical mass flux.

Table 3. Combustion reaction rates for selected hydrocarbon fuels, reproduced Dryer and Westbrook (1981)

Fuel	Structure	A (s ⁻¹ , see note 1)	E _a (kJ/mol)	n	m	ΔH _c (kJ/g)
Methane	CH ₄	8.3×10 ⁵	126	0.3	1.3	50.1
Ethane	C ₂ H ₆	1.1×10 ¹²	126	0.1	1.65	47.1
Propane	C ₃ H ₈	8.6×10 ¹¹	126	0.1	1.65	46.0
Butane	C ₄ H ₁₀	7.4×10 ¹¹	126	0.15	1.6	45.4
Heptane	C ₇ H ₁₆	5.1×10 ¹¹	126	0.25	1.5	44.6
Methanol	CH ₃ OH	3.2×10 ¹²	126	0.25	1.5	20.0
Ethanol	C ₂ H ₅ OH	1.5×10 ¹²	126	0.15	1.6	27.7
Benzene	C ₆ H ₆	2.0×10 ¹¹	126	0.1	1.85	40.1
Polymethylmethacrylate †	PMMA	1.0×10 ⁷	130	0	1	25.2
Polypropylene †	PP	1.0×10 ⁵	94	0	1	43.4
Polystyrene ††	PS	1.0×10 ¹³	245	1	0.3	39.2

† Lyon, Walters and Stoliarov (2006)

†† Stoliarov *et al.* (2016)

Note 1: Units of A are in (s⁻¹(kg/m³)^{1-n-m}) for Stoliarov *et al.* (2016) and in (s⁻¹(mol/cm³)^{1-n-m}) for Dryer and Westbrook (1981).

Note 2: Reaction rates for more fuels are found in Kanury (1977, p. 109) and Reshetnikov and Reshetnikov (1999).

3.1.2.4 Flame radiation fraction

The flame radiation fraction for a given fuel changes with fuel bed size. A small flame that produces little soot has a low emissivity and hence a small radiation fraction. A larger flame is turbulent and contains soot, which increases the radiation fraction. Most data on the radiation fraction has been made available by Tewarson (2002) from tests of 10 cm diameter samples in the ISO 12136 fire propagation apparatus (FPA), where the radiation fraction is related to the combustion efficiency. Some of this data is presented in Tewarson (2004). Quintiere, Lyon and Crowley (2016) provided additional radiation fraction data in the cone calorimeter. In summary, the flame radiation fraction in the two test set-ups varies between 0.25 and 0.60 for several plastics.

The radiation fraction has a linear correlation to the laminar smoke point, as seen in Figure 9.

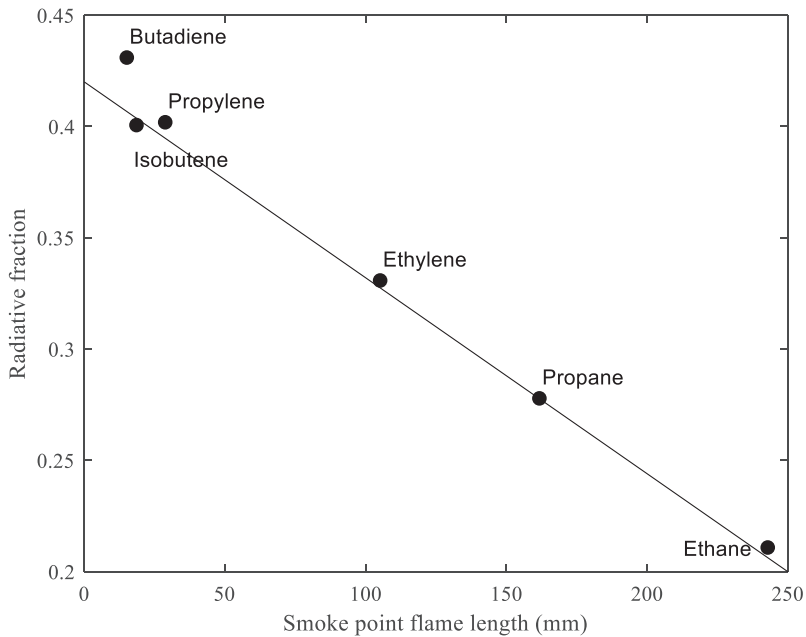


Figure 9. Radiation fraction for turbulent flames vs. laminar smoke point flame length, reproduced from de Ris (1989) by permission

An increase in the flame radiation fraction (or a lower smoke point) decreases the critical mass flux.

3.1.2.5 Fuel mass fraction at the surface

The fuel mass fraction at the surface depends on the amount of inert species (diluent) that are part in the fuel gases. Diluents lower the total combustibility of a unit amount of fuel gases and act as a thermal ballast. Increasing the amount of diluent leads to a reduction of the fuel mass fraction at the surface. This in turn leads to an increase in the required mass flux needed for sustained flaming.

3.1.2.6 Other characteristics

Other material characteristics have also been shown to influence the critical mass flux. Moghtaderi, Novozhilov, Fletcher and Kent (1997) and Atreya and Abu-Zaid (1991) reported that the critical mass flux at ignition increases with an increase of moisture content in Douglas fir, but the amount of dry pyrolysates remain unchanged if water vapour was removed.

3.1.3 Environmental conditions

The environmental conditions during experiments influence the critical mass flux. In Eq. (2.10) this is characterized using:

- the convective heat transfer coefficient, h_c ;
- the specific heat capacity (gas), c_p ;
- the oxygen mass fraction, Y_{ox} ; and
- the ambient temperature, T_∞ .

3.1.3.1 Convective heat transfer coefficient

Córdova and Fernandez-Pello (2000) investigated the influence of the convective heat transfer coefficient to the critical mass flux. They found \dot{m}''_{cr} to be a linear function of h_c . An increase in flow velocity or in the heat transfer coefficient increases the critical mass flux (Rich *et al.*, 2007).

3.1.3.2 Specific heat capacity of gas

The specific heat capacity is slightly temperature dependent, as described in Section 2.5.2, and is also dependent on the fuel gas. Since air consists of 79 vol % nitrogen, and the fuel mass fraction is low, it is deemed reasonable to assume the values of nitrogen or air. A decrease in the specific heat leads to an increase in the critical mass flux.

3.1.3.3 Oxygen mass fraction

Delichatsios (2005) and others (Marquis *et al.*, 2014; Quintiere and Rangwala, 2004; Rich *et al.*, 2007; Xin and Khan, 2007) have explored the variation of critical mass fluxes with oxygen concentration, finding a weak dependency for oxygen concentrations above 18 vol %. If the oxygen mass fraction is lowered (as sometimes is the case at extinction) the critical mass flux is lower.

3.1.3.4 Ambient temperature

An increase in the ambient temperature increases the critical mass flux. This has been investigated by Xin and Khan (2007) who concluded that the ambient temperature does not have a significant effect if it varies less than 40°C.

3.1.3.5 Other environmental factors

Different studies have shown that the critical mass flux is dependent on other environmental factors as well. Ignition of a solid material requires external heating, so that decomposition processes occur. This is not necessarily the case for extinction, however, a flame can be extinguished if the external heat source is removed.

Some researchers have investigated the influence of external heating on the criticalities of flaming combustion. Thomson and Drysdale (1989) observed a small drop in the

critical mass flux as the heat flux approaches the minimum heat flux required for sustained ignition (between 10 and 20 kW/m²). Panagiotou and Quintiere (2004) measured critical mass fluxes in the cone calorimeter for irradiances in the range of 20-60 kW/m². They saw a variation in the critical mass flux for acrylonitrile butadiene styrene (ABS), but otherwise they considered the effect of external heating to be weak or negligible.

Fereres *et al.* (2011) and Jiakun *et al.* (2013) have looked into the influence of pressure on the critical mass flux at ignition, finding slightly lower critical mass fluxes, i.e. an increased fire hazard, in atmospheres of reduced pressure, as is the case in aircraft and spacecraft cabins.

3.1.4 Test apparatus design

The design of the experimental equipment and its operating conditions may influence the result. The subsequent paragraphs describe variations coupled to test set-ups.

3.1.4.1 Definitions of ignition and extinction and impact of igniter

The igniter type and position will have an effect on the experimental results. It is assumed here that the igniter type and position for each presented apparatus has been chosen on the basis of an ideal outcome. A spark igniter has the benefit of producing a non-intrusive, yet high energy ignition source, but is sensitive to the distance from the sample. A glowing wire igniter has benefits similar to the spark igniter but is less efficient than electric sparks. However, it covers a localized region surrounding the wire length. A flame igniter covers a wider range of possible flammable regions above the sample surface than a spark igniter, however, it may also heat the surface of the material locally (Janssens, 2016).

Throughout this thesis, sustained ignition and extinction have been assumed to be similar. Although this is true for many cases, the assumption is not necessarily generic. For ignition to resemble extinction, an igniter is needed since the flame acts as the "igniter" of the flammable mixture at extinction. The extinguishment of flames also has different characteristics, e.g. radiation fraction, mass flux at the point of extinction etc. Jiakun *et al.* (2013) investigated the distance between the surface of a PMMA sample and a 200 W spark igniter in a test setup resembling the cone calorimeter. They found that the critical mass flux decreased as the igniter approached the sample surface (Figure 10), but below 20 mm (for their test setup) the critical mass flux remained constant to increasing.

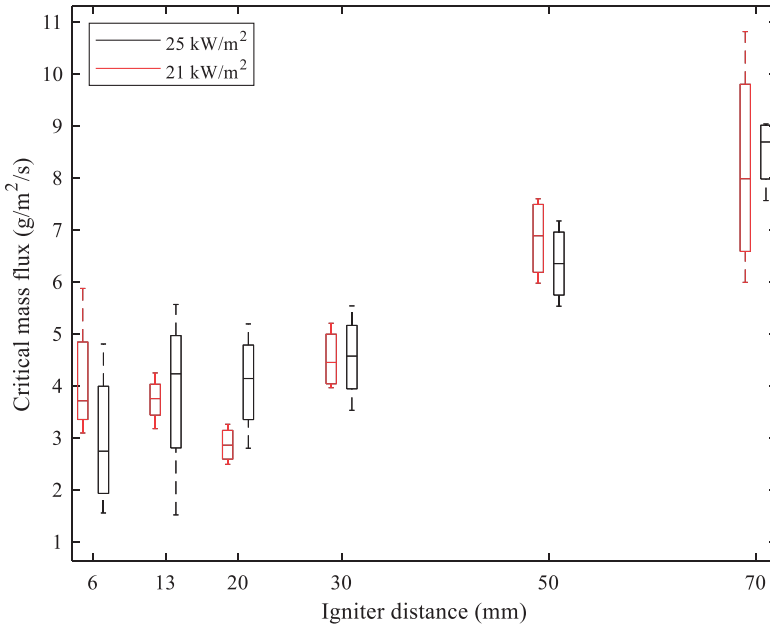


Figure 10. Influence of distance between igniter and sample, reproduced from Jiakun *et al.* (2013) by permission

3.1.4.2 Sample orientation and flow direction and velocity

Sample orientation also has an influence on the flow conditions and will therefore have an effect on the measurements. The top of a vertically placed sample is e.g. heated by the gas stream from the lower parts of the sample. Thus, the vertical and horizontal sample cases require different correlations for the convective heat transfer coefficient.

3.1.4.3 Heating device

Two main types of experimental equipment exist to obtain the critical mass flux: in one type the samples are exposed to a radiant flux, and in the other type the samples are exposed from all sides in a furnace. The first type is most common for ignition measurements; commonly used experimental equipment are described in Section 3.2.

Heat to one side of a sample is commonly applied with electrical heaters. Some experimental equipment uses tungsten filament lamps that produce radiant fluxes with shorter wavelengths than flames in real fires. This is because the wavelength is directly influenced by the temperature of the emitter (Försth and Roos, 2011). High temperature electrical heaters correspond approximately to conditions under fire exposure (Janssens, 2016).

3.1.4.4 Measurement and analysis of mass flux

Measurements of mass are typically conducted by placing the material sample of interest on a load cell. The load cell records the mass at specific time intervals and the mass flux is derived from the measured mass by numerical differentiation. The “measured critical mass flux” is therefore the calculated mass flux at the closest recorded time step to when a sustained flame has visually been observed. The mass measurements from load cells are noisy, especially when the signal is low, e.g. during ignition (Staggs, 2005). The noise is increased by numerical differentiation. Mass flux data is therefore often smoothed so that the true signal appears.

The time step chosen, the resolution and accuracy of the load cell, and the smoothing technique may consequently have an effect on the measurement of the critical mass flux. Another possibility of measuring the mass flux is to transport fuel gases through mass flow meters before combustion.

3.2 Experimental methods

In Figure 11 to Figure 17 and Table 4, a few of the apparatuses for determining the critical mass flux at ignition are presented. Table 4 lists experimental characteristics that may have an impact on the measurements.

3.2.1 Cone calorimeter

Most of the recent critical mass flux measurements have been obtained using the ISO 5660 cone calorimeter (ISO, 2015), illustrated in Figure 11. The cone calorimeter was developed by Babrauskas in the 1980’s and is one of the most frequently used pieces of bench-scale equipment for fire research. It was initially developed to measure the heat release rate (HRR) of building products but was later modified to also measure smoke production (Babrauskas, 2009). A modified version of the cone calorimeter, called controlled atmosphere cone calorimeter (CACC) is sometimes used. The load cell, sample and heater are then enclosed in a sealed chamber, and oxygen and nitrogen are fed to the bottom of the chamber where flow uniformity is ensured (Werrel *et al.*, 2014; Marquis *et al.*, 2014; van Hees *et al.*, 2018).

Table 4. Small-scale equipment used for critical mass flux determination

Apparatus	Heater	Sample (mm)	Igniter	Air flow	Sample orientation	Measurement of mass
ISO 5660 Cone calorimeter (CC)	Electric cone heater	Square, 100*100	Spark, 13 mm above the sample surface	Duct exhaust 10-32 L/s	H/V	Load cell, 0.1 g resolution
ISO 12136 Fire propagation apparatus (FPA)	Four coaxially located electrical heaters	Square, 100*100 or Circular, D=100	Pilot flame, 10 mm above the sample surface	3.3 L/s fed from the bottom of the quartz tube	H/V	Load cell, 0.1 g accuracy
Forced ignition and flame spread test (FIST)	IR radiant panel	Square, 30*30	Nichrome wire, 10 mm downstream, 5 mm above the sample surface	Fan at the downstream end, various flows	H	Load cell, 0.1 mg resolution (Sartorius WZ214S)
Edinburgh University ignition apparatus (EDUJA)	Electric cone heater	Circular, D=60 exposed (samples are 65*65, square)	Spark, 5 mm above the sample surface	Quiescent, exhaust flow not specified	H	Load cell, 0.1 g resolution (Sartorius L610)
Fire point apparatus	Radiant panel	Circular, D=60 exposed (samples are 65*65, square)	Hydrogen diffusion flame, 2 mm above the sample surface	0-60 L/min fed from the bottom of the cylindrical tube	H	Load cell, unspecified resolution (Unimeasure, 80 transducer)
BRE gas burner	None	D=25-100	Propane flame	Quiescent	H/V	Alicat mass flow controllers

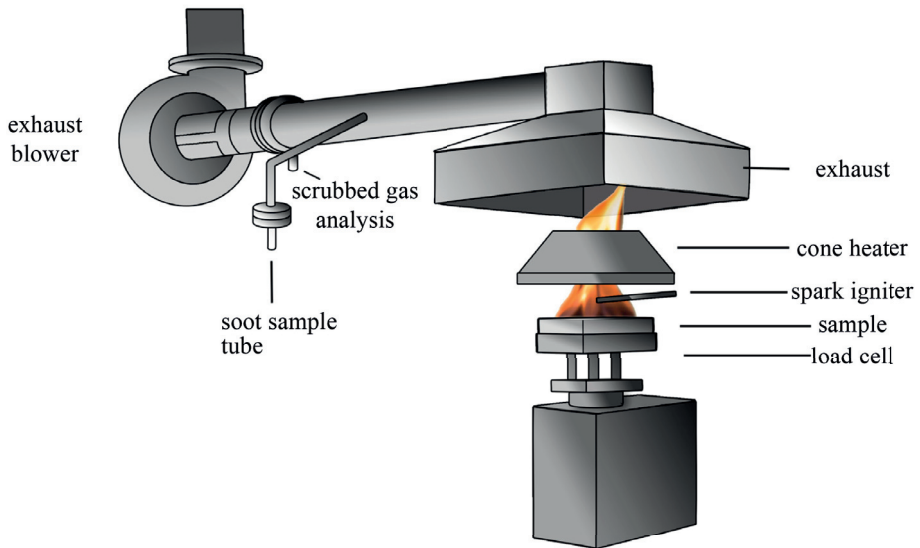


Figure 11. ISO 5660 Cone calorimeter (CC)

A square 100 mm material specimen, between 3 and 50 mm thick, is mounted in a steel retainer frame, so that sample sides and back surfaces are enclosed, and one surface is facing an irradiating cone heater. Upon heating, samples produce gases that are ignited by a spark igniter. The gases are collected in a hood and heat release is quantified by oxygen consumption calorimetry. Mass loss of the specimen is measured by a load cell (ISO, 2015).

According to the ISO 5660 standard, specimen preparation in the cone calorimeter is conducted as follows (see also Figure 12):

- A stainless steel retainer frame is placed on a flat surface, facing down.
- The 100 by 100 mm² specimen is wrapped in aluminium foil, with the shiny side towards the specimen. The foil should cover the bottom and sides of the specimen, and at least 3 mm on the sides of the top surface.
- Then, the wrapped specimen is placed in the retainer frame, with the exposed material surface facing down. The retainer frame should cover 3 mm of the sides of the exposed material surface, so that the exposed surface area becomes 94 by 94 mm².

- A refractory fibre blanket is placed on the backside of the specimen, until one to two 13 mm layers extend above the rim of the retainer.
- The sample holder is finally placed into the retainer frame, on top of the fibre blanket. The retainer frame is pressed down and the holder is secured with small screws. The holder is then flipped, so that the material faces the cone heater.

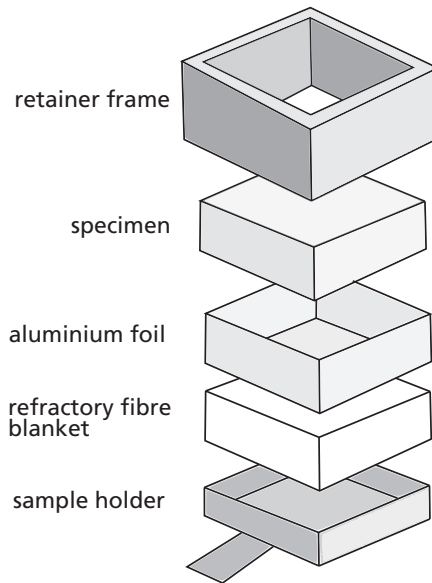


Figure 12. Cone calorimeter sample arrangement

In standard ISO 5660 cone calorimeter testing, samples are square, which introduces a case of non-homogenous heat flux towards the specimen, as the radiation source is circular. The irradiance in the central area (50 by 50 mm) is reported to lie within $\pm 2\%$ (ISO, 2015). The corners, however, receive incident heat radiation between 30-90 % of the centre value. Schartel, Bartholmai and Knoll (2005) found that the incident heat radiation over the specimen centre (a 5 by 5 cm area) is uniform, but the heat flux decreases towards the sample corners. Despite this, the calculated average incident heat radiation over the entire sample reaches 97 % of the incident heat radiation in the centre area. Wilson, Dlugogorski and Kennedy (2003) presented isolines on the square cone calorimeter specimen (intumescent material) that graphically showed the difference in incident heat radiation between the sample centre, edge (44 mm from the centre) and corners (62 mm from the centre). Similarly, Janssens, Huczek and Faw (2008) provided heat flux distributions over the sample area in the cone calorimeter, for irradiances of 27, 52 and 82 kW/m². The distribution for the 27 kW/m² case is reproduced in Figure 13.

Corner effects are significant, with heat fluxes only reaching half of that in the centre of the specimen. The mean heat flux dropped by 13 % compared to the centre heat flux for the three tests.

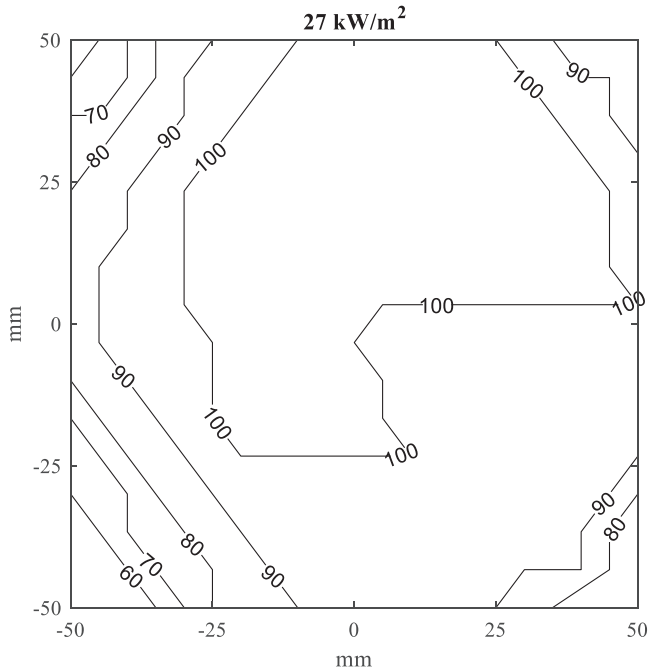


Figure 13. Heat flux distributions in % for cone calorimeter sample surfaces, based on reported measurements in Janssens *et al.* (2008)

3.2.2 Fire propagation apparatus

The ISO 12136 fire propagation apparatus (FPA) tests material samples enclosed in a quartz tube. A user-defined rate of oxygen and nitrogen is fed from the bottom of the tube. Four tungsten filament heaters are placed outside the tube, as seen in Figure 14 (ISO, 2011). The FPA is mainly used to measure the HRR and mass loss. Samples can either be square or circular.

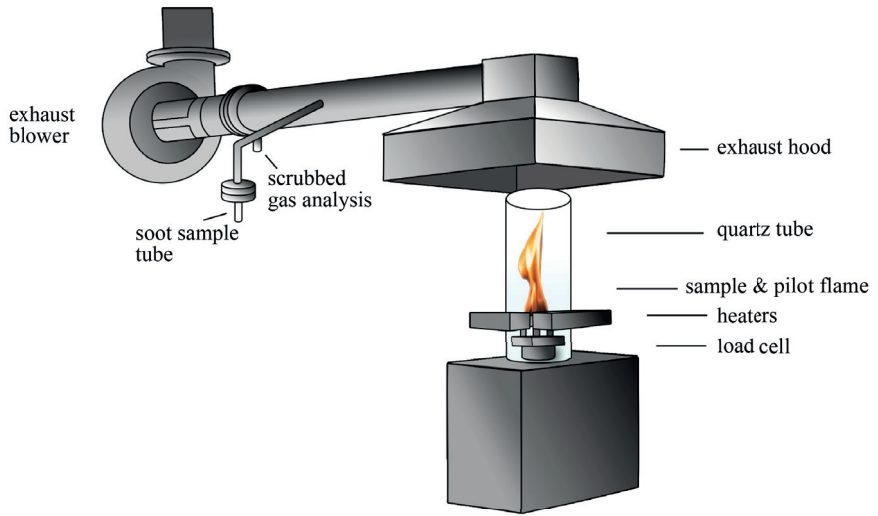


Figure 14. ISO 12136 Fire propagation apparatus (FPA)

3.2.3 Edinburgh University ignition apparatus

The Edinburgh University ignition apparatus (EDUA) was designed and utilized by Drysdale and Thomson (1989). A circular specimen is placed on a load cell and exposed to incident heat radiation from a cone heater, as seen in Figure 15. To decrease external vibration and draught effects on mass loss readings, the sample is surrounded by a non-combustible building board, and the test rig is enclosed in a steel cylinder.

3.2.4 Forced ignition and flame spread test

The forced ignition and flame spread test (FIST) is a small-scale wind tunnel, in which the specimen is placed flush with the bottom wall and exposed to heat by a radiant panel placed on the opposite side of the tunnel. An ignition wire is located downstream from the sample. The wind tunnel allows a variety of pressures and flows and oxygen/nitrogen mixtures. The sample is placed on a high resolution load cell for mass loss measurements (Rich *et al.*, 2007).

3.2.5 Fire point apparatus

The fire point apparatus was designed and utilized by Deepak and Drysdale (1983). It incorporates a radiant panel, a load cell and a flame igniter. A cylindrical tube is fed with

a chosen oxygen/nitrogen mixture. The sample is placed 75 mm under the lip of the tube to ensure burning under the intended mixture conditions. An outer enclosure shields the specimen from draught.

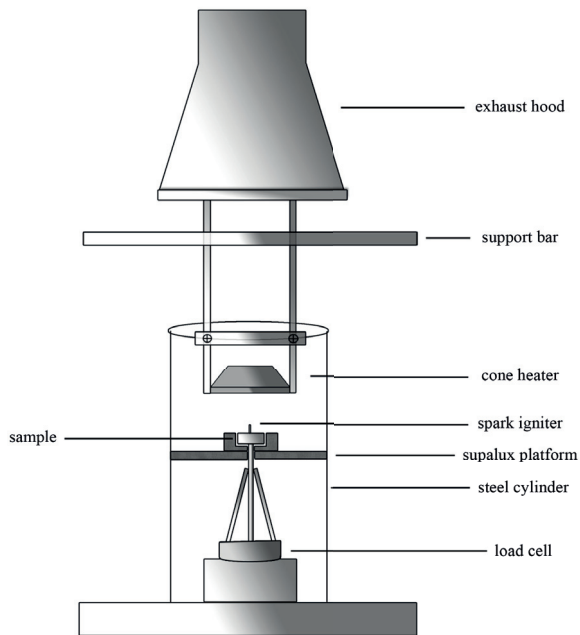


Figure 15. Edinburgh University ignition apparatus (EDUA)

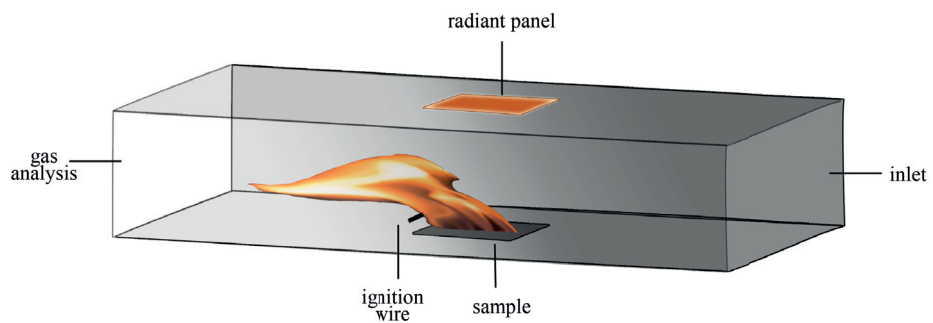


Figure 16. Forced ignition and flame spread test (FIST)

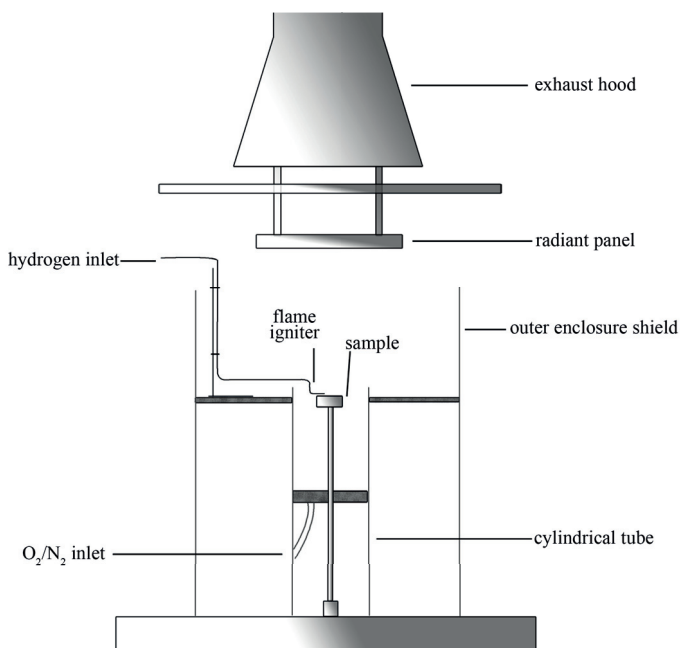


Figure 17. Fire point apparatus

3.2.6 Emulating gas burners

Sustained ignition and extinction are related to locally rapid transition processes. Prior to ignition the mass loss rate increases very slowly. Then, at ignition, an exponential increase in the mass loss rate is initiated which proceeds until the material sample burns at an approximately steady rate. This behaviour makes it difficult to accurately measure the critical mass flux with load cells. The small values of mass loss rate during ignition, along with its strong time dependency may introduce a significant error, especially when samples are irradiated with high heat fluxes, since the processes are faster with increased heat fluxes. This has mainly to do with the experimental definition of ignition time, where the operator manually observes ignition. The strong increase of the critical mass flux at ignition stands in contrast to the temperature-time curve, which has a logarithmic shape, and levels out at ignition, as exemplified in Figure 8 (adapted from Kashiwagi, Inaba and Brown (1986)).

By decoupling the mass and energy balance at the fuel surface from the gas phase mechanisms, it is possible to control the time dependency, and to focus primarily on the gas phase phenomena during ignition and extinction of a diffusion flame. Separation of the gas and solid phases can be done by thermally distilling pyrolysates from a solid fuel

and combusting the pyrolysates separately. Few studies exist that offer data on chemical reactions in the gas phase. Lyon, Walters and Stoliarov (2006) proposed a method to separate the solid and gas phases through pyrolysis-combustion flow calorimetry. They arrived at Arrhenius expressions for combustion of methane and six polymers. Similarly, Brink and Massoudi (1978) studied combustion of wood in a flow reactor.

A simpler method to control the rapid process (i.e. to rule out the effect of time dependency) is by experimentally simulating pyrolysis gases with a gas burner. Corlett (1968, 1970) pioneered the use of gas burners to emulate pool fires. He utilized circular, water cooled burners having 5, 10 and 19 cm diameters. The main purpose of the study was to delineate heat transfer mechanisms from the gas phase to the emulated condensed phase. He concluded that the essential features of burning pools were preserved with the gas burners, and that the magnitude of heat transfer in the burners correspond to the heat transfer of burning liquids. De Ris and Orloff (1972, 1975) used a large scale sintered brass burner, placed at different angles, to study radiation and orientation effects of turbulent diffusion flames over “walls” and “ceilings”. The fuel mass flux stemming from the burner was uniform, unlike ‘real’ solids or liquids but could still represent the burning behaviour of several condensed phase fuels. Kim *et al.* (1971) utilized gas burners to study laminar flames under natural convection. The gas burner data showed excellent agreement with burning rates of methanol but failed to produce the burning rates of high-molecular weight fuels such as toluene and benzene. It was hypothesized that this had to do with the low Lewis numbers associated with high molecular weight fuels. Zhang *et al.* (2014) investigated the flame standoff distance over inclined plates. Results validated the similarity in flame shape and turbulent flow between emulating burners and flat solid surfaces.

Emulation of condensed fuels is a simplified approach to retrieve material data. A recent project – the burning rate emulator (BRE) – has shown that steady burning of liquid and solid fuels is possible to emulate by matching gas burner properties with four properties of real liquids and solids (Zhang *et al.*, 2015; Auth, 2019):

- Chemical heat of combustion
- Laminar smoke point
- Heat of gasification
- Surface temperature

The four fuel properties were selected on the basis of their impact on fuel behaviour in combustion. The chemical heat of combustion is related to flame shape and therefore also to convective and radiative heat fluxes. The laminar smoke point is an indicator for sooting propensity. The heat of gasification is the heat required to gasify the fuel and the surface temperature is related to the boiling point of a liquid. Gas burner experiments by Zhang *et al.* (2015) and Auth (2019) validated possible emulation of steady burning of liquids, e.g. heptane and methanol, as well as solids, such as PMMA and

polyoxymethylene (POM). Their conclusions are based on similarities in flame shape, flame height, convective heat transfer, flame anchoring and flammability regions; this is exemplified in Figure 18. For steady-state burning Zhang *et al.* (2015) showed that there was no need to emulate the surface temperature in the gas burners due to its low impact on the heat transfer in comparison to the heat flux from the flame. Consequently, both Zhang *et al.* (2015) and Auth (2019) emulated fuels without matching surface temperatures.

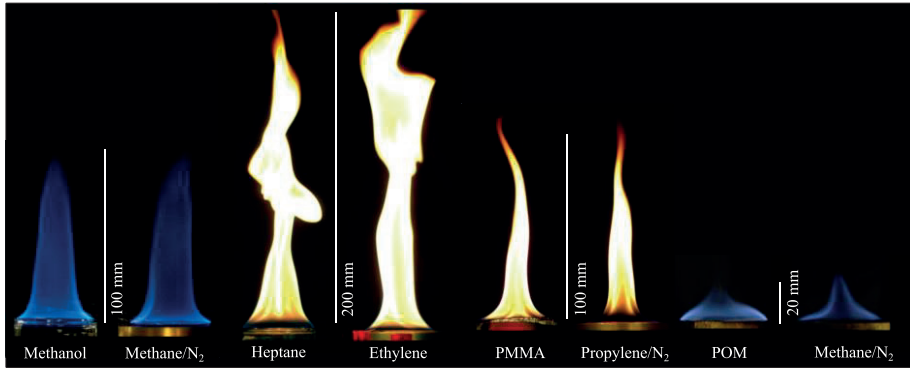


Figure 18. Burner emulated flames compared to condensed phase fuels, from Zhang *et al.* (2015) by permission

Reports on experiments with gas burners emulating the critical points of ignition and extinction have been scarce. Delichatsios and Delichatsios (1997) analysed extinction of diffusion flames using the experimental data by Corlett (1968). They correlated the influence of the convective heat transfer coefficient to the critical mass flux at extinction.

3.2.7 Summary of apparatus evaluation

In summary, the experimental equipment presented in Table 4 have similar functions, which are repeated in Table 5 to remind the reader. The parameter(s) of interest determine which equipment to select.

Table 5. Summary of the evaluated pieces of equipment

	CC	FPA	EDUA	FIST	FP	BRE
Availability	High	High	Low	Medium	Low	Low
Heater	cone	lamps	cone	panel	cone	-
H/V?	H/V	H/V	H	H	H	H/V
Mass flux measurements	Load cell	Load cell	Load cell	Load cell	Load cell	Mass flow controllers
Vary Y_{ox} ?	Yes	Yes	Yes	Yes	Yes	No
Igniter	Spark	Flame	Spark	Wire	Flame	Flame

All the evaluated pieces of equipment have the possibility to vary the oxygen concentration around the test object. The flow field at the sample surface is (for all apparatuses except FIST) perpendicular to the sample at its centre, due to buoyancy and hood extraction. The FIST places the sample at the bottom of a wind tunnel, and it is therefore easy to control the flow over the fuel surface, travelling parallel to the fuel surface. Both natural and forced convection may be applied. The combustion gases are separated from the heaters in the FPA but are in contact with the heater in the cone calorimeter.

Heating is applied with an electrical cone shaped heater or at least one electrical radiant panel. The FPA operates with heaters (tungsten filament lamps) that produce radiant fluxes with shorter wavelengths than flames in real fires. This is because the wavelength is directly influenced by the temperature of the emitter (Försth and Roos, 2011). The other pieces of equipment utilize heaters that correspond approximately to conditions under fire exposure (Janssens, 2016).

The resolution of the load cell is similar for all the above mentioned equipment. It is well known that mass loss data in the cone calorimeter suffers from noise (Staggs, 2005), which would therefore probably also be the case for the other equipment. Noise is usually handled by smoothing the mass loss data to achieve an average value based on adjacent data points, so that the true signal appears. Noise stemming from environmental disturbances (e.g. flow field) can also be handled experimentally by shielding the sample from draught. In the FPA, EDUA and fire point apparatuses shielding is achieved by cylinders surrounding the sample. Additionally, the EDUA has a platform at the same height as the sample that decreases measurement noise (Drysdale and Thomson, 1989). Noise can also be reduced by increasing the number of data points (i.e. decreasing the time step so that improved smoothing can be conducted). For the presented experimental equipment, the minimum time step available is not always reported.

3.3 Measurements of the critical mass flux at ignition

Table 6 presents previous measurements of the critical mass flux at ignition. The table is divided into type and size of material slab, environmental conditions (represented by the convective heat transfer coefficient h_c), equipment design (represented by name of apparatus, incident heat flux and sample orientation).

Specific characteristics of the tested material is indicated in the table by the differences in the critical mass flux, which varies for different materials. Tewarson (1982) measured the critical mass flux for several materials under the same testing conditions. Plastics were subjected to natural convection ranges between 1.9 and 3.2 g/m²/s in the Tewarson study. Values obtained for wood (plywood) had natural convection in the range of 2.0-3.8 g/m²/s according to Delichatsios (2005). One consideration that is important to mention in fire testing is that materials are often labelled only with their generic material name, such as

PMMA. These generic material names are in reality group names, for which material properties of individual specimens are likely to differ. These differences not only stem from differences in polymerization etc., but also from the amount of additives present. The materials in Paper II of this thesis are from the same manufacturer and batch, which allows for a comparison between tests (Grayson, 2018). However, it should be noted that the material properties from Table 6 are not directly comparable and their actual material properties, apart from the critical mass flux, are to be found in the original references.

Table 6 also shows that the critical mass flux varies between different pieces of equipment. This is due, in part, to sample size, flow conditions, igniter energy and location and type of heater. Table 6 presents sample sizes and their characteristic lengths (L^*), which are used in heat transfer correlations for Nu . In general terms, L^* is the height of the plate for vertical plates and $L^* = S / P$ (area/perimeter) for horizontal surfaces. One example of when the sample size is probably influencing the critical mass flux values is the comparison of different studies of PMMA. Zhubanov and Gibov (1988) tested 1 cm diameter PMMA samples that had much higher critical mass flux values (19.2 g/m²/s) than larger samples tested by e.g. Thomson and Drysdale (1989) (2.0 g/m²/s).

Table 6 also indicates that the critical mass flux may be dependent on the incident heat flux. This is seen in the values measured by Rasbash *et al.* (1986), where the critical mass flux for PMMA drops at low incident heat fluxes.

There are also differences between results for natural/mild and forced convection (given as h_c in Table 6), where an increase in flow velocity increases the critical mass flux (Rich *et al.*, 2007). Sample orientation also has an influence on the flow conditions and will therefore have an effect on the measurements.

Table 6. Critical mass fluxes at sustained ignition

Plastics	\dot{m}_{cr} (g/m ² /s)	q''_{inc} (kW/m ²)	Test	L* (mm)	Orientation	h_c (W/m ² /K)	Reference
ABS	8.2	50	CC	25	H	10	(Panagiotou and Quintiere, 2004)
Bamboo (laminated)	3	15	CC	25	H	10	(Solarie, Hidalgo and Torero, 2018)
Bamboo (laminated)	2.1	16	CC	25	H	10	(Solarie, Hidalgo and Torero, 2018)
Bamboo (laminated)	3.9	40	CC	25	H	10	(Solarie, Hidalgo and Torero, 2018)
Deal, oak and pine	2.5	18-54	Batswing burner	2*230	V	-	(Bamford <i>et al.</i> , 1946)
Douglas fir	2.2-5.8	18-34	Similar to FIST	25.4	H	-	(Atreya and Abu-Zaid, 1991)
HIPS	1.8	17	CC	25	H	10	(Panagiotou and Quintiere, 2004)
HIPS	1.9	50	CC	25	H	10	(Panagiotou and Quintiere, 2004)
PE	1.9	-	FPA	100	H	10	(Tewarson, 1982)
PE	2.5	-	FPA	100	H	13	(Tewarson, 1982)
PE-chl	6.6-7.6	-	FPA	100	H	13	(Tewarson, 1982)
Plywood	2.0	25	CACC (at 21 vol-% O ₂)	25	H	-	(Delichatsios, 2005)
Plywood	2.8	35	CACC (at 21 vol-% O ₂)	25	H	-	(Delichatsios, 2005)
Plywood	3.0	50	CACC (at 21 vol-% O ₂)	25	H	-	(Delichatsios, 2005)
Plywood (fire retarded)	3.4	25	CACC (at 21 vol-% O ₂)	25	H	-	(Delichatsios, 2005)

Plastics	m''_{cr} (g/m ² /s)	q''_{inc} (kW/m ²)	Test	L* (mm)	Orientation	h_c (W/m ² /K)	Reference
Plywood (fire retarded)	3.4	35	CACC (at 21 vol-% O ₂)	25	H	-	(Delichatsios, 2005)
Plywood (fire retarded)	3.8	50	CACC (at 21 vol-% O ₂)	25	H	-	(Delichatsios, 2005)
POM	1.7	13	EDUA	15	H	10	(Drysdale and Thomson, 1989)
POM	1.8	17	CC	25	H	10	(Panagiotou and Quintiere, 2004)
POM	3.5	30	CC	25	H	10	(Panagiotou and Quintiere, 2004)
POM	0.7	50	CC	25	H	10	(Panagiotou and Quintiere, 2004)
POM	3.9	-	FPA	100	H	10	(Tewarson, 1982)
POM	4.5	-	FPA	100	H	13	(Tewarson, 1982)
PMMA	19.2	-	Irradiating device	2.5	H	-	(Zhubanov and Gibov, 1988)
PMMA	4	12	Fire point apparatus	60	H	-	(Rasbash, Drysdale and Deepak, 1986)
PMMA	4.8	16	Fire point apparatus	60	H	-	(Rasbash <i>et al.</i> , 1986)
PMMA	5.4	19	Fire point apparatus	60	H	-	(Rasbash <i>et al.</i> , 1986)
PMMA	5.3	24	Fire point apparatus	60	H	-	(Rasbash <i>et al.</i> , 1986)
PMMA	5.2	26	Fire point apparatus	60	H	-	(Rasbash <i>et al.</i> , 1986)
PMMA	1.9	13	EDUA	15	H	10	(Drysdale and Thomson, 1989)
PMMA	2.0	33	EDUA	15	H	10	(Drysdale and Thomson, 1989)
PMMA	3.2	-	FPA	100	H	10	(Tewarson, 1982)

Plastics	m''_{cr} (g/m ² /s)	q''_{inc} (kW/m ²)	Test	L* (mm)	Orientation	h_c (W/m ² /K)	Reference
PMMA	1.9	18	FIST	7.5	H	10	(Rich <i>et al.</i> , 2007)
PMMA	2.1	16	FIST	7.5	H	-	(Feres <i>et al.</i> , 2011)
PMMA	4.4	-	FPA	100	H	13	(Tewarson, 1982)
PMMA	3.2	50	CC	25	H	10	(Panagiotou and Quintiere, 2004)
PMMA	4.9	20	CC	25	H	10	(Vermesi <i>et al.</i> , 2016)
PMMA	1.5	25.4	Irradiating device	12.5	H	-	(Jiakun <i>et al.</i> , 2013)
PMMA	2.5	21.2	Irradiating device	12.5	H	-	(Jiakun <i>et al.</i> , 2013)
PMMA	4	-	Irradiating device	12.5	H	7	(Peng <i>et al.</i> , 2015)
PMMA	12	-	Irradiating device	12.5	V	8	(Peng <i>et al.</i> , 2015)
PP	1.1	25	EDUA	15	H	10	(Drysdale and Thomson, 1989)
PP	2.2	-	FPA	100	H	10	(Tewarson, 1982)
PP	2.7	-	FPA	100	H	13	(Tewarson, 1982)
PP/GL	1.4	18	FIST	7.5	H	10 or $0.54k \cdot Ra^{1/4}/L^*$	(Rich <i>et al.</i> , 2007)
PS	0.9	33	EDUA	15	H	10	(Drysdale and Thomson, 1989)
PS	3.0	-	FPA	100	H	10	(Tewarson, 1982)
PS	4.0	29	FPA	100	H	13	(Tewarson, 1982)

Plastics	m''_{cr} (g/m ² /s)	q''_{inc} (kW/m ²)	Test	L* (mm)	Orientation	h_c (W/m ² /K)	Reference
PUR (rigid)	6.9-8.4	-	FPA	100	H	13	(Tewarson, 1982)
PIR (rigid)	5.5-6.8	-	FPA	100	H	13	(Tewarson, 1982)
Wood	1-22	-	Fire point apparatus	60	H	-	(Koochyar et al., 1968)

denotes that the information is not specified in the paper

3.4 Measurements of the critical mass flux at extinction

It is not entirely straightforward to obtain critical mass flux data for flame extinction of solids, since most tests rely on continuous heating of the specimen to aid combustion until the material burns out, and burn-out is not representative of flame extinction (recall Section 2.5). Some experimental research, by Delichatsios and Delichatsios (1997), has been devoted to auto-extinction. Magee and Reitz (1975) have obtained critical mass flux values by adding water until extinction. Beyler (1992) has theoretically investigated the application of fire point theory to suppressants; however, measurements taken by adding suppressants may be higher due to fuel “splashing” into the flame (Rasbash *et al.*, 1986). In Table 7 critical mass fluxes at extinction are presented. Similar to Table 6, values of the critical mass flux vary with material and between tests. The values for the critical mass flux are generically somewhat higher than in Table 6.

The critical mass flux at extinction of a flame vary with the same parameters as ignition. However, extinction does not vary considerably with the position of the ignition source, since the flame itself is the igniter. If extinction occurs in a compartment post flashover, the oxygen concentration in the environment is likely to be reduced, and external radiation is likely to be larger due to a smoke layer. The char depth of a charring material is expected to be deeper. However, these effects are possible to include in the theory described in Section 2.5.2.

Table 7. Measured critical mass flux at extinction

Material	m''_{cr} (g/m ² /s)	Test	Reference
CLT	4	Large-scale compartment (2.75×2.75×2.95 m ³)	(Bartlett <i>et al.</i> , 2017)
Douglas fir	4	Bench-scale compartment	(Quintiere and Rangwala, 2004)
Heptane	1	Bench-scale compartment	(Quintiere and Rangwala, 2004)
Methanol	2.5	Bench-scale compartment	(Quintiere and Rangwala, 2004)
Particle board	7	FPA	(Delichatsios and Delichatsios, 1997)
PE	11.0	Flammability apparatus, similar to the CC with vertically placed samples	(Magee and Reitz, 1975)
PMMA	6.0	Flammability apparatus, similar to the CC with vertically placed samples	(Magee and Reitz, 1975)
PMMA	1.5	Bench-scale compartment	(Quintiere and Rangwala, 2004)
POM	4.0	Flammability apparatus, similar to the CC with vertically placed samples	(Magee and Reitz, 1975)

Material	\dot{m}''_{cr} (g/m ² /s)	Test	Reference
PS	9.0	Flammability apparatus, similar to the CC with vertically placed samples	(Magee and Reitz, 1975)
PS	1.5	Bench-scale compartment	(Quintiere and Rangwala, 2004)
Timber	2.6-8.3	Mass loss calorimeter with sample in vertical position	(Emberley <i>et al.</i> , 2017)

4 Selecting parameters based on a sensitivity analysis

This chapter explains the motives involved in the choice of parameters that are further investigated. A sensitivity analysis of the properties included in Eq. (2.10) has been the basis for the selection of the parameters.

4.1 Sensitivity analysis

All models are simplified representations of real phenomena. Predicting a phenomenon with the accuracy required by the application depends on whether the model is capable of predicting the phenomenon (trueness) and the spread in results based on variations in the input parameters (uncertainty). A parameter sensitivity study indicates which input parameters contribute the most to variability in results. Focus can then be placed on reducing the uncertainty of the most sensitive parameters.

Equation (2.10) describes the parameters that are important in producing sufficient pyrolysates for a sustained flame. The equation is repeated below for convenience. These parameters vary based on the material (as described in Section 3.1.2) and the environment (Section 3.1.3).

$$\dot{m}_{cr}'' = \left(\frac{h_c}{c_p} \right) \ln \left[1 + \frac{[Y_{O_2,\infty}(1-X_r)\Delta H_{ox} - c_p(T_s - T_\infty)]}{\Delta H_c Y_{F,0}(1-X_r) + c_p(T_s - T_\infty) - c_p(T_f - T_\infty) \left(1 + \frac{\Delta H_c Y_{F,0}}{\Delta H_{ox} Y_{O_2,\infty}} \right)} \right] \quad (2.10)$$

Since the specific heat (gas) is dependent on the flame temperature, it is calculated from the flame temperature as $c_p = .001 + 5 \cdot 10^{-10} T_f$ where the equation is retrieved from Wickström (2016). This is due to avoid covariance problems arising in the sensitivity model where interdependent parameters are used. The c_p range presented in Table 8 is the range represented by variations in the flame temperature.

Table 8 provides typical ranges for each parameter in Eq. (2.10) that were used in a parameter sensitivity analysis; the results are shown in Figure 19. The sensitivity analysis used here is a global approach, based on probability distributions of the parameters and ranked data correlations (referred to as Kendall's τ_b). Kendall's τ_b can be viewed as a coefficient of determination that is not sensitive to the type of correlation. This means

that the correlation between the dependent parameter ($\dot{m}_{c'}''$) and the influential parameters does not have to be linear. The concept of this approach is described elsewhere (Saltelli *et al.*, 2008). The ranges are based on a black PMMA sample burned in the cone calorimeter, where each range is obtained by the references quoted in the table.

Table 8. Parameter ranges of input properties for Eq. (2.10)

Parameter	Unit	Range, black PMMA	Reference
c_p	kJ/kg/K	1.3-1.4	(Wickström, 2016)
h_c	W/m ² /K	9-15	(Staggs, 2011)
ΔH_c	kJ/g	23-27	(Tewarson, 2002)
ΔH_{ox}	kJ/g-O ₂	13.1±0.1	Assumed. For all materials: 13.1±0.1 (Tewarson, 2002)
T_f	K	1450-1600	(Quintiere and Rangwala, 2004)
T_{∞}	K	290-300	Assumed
T_s	K	587-620	(Lyon and Janssens, 2005; Thomson <i>et al.</i> , 1988; Rhodes and Quintiere, 1994)
X_r	-	0.25-0.33	(Tewarson, 2004; Quintiere <i>et al.</i> , 2016)
$Y_{F,0}$	-	0.99-1	(Wichman, 1986)
Y_{ox}	-	0.233±0.02	Assumed

Figure 19 provides the results of the sensitivity analysis. Values of Kendall’s τ_b range between -1 and 1, where -1 and 1 both indicate a 100 % ordinal association between the dependent and independent (influential) variables.

4.2 Motivation for parameter selection

It is clear from Figure 19 that the critical mass flux is sensitive to the convective heat transfer coefficient. The convective heat transfer coefficient is therefore selected for further investigation.

Although the parameter sensitivity shows, that for black PMMA, the convective heat transfer coefficient has the largest impact, the chemical heat of combustion for an arbitrary selection of common materials and liquids range between ~2 and 50 kJ/g. The selection of material will therefore have a large impact on the outcome. Consequently, the influence of the chemical heat of combustion is a parameter that will be investigated further.

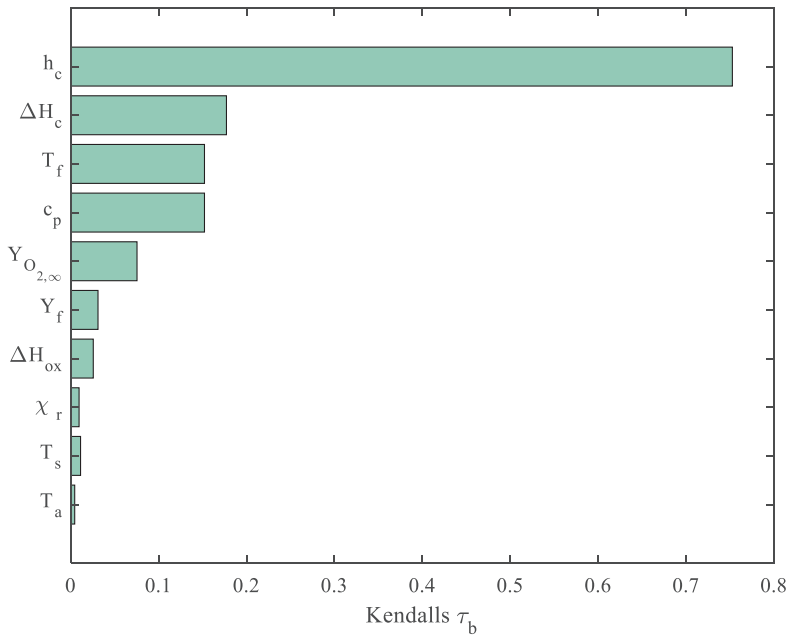


Figure 19. Parameter sensitivity of Eq. (2.10) for black PMMA

Despite the theoretical statement in Eq. (2.10), researchers have assessed a variation of the critical mass flux at different incident radiation fluxes (Drysdale and Thomson, 1989; Xin and Khan, 2007). The influence of the incident radiation flux upon the critical mass flux is therefore of interest. If the incident radiation flux has a large influence it may prove that the theory is unable to predict reality. Investigating the influence of the incident radiation flux on the critical mass flux will give an indication of the trueness of the model. Therefore, the incident radiation flux is selected as one of the possible influential parameters.

5 Selection and development of experimental methods

In order to meet the objectives of this thesis – to assess the critical mass flux and its dependence on key factors at the limiting points – experiments are needed. The experimental pieces of equipment have been chosen based on their ability to vary and investigate the selected parameters. The experimental modifications are further described in Papers II-IV.

Two experimental methods for obtaining critical mass flux values have been chosen for the experiments in this thesis. The first experimental set-up had the primary objective of testing with a uniform heat flux, so that, if a dependence on incident radiation flux was obtained, this dependence could be quantified. Testing was therefore conducted by using a standardized cone calorimeter, but with modifications to obtain an even more uniform incident heat radiation. This first experimental set-up is presented in Paper II. The latter experimental method was chosen partly due to its possibility of decoupling heat and mass transport. The experimental set-up was intended to explore the influence of the convective heat transfer coefficient on flames in quiescent air and the combustibility of fuel gases. The second set-up is a porous gas fuelled burner that emulates burning of condensed phase fuels; this set-up was used in Papers III and IV.

5.1 Cone calorimeter modification

The cone calorimeter utilizes electrical heaters that correspond approximately to conditions under fire exposure, however, the incident heat radiation on the sample surface is not uniform. Provided that the emitted heat radiation is uniform over the inner surface of the cone, a theoretical expression for the view factor F between each element of the sample surface (at distance d from the centre) to the cone is found in Wilson *et al.* (2003), and presented in Eq. (5.1). In Eq. (5.1), the shape of the heater is simplified as a cone without the cylindrical base.

$$H_1 = z/d$$

$$R_1 = r_1/d$$

$$Z_1 = 1 + H_1^2 + R_1^2$$

$$H_2 = (z + h)/d$$

$$R_2 = r_2/d$$

$$Z_2 = 1 + H_2^2 + R_2^2$$

$$F_{d_{sample} \rightarrow cone} = \frac{1}{2} \left[\left(1 - \frac{1+H_1^2-R_1^2}{\sqrt{Z_1^2-4R_1^2}} \right) - \left(1 - \frac{1+H_2^2-R_2^2}{\sqrt{Z_2^2-4R_2^2}} \right) \right] \quad (5.1)$$

The individual denotations in Eq. (5.1) are explained in Figure 20. To validate the expression by Wilson *et al.* (2003) the view factor between the cone and sample surface can also be modelled in Comsol Multiphysics version 5.4 (Comsol, 2019). In the Comsol model results provided here, the cone heater was represented by an irradiating surface, to which only boundary conditions were applied. The size complied with the size of the inner shell dimensions as specified in ISO 5660, where the base of the cone has a short 13 mm cylindrical section, seen in Figure 20. The sample was represented by a 20 mm by 20 mm surface, 25 mm below the frustum of the cone.

Further modelling assumptions were that air was not participating in radiation, (i.e. no flame was modelled) and that absorptivity and emissivity were equal. Radiation was modelled with the surface-to-surface radiation interface in Comsol, utilizing the hemicube method (resolution 1024), to account for possible shadowing effects, and because small gaps and sharp angles may have caused problems if a direct area integration method had been used.

For an efficient evaluation, the cone and sample surface were modelled with approximately the same number of mesh elements. The maximum element size was based on the respective surface area. The total number were 1946 triangular elements with an element/area ratio of 0.14.

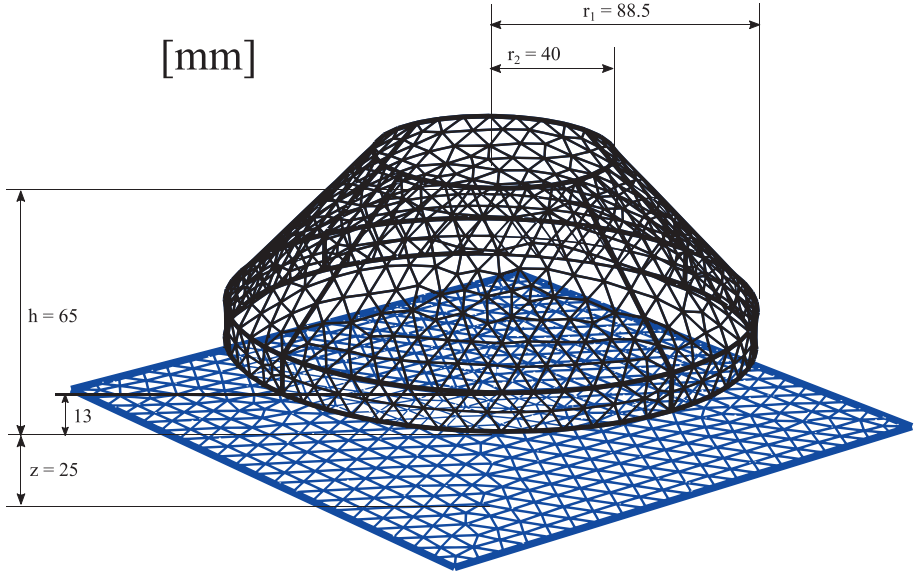


Figure 20. Modelled geometry and mesh

Figure 21 shows a comparison of the view factor evaluated in Comsol prior to simulations, and the theoretical expression given by Eq. (5.1). The calculated and modelled view factors are in agreement for the entire sample, which indicates that the equation by Wilson *et al.* (2003) (Eq. (5.1)) is reasonable (for materials that do not recede or intumesce upon heating).

The incident heat radiation \dot{q}''_{inc} to the sample surface was calculated from the cone heater's average temperature T as:

$$\dot{q}''_{inc} = F_{d_{sample} \rightarrow cone} \varepsilon \sigma T^4 \quad (5.2)$$

where σ and ε denotes the Stefan-Boltzmann constant and surface emissivity of the heating coil, respectively. The view factor determines the heat flux distribution over the sample, hence emissivity of the cone heater was set to unity and a temperature was specified so that the centre area would equal the intended incident heat radiation.

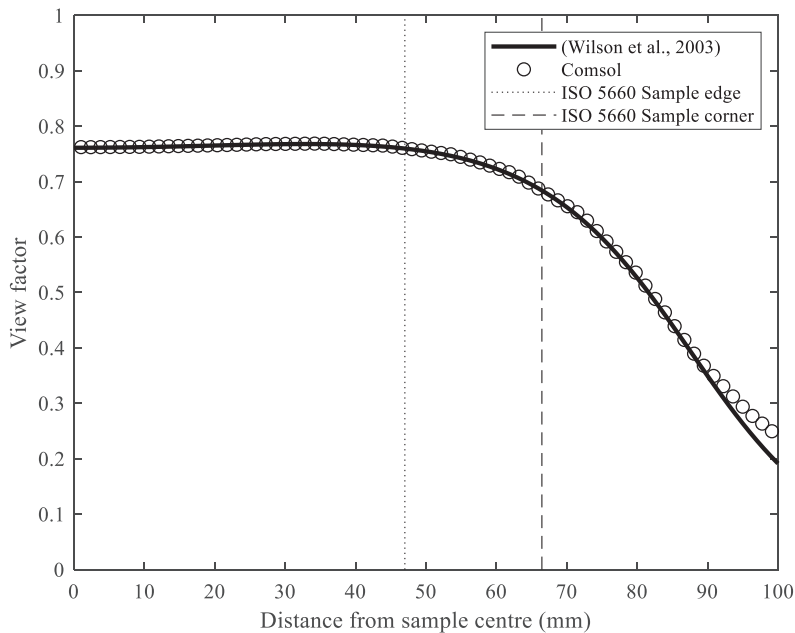


Figure 21. View factor between the sample surface and the cone heater

Most of the energy in a flame (and cone heater) is in the IR part of the spectrum, with relatively long wavelengths ($2 \mu\text{m}$ or longer). Boulet *et al.* (2014) measured the spectral emission of the cone heater and compared it to Planck's curves, showing that the cone heater may be approximated by a blackbody with an emissivity of unity. Consequently, the blackbody assumption for the cone heater made in this study is deemed acceptable.

Figure 22 shows the results from the simulations presented as isocurves of incident radiation. The incident heat radiation to the sample surface is dependent on the emitted radiation from the cone shaped heater and the view factor. The ISO 5660 standard states that the central 50 mm by 50 mm area of the specimen surface should be exposed to a uniform heat flux within an error margin of $\pm 2\%$, when the heat flux is 50 kW/m^2 (ISO, 2015). In Figure 22 this central area is represented by a red dashed line, where the corner parts of the central area are exposed to a heat flux of 47 kW/m^2 . However, the mean heat flux in the central area is 49.6 kW/m^2 , which lies within the error margin of $\pm 2\%$. The results of Figure 22 concur with the findings by Janssens *et al.* (2008), as the simulated incident heat radiation is uniform in the central area and decreases to 60 % of its original flux in the sample corners.

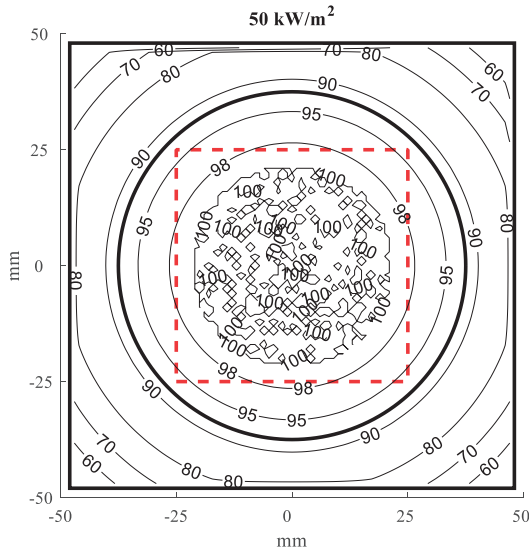


Figure 22. Simulated incident heat radiation (in %) to a square or a circular sample (black lines) at 50 kW/m². The red dashed line marks the central 50 by 50 mm area.

Table 9 presents the results of simulations for heat fluxes of 10, 30, 50 and 75 kW/m². Mean incident heat radiation levels are quantified over circular and square samples for a few given radiositivities. Table 9 shows that there is no significant difference in distribution or percent of decrease depending on the heat flux from the heater. All of the mean incident heat radiation to the square sample is within 82 % of the maximum value. If a circular sample with a 75 mm diameter is used, the mean incident heat radiation would be 97 % of the maximum value. The inner 50 by 50 mm area has an average incident heat radiation of 99 % of the maximum value.

Table 9. Incident heat radiation to the sample surface

Cone heat flux (kW/m ²)	Incident heat radiation (kW/m ²)				
	Central area	Circular sample	Square sample		
	Mean	Mean	Min	Max	Mean
10	9.96	9.8	5.0	10.0	8.2
30	29.7	29.2	14.9	30.0	24.7
50	49.6	48.7	24.7	50.0	41.3
75	74.4	73.1	37.2	75.0	61.6

In summary, it is clear that the heat flux distribution over the sample surface is non-uniform.

In order to experimentally reduce some of the boundary effects a proposed method in Paper II is to prepare specimens according to Figure 23, namely by removing both the effects of the retainer frame and the geometrical effect of the specimen. This procedure is as follows:

- The specimen is cut into a circular shape.
- The specimen is wrapped in aluminium foil or aluminium tape.
- Both back and sides of the sample are wrapped with ceramic wool, so that it fills out the void in the retainer frame.
- Finally, the ceramic wool is covered with aluminium tape.

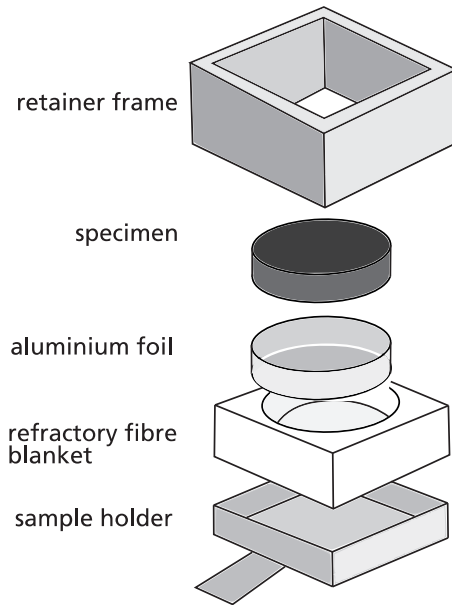


Figure 23. Sample set-up in Paper II

A photo of the circular sample is presented in Paper II. Apart from the sample preparation, tests were conducted according to the ISO 5660 standard (ISO, 2015). Sample mass loss is measured with a load cell. According to ISO 5660, this weighing device should have an accuracy of at least ± 3 g and a resolution of 0.1 g (ISO, 2015). The mass flux is derived from the measured mass by numerical differentiation. ISO 5660 recommends the use of a high-order scheme. The chemical heat of combustion is averaged over the entire test period subsequent to ignition such that

$$\Delta H_c = \frac{\sum \dot{Q}'' \Delta t}{m_{ig} - m_{end}} \quad (5.3)$$

where \dot{Q}'' is the heat release at time t , and Δt is the sampling time interval. m_{ig} and m_{end} are the mass of the specimen at sustained flaming and at the end of the test respectively.

Cone calorimeter measurements of mass of a burning specimen is inherently noisy. This noise is amplified in the derived mass flux. This is especially a problem when the signal is low, e.g. during ignition (Staggs, 2005).

Drysdale and Thomson (1989) reduced some measurement noise in the Edinburgh University apparatus by (1) surrounding the sample with a platform at the same height as the sample, and (2) by shielding the sample from draught by a steel cylinder, which would give a similar effect as the protecting shield in the cone calorimeter. This indicates that noise does not only stem from surface bubbling as presented by Fereres *et al.* (2011), Rasbash *et al.* (1986) and Rich *et al.* (2007), but also from environmental disturbances.

The noise in the cone calorimeter is normally handled by smoothing the results so that the signal appears. In Figure 24 smoothing of data is performed with a moving average. Data points can also be taken at a shorter time-step than the 5 s time step recommended in ISO 5660-1. In Paper II, measurements were taken at 1 s intervals. However, in Paper II it was seen that the signal-to-noise ratio is sometimes too low at ignition, even if a smoothing technique is used. Also, by using a smoothing technique, the output is calculated on the basis of adjacent data points. This results in values which are not necessarily “true”. The enhancement of Figure 24 (top right corner) shows that the unfiltered signal at ignition lies between 0 and 5 $\text{g m}^{-2} \text{s}^{-1}$ while the filtered signal suggests a critical mass flux of 1 $\text{g m}^{-2} \text{s}^{-1}$.

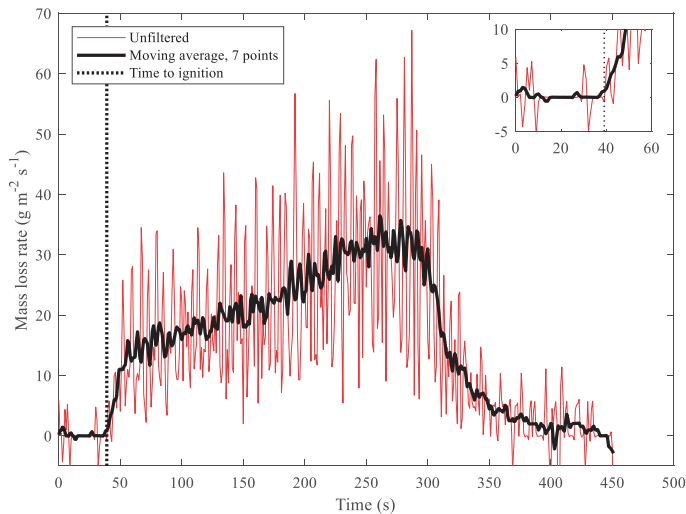


Figure 24. Example of noisy output in the cone calorimeter. PMMA. Test start: $t=0$.

The conclusion is that the cone calorimeter load cell is not always precise enough during ignition to measure the critical mass flux. Other methods or an improved load cell configuration are needed.

5.2 Burning rate emulator (BRE)

Papers III and IV are part of the same project as the Zhang *et al.* (2015) and Auth (2019) studies described in Section 3.2.6 – but with a focus on the ignition and extinction limits. The physical description of the limiting conditions is found in the equations in Section 2.5.2. The B number (Eq. (2.8)) represents the ratio of energy produced by the flame to the energy required to vaporize fuel in dimensionless terms. The flame temperature is described in Eq. (2.9). This equation contains the heat losses. Combining the two equations into Eq. (2.10) yields an expression in which the heat of gasification (L_m) disappears. In other words, Eq. (2.10) states that the critical mass flux does not depend on the condensed phase nor the heat loss to the burner. As a consequence, at ignition and extinction, three properties are required for emulation:

- Chemical heat of combustion
- Laminar smoke point
- Surface temperature

Temperatures at the burner surface have not been matched, but measurements have been made with K-type thermocouples mounted on the burner surfaces. Calculation of the matching properties are based on the mass fraction of the fuel (Y_f). First, a chemical heat of combustion (ΔH_c) is given by

$$\Delta H_c = Y_f \Delta H_f \quad (5.4)$$

where ΔH_f is the chemical heat of combustion of the pure fuel gas. Secondly, the laminar smoke point of the gaseous mixture (L_{sp}) is calculated by

$$L_{sp} = \left(Y_f / L_{sp,f} + Y_{N_2} / L_{sp,N_2} \right)^{-1} \quad (5.5)$$

where $L_{sp,f}$ and L_{sp,N_2} are the laminar smoke points of fuel and diluent respectively, and Y_f and Y_{N_2} are the mass fractions of fuel and diluent. By using different fuel gases, a variation of results due to different smoke points can be achieved, visible through the flame colour and smoke production. The relationship between the chemical heat of combustion and the smoke point is illustrated in Figure 25, where the lines of the gas mixtures are from the experiments in Paper IV, and the solid and liquid data is from Li

and Sunderland (2012) and Tewarson (2002). A lower chemical heat of combustion indicates a higher smoke point.

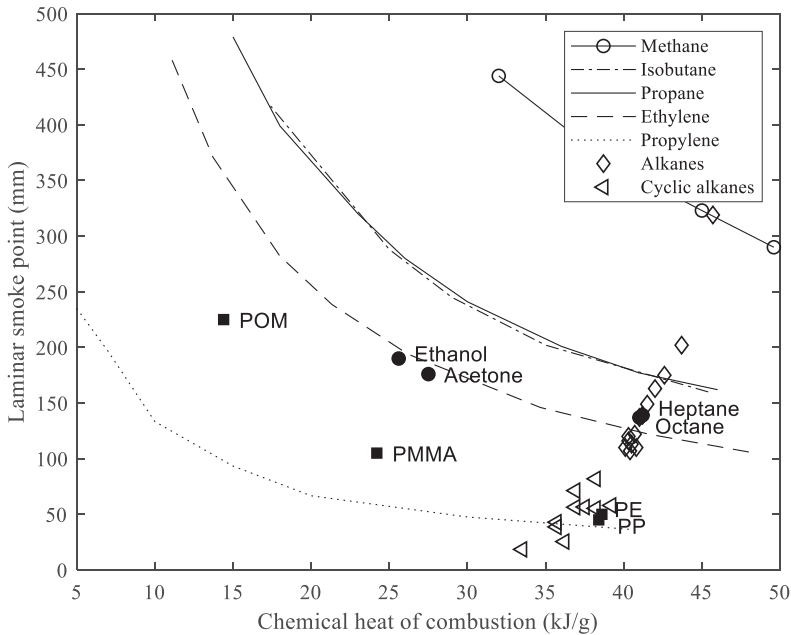


Figure 25. Relation between the chemical heat of combustion and the laminar smoke point

In Papers III and IV the burners were fed with one of four fuel gases (methane, propane, ethylene or iso-butane) and a diluent (nitrogen) that were mixed before entering the burner outlet. Propylene was also used in the 25 mm burner but not reported in the papers. The fuel gases were used so that a variety of flame characteristics could be achieved. Methane, for example, is known for its low burning velocity, and iso-butane has a relatively high molecular weight. The variety of gases ensured that the gases would represent a wide range of solid pyrolysates and liquid vapours with different smoke points. Properties of the fuel gases are described in Table 10.

The conversion from volume to mass flow was calculated with the ideal gas law, so that the mass flux of the gaseous mixture in the burner outlet is

$$\dot{m}'' = \frac{\dot{Q}/\rho}{\pi(D/2)^2} = \frac{(P(\text{Pa}) \cdot \dot{Q}(\text{slpm})/60 \cdot MW(\text{g/mole})) / (1000 \cdot R \cdot T(\text{K}))}{\pi(D(m)/2)^2} \quad (5.6)$$

where the volumetric flow rate of the mixture (\dot{Q}) and the mixture's density (ρ) are in the numerator and the burner surface area is in the denominator. P is the inlet pressure, MW

is molecular weight of the fuel mixture, R is the universal gas constant, T is inlet temperature.

Table 10. Gas properties used in the BRE

Name	Formula	MW (g/mole)	ΔH_c (kJ/g)	X_f	L_{sp} (mm)
Methane	CH ₄	16	49.6	0.14	290
Propane	C ₃ H ₈	44	43.7	0.27	162
Ethylene	C ₂ H ₄	28	41.5	0.25	106
Isobutane	C ₄ H ₁₀	58	42.6	0.29	160
Propylene	C ₃ H ₆	42	40.5	0.32	32.8
Nitrogen	N ₂	28			

Mass loss data was measured by *Alicat* gas mass flow controllers (pt. no. MC-2SLPM-D, 0.001 SLPM resolution), which are customized for low gas flows, such as the flows of pyrolysates at ignition and extinction. The step size chosen for increasing amounts of fuel gas until ignition occurred was 0.01 SLPM, which corresponds to approximately 0.1 g/m²/s, but this depends on the fuel used and the area of the burner outlet. Compared to e.g. the load cell in the cone calorimeter, the mass loss data in this experimental set-up has a high resolution.

The mass flow controller operating range (between 0 and 2 SLPM) allowed for a study of mass fluxes between approximately 0.5 and 50 g/m²/s. The lower bound is determined by the critical mass flux of the pure fuel, and the upper bound is determined by whether the flow was buoyancy controlled or not.

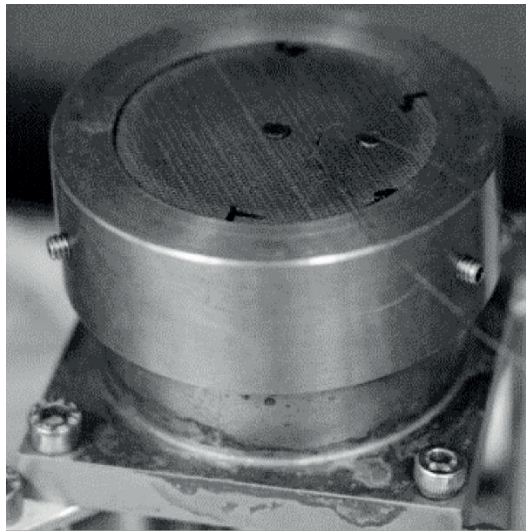
In total, three sets of burner prototypes were developed for the project, all which are referred to as BRE. These burners are fabricated based on the burners by de Ris and Orloff (1972) and have been modified and improved during the research project. The two first sets have been tested in Papers III and IV. Table 11 provides specifications on the burner characteristics.

The first set of prototypes were constructed mainly of brass, similar to the Corlett (1968) and the de Ris and Orloff burners (1972) (see Figure 26). The second set of burners were constructed using a thick copper plate, so that a better surface temperature distribution could be achieved; thus improving the heat flux measurements (see Figure 27). It also had the benefit of acting as a slug calorimeter, to achieve average heat flux measurements on the surface. The top plate was painted black and emissivity and absorptivity of the paint was quantified by pilot experiments. Stainless steel was chosen as the burner body material, to minimize heat transfer from the top plate to the burner walls. The mixing plenum was also designed to minimize heat transfer from the copper plate to the steel part of the burner. Gas leakage was prevented with rubber O-rings.

Table 11. Gas burner characteristics

	BRE1	BRE2	BRE3
Top plate material	Brass mesh	7 mm thick perforated copper	7 mm thick perforated copper
Gas flow uniformity	Glass beads	Ceramic honeycomb	Aluminium honeycomb
Sidewalls	Brass	1 mm thick stainless steel	Insulated stainless steel
Heat flux sensors	Medtherm thermopile, 1/8 inch diameter, located at the centre and offset radius R*	Medtherm thermopile, 1/8 inch diameter, located at the centre and offset radius R*	Medtherm thermopile, 1/8 inch diameter, located at the centre and offset radius R*
Temperature	K-type thermocouples, located at the centre and offset radius R*	K-type thermocouples, located at the centre and offset radius R*	K-type thermocouples, located at the centre and offset radius R*

Experiments by e.g. Zhang, Kim, Sunderland, Quintiere and de Ris (2016) and Zhang *et al.* (2015), and Papers III and IV in this thesis, have led to the development of the final (third) set of burners. The third set of burner walls consist of stainless steel, but with insulation surrounding it so that convective losses from the housing is minimized.

**Figure 26.** BRE gas burner, set I

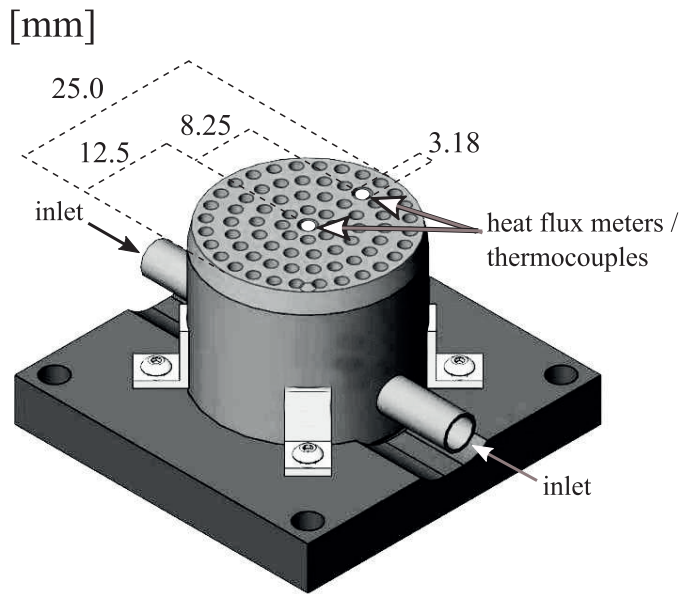


Figure 27. BRE gas burner, set II

6 Correlating the critical mass flux to fuel and environmental factors

In this chapter experimental findings are outlined and put into a theoretical context. The influence of fuel type on the critical mass flux, represented by the chemical heat of combustion, is presented in Section 6.1. The influence of the environment on the critical mass flux, characterised by the convective heat transfer coefficient and the incident heat flux, is described in Sections 0 and 6.3 for the two parameters respectively. These influences have been quantified in Papers II-IV, by utilizing the adapted sample preparation procedure for the cone calorimeter and the gas burners presented in Chapter 5.

6.1 The influence of fuel

The chemical structure of a fuel is closely related to its net heat of complete combustion. This is evidenced by the additivity principle in which the heat of combustion can be related to the summation of a fuel's chemical group and contribution of chemical bonds. The additivity principle is explained elsewhere (Van Krevelen, 1990), but its effect is that different types of fuels can be discussed in terms of their chemical heats of combustion.

6.1.1 Chemical heat of combustion

If oxygen is present in large excess, and the temperature is sufficiently high, complete combustion prevails. In real fires, however, complete combustion is seldom achieved. Products of incomplete combustion, such as CO, ethylene and carbon, are common, at the expense of products of complete combustion, such as CO₂ and H₂O. This results in decreased consumption of O₂, as stated by the combustion efficiency χ in Eq. (6.1)

$$\Delta H_c = \chi \Delta H_{net} = \frac{\dot{Q}''}{\dot{m}''} = \frac{\Delta H_{ox} \dot{C}_O''}{\dot{m}''} \quad (6.1)$$

where ΔH_c and ΔH_{net} are the chemical and net heats of combustion respectively. \dot{Q}'' is the (chemical) HRR measured by a calorimeter and \dot{m}'' is the mass loss rate. The factor \dot{C}_O'' is the mass consumption rate of oxygen. The combustion efficiency for common products

ranges between 0.46 and 1, with extinction at χ below 0.4 (Tewarson, 2002). For well-ventilated flames, the combustion efficiency for many materials approaches unity.

The correlation between the critical mass flux and the chemical heat of combustion is shown by the results from Paper IV (Figure 28) where measurements have been conducted using different fuel/air mixtures in the gas burners. A higher critical mass flux or a lower chemical heat of combustion is associated with a lower ignitability.

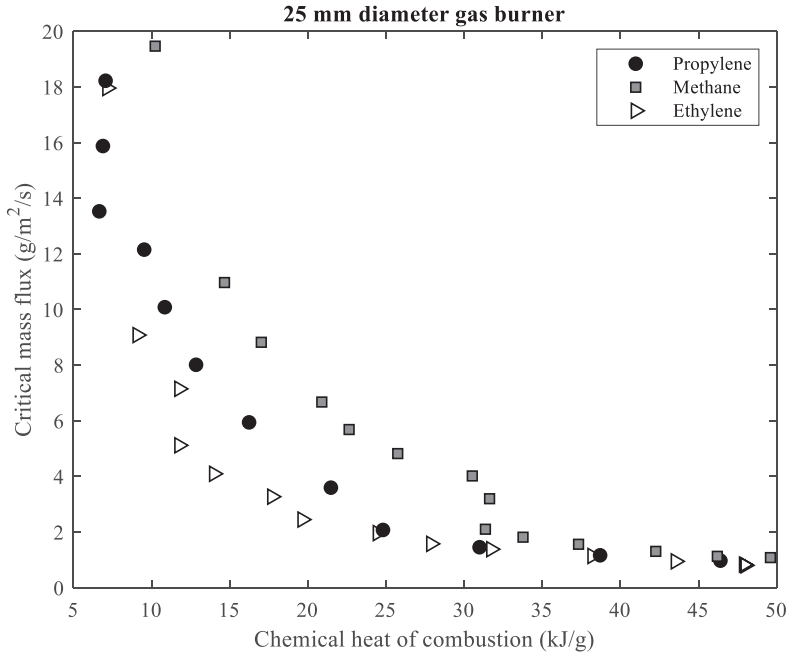


Figure 28. Critical mass flux at ignition

The results in Figure 28 are scattered due to variations in smoke point of the fuel gases used, which gives a span that many real solid and liquid substances would fit within (recall Figure 25). Similarly, Figure 29 presents the critical heat release rate ($58 \pm 9 \text{ kW/m}^2$) from Paper II, for a few hydrocarbon fuels burnt in the cone calorimeter.

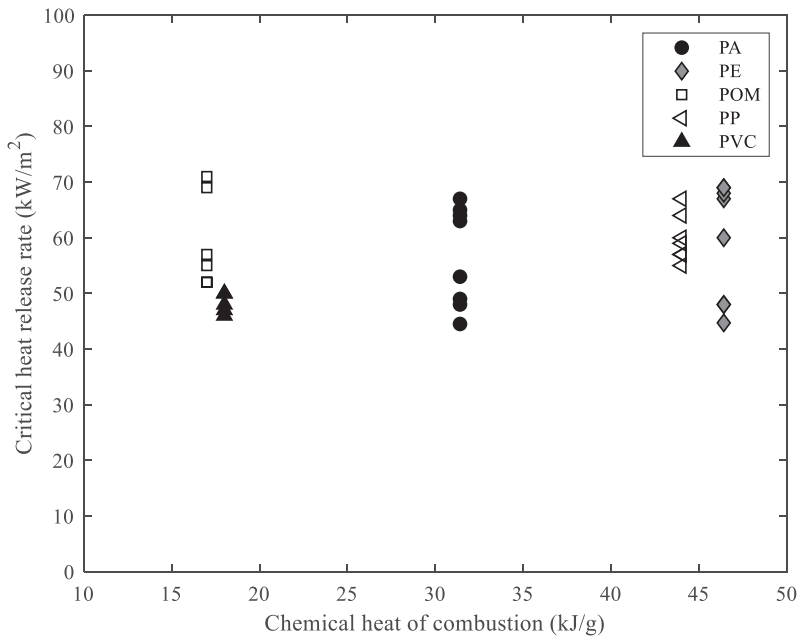


Figure 29. Critical heat release rate at ignition, measured in the cone calorimeter

Figure 29 illustrates that the critical heat release rate is independent on the chemical heat of combustion (for the materials used in Paper II). Since the chemical heat of combustion roughly represents the combustion characteristics of a material’s pyrolysates, the critical heat release rate is approximately fuel independent.

Figure 29 shows the trend for materials with heats of combustion between 17 and 46 kJ/g. A wider range of heats of combustion was investigated in Papers III and IV, with results shown in Table 12

. The table provides results from the same data set, but mean critical heat release rates are calculated over different ranges of heats of combustion: 5-50, 10-50, and 15-50 kJ/g. Both the mean and the standard deviation (Std) are remarkably higher when data points between 5 and 10 kJ/g are included in the range. A Student’s t-test is used to check whether the ranges provide significantly different values ($p < .05$) for the critical heat release rate (Student, 1908). Calculated p-values are presented in Table 12 together with clarification in parenthesis on whether the mean critical heat release rates differ.

The conclusion is that a constant critical heat release rate is a good approximation for materials with effective heats of combustion between 10 and 50 kJ/g. In other words, practitioners and modellers do not have to search for fuel specific \dot{Q}''_{cr} values in the literature if materials have chemical heats of combustion above 10 kJ/g. For materials

with chemical heats of combustion below 10 kJ/g some consideration needs to be taken. For instance, one may model using a critical mass flux value retrieved from experiments. Materials with low chemical heats of combustion are typically charring or fire retarded, as seen in Table 13.

Some variability is expected, not only with the chemical heat of combustion, but also with reactivity of the fuel gas. The fuel reactivity is not fully captured by the chemical heat of combustion property. Some fuel gases have exceptionally high (e.g. hydrogen) or low (e.g. methane) burning velocities (oxidation rates) under appropriate conditions. This is not evident in intermediate combustion steps, but if a fuel gas, either entirely or largely, consists of such a gas, it is seen in the results. In Paper IV this effect was indicated by the outlying trend of methane compared to the other fuel gases fed into the burners (i.e. propane, ethylene and iso-butane). Theoretically, the reactivity can be handled by lowering the chosen limiting flame temperature accordingly for vapours with low reactivity or lowering the flame temperature for gases with high reaction rates.

Reactivity of fuel gases is more fundamentally seen in measured Arrhenius combustion properties (A, E_a, n, m) and listed in Table 3; chemically inhibited flames have a higher activation energy (Quintiere and Rangwala, 2004). In this thesis it is however represented in a simpler format by the adiabatic flame temperature at extinction. Adiabatic flame temperatures for common hydrocarbons at extinction are somewhat fuel dependent, where Peters (1979) measured flame temperatures between 1650 K for methane to 1880 K for iso-octane. Findings in Paper IV confirm the statement of Williams (1981), i.e. that the ordering of flame temperatures at extinction is consistent with the reactivity of fuels in combustion, where a low flame temperature at extinction corresponds to a reactive fuel.

Table 12. Average critical heat release rates for three burners (BRE 1) in Paper IV

D = 25 mm			D = 50 mm			D = 100 mm		
ΔH_c (kJ/g)	\dot{Q}_{cr} (kW/m ²)		ΔH_c (kJ/g)	\dot{Q}_{cr} (kW/m ²)		ΔH_c (kJ/g)	\dot{Q}_{cr} (kW/m ²)	
	Mean	Std		Mean	Std		Mean	Std
15-50	46	5	0.2† (No)	36	2	0.2† (No)	29	1
10-50	49	7	0.03†† (Yes)	38	6	0.04†† (Yes)	30	1
5-50	122	120		60	44		30	1

† test of difference between 10-50 and 15-50 kJ/g ranges

†† test of difference between 5-50 and 10-50 kJ/g ranges

Table 13. Chemical heats of combustion of materials (from Tewarson, 2002)

Liquids		Ordinary polymers		Wood		Low combustibility materials	
Material	ΔH_c (kJ/g)	Material	ΔH_c (kJ/g)	Material	ΔH_c (kJ/g)	Material	ΔH_c (kJ/g)
Heptane	41.2	PE	38.4	Douglas fir	13.0	PUR-FR	14.8
Kerosene	40.3	PP	38.6	Red oak	12.4	PE-FR	7.2
Acetone	27.9	PS	27.0			PVC	5.7
Methanol	19.1	PMMA	24.2			Gypsum	4.3
		POM	14.4			Teflon	1.3

6.2 The influence of the convective heat transfer coefficient

Convection is heat transfer by a fluid flow. For example, in a free-burning fire, the heat released in the flame (or by a hot surface) creates buoyancy induced flows that carry away the heated gas by convection. The magnitude of convective flow is represented by a convective heat transfer coefficient. Typical values for natural convection (buoyancy induced flows) are 5-50 Wm⁻²K⁻¹ and 25-250 Wm⁻²K⁻¹ for forced convection (induced by e.g. a fan). The convective heat transfer coefficient in natural convection is a function of the Rayleigh number (Ra), which is dependent on the size of the fuel bed, as presented by Eqns. 2.7-2.15.

Paper IV explored the influence of flow on the ignition and extinction thresholds by varying the fuel bed size at critical conditions. Three gas burners with different diameters were used in the experiments (25, 50 and 100 mm). This allowed for a scalability study within the laminar and convection-controlled flow range.

The results were also compared to existing data taken in the cone calorimeter. An approximate convective heat transfer coefficient for the cone calorimeter is well known and has been investigated by e.g. Staggs (2009). For the gas burners, h_c has been calculated from heat transfer theory in the literature.

Based on the three burner diameters used in paper IV, the mass flux is dependent on the diameter as:

$$m''_{cr} = (0.14/D + 5/\sqrt[4]{D})(1/(0.43\Delta H_c - 1.9)) \quad (6.2)$$

The *lowest expected* critical mass flux for a given fuel bed diameter is illustrated by the lines in Figure 30. A smaller diameter requires a higher mass flux for a flame to sustain. Three virtual materials are presented, with heats of combustion of 10, 25 and 50 kJ/g.

The correlations give the lowest possible mass fluxes for materials at initiation or extinction of flaming. Materials tested in transient conditions, such as cone calorimeter testing, do not have the advantage of producing step-wise measurements, and therefore measurements of 'real materials' give higher critical mass fluxes, as seen by the points. For example, PMMA and polyurethane (PUR) have chemical heats of combustion of approximately 25 kJ/g. The critical mass flux measured in the cone calorimeter is 2.5 and 2.0 g/(m²s) for PMMA and PUR respectively (Lyon and Quintiere, 2007). The burner results give the conservative value of ~1.8 g/(m²s), i.e. the limit below which a material with $\Delta H_c \approx 25$ kJ/g would not burn. Another case to consider is polypropylene (PP) and high-density polyethylene (HD-PE) from Paper II, which have chemical heats of combustion of ~45 kJ/g. These materials have critical mass fluxes of 1.2-1.4 g/(m²s), whilst the correlation from Paper IV yields a critical heat release of 0.8 g/(m²s).

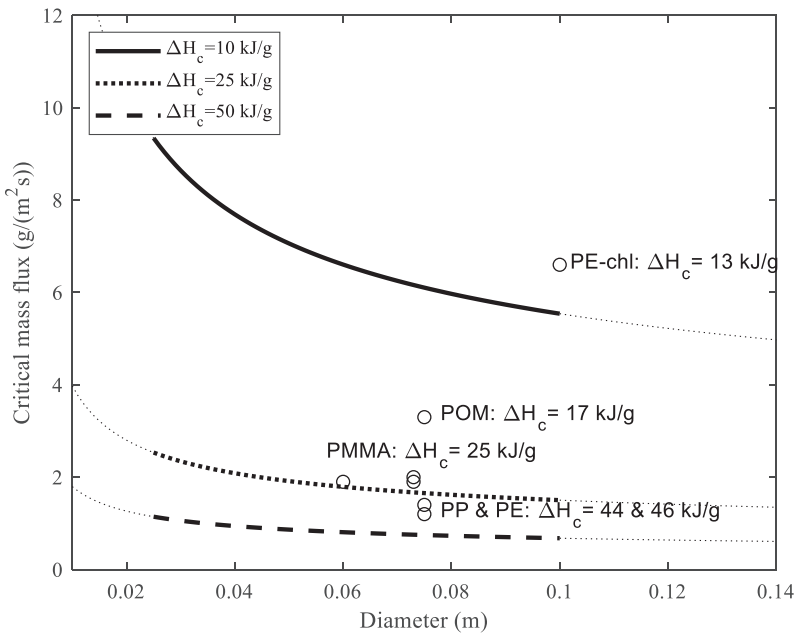


Figure 30. Critical mass flux: Influence of fuel bed size

Rayleigh number analysis of flames is valid when flames are buoyant. As the rate of fuel supply and inert gas was increased in the burners, a lift-off effect of flames was seen. The Froude number (Fr) is used in fire research to classify the relative importance of momentum and buoyancy in a flame (Drysdale, 2011, p. 122). For a Froude number below unity, the flame is primarily driven by buoyancy. In order to validate that the burners were not fed at fuel rates that established a momentum-driven flame, the Froude number was calculated. In most cases, Fr was much lower than unity. In a few points, a transitional flow for the 25 mm burner could be seen. Overall, a Rayleigh number analysis was deemed sufficient for the burner measurements.

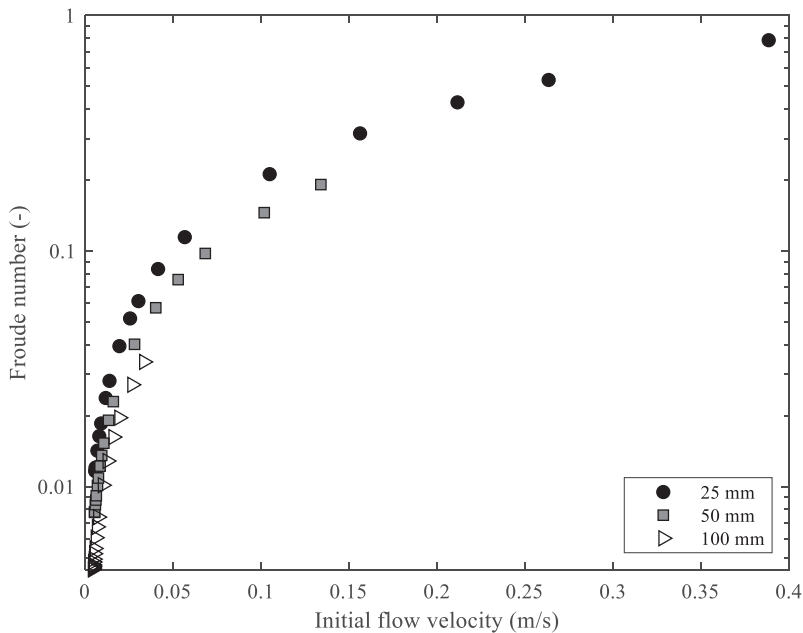


Figure 31. Froude number for gas mixtures in burners of 25, 50 and 100 mm diameter

In summary, since the critical mass flux and critical heat release rate are dependent on the flow conditions, different results will be achieved in different test conditions due to differences in impinged flow and the size and orientation of the sample. The results in this study are valid for laminar flames in quiescent air for samples having diameters approximately between 25 and 100 mm. By using the appropriate convective heat transfer coefficient, configurations other than horizontal burning can be assessed, but without the experimental validation from the burners.

6.3 The influence of incident heat flux

In Paper II, five materials were subjected to different incident heat fluxes (20-50 kW/m²) in the cone calorimeter to assess the influence of external heating. These materials were polyamide 6 (PA6), HD-PE, POM-C, polypropylene (PP) and polyvinylchloride (PVC).

Linear fits are produced for each material, so that slope coefficients are obtained. A Student's t-test can be used to check whether the slopes of fitted linear regression lines are significantly different from 0, i.e. if there is a significant increase in the critical mass

flux with an increase in the incident heat radiation. Although each calculated slope is built on a small sample size ($n \leq 15$), and a t-test is sensitive to small sample sizes, Student, originally formulated and validated the test on the basis of a sample size of 4 (Student, 1908). The slope is assumed to be significant if the probability value (p-value) is less than 0.05. Table 14 illustrates the critical mass flux versus the incident heat flux for the five materials.

Table 14 indicates that the critical mass flux is not dependent on the incident heat flux. Calculated slopes of critical mass flux data vs. the incident heat flux for the materials are not significantly different from 0. This indicates that the incident heat flux is not a factor that influences the critical mass flux value for a given material.

Table 14. Regression fits to data in Paper II

Material	n	r^2	Fitted equation	Significant slope? (p-value)
PA6	15	.24	$\dot{m}''_{cr} = 0.01 \cdot \dot{q}''_{inc} + 1.4$	No (0.07)
POM	14	.001	$\dot{m}''_{cr} = 0.02 \cdot \dot{q}''_{inc} + 2.6$	No (0.13)
HDPE	12	.18	$\dot{m}''_{cr} = -0.01 \cdot \dot{q}''_{inc} + 1.2$	No (0.91)
PP	12	.45	$\dot{m}''_{cr} = 6 \cdot 10^{-3} \cdot \dot{q}''_{inc} + 1.16$	Yes (0.02)
PVC	9	.42	$\dot{m}''_{cr} = -7 \cdot 10^{-3} \cdot \dot{q}''_{inc} + 2.9$	No (0.10)

An apparent dependence on the incident heat flux may be explained in a few ways. Firstly, by exposing the sample to a higher incident heat flux means that decomposition processes within the sample go faster, and that the time to ignition consequently is shorter. Also, the transport and mixing of fuel gas and air is faster, hence the operator has a shorter time interval to log the “correct” time of ignition.

Secondly, the heat penetrates deeper into the sample before ignition at low heat fluxes. This allows for ignition to occur at lower surface temperatures, as explained by Long *et al.* (2000). The critical mass flux in the boundary layer is weakly dependent on the sample surface temperature as stated in Eq. (2.10).

However, the uniformity of external heating has been shown to be important to other ignitability parameters, such as the time to ignition. This is due to the strong dependence between t_{ig} and thermal inertia. Two other ignition parameters which would likely be influenced by the uniformity of the external heating are the ignition temperature and the critical heat flux. Since the critical mass flux (and the critical heat release rate) are not associated with the incident heat flux it would suggest that this is a more robust threshold for testing and modelling of ignition. This theory is strengthened by recent work at the University of Edinburgh where researchers have explored different ignition thresholds when samples are exposed to step-wise increasing heat exposures in the cone calorimeter. Their studies show that the critical mass flux provides more accurate modelling results than both ignition temperature and critical heat flux (Vermesi *et al.*, 2016).

6.4 Summary of influencing parameters

The main purpose of this chapter has been to examine certain parameters that have an influence on the critical mass flux and to quantify these influences. Essentially, results suggest that the convective heat transfer coefficient indeed has a significant effect on the critical mass flux at ignition and extinction. The data also suggest that fuel dependence can be neglected if a critical heat release rate is used instead of a critical mass flux, but not for materials with chemical heats of combustion below 15 kJ/g. The critical mass flux is not dependent on the incident heat flux and may thus be a robust ignition threshold compared to other simplified thresholds.

Investigation of influential parameters for the critical mass flux, based on the theoretical model, shows that the results vary. This may have an impact when this parameter is used as input in modelling.

7 Discussion

This thesis aims to assess the critical mass flux needed for sustained flaming. Two experimental pieces of equipment have been utilized to explore the threshold. The first experimental device (presented in Section 5.1), provides evidence that the standard sample preparation and geometry in the cone calorimeter results in a non-uniform heat exposure during testing. The modified test procedure limits this effect, which enables quantification of the influence of external heating on the critical mass flux at ignition. It is shown that the critical mass flux is not dependent on the level of incident heat radiation. This work was conducted to test the theoretical model and shows that the theoretical expression holds. This is discussed further in Section 7.2.3 while limitations of the experimental device are discussed in Section 7.1.1.

One of the issues remaining in the cone calorimeter, despite modifications, is the strong time dependency of the critical mass flux. The second piece of experimental equipment (presented in Section 5.2) is an attempt to remove the time dependency by the use of a diffusion flame gas burner. Gas burners decouple the solid and gas phase mechanisms and therefore also the dependence of the reaction time of the operator.

The gas burners have been employed to study the effect of h_c in terms of the fuel bed size and fuel type on the critical mass flux for ignition and extinction. It is shown that the critical mass flux is expected to decrease with increasing fuel bed diameter and increasing chemical heat of combustion, respectively. These correlations are discussed in Sections 7.2.1-7.2.2 and the validity of the experimental equipment is discussed in Section 7.1.

The end of this chapter (Section 7.3) provides context for the findings by presenting the critical mass flux in different types of existing fire prediction models.

7.1 Experimental instrumentation

Both experimental set-ups used in this thesis (cone calorimeter and gas burner) were used with the primary objective of assessing critical mass fluxes at sustained ignition and extinction. The validity of experimental instrumentation and the results from the tests are first summarised. Then practical implementations of the studies are suggested, together with their respective limitations.

7.1.1 Cone calorimeter modification

By modifying the specimen geometry in the cone calorimeter, from square to circular, the incident heat radiation to the sample surface becomes more uniform, which has been validated by modelling in Comsol Multiphysics. This enables a better quantification of a possible dependence of the critical mass flux to the incident heat flux. Although it was shown that the critical mass loss rate is not dependent on the incident heat flux, other ignitability parameters are strongly dependent, such as ignition temperature and the critical heat flux. It is therefore a practical modification if one wishes to assess all ignition thresholds simultaneously, e.g. for comparative studies.

Another general finding regarding mass flux testing in the cone calorimeter is that there is a need for a higher resolution of mass loss data to achieve improved ignitability results. There is significant noise in the mass loss rate data stemming from (1) enhancement of noise when deriving the measured mass loss; (2) flow disturbance to the sample, and; (4) surface bubbling and/or other surface phenomena.

Noise stemming from the load cell may possibly be decreased by decoupling the exhaust system from the heating and mass measurement devices, since vibrations from the exhaust system affect the equipment in the present configuration. This effect has not been quantified in this thesis and newer cone calorimeters already use separate housings for the exhaust system and the load cell.

7.1.2 Burning rate emulator

Throughout this thesis, it has been proposed that sustained ignition as well as extinction of solid fuels can be effectively investigated using porous gas burners. Gas burners enable decoupling of gas phase combustion from the pyrolysis and energy balance at the fuel surface. Unlike the mass flow rate from a solid specimen, the fuel flow in a gas burner may be controlled, and the critical mass flux investigated separately. Such a separation simplifies both experimental interpretation and analysis. In this thesis, the gas burner results have given rise to empirical correlations for the influence of burner diameter on the critical mass flux. In addition, they have provided correlation data for the influence of the chemical heat of combustion on the critical mass flux. The gas burners have also provided an experimental method in which critical mass fluxes for both sustained ignition *and* extinction can be determined.

This method is founded on the idea that sustained ignition and extinction occur at the moment for which the fuel supply rate (rate of pyrolysis products for a solid) is not sufficient to sustain a flame. These experiments have provided data that would be difficult to obtain from other types of experiments on solids due to the rapid, closely coupled phenomena that occur during sustained ignition and extinction.

Several questions may arise regarding this method, hence some considerations are discussed below. An initial consideration is that the decoupling of gas phase combustion from “solid phase pyrolysis” may not provide realistic representations of the critical mass

fluxes stemming from liquid or solid fuels. This argument has been addressed by Delichatsios, Gummala and Vlachos (2013), who compared two models: one in which the two phases were decoupled, and one in which the two phases were linked. They received almost identical results for the critical mass loss at extinction.

It may also be argued that the fuel gases that are fed into the burners do not represent pyrolysates from solid and liquid fuels. The burner gases were pure compounds (methane, propane, ethylene, iso-butane and propylene), each of which were diluted with increasing amounts of nitrogen until the mass flow rate controller for nitrogen fed the burner at maximum capacity. “Real” hydrocarbon pyrolysates contain hetero-atom fragments of the solid fuel. These are broken down in the flame into smaller hydrocarbon groups, carbon monoxide and hydrogen, etc., as are the fuel gases in this study. The variety of fuel gases used was deemed to produce a range of smoke points similar to real condensed phase fuels. However, propylene, which represents critical mass flux results for materials with low smoke points has only been used for the 25 mm burner. As a consequence, the range of accurate emulation results is limited. Materials with low smoke points are, for instance, alkenes and alkynes. More fuel gases with low smoke points, and various types of diluent gases would improve the gas burner results and further validation would be provided if real pyrolysates were fed into the burners.

Another consideration with the burner emulation is that the flow velocity stemming from the surface of the gas burner is uniform while a flame from a solid or liquid fuel has a heat flux distribution over its surface, and hence also a distributed surface velocity. Akita and Yumoto (1965) showed that the heat flux distribution for small pools take an exponential form, for which the centre is exposed to the lowest heat flux. In Paper III, delineating flame appearance was part of this study, as shown in Figure 32. Zhang *et al.* (2015) similarly validated that there were strong similarities between the gas burners and condensed phase fuels regarding flame appearance and mass fluxes for steady-state burning. Results suggest that the uniform flow at the surface rapidly equilibrates to diffusional flows similar to those for solids and liquids after a flame becomes attached.

The theoretical expression of the convective heat transfer coefficient was found to be best represented with a pure conductive solution. The engineering correlation for other flames is only valid for flames in quiescent air.

A special consideration regarding the fuel is that several common building products, e.g. wood and gypsum, contain water. Upon heating of such materials, water vapour is released together with the pyrolysates, which is recorded by the load cell. This has not been explicitly tested in the gas burners, nor for the materials tested in the cone calorimeter. Moghtaderi *et al.* (1997) recorded critical mass flux values of 1.8 g/m²/s for dry pine, compared to 4 g/m²/s for pine with a moisture content of 30 %. A similar trend is seen for measurements of time to ignition, which increases with increasing moisture content of the fuel. Since the model assumes that the burning rate in the gas phase equals the mass flux from the surface, i.e. that no inerts or other incombustible/reductional gases are part of the pyrolysates, it is not recommended to use the model for materials with gases containing water. However, since the fuel mass fraction at the surface is part of the

model, it is possible to relax this assumption. The effect of water in the gases has not been assessed in the thesis.

7.2 Experimental results

As was shown in Chapters 2 and 3, ease of ignition (or extinction) may be identified by several material properties. A material will be hard to ignite if the chemical heat of combustion is low – or if its critical mass flux is high. Moreover, the reactivity of the volatiles (given by either the activation energy or the flame temperature) are of importance to a material’s ignitability. Materials with different ignitabilities may be chosen directly based on the above-mentioned properties, or, if the aim is to enhance fire safety of a material, fire retardants may be added to alter the aforementioned property values.

7.2.1 Fuel dependence

For the gas burners, the chemical heat of combustion of volatiles equals the chemical heat of combustion of the emulated “solid”. However, for comparison with data for materials that leave a residue (e.g. charring materials), this difference needs to be accounted for. During a fire, the solid material surface is heated to a range of temperatures and volatiles are generated anaerobically at the surface, resulting in a range of atomic compositions with different molecular weights. Often low molecular weight species are released initially, followed by compounds of higher molecular weight fuels in the latter stages of the fire. For a charring material, the instantaneous chemical composition of gas differs from the original material, where hydrogen is released at high temperature decomposition, leaving a carbonaceous char layer (Cullis and Hirschler, 1981). The chemical heat of combustion of the volatiles stemming from a material therefore varies with time. A constant chemical heat of combustion of the volatiles is a simplification, but continuous determination has previously been conducted as averaged or instantaneous values in fire material testing (Walters, 2013). Averaged values for the chemical heats of combustion of the materials are calculated using the cone calorimeter. This is a reasonable approach for homogenous materials exhibiting one mode of degradation, such as organic liquids. Many building products however consist of composites, or experience charring. The chemical heat of combustion of the fuel gas can therefore be better obtained over the full length of the fuel generation process.

Charring has been included in the full theory by Quintiere and Rangwala (2004), through the L_m term.

The chemical heat of combustion has been shown to not influence the critical heat release rate (Tewarson, 2002; Lyon and Quintiere, 2007). In other words, \dot{Q}''_{cr} is approximately fuel independent (as presented in Section 6.1). This is an important

finding, since ignition criteria that are not fuel dependent are beneficial in fire modelling. In a compartment fire, many items may burn simultaneously, and these items may also consist of several individual materials. Hence, it is a complex task to model all combustible gases individually, therefore a fuel independent criterion simplifies modelling.

The experimental data from Paper II corroborates the Lyon and Quintiere data. However, in Papers III and IV, gases were tested at a wider range of chemical heats of combustion than in previous studies. For effective heats of combustion below ~ 10 kJ/g, the constancy no longer holds. The implication of this result is that some caution needs to be taken when using the critical heat release rate in fire modelling of low combustible materials. However, it also implies that there is a limit for the chemical heat of combustion, below which flaming will not be sustained.

A limited number of fuel gases have been tested in this thesis. In the cone calorimeter, five different plastics were tested, and the gas burners used five different types of fuel gas. As stated in Paper I, many materials crack upon heating and thereby expose a larger area to the flame. Other composites delaminate. Some materials collapse before ignition or swell when exposed to radiation. In other configurations, several materials melt away from the igniter flame, or drip. Many materials leave a residue, e.g. a char or a tar. Several materials are fire retarded. Consequently, conclusions drawn for all different types of fuel are not fully validated.

7.2.2 The influence of the heat transfer coefficient and fuel bed size

The convective heat transfer coefficient has a strong influence on the critical mass flux. This has been described by theoretical expressions such as Eq. (2.10) in Section 2.5.2 of this thesis and the parameter sensitivity in Section 4.1. It has also been shown by experimental work, such as the Córdova and Fernandez-Pello (2000) study.

In this thesis, the investigation of the influence of h_c has been limited to laminar flames in quiescent air. The quiescent scenario has enabled the flow field to be varied by using a set of three burners with different diameters: 25, 50 and 100 mm (Paper IV). The results have been compiled into a formula that can be used to calculate the critical mass flux based on the chemical heat of combustion and the diameter of the fuel bed. It is important to note that it is not intended for use in large pool fires, or when radiation is the dominating heat transfer mode, or for turbulent flows.

One problem with the investigation of fuel bed diameters that directly manifests itself is that the fuel bed size and the size of the flame base are not necessarily the same at the moment a flame appears/vanishes. This is illustrated for the gas burners in Figure 32, where the burner to the far left shows a flame that is not covering the burner surface.

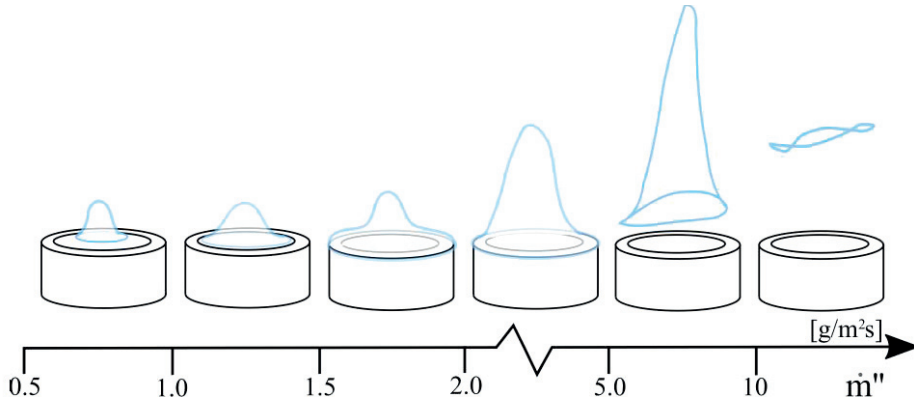


Figure 32. BRE burner flames

By increasing the amount of gas, the flame base increases its diameter and finally reaches the “anchor point”, i.e. the minimum amount of gas mixture needed to cover the burner (or sample) surface. The same problem exists for real materials. Testing in the cone calorimeter initially produces a flame that does not cover the entire sample. It then rapidly widens to cover the full sample surface. The process is illustrated in Figure 33 for two 75 mm diameter circular samples in the cone calorimeter, using two materials (POM and PP). Time $t = 0$ s denotes when the first flash leading to a sustained flame hits the fuel surface. The data is retrieved with the Matlab image processing toolbox. It takes approximately 2.5 s for the flame to cover the entire sample (reach the anchor point), however over 70 % of the surface is covered already after 0.5 s. Times less than a second are too small to capture the mass flux at the fire point in the cone calorimeter.

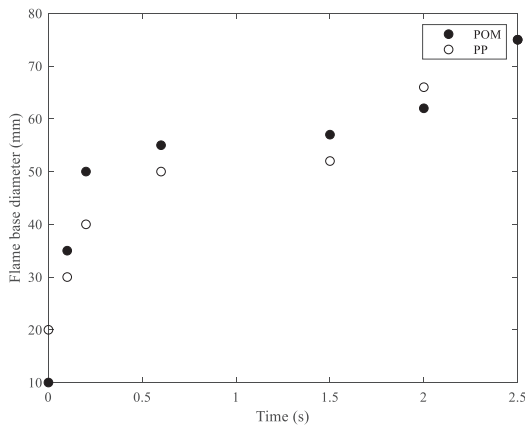


Figure 33. Evolution of the flame base diameter at ignition in the cone calorimeter for two different fuels

In light of this finding, it can be questioned whether the first visual observation of a flame or the anchor point is the better definition of ignition. The critical mass flux needed for the anchor point is considerably higher than that of the fire point, as explained in Papers III and IV. The theoretical expression for Nu however requires the diameter of the plate (the sample or burner diameter). The expression has been used by Sunderland *et al.* (2011) to express heat transfer in candle flames. They used the wick diameter (which is smaller than the flame base) to express Nu .

7.2.3 The influence of incident heat flux

The ignition time of solid fuels is affected by external heating, a component which has not been explored for the gas burners. Contrary to fuels that are already in a gaseous state, fuels that are initially solids require external heating for ignition to occur. The heat flux level affects the time it takes for ignition to occur. Returning to Section 2.4, it is clear that reduced incident heat fluxes will increase the pyrolysis time. Although the mass flux is related to all three time components, and especially the pyrolysis time, the *critical* mass flux is only related to the mixing and chemical times, which are much smaller (Drysdale, 2011, p. 263). Section 3.4.3 also verifies that varying the incident heat flux has no influence on the critical mass flux.

7.2.4 Scalability of small-scale data

One drawback with both the cone calorimeter modification and the gas burners is that small-scale experimental data cannot be used directly to predict larger scale fires. This was discussed in Paper I, especially in regard to empirical models. The work by Blinov and Khudiakov (1957), reviewed by e.g. Emmons (1965) and Alpert (2002), provides some insight into the problem of edge effects associated with small samples. In their study of liquid pool fires, heat loss through the container walls were deemed excessive at fuel bed diameters below 0.1 m. However, they presented data on liquids, so an analogy is best suited for thermally conducting solid materials. The circular sample size in Paper II was restricted to a small diameter ($d = 75$ mm) since the study was restricted by the standard cone calorimeter dimensions. Improved results would possibly be produced by a larger cone heater so that a larger insulated circular sample could be tested.

Another problem of using small sample sizes is that fire test data dominated by convective heat transfer cannot be used directly to assess fire hazard or predict full-scale fire behaviour, since the dominating heat transfer mode in a large scale fire is radiation. It has been shown that pools with diameters beyond 0.2-0.3 m produce flames that are radiation dominated (Drysdale, 2011, p. 130). In order to produce radiation dominated (hotter, more sooty and emissive flames) at the smaller scale it is possible to enhance the

oxygen content surrounding the flame (Tewarson, Lee and Pion, 1981). This can be taken into consideration in future work. Another way to investigate the role of radiation, which has been conducted for the gas burners, is testing in a microgravity environment. Combustion phenomena that are masked in normal gravity are easier to examine in microgravity due to the lack of gravitational settling of the flame and the suppression of buoyancy induced flows. One example of an effect that can be examined is radiation heat loss from the flame (soot and gas) on the extinction limits (Atreya and Agrawal, 1998). Since the studies in papers III and IV were conducted, the new burners have been operated in microgravity environments (Quintiere *et al.*, 2017). Initial results provide evidence that gas phase radiation plays a role for ≥ 50 mm diameter burners (Markan *et al.*, 2018).

7.3 The critical mass flux in fire modelling

The critical mass flux has been used in several theoretical descriptions for sustained ignition and flame spread as described in Appendix A. The sensitivity of predictions to the chosen critical mass flux value depends on the model equation and also on the expected parameter variation.

Amongst the gas phase properties, the critical mass flux is the parameter which has the most influence on the result of time to ignition modelling. However, solid phase properties, such as thermal conductivity, have a larger influence.

Despite its relatively small influence in fire modelling, the theoretical expressions for the critical mass flux form a promising tool for evaluating e.g. hypoxic air systems (due to the theoretical presence of Y_{ox}), or the amount of water required to suppress a flame. With the appropriate theoretical expressions (laminar or turbulent flow; inclusion or not of flame radiation; inclusion or not of water application) the extinction conditions of a flame can be reasonably predicted.

The critical mass flux at ignition can be coupled to a comprehensive pyrolysis model so that reliable ignition times can be calculated. The benefit of using a critical mass flux is that it can be directly calculated from environmental properties and fuel properties.

8 Conclusions

In this thesis, a threshold for sustained ignition and extinction - the critical mass flux - is studied. The first objective was to evaluate different small-scale experimental equipment used to measure the critical mass flux, and to select appropriate devices to study the effect of environmental and fuel specific influences.

Five of the six evaluated pieces of small-scale equipment had similar functions, where heating of a sample leads to pyrolysis and the mass loss is measured with a load cell. Differences in these five apparatuses are the type of heater, type of igniter and type of oxidizer flow. The load cells have similar resolution and accuracy. The flow velocity is low in all pieces of equipment except one. The sixth evaluated piece of equipment was a gas burner. This device is fed by gas mixtures with mass flow controllers so that specific amounts of pyrolysates are emulated to rise from a porous surface. Two apparatuses were selected for the experimental work in this thesis: the cone calorimeter and gas burners. The cone calorimeter was selected because the heat exposure from high temperature electrical heaters in this apparatus are similar to real fire exposure compared to tungsten filament lamps (used in the FPA) and are therefore of more interest when the influence of external heating is investigated. It is also an apparatus that is extensively used in small-scale testing. The second selected device was gas burners. Gas burners can emulate the gas stream so that the time step is not a factor that affects mass loss measurements. Additionally, mass loss measurements in mass flow controllers do not suffer from as much noise load cells.

The second objective was to propose modifications to the selected experimental equipment. Cone calorimeter samples were modified so that a more uniform incident heat radiation was achieved. Samples were cut in a circular shape and were insulated on the sides. The main benefits of the cone calorimeter for obtaining critical mass flux measurements are:

- The sample is exposed to an incident heat radiation with wavelengths similar to those in real fires.
- The cone calorimeter is available in most fire labs and is standardized equipment for small-scale fire testing.

In particular, by using the modified cone calorimeter as developed in this thesis, the benefits are:

- The incident heat radiation upon the modified sample is uniform. This enables better quantification of the dependence on external heating.
- The uniform incident heat radiation also provides a way to accurately obtain (and compare) different ignition thresholds simultaneously, since most ignition thresholds are dependent on external heating.

However, testing with the cone calorimeter indicated that there is a need for higher data resolution to achieve better ignitability results. There is much noise in the mass loss rate data, stemming from (1) the accuracy of the load cell and the enhancement of noise when deriving the measured mass loss; (2) flow disturbance to the sample, and; (3) surface bubbling and/or other surface phenomena.

The second test set-up, the BRE gas burner, was proposed due to its ability to decouple the heat and mass phenomena at the transient moments of ignition and extinction. Modifications to the burners prior to testing included fine-tuning of the existing burners e.g. fixing gas leakage. The main benefits of exploring the critical mass flux with gas burners are:

- The burners allow for exploring critical mass flux variations for a wide range of fuel/oxidizer gas mixtures. This is a simpler (and cheaper) approach than the testing of real solids and liquids.
- Measurements at ignition and extinction are "frozen in time".
The gas burners' ability to decouple heat and mass phenomena at ignition and extinction allow for the operator to investigate critical conditions without regard to any transient mechanisms. Possible errors introduced by logging the mass loss at the correct time-step are thereby removed. This approach is not possible for real solids and liquids without separating the heated specimen from the combusting gases.
- Mass loss data is controlled with mass flow controllers.
It has been shown that the load cell in the cone calorimeter provides low resolution mass loss data at ignition. Mass flow controllers customized for low flow rates improve the resolution in measured ignition mass flux data.
- Ignition and extinction may be tested in the same piece of equipment
In Sections 3.3 and 3.4 it was shown that ignition and extinction of solid fuels are not measured in the same devices. The gas burners enable testing of both ignition and extinction, and the ignition and extinction values can consequently also be compared.
- Testing with gas burners that emulate flames from condensed phase fuels have been done previously. However, emulation of ignition and extinction has been scarce and the results from Papers III and IV fill part of this research gap.

- Little is known about combustion chemistry of fuels involved in fire. Gas burner experiments provide a possible simplification to this problem. However, the gas burners have not yet been validated with experiments in which actual condensed phase fuel gas is used.

The third objective was to identify and investigate key factors responsible for producing variations in critical mass flux measurements. A parameter sensitivity analysis showed that variations in the convective heat transfer coefficient and the chemical heat of combustion were responsible for most of the measurement variations in the critical mass flux. A third parameter, the incident heat flux, was selected for further investigation because previous research has claimed it to be influential, however the theoretical expression used in this thesis argues against this claim.

The convective heat transfer depends on flow conditions. Flow conditions of a small flame burning in natural convection is described by the Rayleigh number. This in turn is influenced by the fuel bed size. Therefore, a scalability study of small fuel beds (0.025-0.1 m) was conducted. The findings showed that the critical mass flux for both sustained ignition and extinction decreases with a decreasing convective heat transfer coefficient (or a larger fuel bed diameter).

The critical mass flux is fuel dependent. Most of this dependency is captured by the chemical heat of combustion of the material. However, some fuel gases with relatively high or low reactivity are shown to deviate from the trend of common fuels. For engineering calculations this may be handled by modification of the flame temperature. A related threshold, the critical heat release rate, is shown to be independent of the chemical heat of combustion. However, this independence only applies to materials with chemical heats of combustion above ~ 10 kJ/g. Finally, an engineering correlation was derived for the critical mass flux of laminar horizontal flames burning in quiescent air, based on the investigated parameters:

$$\dot{m}''_{cr} = (0.14D + 5/\sqrt[4]{D})(1/(0.43 \Delta H_c - 1.9))$$

Solid fuels require incident heating for ignition to occur. Therefore, the influence of an external heat source has been explored through the modified cone calorimeter. Results show a negligible dependency, where the critical mass flux is not significantly depending on the irradiance.

9 Future work

One of the limitations of this work is that it focuses merely on one ignition / extinction threshold, i.e. the critical mass flux. Much research efforts have previously been devoted to other simplified thresholds, such as the ignition temperature. Limited research has, however, been conducted on the more fundamental threshold, the Damköhler number (which is the ratio of the diffusion time to the chemical reaction time). This is because little information exists about combustion reaction characteristics of fuel gases emerging from solids. Some work is found in scattered articles in conferences, textbooks and journals, but there is no real collection of data available. In the *SFPE handbook of fire safety engineering* (5th Ed.) decomposition properties (A and E_a etc) for pyrolysis reactions of a variety of materials are gathered in one chapter (Witkowski, Stec and Hull, 2016). Similarly, heats of combustion for a variety of materials are presented in another chapter (Khan, Tewarson and Chaos, 2016). Simple combustion properties, such as A and E_a etc. for combustion are, however, not easily found. Future work could provide simple combustion reaction schemes for a variety of materials in order to know the feasibility of this type of modelling in fire safety engineering.

The critical mass flux is dependent on several factors and not all have been explored in this thesis. Although time to ignition is mainly sensitive to the solid phase properties, ignition will not occur without the right amount of fuel gas in the combustion zone. Future work may be devoted to understanding the implications of varying the mass loss in different types of models and for different types of materials, and to compare the critical mass flux to other thresholds available.

Also, it has been shown that the resolution of the load cell in the cone calorimeter may not be high enough for ignition testing in order to determine the critical mass flux criteria. However, the actual resolution needed has not been investigated in this work and is a possible subject for further research. It is recommended that the effects of resolution and accuracy of the load cell for ignitability testing are quantified, and that ways to prevent noise are investigated in the load cell configuration.

Additional validation is needed for the BRE burners: the first is to feed the burners with real pyrolysates from condensed phase fuels in order to validate that gas mixtures may represent condensed phase fuels. Additionally, the effects of heat losses to the burner housing have not been quantified, and it is recommended that these questions are resolved before the device is used for screening of materials on the basis of their gas properties. The fuel gases used in the burner have laminar smoke points between approximately 50 and 300 mm. This means that they may represent gases from condensed fuels having

smoke points within this range. However, fuels with smoke points outside this range are not properly represented in the present analysis. Fuel gases with different smoke points would be of interest to test.

The critical mass flux in radiation dominated flames and turbulent flames has not been assessed. Future studies should focus on these phenomena.

References

- Akita, K., & Yumoto, T. (1965). Heat Transfer in Small Pools and Rates of Burning of Liquid Methanol. *Proceedings of the Combustion Institute*, 10(1), 943–948.
- Alpert, R. L. (2002). Review of Blinov and Khudiakov's Paper on "Certain Laws Governing Diffusive Burning of Liquids" by Hoyt. C. Hottel. *Journal of Fire Protection Engineering*, 12(1), 5-7.
- Atreya, A. (1998). Ignition of Fires. *Philosophical Transactions: Mathematical, Physical and Engineering Sciences*, 356(1748), 2787–2813.
- Atreya, A., & Abu-Zaid, M. (1991). Effect of Environmental Variables on Piloted Ignition. *Fire Safety Science*, 3, 177-186. doi:10.3801/IAFSS.FSS.3-177
- Atreya, A., & Agrawal, S. (1998). Effect of Radiative Heat Loss on Diffusion Flames in Quiescent Microgravity Atmosphere. *Combustion and Flame*, 115(3), 372-382.
- Atreya, A., & Wichman, I. S. (1989). Heat and Mass Transfer During Piloted Ignition of Cellulosic Solids. *Journal of Heat Transfer*, 111(3), 719-725.
- Babrauskas, V. (2002). Ignition of Wood : A Review of the State of the Art. *Journal of Fire Protection Engineering*, 12(3), 163-189.
- Babrauskas, V. (2003). *Ignition Handbook*. Issaquah, WA: Fire Science Publishers.
- Babrauskas, V. (2009). The Cone Calorimeter. In V. Babrauskas & S. J. Grayson (Eds.), *Heat Release in Fires* (pp. 61-92). London, UK: Interscience Communications.
- Bal, N. (2012). *Uncertainty and Complexity in Pyrolysis Modelling* (Doctoral dissertation, University of Edinburgh, Edinburgh, UK). Retrieved from <http://hdl.handle.net/1842/6511>
- Bamford, C. H., Crank, J., & Malan, D. H. (1946). The Combustion of Wood. Part I. *Mathematical Proceedings of the Cambridge Philosophical Society*, 42(2), 166–182.
- Bartlett, A. I., Hadden, R. M., Hidalgo, J. P., Santamaria, S., Wiesner, F., Bisby, L. A., ... Lane, B. (2017). Auto-Extinction of Engineered Timber: Application to Compartment Fires with Exposed Timber Surfaces. *Fire Safety Journal*, 91, 407–413.
- Beaulieu, P. A. (2005). *Flammability Characteristics at Heat Flux Levels up to 200 kW/m² and the Effect of Oxygen on Flame Heat Flux* (Doctoral dissertation, Worcester Polytechnic Institute, Worcester, MA). Retrieved from <https://web.wpi.edu/Pubs/ETD/Available/etd-121905-082146/unrestricted/beaulieu.pdf>.
- Beyler, C. (1992). A Unified Model of Fire Suppression. *Journal of Fire Protection Engineering*, 4(1), 5–16.

- Blinov, V. I., & Khudiakov, G. N. (1957). Certain Laws Governing Diffusive Burning of Liquids. *Doklady Akademii Nauk SSSR*, 113, 1094-1098.
- Boulet, P., Parent, G., Acem, Z., Collin, A., Försth, M., Bal, N., ... Torero, J. L. (2014). Radiation Emission from a Heating Coil or a Halogen Lamp on a Semitransparent Sample. *International Journal of Thermal Sciences*, 77, 223-232.
- Brink, D. L., & Massoudi, M. S. (1978). A Flow Reactor Technique for the Study of Wood Pyrolysis. I. *Experimental. Journal of Fire & Flammability*, 9, 176-188.
- Burke, S. P., & Schumann, T. E. W. (1928). Diffusion Flames. *Industrial & Engineering Chemistry*, 20(10), 998-1004.
- Comsol (2019). *Introduction to Comsol Multiphysics*. Retrieved from <https://cdn.comsol.com/documentation/5.4.0.225/IntroductionToCOMSOLMultiphysics.pdf>
- Córdova, J. L., & Fernandez-Pello, A. C. (2000). Convection Effects on the Endothermic Gasification and Piloted Ignition of a Radiatively Heated Combustible Solid. *Combustion Science and Technology*, 156(1), 271-289.
- Córdova, J. L., Walther, D. C., Torero, J. L., & Fernandez-Pello, A. C. (2001). Oxidizer Flow Effects on the Flammability of Solid Combustibles. *Combustion Science and Technology*, 164(1), 253-278.
- Corlett, R. C. (1968). Gas Fires with Pool-Like Boundary Conditions. *Combustion and Flame*, 12(1), 19-32.
- Corlett, R. C. (1970). Gas Fires with Pool-Like boundary Conditions: Further Results and Interpretation. *Combustion and Flame*, 14(3), 351-360.
- Cullis, C. F. & Hirschler, M. M. (1981). *The Combustion of Organic Polymers*. Oxford, UK: Clarendon Press.
- de Ris, J. L. (1989). A Scientific Approach to Flame Radiation and Material Flammability. *Fire Safety Science*, 2, 29-46. doi: 10.3801/IAFSS.FSS.2-29
- de Ris, J. L., & Orloff, L. (1972). A Dimensionless Correlation of Pool Burning Data. *Combustion and Flame*, 18(3), 381-388.
- de Ris, J. L., & Orloff, L. (1975). The Role of Buoyancy Direction and Radiation in Turbulent Diffusion Flames on Surfaces. *Symposium (International) on Combustion*, 15(1), 175-182.
- Deepak, D., & Drysdale, D. D. (1983). Flammability of Solids: An Apparatus to Measure the Critical Mass Flux at the Firepoint. *Fire Safety Journal*, 5(2), 167-169.
- Delichatsios, M. A. (2005). Piloted Ignition Times, Critical Heat Fluxes and Mass Loss Rates at Reduced Oxygen Atmospheres. *Fire Safety Journal*, 40(3), 197-212.
- Delichatsios, M. A., & Delichatsios, M. M. (1997). Critical Mass Pyrolysis Rates for Extinction in Fires Over Solid Materials. *Fire safety science*, 5, 153-164. doi:10.3801/IAFSS.FSS.5-153
- Delichatsios, M. A., Gummala, M., & Vlachos, D. G. (2013). Extinction of Surface Stabilized Gaseous Diffusion Flames: Part I Simplified Numerical Model and Implications for Solid Fuels in Fires. *Fire Safety Journal*, 55, 152-159.
- Deverall, L. I., & Lai, W. (1969). A Criterion for Thermal Ignition of Cellulosic Materials. *Combustion and Flame*, 13(1), 8-12.

- Dryer, F. L., & Westbrook, C. K. (1981). Simplified Reaction Mechanisms for the Oxidation of Hydrocarbon Fuels in Flames. *Combustion Science and Technology*, 27(1–2), 31–43.
- Drysdale, D. D. (2011). *An Introduction to Fire Dynamics* (3rd Ed.). Chichester, UK: John Wiley & Sons.
- Drysdale, D. D., & Thomson, H. E. (1989). Flammability of Plastics II: Critical Mass Flux at the Firepoint. *Fire Safety Journal*, 14(3), 179–188.
- Emberley, R., Do, T., Yim, J., & Torero, J. L. (2017). Critical Heat Flux and Mass Loss Rate for Extinction of Flaming Combustion of Timber. *Fire Safety Journal*, 91, 252–258.
- Emmons, H. W. (1965). Fundamental Problems of the Free Burning Fire. *Symposium (International) on Combustion*, 10, 951–964.
- Evarts, B. (2018). *Fire Loss in the United States During 2017* (NFPA#FLX10). Quincy, MA: National Fire Protection Association.
- Fereres, S., Lautenberger, C., Fernandez-Pello, C., Urban, D., & Ruff, G. (2011). Mass Flux at Ignition in Reduced Pressure Environments. *Combustion and Flame*, 158(7), 1301–1306.
- Fernandez-Pello, C. (2011). On Fire Ignition. *Fire Safety Science*, 10, 25–42. doi: 10.3801/IAFSS.FSS.10-25
- Försth, M., & Roos, A. (2011). Absorptivity and its dependence on heat temperature and degree of thermal breakdown. *Fire and Materials*, 35(5), 285–301.
- Gebhart, B. (1971). *Heat Transfer*. New York, NY: McGraw-Hill Book Co.
- Grant, G. & Drysdale, D. (1995). Numerical Modelling of Early Flame Spread in Warehouse Fires. *Fire Safety Journal*, 24(3), 247–278.
- Grayson, S. (2018). Letter to Fire Journal Editors on Materials Identification in Comparison of Results among Fire Scaling and Flammability Studies. *Fire and Materials*, 42(6), 581–582.
- Heskestad, G. (1980). The Role of Water in Suppression of Fire: A Review. *Journal of Fire and Flammability*, 11, 254–262.
- Hirano, T. I., Noreikis, S. E., & Waterman, T. E. (1974). Measured Velocity and Temperature Profiles Near Flames Spreading Over a Thin Combustible Solid. *Combustion and Flame*, 23(1), 83–96.
- Huggett, C. (1980). Estimation of the Rate of Heat Release by Means of Oxygen Consumption. *Journal of Fire and Flammability*, 12, 61–65.
- International Organization for Standardization. (2011). *Reaction-to-fire Tests – Measurement of Material Properties using a Fire Propagation Apparatus* (ISO Standard No. 12136: 2011). Retrieved from <https://www.iso.org/standard/51237.html>
- International Organization for Standardization. (2015). *Reaction-to-fire Tests — Heat Release, Smoke Production and Mass Loss Rate — Part 1: Heat Release Rate (Cone Calorimeter Method) and Smoke Production Rate (Dynamic Measurement)* (ISO Standard No. 5660-1: 2015). Retrieved from <https://www.iso.org/standard/57957.html>

- International Organization for Standardization. (2017a). *Fire safety – Vocabulary* (ISO Standard No. 13943:2017). Retrieved from <https://www.iso.org/standard/63321.html>
- International Organization for Standardization. (2017b). *Petroleum and Related Products – Determination of flash and fire points – Cleveland open cup method* (ISO Standard No. 2592:2017). Retrieved from <https://www.iso.org/standard/67910.html>
- Janssens, M. L. (1991). Measuring Rate of Heat Release by Oxygen Consumption. *Fire Technology*, 27(3), 234–249.
- Janssens, M. L. (2006). Fundamental Measurement Techniques. In V. B. Apte (Ed.), *Flammability Testing of Materials used in Construction, Transport and Mining* (pp. 22–64). Cambridge, UK: Woodhead.
- Janssens, M. L. (2016). Calorimetry. In M. J. Hurley (Ed.), *SFPE Handbook of Fire Safety Engineering* (3rd ed., pp. 3.38-3.62). Quincy, MA: National Fire Protection Association.
- Janssens, M. L., Huczek, J., & Faw, A. (2008). Effect of Specimen Size on Test Results Obtained in the Cone Calorimeter. In *19th Annual Conference on Recent Advances in Flame Retardancy of Polymeric Materials* (pp. 347–356). Red Hook, NY: Curran Associates.
- Jiakun, D., Delichatsios, M. A., & Lizhong, Y. (2013). Piloted Ignition of Solid Fuels at Low Ambient Pressure and Varying Igniter Location. *Proceedings (International) of the Combustion Institute*, 34(2), 2497–2503.
- Johansson, N., & van Hees, P. (2012). *Slutrapport: Varför blir vissa små bränder stora?* (LUTVDG/TVBP-3167-SE; Vol. 3167). Lund, Sweden: Department of Fire Safety Engineering and Systems Safety, Lund University.
- Kanury, A. M. (1977). *Introduction to Combustion Phenomena (for Fire, Incineration, Pollution and Energy Applications)* (2nd Ed.). New York, NY: Gordon and Breach.
- Kanury, A. M. (2002). Ignition of Liquid Fuels. In P. J. DiNenno (Ed.), *SFPE Handbook of Fire Protection Engineering* (3rd ed., pp. 2.188-2.199). Quincy, MA: National Fire Protection Association.
- Kashiwagi, T. (1973). A Radiative Ignition Model of a Solid Fuel. *Combustion Science and Technology*, 8(5), 225–236.
- Kashiwagi, T. (1994). Polymer Combustion and Flammability-Role of the Condensed Phase. *Proceedings (International) of the Combustion Institute*, 25(1), 1423–1437.
- Kashiwagi, T., Inaba, A., & Brown, J. E. (1986). Differences in PMMA Degradation Characteristics and Their Effects on its Fire Properties. *Fire Safety Science*, 1, 483-493. doi: 10.3801/IAFSS.FSS.1-483
- Khan, M. M., & de Ris, J. L. (2005). Operator Independent Ignition Measurements. *Fire Safety Science*, 8, 163–174. doi:10.3801/IAFSS.FSS.8-163
- Khan, M. M., Tewarson, A., & Chaos, M. (2016). Combustion Characteristics of Materials and Generation of Fire Products. In M. Hurley (Ed.), *SFPE Handbook of Fire Protection Engineering* (5th ed., pp. 1143–1232). New York, NY: Springer.
- Kim, J. S., de Ris, J., & William Kroesser, F. (1971). Laminar Free-Convective Burning of Fuel Surfaces. *Symposium (International) on Combustion*, 13(1), 949–961.

- Kobes, M., & Groenewegen, K. (2009). *Consumer Fire Safety: European Statistics and Potential Fire Safety Measures* (Report No. 431N8032/3.0). Arnhem, Netherlands: Netherlands Institute for Safety NIBRA.
- Koohyar, A. N., Welker, J. R., & Sliepcevich, C. M. (1968). The Irradiation and Ignition of Wood by Flame. *Fire Technology*, 4(4), 284–291.
- Lautenberger, C. (2002). *CFD Simulation of Soot Formation and Flame Radiation* (Master's thesis, Worcester Polytechnic Institute, Worcester, MA). Retrieved from <https://digitalcommons.wpi.edu/etd-theses/104/>
- Lautenberger, C., & Fernandez-Pello, C. (2005). Approximate Analytical Solutions for the Transient Mass Loss Rate and Piloted Ignition Time of a Radiatively Heated Solid in the High Heat Flux Limit. *Fire Safety Science*, 8, 445–456. doi:10.3801/IAFSS.FSS.8-445
- Lautenberger, C., Torero, J., & Fernandez-Pello, C. (2006). Understanding Materials Flammability. In V. B. Apte (Ed.), *Flammability Testing of Materials Used in Construction, Transport and Mining* (pp. 1–21). Cambridge, UK: Woodhead.
- Law, C. K. (1984). Heat and Mass Transfer in Combustion: Fundamental Concepts and Analytical Techniques. *Progress in Energy and Combustion Science*, 10(3), 295–318.
- Li, L., & Sunderland, P.B. (2012). An Improved Method of Smoke Point Normalization. *Combustion Science and Technology*, 184(6), 829–841.
- Long, R. T., Torero, J. L., Quintiere, J. G., & Fernandez-Pello, A. C. (2000). Scale and Transport Considerations on Piloted Ignition of PMMA. *Fire Safety Science*, 10, 567–578. doi:10.3801/IAFSS.FSS.6-567
- Lyon, R. (2004). Plastics and Rubber. In C. A. Harper (Ed.), *Handbook of Building Materials for Fire Protection* (pp. 3.1-3.51). New York, NY: McGraw-Hill Education.
- Lyon, R., & Janssens, M. L. (2005). *Polymer Flammability* (DOT/FAA/AR-05/14). Washington DC, VA: Federal Aviation Administration.
- Lyon, R., & Quintiere, J. G. (2007). Criteria for Piloted Ignition of Combustible Solids. *Combustion and Flame*, 151(4), 551–559.
- Lyon, R., Walters, R., & Stoliarov, S. (2006). A Thermal Analysis Method for Measuring Polymer Flammability. *Journal of ASTM International*, 3(4), 1-18.
- Maček, A. (1976). *Flammability Limits: Thermodynamics and Kinetics* (PB-254 180). Gaithersburg, MD: National Bureau of Standards.
- Magee, R. S., & Reitz, R. D. (1975). Extinguishment of Radiation Augmented Plastics Fires by Water Sprays. *Symposium (International) on Combustion*, 15(1), 337–347.
- Markan, A. (2018). *Development and Analysis of a Burning Rate Emulator (BRE) for Study in Microgravity* (Doctoral dissertation, University of Maryland, College Park, MD). Retrieved from <https://drum.lib.umd.edu/handle/1903/21351>
- Markan, A., Sunderland, P. B., Quintiere, J. G., de Ris, J. L., Stocker, D. P., & Baum, H. R. (2018). A Burning Rate Emulator (BRE) for Study of Condensed Fuel Burning in Microgravity. *Combustion and Flame*, 192, 272–282.

- Marquis, D. M., Guillaume, E., & Camillo, A. (2014). Effects of Oxygen Availability on the Combustion Behaviour of Materials in a Controlled Atmosphere Cone Calorimeter. *Fire Safety Science*, *11*, 138–151. doi: 10.3801/IAFSS.FSS.11-138
- Martin, S. (1965). Diffusion-Controlled Ignition of Cellulosic Materials by Intense Radiant Energy. *Symposium (International) on Combustion*, *10*(1), 877-896.
- McAllister, S., Chen, J.-Y., & Fernandez-Pello, A. C. (2011). Fundamentals of Combustion Processes. New York, NY: Springer.
- Melvin, A., Moss, J. B., & Clarke, J. F. (1971). The Structure of a Reaction-Broadened Diffusion Flame. *Combustion Science and Technology*, *4*(1), 17–30.
- Moghtaderi, B., Novozhilov, V., Fletcher, D. F. & Kent, J. H. (1997). A New Correlation for Bench-Scale Piloted Ignition Data of Wood. *Fire Safety Journal*, *29*(1), 41-59.
- Mowrer, F. W. (2003). An Analysis of Effective Thermal Properties of Thermally Thick Materials. *Fire Safety Journal*, *40*(5), 395-410.
- Nelson, M. I., Brindley, J., & McIntosh, A. (1995). The Dependence of Critical Heat Flux on Fuel and Additive Properties: A Critical Mass Flux Model. *Fire Safety Journal*, *24*(2), 107–130.
- Nelson, M. I., Brindley, J., & McIntosh, A. (1996a). Ignition Properties of Thermally Thin Materials in the Cone Calorimeter: A Critical Mass Flux Model. *Combustion Science and Technology*, *113*(1), 221–241.
- Nelson, M. I., Brindley, J., & McIntosh, A. (1996b). Polymer ignition. *Mathematical and Computer Modelling*, *24*(8), 39–46.
- Pagni, P. J. (1981). Diffusion Flame Analyses. *Fire Safety Journal*, *3*(4), 273-285.
- Panagiotou, J., & Quintiere, J. G. (2004). Generalizing Flammability of Materials. In S. Grayson (Ed.), *Interflam - Tenth International Fire Science and Engineering Conference* (pp. 895–906). Greenwich, UK.: Interscience Communications.
- Peng, F., Zhou, X., Zhao, K., Wu, Z., & Yang, L. (2015). Experimental and Numerical Study on Effect of Sample Orientation on Auto-Ignition and Piloted Ignition of Poly(methyl methacrylate). *Materials*, *8*(7), 4004–4021.
- Peters, B. D. (1979). *Mass Burning Rates in a Spark Ignition Engine Operating in the Partial-Burn Regime*. Paper presented at the Institute of Mechanical Engineers Conference on Fuel Economy and Emissions in Lean Burn Engines (Paper C92/79), London, UK.
- Quintiere, J. G. (2006a). A Theoretical Basis for Flammability Properties. *Fire and Materials*, *30*(3), 175–214.
- Quintiere, J. G. (2006b). *Fundamentals of Fire Phenomena*. Chichester, UK: Wiley.
- Quintiere, J. G., Lyon, R. E., & Crowley, S. B. (2016). An Exercise in Obtaining Flame Radiation Fraction from the Cone Calorimeter. *Fire and Materials*, *40*(6), 861-872.
- Quintiere, J. G., & Rangwala, A. S. (2004). A Theory for Flame Extinction Based on Flame Temperature. *Fire and Materials*, *28*(5), 387–402.
- Quintiere, J. G., Markan, A., Sunderland, P. B., Baum, H. R., de Ris, J. L., Stocker, D. P., & Vermina Lundström, F. (2017, July). A Gas Burner Emulator for Condensed-Phase Burning. Paper presented at the 9th International Seminar on Flame Structure, Novosibirsk, Russia.

- Rangwala, A. S. (2016). Diffusion Flames. In M. Hurley (Ed.), *SFPE Handbook of Fire Protection Engineering* (5th ed., pp. 350–372). New York, NY: Springer.
- Rasbash, D. J. (1975). Relevance of Firepoint Theory to the Assessment of Fire Behaviour of Combustible Materials. In *International Symposium on Fire Safety of Combustible Materials* (pp. 169-178). Edinburgh, UK: University of Edinburgh Centre for Industrial Consultancy and Liaison.
- Rasbash, D. J. (1976). A Flame Extinction Criterion for Fire Spread. *Combustion and Flame*, 26, 411–412.
- Rasbash, D. J. (1986). The Extinction of Fire with Plain Water: A Review. *Fire Safety Science*, 1, 1145–1164. doi:10.3801/IAFSS.FSS.1-1145
- Rasbash, D. J., Drysdale, D. D., & Deepak, D. (1986). Critical Heat and Mass Transfer at Pilot Ignition and Extinction of a Material. *Fire Safety Journal*, 10(1), 1–10.
- Reshetnikov, S. M. & Reshetnikov, I. S. (1999). Oxidation Kinetic of Volatile Polymer Degradation Products. *Polymer Degradation and Stability*, 64(3), 379-385.
- Rhodes, B.T., Quintiere, J. (1994). Burning Rate and Flame Heat Flux for PMMA in the Cone Calorimeter. *Fire Safety Journal* 26(3), 221-240.
- Rich, D., Lautenberger, C., Torero, J. L., Quintiere, J. G., & Fernandez-Pello, C. (2007). Mass Flux of Combustible Solids at Piloted Ignition. *Proceedings of the Combustion Institute*, 31(2), 2653–2660.
- Ritchie, S., Steckler, K., Hamins, A., Cleary, T., Yang, J., & Kashiwagi, T. (1997). The Effect of Sample Size on the Heat Release Rate of Charring Materials. *Fire Safety Science*, 5, 177–188. doi:10.3801/IAFSS.FSS.5-177
- Roslon, M., Olenick, S., Walther, D., Torero, J. L., Fernandez-Pello, A. C. & Ross H. D. (2000). Microgravity Ignition Delay of Solid Fuels in Low Velocity Flows. *AIAA Journal*, 39(12), 2336-2342.
- Saltelli, A., Ratto, M., Andres, T., Campolongo, F., Cariboni, J., Gatelli, D., Saisana, M., & Tarantola, S. (2008). *Global Sensitivity Analysis. The Primer*. West Sussex, UK: Wiley.
- Sauer, F. M. (1956). The Charring of Wood During Exposure to Thermal Radiation (AFSWP-868). Washington, DC: US Department of Agriculture.
- Schartel, B., Bartholmai, M., & Knoll, U. (2005). Some Comments on the use of Cone Calorimeter Data. *Polymer Degradation and Stability*, 88(3), 540–547.
- Simmons, R. F., & Wolfhard, H. G. (1957). Some Limiting Oxygen Concentrations for Diffusion Flames in Air Diluted with Nitrogen. *Combustion and Flame*, 1(2), 155–161.
- Solarte, A., Hidalgo, J. P., & Torero, J. L. (2018). *Flammability Studies for the Design of Fire-Safe Bamboo Structures*. Paper presented at 2018 World Conference on Timber Engineering (WCTE). Seoul, Korea.
- Spalding, D.B. (1953). The Combustion of Liquid Fuels. *Proceedings of the Combustion Institute*, 4, 847-864.
- Staggs, J. E. J. (2005). Savitzky – Golay Smoothing and Numerical Differentiation of Cone Calorimeter Mass Data. *Fire Safety Journal*, 40(6), 493–505.

- Staggs, J.E.J. (2009). Convection Heat Transfer in the Cone Calorimeter. *Fire Safety Journal*, 44(4), 469–474.
- Staggs, J.E.J. (2011). A Reappraisal of Convection Heat Transfer in the Cone Calorimeter. *Fire Safety Journal*, 46(3), 125-131.
- Staggs, J.E.J., & Nelson, M.I. (2001). A Critical Mass Flux Model for the Flammability of Thermoplastics. *Combustion Theory and Modelling*, 5(3), 399–427.
- Stoliarov, S. I., Raffan-Montoya, F., Walters, R. N., and Lyon, R. (2016). Measurement of the Global Kinetics of Combustion for Gaseous Pyrolyzates of Polymeric Solids Containing Flame Retardants. *Combustion and Flame*, 173, 65-76.
- Student. (1908). The probable error of a mean. *Biometrika*, 6(1), 1-25.
- Särdqvist, S. (2002). *Water and Other Extinguishing Agents*. [PDF file]. Karlstad: Räddningsverket. Retrieved from <https://www.msb.se/RibData/Filer/pdf/23061.pdf>
- T'ien, J. S., & Endo, M. (2013). Material Flammability: A Combustion Science Perspective. *Procedia Engineering*, 62, 120–129.
- Tewarson, A. (1982). Experimental Evaluation of Flammability Parameters of Polymeric Materials. In M. Lewin., S. M. Atlas, & E. M. Pearce (Eds.), *Flame Retardant Polymeric Materials* (pp. 97–153). New York, NY: Plenum Press.
- Tewarson, A. (1994). Flammability Parameters of Materials: Ignition, Combustion, and Fire Propagation. *Journal of Fire Sciences*, 12(4), 329–356.
- Tewarson, A. (2002). Generation of Heat and Chemical Compounds in Fire. In P. J. DiNenno (Ed.), *SFPE Handbook of Fire Protection Engineering* (3rd ed., pp. 3.82-3.161). Quincy, MA: National Fire Protection Association.
- Tewarson, A. (2004). Combustion Efficiency and its Radiative Component. *Fire Safety Journal*, 39(2), 131-141.
- Tewarson, A., Lee, J. L. & Pion, R. F. (1981). The influence of oxygen concentration on fuel parameters for fire modelling. *Proceedings of the Combustion Institute*, 18(1), 563–570.
- Thomson, H. E., & Drysdale, D. D. (1989). Critical Mass Flowrate at The Firepoint Of Plastics. *Fire Safety Science*, 2, 67–76. doi:10.3801/IAFSS.FSS.2-67
- Thomson, H. E., Drysdale, D. D., & Beyler, C. L. (1988). An Experimental Evaluation of Critical Surface Temperature as a Criterion for Piloted Ignition of Solid Fuels. *Fire Safety Journal*, 13(2), 185–196.
- Thornton, W. M. (1917). The Relation of Oxygen to the Heat of Combustion of Organic Compounds. *The London, Edinburgh, and Dublin Philosophical Magazine and Journal of Science*, 33(194), 196-203.
- Torero, J. L. (2016). Flaming Ignition of Solid Fuels. In M. J. Hurley (Ed.), *SFPE Handbook of Fire Protection Engineering* (5th ed., pp. 633-661). New York, NY: Springer.
- Tzeng, L. S., Atreya, A., & Wichman, I. S. (1990). A One-Dimensional Model of Piloted Ignition. *Combustion and Flame*, 80, 94-107.
- van Krevelen, D. W. (Ed.). (1990). *Properties of Polymers* (3rd ed.), New York, NY: Elsevier Scientific.

- Vermesi, I., Roenner, N., Pironi, P., Hadden, R. M., & Rein, G. (2016). Pyrolysis and Ignition of a Polymer by Transient Irradiation. *Combustion and Flame*, *163*, 31–41.
- Vermina Lundström, F., Sunderland, P. B., Quintiere, J. G., van Hees, P., & de Ris, J. L. (2017). Study of Ignition and Extinction of Small-Scale Fires in Experiments with an Emulating Gas Burner. *Fire Safety Journal*, *87*, 18–24.
- Vermina Lundström, F., van Hees, P., & Guillaume, E. (2017). A Review on Prediction Models for Full-Scale Fire Behaviour of Building Products. *Fire and Materials*, *41*(3), 225–244.
- Vermina Plathner, F., & van Hees, P. (2019). Experimental Assessment of Bench-Scale Ignitability Parameters. *Fire and Materials*, *43*(2), 123-130.
- Walters, R. N. (2013). Development of Instrumental and Computational Tools for Investigation of Polymer Flammability (Doctoral dissertation, University of Central Lancashire, Preston, UK). Retrieved from <http://clock.uclan.ac.uk/9268/1/Walters%20Richard%20Final%20e-Thesis%20%28Master%20Copy%29.pdf>
- Weatherford, W. D., & Sheppard, D. M. (1965). Basic Studies of the Mechanism of Ignition of Cellulosic Materials. *Symposium (International) on Combustion*, *10*(1), 897-910.
- Werrel, M., Deubel, J. H., Krüger, S., Hofmann, A., & Krause, U. (2014). The calculation of the heat release rate by oxygen consumption in a controlled-atmosphere cone calorimeter. *Fire and Materials*, *38*(2), 204-226.
- Wichman, I. S. (1986). A Model Describing the Steady-State Gasification of Bubble-Forming Thermoplastics in Response to an Incident Heat Flux. *Combustion and Flame*, *63*(1-2), 217-229.
- Wickström, U. (2016). *Temperature Calculation in Fire Safety Engineering*. Basel, Switzerland: Springer.
- Williams, F. A. (1981). A Review of Flame Extinction. *Fire Safety Journal*, *3*(3), 163–175.
- Wilson, M. T., Dlugogorski, B. Z., & Kennedy, E. M. (2003). Uniformity of Radiant Heat Fluxes in Cone Calorimeter. *Fire Safety Science*, *7*, 815–826. doi:10.3801/IAFSS.FSS.7-815
- Witkowski, A., Stec, A. A., & Hull, T. R. (2016). Thermal Decomposition of Polymeric Materials. In M. J. Hurley (Ed.), *SFPE Handbook of Fire Protection Engineering* (5th ed., pp. 167–254). New York, NY: Springer.
- Xin, Y., & Khan, M. M. (2007). Flammability of Combustible Materials in Reduced Oxygen Environment. *Fire Safety Journal*, *42*(8), 536–547.
- Yuen, W. W., & T'ien, C. L. (1977). A Simple Calculation Scheme for the Luminous-Flame Emissivity. *Symposium (International) on Combustion*, *16*(1), 1481–1487.
- Zabetakis, M. G. (1965). Flammability Characteristics of Combustible Gases and Vapors (AD 701576). Washington, DC: Bureau of Mines.
- Zhang, Y., Bustamante, M. J., Gollner, M. J., Sunderland, P. B., & Quintiere, J. G. (2014). Burning on Flat Wicks at Various Orientations. *Journal of Fire Sciences*, *32*(1), 52-71.

- Zhang, Y., Kim, M., Guo, H., Sunderland, P. B., Quintiere, J. G., Ris, J. L. de, & Stocker, D. P. (2015). Emulation of Condensed Fuel Flames with Gases in Microgravity. *Combustion and Flame*, 162(10), 3449–3455.
- Zhang, Y., Kim, M., Sunderland, P. B., Quintiere, J. G., & de Ris, J. (2016). A Burner to Emulate Condensed Phase Fuels. *Experimental Thermal and Fluid Science*, 73, 87–93.
- Zhubanov, T. B. & Gibov, K. M. (1988). Oxygen Index and Minimum Tasks of Polymer Combustion. *Fire and Materials*, 12, 169-172.

Appendix A: The critical mass flux in ignition and flame spread modelling

A.1 Introduction

The critical mass flux has been used in several theoretical descriptions for sustained ignition and for flame spread predictions. This Appendix aims to describe the use of the critical mass flux in ignition modelling by providing a few examples, and to explore its impact on different modelling results. The critical mass flux for nascent flaming has a stand-alone importance, since it is a threshold that depicts whether a flame can be sustained. Despite this, the value used may not have a large effect on the modelling outcome. Prediction models differ in complexity and assumptions, therefore, the critical mass flux may have a larger impact in some models than in others.

Classical ignition theory provides two equations for the time to ignition, depending on the thermal thickness of the material (Quintiere, 2006a)

$$t_{ig} = \rho c \delta \frac{T_{ig} - T_{\infty}}{\dot{q}_{ext}''} \quad (\text{A.1a, thin})$$

$$t_{ig} = \frac{\pi}{4} k \rho c \frac{(T_{ig} - T_{\infty})^2}{\dot{q}_{ext}''^2} \quad (\text{A.1b, thick})$$

where Eq. (A.1b) is valid for high incident heat flux levels. ρ , c , k , and δ constitute the density, specific heat, thermal conductivity and thickness, T_{ig} and T_{∞} are temperatures at ignition and the surroundings respectively, \dot{q}_{ext}'' is the incident heat flux. These equations are valid when the ambient and initial temperatures are equal and for relatively short times to ignition.

From classical theory it is well-known that solid properties such as k , ρ , and c (that together constitutes the thermal inertia of the material) govern the temperature within the material and thus are also the most influential properties for the time to ignition (Mowrer,

2003). However, the theory underpredicts ignition times at high incident heat fluxes. This may partly be explained by the assumption that ignition occurs at a specified ignition temperature, which has been shown to be dependent on the incident heat radiation (Beaulieu, 2005; Thomson, Drysdale and Beyler, 1988). It has been proposed that the critical mass flux would be a more suitable threshold at varying levels of heat exposure (Lautenberger, 2002).

The objective of this Appendix is to provide the reader with a few modelling examples where the critical mass flux has been used, along with a description of parameter input sensitivity. The sensitivity analysis is conducted in order to illustrate the impact of parameter variation in ignition modelling.

A.2 Method

A sensitivity analysis is performed in order to see how the variation in the output quantity correspond to the ranges of the inputs.

A.2.1 Sensitivity model

Parameter sensitivity analysis refers to the study of how the uncertainty of the output (e.g. time to ignition) can be allocated to variations in the input parameters in a model. There are several different methodologies to obtain this relationship between the input and output parameters. In this Appendix, a correlation analysis is conducted with Kendall's tau. This model is simple, yet appropriate for small, sample data that is not linearly correlated.

Given an input variable X and an output variable Y , the method is based on a ranking system of concordant (i, j) pairs, i.e. the pairs where $(X_i - X_j)$ and $(Y_i - Y_j)$ have the same sign. In other words, concordant pairs mean that the larger of the two values in X corresponds to the larger of the two values in Y . Their correlation coefficient τ_b is given by

$$\tau_b = \frac{2 \sum_{i=1}^{n-1} \sum_{j=i+1}^n E(X_i, X_j, Y_i, Y_j)}{n(n-1)} \quad (\text{A.2})$$

where n is the number of pairs. $E(X_i, X_j, Y_i, Y_j)$ in Eq. (A.2) is the probability of concordance, ties and discordance and are given by

$$E(X_i, X_j, Y_i, Y_j) = \begin{cases} 1 & \text{if } (X_i - X_j)(Y_i - Y_j) > 0 \\ 0 & \text{if } (X_i - X_j)(Y_i - Y_j) = 0 \\ -1 & \text{if } (X_i - X_j)(Y_i - Y_j) < 0 \end{cases} \quad (\text{A.3})$$

A.2.2 Parameter data

Two sets of parameter data are used in the sensitivity analysis: one that is based on an expected range of material properties for black PMMA, taken from Bal (2012), and one for which the property ranges are $\pm 10\%$ of the mean value of that range. The data is presented in Table A.1 and the parameters are explained in the nomenclature list.

Table A.1 Parameters used in the sensitivity analysis

Parameter	Expected value	Expected range (from Bal, 2012)	Unit
A	5·108	[2·104 ; 9·1013]	1/s
α_s	0.945	[0.945 ; 1]	-
c	1665	[1420 ; 2090]	J/kg·K
E_a	125	[74 ; 196]	kJ/mol
ε_f	0.15	[0.1 ; 0.2]**	-
ε_s	0.945	[0.945 ; 1]	-
h_c	10	[5 ; 25]	W/m ² /K
ΔH_c	25	[24 ; 26]*	kJ/g
ΔH_g	1.5·106	[1.4·106 ; 1.6·106]*	J/kg
HRP	14.5	[14 ; 15]*	-
k	0.21	[0.19; 0.27]	W/m/ K
m_{cr}''	2.42	[1.82 ; 3.75]	g/m ² /s
ρ	1188	[1180 ; 1191]	Kg/m ³
\dot{q}_{ext}''	50	[50 (-13 %) ; 50 (+13 %)]	kW/m ²
T_0	298	[290 ; 308]	K
T_∞	298	[290 ; 308]	K
T_f	1600	[1500 ; 1650]	K
T_s	550	[540 ; 560]	K

*values from Tewarson (2002)

**values from Yuen and T'ien (1977) and Staggs and Nelson (2001)

A.3 Models

This section provides a few modelling examples where the critical mass flux has been used. A sensitivity analysis is conducted for a few models in order to establish its impact in ignition modelling.

A.3.1 Ignition temperature

Nelson, Brindley and McIntosh (1995, 1996a, 1996b) developed a model to predict the ignition temperature of a thermally thin slab. They assumed a constant gas phase

temperature ($T_f = T_\infty$) prior to ignition and could thereby decouple solid and gas phase mechanisms. They derived an expression for the ignition temperature based on the critical mass flux and decomposition properties of the solid

$$T_{ig} = \frac{E_a}{R \ln\left(\frac{A m(0)}{\dot{m}_{cr}'' S}\right)} \quad (\text{A.4})$$

where $m(0)$ is initial mass of the sample, R is the universal gas constant, E_a is the activation energy, A is the pre-exponential factor, \dot{m}_{cr}'' is the critical mass flux at ignition, and S is the sample surface area. They predicted the ignition temperature to be 639 K for a 1 mm thin wooden slab.

Intuitively one can see that E_a has the largest effect on the ignition temperature, since the other variables are logarithmic. The sensitivity analysis confirms that variations in the critical mass flux has no large impact on ignition temperature in Nelson's model. Results are shown in Figure A.1. The initial mass has been calculated from the surface area, the sample thickness (assumed to be 1 mm) and the density.

Lautenberger and Fernandez-Pello (2005) solved the governing equations analytically and produced an approximate solution for the ignition temperature of a thermally thick solid slab

$$T_{ig} = T_0 \left(\frac{T_a^v \dot{q}_{ext}'' \dot{m}_{cr}''}{\mu k \rho A T_0 e^{T_a/T_1}} \right)^{T_2/T_a} \quad (\text{A.5})$$

where v , μ , T_1 and T_2 represent constants. T_0 is the initial temperature, \dot{q}_{ext}'' is the incident heat flux, k is the thermal conductivity, ρ is density, \dot{m}_{cr}'' is the critical mass flux at ignition, and T_a is the activation temperature. The authors fitted these constants to common material parameters and found that $v = 0.85$, $\mu = 341.3$, $T_1 = 357$ K, and $T_2 = 615$ K. A sensitivity analysis of the parameters indicates that the critical mass flux has some influence on the outcome (Figure A.2), but variations in decomposition kinetics (A) have a larger effect.

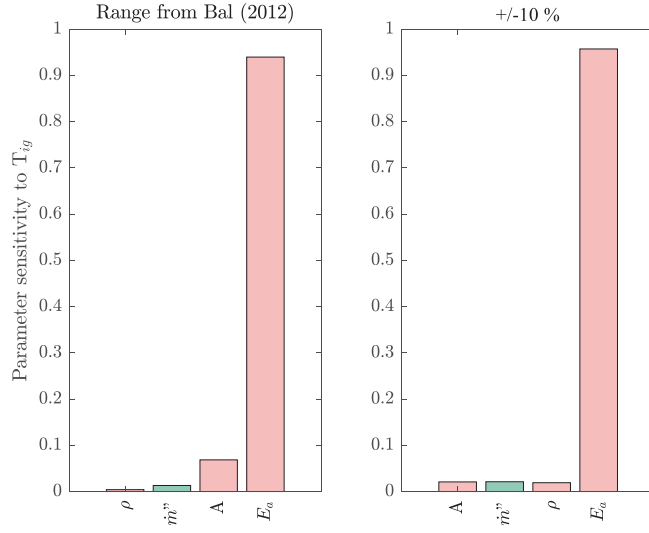


Figure A.1 Sensitivity analysis of Eq. (A.4)

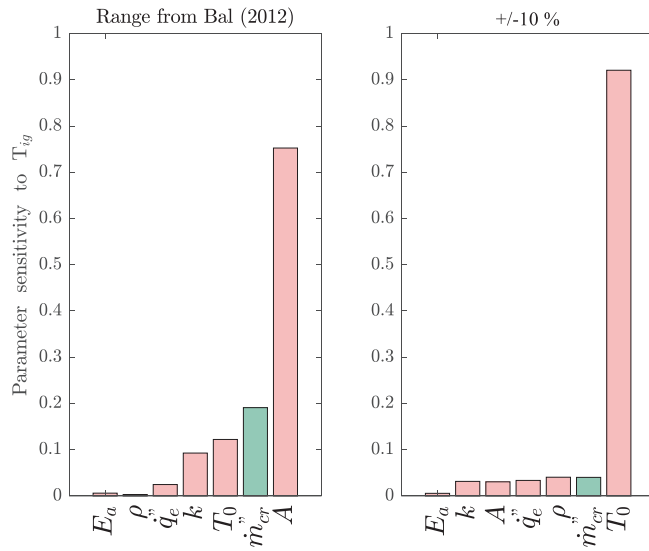


Figure A.2 Sensitivity analysis of Eq. (A.5)

A.3.2 Critical heat flux

Nelson *et al.* (1995) extended Eq. (A.4) and provided a correlation for the critical heat flux (\dot{q}_{cr}'') needed for ignition of a thermally thin slab, based on the assumptions mentioned in section A.3.

$$\dot{q}_{cr}'' = \frac{\Delta H_g \dot{m}_{cr}'' S + h_c (T_{ig} - T_f) + \sigma S (\epsilon_s T_{ig}^4 - \alpha_s \epsilon_f T_f^4)}{(1 - \alpha_s) S} \quad (A.6)$$

They arrived at a value of 24 kW/m² for thin wood. In Eq. (A.6) ΔH_g is the heat of gasification, h_c denotes the convective heat transfer coefficient, σ is the Stefan-Boltzmann constant, ϵ_s and ϵ_f are the emissivities of surface and flame, and α_s is the absorptivity of the surface. T_f denotes the flame (gas) temperature. The remaining parameters were explained in Eq. (A.4). A sensitivity analysis is conducted for Eq. (A.6), based on values in Table A.1. The critical mass flux has little impact on the critical heat flux in Nelsons model, as seen in Figure A.3.

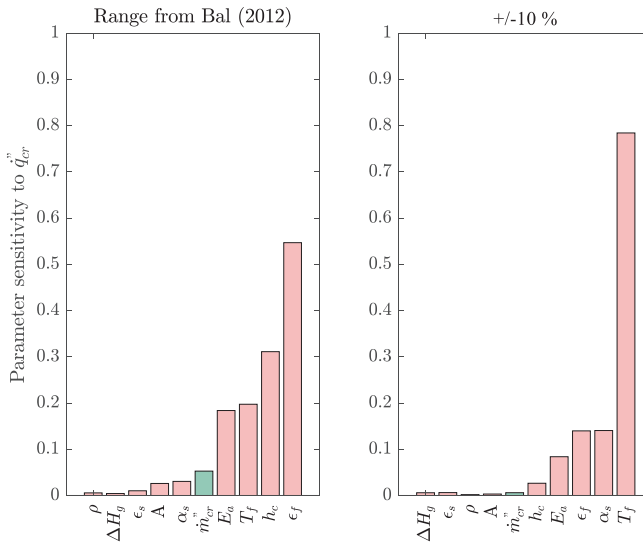


Figure A.3 Sensitivity analysis of Eq. (A.6)

Ritchie *et al.* (1997) developed a model to determine the incident heat flux (\dot{q}_{inc}'') to a thermally thick Douglas fir sample before and after a flame had been sustained.

$$\dot{q}''_{inc} = \begin{cases} (1-r)\dot{q}''_{ext} & \dot{m}'' < \dot{m}''_{cr} \\ (1-r)(\dot{q}''_{ext} + \dot{q}''_{f,r}) + \dot{q}''_{f,conv} & \dot{m}'' \geq \dot{m}''_{cr} \end{cases} \quad (\text{A.7})$$

where the critical mass flux (\dot{m}''_{cr}) for Douglas fir was set to 3 g/m²s. In the equation r denotes reflectivity, \dot{q}''_{ext} , $\dot{q}''_{f,r}$ and $\dot{q}''_{f,conv}$ denotes external, flame radiation, and flame convective heat fluxes respectively. This model indicates the stand-alone importance of the critical mass flux, as it is clear in Eq. (A.7) that the incident heat flux depends strongly on the chosen threshold value. After the mass flux has reached the critical value, additional heat fluxes increase the incident heat flux from 25 to almost 40 kW/m².

A.3.3 Time to ignition

Lautenberger and Fernandez-Pello (2005) extended the analysis in Eq. (A.5) to predict time to ignition, based on a mass flux threshold. They derived the following correlation for a thermally thick material

$$t_{ig} = \frac{\pi}{4} k \rho c \left(\frac{T_0}{\dot{q}''_e} \right)^2 \left(\left[\frac{\dot{q}''_e \dot{m}''_{cr}}{(\mu/T_a^v) \rho e^{-T_a/T_1} A k T_0} \right]^{T_2/T_a} - 1 \right)^2 \quad (\text{A.8})$$

In Eq. (A.8), the only parameter added is specific heat (c), but the equation itself determines the parameter sensitivity. As expected, conductivity and specific heat have a large influence on the result, as seen in Figure A.4. However, variations in A lead to most of the spread in ignition time. The critical mass flux also has a large influence on the results.

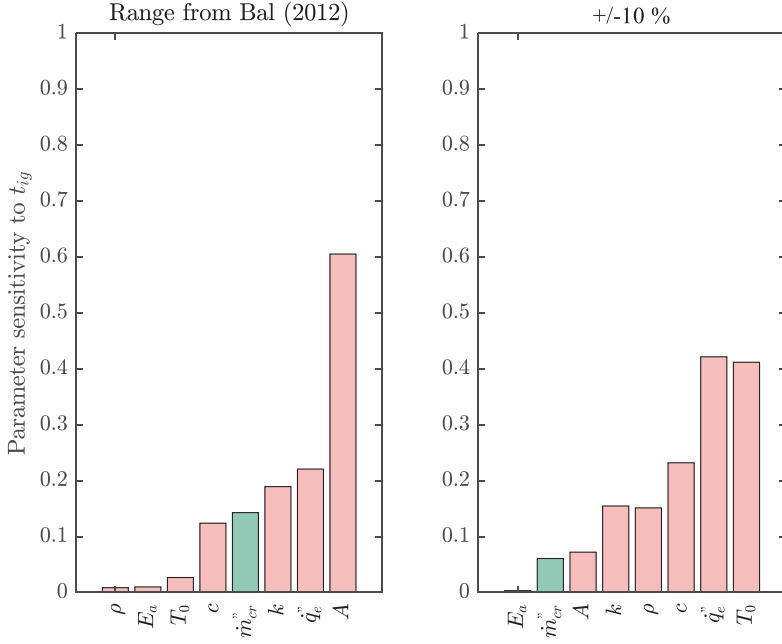


Figure A.4 Sensitivity analysis of Eq. (A.8)

Atreya and Wichman (1989) conducted a theoretical and experimental investigation on the ignition of wood. They related the ignition temperature to the critical mass flux by two dimensionless equations, where (*) denotes a dimensionless number

$$\dot{m}_{solid}''^* = \frac{A^*(1-\rho_g^*)}{\Phi_s E^*} (T_s^* + 1)^2 e^{-E^*/(T_s^*+1)} \left[1 - \frac{e^{[-E^*(T_s^*/(T_s^*+1))]} }{(T_s^*-1)^2} \right] \quad (A.9)$$

$$\dot{m}_{gas}''^* = \frac{Y_{ox} c_s (T_f^* - T_s^*) / \Delta H_{ox} c_p}{\left(\frac{-Y_{ox} \Delta H_c}{c_p T_\infty \Delta H_{ox}} \right) - T_f^* - Y_{ox} \left(\frac{T_f^* - T_s^*}{\Delta H_{ox}} \right)} \quad (A.10)$$

Eq. (A.9) is an expression of pre-ignition mechanisms and Eq. (A.10) describes the gas phase energy balance at ignition using the critical flame temperature needed for sustained flaming. The parameters are explained in the nomenclature list. The intersection between the two equations provides the point of ignition and thereby determines the time to ignition, as seen in Figure A.5. The figure also reveals that the ignition temperature is more sensitive to decomposition kinetics (A) than the critical mass flux is.

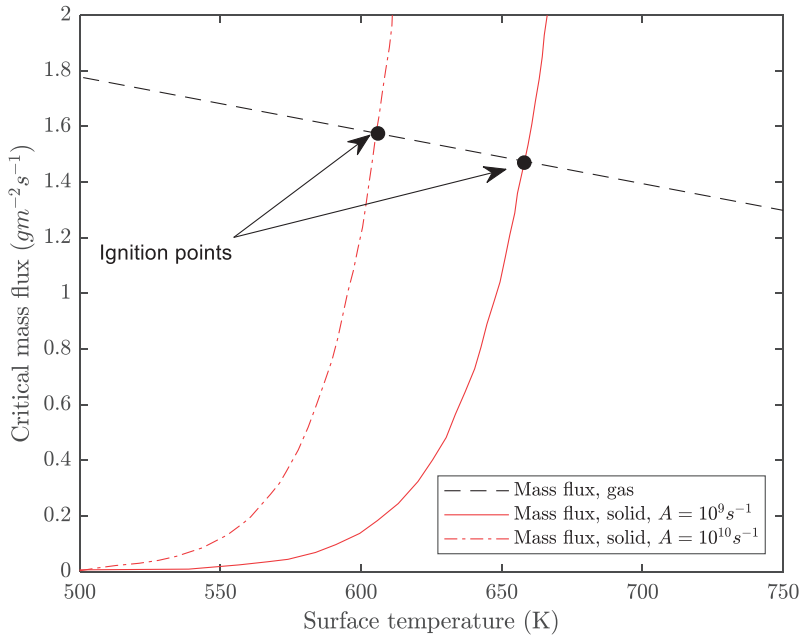


Figure A.5 Graphical example of Eqns. (A.9) and (A.10), adapted from Atreya and Wichman (1989) by permission

For thermally thin solids, if Nelson’s model is used in classical ignition theory (Eq. (A.1a)), a sensitivity analysis can be conducted for parametric ranges given in Table A.1. Results are presented in Figure A.6. It is clear that the critical mass flux has very little influence on the time to ignition in Nelson’s model.

Bal (2012) investigated numerical models having various levels of complexity for time to ignition and the parameters needed to predict it. He concluded that time to ignition predictions are more sensitive to thermal inertia and to the external heat flux than to gas phase properties like the critical mass flux. Figure A.7 is reproduced from Bal (2012) for a PMMA sample under a 50 kW/m² irradiance. However, amongst the gas phase properties, the critical mass flux is the property that has the most influence on the prediction of time to ignition.

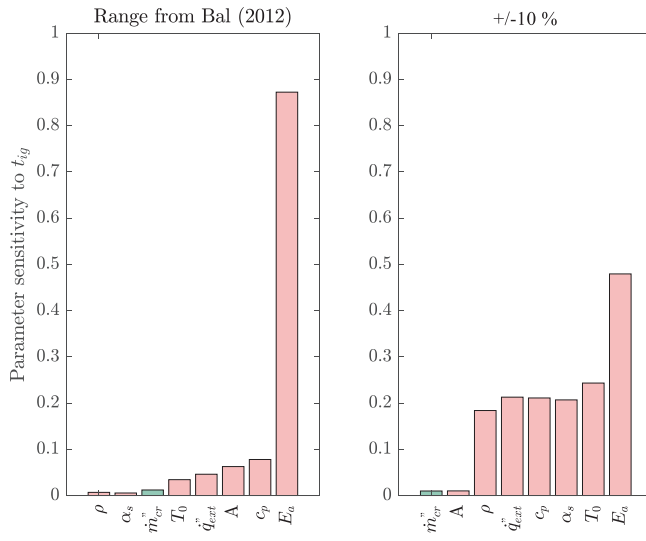


Figure A.6 Sensitivity analysis of Eq. (A.1a)

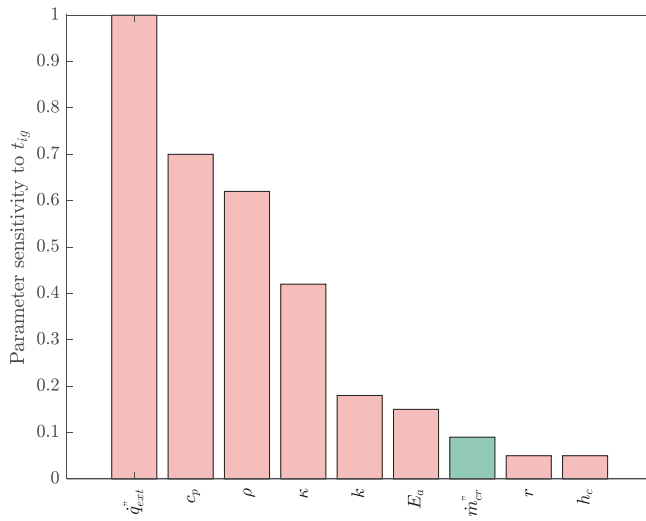


Figure A.7 Relative sensitivity to t_{ig} , reproduced from Bal (2012) by permission

A.3.4 Flame spread

Quintiere (2006a) approximated the limiting external heat flux for upward flame spread as

$$\dot{q}_{ext,f}'' = \sigma(T_s^4 - T_\infty^4) - h_c \left(1 - \frac{1}{HRP}\right) (T_{f,cr} - T_\infty) + \frac{\Delta H_c}{HRP} \dot{m}_{cr}'' \quad (\text{A.11})$$

where σ is the Stefan-Boltzmann constant, T_s , T_∞ and T_f are surface, ambient and flame temperatures, respectively, HRP is the heat release parameter, \dot{m}_{cr}'' is the critical mass flux, ΔH_c is the chemical heat of combustion, and h_c is the convective heat transfer coefficient. Parameter sensitivity for Eq. (A.11) is presented in Figure A.8. The convective heat transfer coefficient has an important role for the resulting variation, seconded to the critical mass flux.

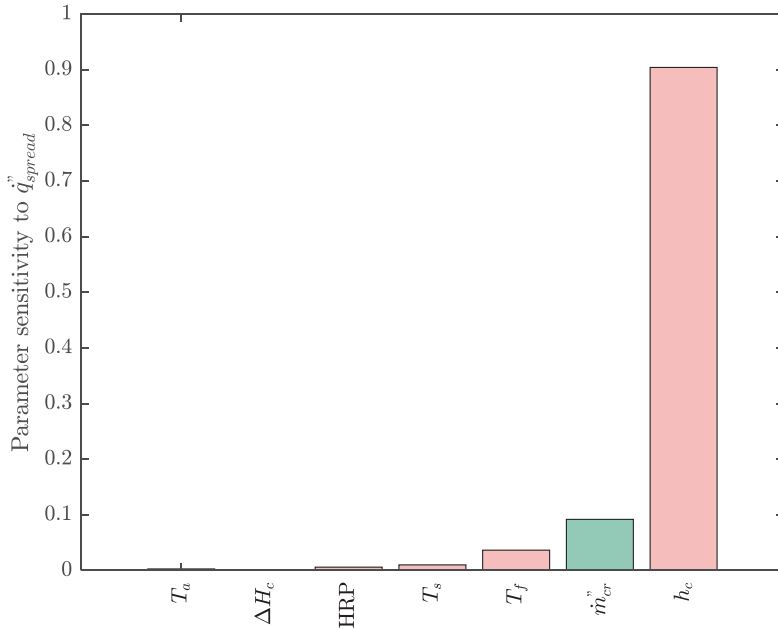


Figure A.8 Sensitivity analysis of Eq. (A.11)

A.4 Conclusions

The critical mass flux has been used in the modelling of a few ignition parameters for both thermally thin and thick materials, and also in flame spread models. From the sensitivity analyses in Section A.3 it is clear that the influence of the critical mass flux compared to other input parameters depends on the model used, the output parameter that is modelled, and the variation chosen for each parameter.

Generally, an expected range (e.g. the ranges from Bal (2012)) for each parameter is a better way to explore parameter sensitivity, however the percental deviations provide information on the extent to which each property varies due to the modelled equation itself.

Time to ignition is generally more sensitive to solid phase properties, but the critical mass flux seems to be the most influential gas phase parameter in modelling. It appears that the chosen value of the critical mass flux will have some impact on the modelling of ignition temperature, time to ignition and flame spread, depending on the model chosen.

Paper I



A review on prediction models for full-scale fire behaviour of building products

Frida Vermina Lundström^{1,2,*}, Patrick van Hees¹ and Éric Guillaume³

¹Department of Fire Safety Engineering, Lund University, P.O. Box 118SE-22100Lund, Sweden

²Danish Institute of Fire and Security Technology (DBI), Jernholmen 12DK-2650Hvidovre, Denmark

³Ejectis – Espace Technologique, Bât Apollo, Route de l'Orme des Merisiers FR-91193 Saint Aubin, France

SUMMARY

This study aims to give an overview over different reaction-to-fire prediction models developed over the last decades by finding similarities and differences between models, as well as identifying their robustness in scaling. The models have been divided into four categories – empirical, thermal, polynomial and comprehensive – depending on how pyrolysis is modelled. Empirical models extrapolate bench-scale test results to larger scales. These models are pertinent to applications that they have been validated for, but surfacic parameters used may not be scalable. In thermal models, pyrolysis is represented by heat transfer rates. The models are feasible for materials with high activation energies and where little pyrolysis occur before ignition. Polynomial models are empirical models that also take the environment into account. The validity of scaling is yet to be established. The comprehensive methodology includes chemical kinetics in the condensed phase. It has the potential to be used for any application; however, many parameters are needed. This increases the degrees of freedom versus data available for the description of the problem. Consequently, possible errors are introduced, and uncertainty is increased. A comprehensive multi-scale methodology is a way forward, where many steps of validation are possible. Copyright © 2016 John Wiley & Sons, Ltd.

Received 11 May 2015; Revised 20 May 2016; Accepted 20 May 2016

KEY WORDS: prediction model; reaction-to-fire; building products; pyrolysis; flame spread; cone calorimeter; multi-scale; performance-based design

1. INTRODUCTION

Achieving a fire-safe environment is accomplished by two strategies: the first aims to prevent fire ignition and growth, and the second strategy aims to manage fire impact in case a fire spreads [1]. These two strategies are implemented in fire safety regulations and influence standard material fire testing principles [2]; namely two areas are employed for depicting fire behaviour of a material: reaction to fire and fire resistance [3]. Reaction to fire is the analysis of a product's contribution to fire growth, especially in the early stages of the fire. Reaction-to-fire testing includes investigation of *ignitability*, *surface flame spread*, *heat release rate* (HRR) and *smoke production* [4]. *Toxicity* is not included in standard testing but may be of vital importance in real fires [5]. Fire resistance testing, on the other hand, focuses on the structure's integrity, for example, time frame in which a construction element may withstand fire.

The conventional approach to evaluate fire behaviour of materials used in building construction systems consists of performing a full-scale or intermediate-scale standard fire test on the material or system of interest. The outcome of standard fire tests is decisive for the building industry; following

*Correspondence to: Frida Vermina Lundström, Department of Fire Safety Engineering, Lund University, P.O. Box 118, SE-221 00 Lund, Sweden.

†E-mail: frida.vermina_lundstrom@brand.lth.se

prescriptive building codes outlining which materials or construction elements that may be used where – the safety of the building product is implicitly included in the test results. However, the outcome of the fire test has deficiencies: Material consumption and work efforts of performing such a test make the experiment costly [6]. Additionally, performance demonstration protocols of the test present results in discrete values, as pass/fail results, or rather results in ‘classes’ of fire behaviour; therefore, usage of test results in performance-based fire engineering is inflexible [7, 8]. Little information is given on the actual fire behaviour of the material tested, and extrapolation of the outcome to scenarios outside the actual experiment is an onerous task [9].

An alternative approach for fire safety in building design, which has been employed since the 1980s, is predictive modelling. Predictive modelling aims to predict the large-scale fire performance of building products from small-scale test results. Small-scale tests (micro-scale and/or bench-scale) are used as screening tests for the product manufacturers; hence, prediction models are more flexible and may significantly reduce the number of large-scale tests for the building product industry. They may also be used for increasing the understanding of physical progressions in the material during heating [8].

Prediction models are employed by both researchers for studies and private firms on actual design projects [10]. This wide-spread usage of prediction models highlights the need to review the state-of-the-art prediction models available and their subsequent applicability. In this study, a number of specific objectives have been defined, in order to exploit the state-of-the-art in predictive modelling of building products:

- i. *What existing types of models are available?*
- ii. *What features do the investigated models capture?*
- iii. *What are the most common output quantities?*
- iv. *What application areas are the models suitable for?*
- v. *Where are the gaps in existing models?*

The aim of this paper was to provide researchers and consultants with an overview over different reaction-to-fire prediction models that have been developed over the last decades. Four modelling strategies have been identified, which the models are categorized by. These categories are used to find similarities and differences between model types and to discuss the applicability and limitations of the models. The limitations of the model types reveal gaps in which more research is needed.

The ultimate goal of a predictive model is to capture fundamental phenomena in small scale as a basis for accurate modelling of building products in end-use condition. In testing, a ‘real’ fire scenario is represented by a large-scale fire test. Thus, most screening models have been aiming at predicting large-scale tests. In this study the main focus is therefore models that predict large-scale fire tests comparable to residential compartments such as the EN 13823 Single Burning Item test (SBI) [11] or the ISO 9750 Room/Corner test (R/C) [12]. Predictive models for façades, or external roofing, or industrial applications such as storage racks are not enclosed in this study. Enclosure fire models are the main target. Numerous efforts have been made on predicting fire behaviour. Not all exertions will be mentioned in this review, some models may be disregarded. It is the authors’ hope that the milestones and state-of-the-art models mentioned will give insight into the predictive modelling strategies as of today.

2. MODELLING STRATEGIES

When a solid material is heated, a pyrolysis process may be initiated; this is sometimes viewed as the starting point of the material’s contribution to the fire. Depending on the underlying assumptions of gaseous fuel production, the various prediction methodologies for fire behaviour of building products have been divided into four categories, identified by previous authors [10,13–18]. Tables of individual models are presented in the findings section:

- i. Empirical Models
- ii. Thermal Models

- iii. Polynomial Models
- iv. Comprehensive Models

Empirical models address, as the name suggests, empirical substitutes to pyrolysis and other fundamental phenomena. The methodologies are based on analysis of bench-scale experimental data for direct extrapolation to larger scale experiments. *Thermal models* include pyrolysis by presence of heat transfer theory. An infinitely thin pyrolysis front represents in-depth decomposition inside the solid material. The output, for example, HRR, is dependent on the temperature and net heat flux. *Polynomial models* highlight the importance of considering environmental factors for the extrapolation of bench-scale results to larger scales. Bench-scale results at different external heat fluxes and oxygen concentrations are used as input for the full-scale results. *Comprehensive models* take account of reaction rates in the condensed phase. A number of factors are used as input to these models, including Arrhenius constants. Usually the comprehensive models use bench-scale or intermediate-scale validation steps.

The methodologies categorized here may be comprehensive regarding fluid dynamics, irrespective of whether the model is empirical, thermal, polynomial or comprehensive. The factor on which they are categorized is solely pyrolysis.

2.1. Empirical models

Simplicity is the key advantage of the empirical models. Measured data from a bench-scale test (e.g. ISO 5660 Cone Calorimeter [19]) is mathematically emulated with arbitrary correction parameters to gain the results of a large-scale experiment (e.g. R/C [12]).

A classical assumption for extrapolating bench-scale data to larger scales is the use of surfacic parameters: results are expressed in relation to the surface of the material. For instance mass loss rate, HRR and incident radiation are commonly expressed per unit area.

Most empirical correlations deal with predicting HRR. Typically, heat release in full-scale (\dot{Q}_{full}'') is assumed proportional to the results of a bench-scale test; multiplying the bench-scale HRR with a factor or by a function, for example, an empirical equation of expanding burning area [20, 21]:

$$\dot{Q}_{full}'' \propto \dot{Q}_{bench}'' \tag{1}$$

Other common assumptions for empirical models are as follows [22]:

- i. Boundary conditions in bench-scale are negligible.
- ii. No mass loss occurs before the surface has reached a critical ignition temperature for the specific material, T_{ig} .
- iii. Surfacic parameters, for example, incident irradiance per exposed area, are similar between scales. Incident heat flux in bench scale is representative for the large-scale fire. The only parameters that vary are geometric.

Most empirical models for smoke production combine bench-scale HRR with a bench-scale smoke production rate to gain full-scale results. Smoke production has also been predicted by calculating smoke yields from bench scale and taking openings and room environment into account, calculating species concentrations [23]. Smoke yield is often assumed to depend solely on the material. This assumption has come under scrutiny, because fire environment has been proved to play a role [24–28].

Empirical models may subsequently be divided into three sub-categories, namely ‘Regression Models’, ‘Fire Growth Models’ and ‘Compartmental Models’ [13, 14].

A. Regression Models

Regression models express a correlation between bench-scale test data and specific indices, such as heat release parameters (e.g. peak heat release) or smoke production parameters (e.g. total smoke production) in larger tests [13]. An example of such a correlation is found in a paper by Tsantaridis and Östman [29], in which the time to flashover (t_{FO}) in the R/C [12] is predicted by measurements of time to ignition (t_{ig}), density (ρ) and total heat release (THR) 300 s after ignition in the cone calorimeter:

$$t_{FO} = 0.07 \frac{t_{ig}^{0.25} \cdot \rho^{1.7}}{THR_{300}^{1.3}} + 60 \quad (2)$$

B. Fire Growth Models

Fire growth models predict time-dependent parameters, like HRR. However, environmental and geometrical aspects are not accounted for. One example is found in the Ph.D. dissertation by Karlsson [30]. In this analytical model, Karlsson ignores pre-heating from a hot gas layer. Instead, he assumes that time to ignition in the R/C directly corresponds to that in the cone calorimeter. By measuring the HRR in the cone calorimeter, using arbitrary fitting constants, an HRR in full-scale is received. Another renowned example is the SP model Conetools in which the R/C or SBI test results are predicted from cone calorimeter data. HRR per unit area is assumed to be identical for the large-scale test and the cone calorimeter. In Figure 1 three theoretically possible paths of fire growth are displayed. Whether the material burns along route II or III depends on if an assumed surface temperature has been reached. This is depicted in the cone calorimeter. Likewise, as the burner heat output is raised (IV), the fire may grow according to path V or VI.

C. Compartmental Models

Compartmental models, which use room effects for fire growth predictions, although still empirical, may in fact be rather advanced in their treatment of fluid dynamics. A compartmental model includes heat feedback from the hot gas layer. Such a model may use a CFD code, a zone model or hand calculations. As an example, Lattimer *et al.* [31, 32] propose a two-zone model in conjunction with a flame spread software. The coupled codes use data from the cone calorimeter to model gas temperature in the hot gas layer and HRR as a function of burning area. The solid surface is divided into cells. A cell is ignited when the surface temperature reaches a specified ignition temperature or lateral flame spread calculations depict cell ignition. HRR in that cell is then dependent on net heat flux into the material.

2.2. Thermal models

Thermal models, compared with empirical, increase the level of complexity. Reaction rates are not included in the thermal pyrolysis model; however, *pyrolysis is represented by heat transfer rates*. Decomposition is assumed to start when the material-dependent pyrolysis temperature, T_p , is reached. Common assumptions for thermal models are as follows [33–35]:

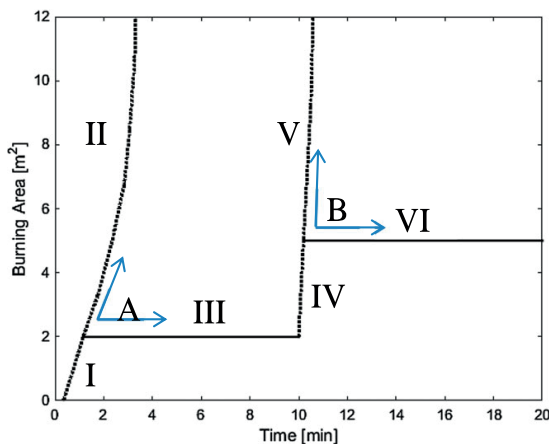


Figure 1. Conetools: burning area growth in the Room/Corner test. Reproduced from [20]. [Colour figure can be viewed at wileyonlinelibrary.com]

- i. Decomposition is assumed to start when a critical pyrolysis temperature (T_p) is reached at the solid surface and the solid is considered thermally inert previous to that point. This is justified with the statement that many condensed-phase fuels have relatively high activation energies (E_a). In other words, the Arrhenius description of reaction rates shows that such fuels experience a slow decomposition before a specific point (T_p) is reached but increases rapidly with temperature as it approaches this critical value.
- ii. 1D heat transfer.
- iii. Pyrolysis temperature is sometimes assumed equal to ignition temperature ($T_p = T_{ig}$).
- iv. Surface temperature remains constant ($T_s = T_p$) throughout the entire stage of mass loss.
 - v. Chemical kinetics are ignored.
 - vi. Release of combustible volatiles occurs in an infinitely thin surface region for non-charring solids (ablation models) and in an infinitely thin pyrolysis front between char and virgin layer for charring solids.
 - vii. Mass transfer in protective layers (char, melt) may be ignored.
 - viii. Thermal properties are invariant.

Mass loss rate is mathematically determined by solving an energy balance at the thin pyrolysis front. The chosen solution method of the heat conduction equation and boundary conditions depends on assumptions and differs between the various models.

A postulation, used by van Hees [36] amongst others [37–39], is that the one-dimensional heat conduction equation with boundary and initial conditions, as follows in Equations (3–6), may be divided into smaller strips. The transient heat conduction in a thermally thick solid may then be simplified to Equation (7) by a Duhamel integral [40]:

$$\frac{\partial^2 T}{\partial x^2} = \frac{1}{\alpha} \frac{\partial T}{\partial t} \tag{3}$$

$$\dot{q}_{net}''(0, t) = k \frac{\partial T}{\partial x} \tag{4}$$

$$\dot{q}_{net}''(0, t) = \dot{q}_f'' + \dot{q}_c'' + \dot{q}_e'' + \dot{q}_{co}'' + \dot{q}_r'' \tag{5}$$

$$T(x, 0) = T_\infty \tag{6}$$

$$T_s(t) = T_\infty + \frac{1}{\sqrt{\pi k \rho c}} \int_0^t \frac{\dot{q}_{net}''(\tau)}{\sqrt{t - \tau}} d\tau \tag{7}$$

The terms in Equations (3–8) are explained in the nomenclature list.

As the surface temperature reaches a critical ignition temperature, the specimen is considered ignited. In this way an expanding burning area may be achieved [41, 42].

Another approach to solve the differential equation is made by Delichatsios *et al.* [43] whereby an exponential temperature profile is employed across the examined wall in the heating-up stage. As the temperature reaches a designated pyrolysis temperature (T_p), the heat up process is terminated, and the temperature remains constant during the process of pyrolysis. The temperature profile used transforms the transient heat conduction equation into an ordinary differential equation. Moghtaderi *et al.* [44] have utilized the same solution technique to the partial differential heat conduction equation, however employed a quadratic temperature profile.

Yan and Holmstedt [45] solved the equation numerically. For temperatures below T_p , Equation (3) is solved by FDM. Pyrolysis initiates as the temperature reaches the prescribed pyrolysis temperature; thereafter, the temperature remains constant.

$$\Delta H_p \frac{\partial \rho}{\partial t} = \frac{\partial}{\partial x} \left(k \frac{\partial T}{\partial x} \right) \quad (8)$$

2.3. Polynomial models

Polynomial models are categorized as *empirical models that take the environment into account*. Mass loss rate is tabulated as a function of incident heat flux and oxygen concentration. Each input parameter is described by the use of a polynomial equation of second order, in which thermal parameters and enthalpies are masked in the coefficients [46]:

$$y = a_0 + \sum_{i=1}^N a_i x_i + \sum_i a_{ii} x_i^2 + \sum_{i \neq j} a_{ij} x_i x_j + \dots + \sum_{i \neq j \neq k} a_{ijk} x_i x_j x_k + a_{i\dots N} x_i \dots x_N \quad (9)$$

where x in Equation (9) is, for example, oxygen concentration or irradiance level, giving a function for the mass loss rate (y). The polynomials are illustrated by the vectors created by the red dots in Figure 2, resulting in a matrix description for mass loss rate.

The experimental results are derived from several tests in the Controlled Atmosphere Cone Calorimeter. One example of this is a model created by Hermouet, which is validated for Acrylonitrile-Butadiene-Styrene (ABS) material. The thermal parameters are not explicit in this kind of model, but they exist in the coefficients of the polynomial equation. The number of datapoints chosen compared with the complexity of the model is very important to avoid overadjustment or under-adjustment. One of the weak points still under research is the behaviour of this model when datapoints are determined in fixed conditions, that is, at constant irradiance and the application concerns variable heating.

2.4. Comprehensive models

Comprehensive models refer to those that *include chemical kinetics*. In general, and according to Rogers and Ohlemiller [48, 49], the modelistic approach is used, which means that the application of the model presupposes establishment of a chemical model, describing reaction paths and intermediate species.

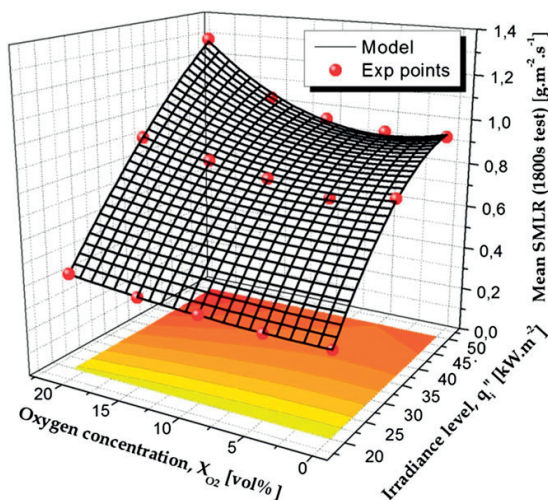


Figure 2. Mass loss rate application example; reprinted from [47], by permission. [Colour figure can be viewed at wileyonlinelibrary.com]

Pyrolysis is thus driven by reaction rates rather than heat transfer. That is to say, gasification rate is calculated based on local temperature, instead of being represented by a heat balance at a thin pyrolysis front. In many cases, chemical kinetics is modelled by some form of an Arrhenius expression:

$$\dot{\omega} = A \cdot e^{-\frac{E_a}{RT}} \quad (10)$$

where $\dot{\omega}$ is reaction rate, A is pre-exponential factor, E_a is activation energy, R is the ideal gas constant and T is temperature. This expression commonly includes representative mass fractions of oxygen ($Y_{O_2}^\delta$) and solid fuel ($Y_F^{n_i}$) with reaction orders δ and n_i [34]. Fuel production at the material's surface ($\dot{m}_p''(0, t)$) is then expressed as an in-depth integral of the material's permeability and reaction rate for each cell (shown here as a one-dimensional expression for simplicity) [34]:

$$\dot{m}_p''(0, t) = \int_0^{z_{FP}} \chi(x, t) Y_{F,s}(x, t) \sum_{i=1}^{i=N} \omega(x, t) dx \quad (11)$$

The terms in Equation (11) are explained in the nomenclature list. Comprehensive models are not truly fundamental; they may neglect or disregard numerous thermophysical and thermomechanical phenomena. Common assumptions are as follows:

- i. Volatiles are instantaneously transported to the surface;
- ii. First order, single-step reaction;
- iii. Negligible surface regression or expansion;
- iv. Thermomechanical failures, like cracking, bending, delamination, etc. are not accounted for;
- v. Negligible fuel production beyond the reactive depth;
- vi. Density is independent of temperature;
- vii. Negligible porosity;
- viii. No radiation in the solid.
- ix. Melt flow/dripping is often neglected.

The properties needed for simulation are often experimentally depicted in micro-scale apparatuses, for example, thermogravimetric analysis. Marquis *et al.* describe a common way of interpreting material property data from TG experiments. In the study it is also demonstrated that a solution of the ordinary differential equation for such models both exist and that it is unique [50]. Nonetheless, sometimes optimization techniques together with bench-scale tests are used for retrieving material properties [51]. To achieve a physically and chemically validated solution, the modeller should be aware that experimentally determined properties are more accurate. This is because optimized data may not be adequate to extrapolate, as data are received from, for example, HRR in a bench-scale test. The optimized properties are thus strictly empirical, and effects of boundary conditions, environment, etc. from the bench-scale test are embedded into the optimized properties. Another way of gaining properties is from literature or data sheets. It should also be noted that experimental measurements of material properties give better agreement than literature data, because of variations in material composition. Kempel *et al.* [52] have shown that especially acknowledging temperature-dependence of certain material properties can also enhance model predictions.

Examples of comprehensive models are the Ph.D. dissertations by Camillo [53, 54] and Bustamante [55] predicting materials involved in railway car fires and polyurethane foam, respectively. Other comprehensive studies are conducted by Marquis *et al.* [56–58] (fibre-reinforced plastics) and Fateh [59] (plywood).

Batiot explains a few elements related to model validation and the sensitivity of choosing the correct reaction properties. It is shown that the position and amplitude of a predicted MLR peak is driven by A and E_a , while asymmetry of the peak is driven by n . In comprehensive modelling, this knowledge is useful for diagnosing faulty results, etc. [60].

3. FINDINGS AND DISCUSSION

In order to obtain an idea of what kinds of prediction models there are, a short overview on the outcome of reaction-to-fire models is presented in Table I. Burning area and flame spread rate are both labelled V_p , and pyrolysis temperature is named T_{ig} for simplicity.

Table I. Predicted reaction-to-fire parameters.

Model	Surface flame		HRR	Smoke production	Toxic species
	Ignitability	spread			
Bustamante [55]	\dot{m}_{cr}^*		HRR	MLR	
Camillo [53]	\dot{m}_{cr}^*	V_p	T		Species
Carlsson [61]	\dot{m}_{cr}^*		HRR		
CONETOOLS [20, 21]	T_{ig}^*	V_p	HRR		
Delichatsios <i>et al.</i> [43]	T_{ig}^*	V_p			
Dietenberger [62, 63]	T_{ig}^*		HRR, T_{FO}	SEA	
Dietenberger, Grexa [64]					
Fateh [59]	\dot{m}_{cr}^*			MLR	
Gollner [65]	T_{ig}^*	V_p			
Grant [66]	T_{ig}^*	V_p	HRR		
Hansen [67]	T_{ig}^*		T_{FO}		
Hansen, Hovde [68, 69]				SMOGRA, TSP	
Hasemi <i>et al.</i> [70]	T_{ig}^*	V_p			
Hermouet <i>et al.</i> [46, 47, 71]				MLR	
Heskestad, Hovde [72]				S_Q	
Hostikka, McGrattan [73]	\dot{m}_{cr}^*		HRR		
Janssens [63,74]	T_{ig}^*	V_p	HRR	Smoke production rate	
Karlsson model 1	T_{ig}^*				
Karlsson model 2 [30,75–77]	T_{ig}^*	V_p	HRR		
Kwon [78]	\dot{m}_{cr}^*		HRR		
Lattimer [31, 32] Beyler [79]	T_{ig}^*		HRR	Smoke levels	Species
Linteris <i>et al.</i> [80]	T_{ig}^*		HRR		
Magnusson, Sundström [76,81]	\dot{q}_{ig}^*		HRR		
Marquis [9,82]	\dot{m}_{cr}^*			MLR	
Mitler [83]	T_{ig}^*	V_p			
Moghaddam <i>et al.</i> [84]	T_{ig}^*		HRR		
Moghtaderi [44]	T_{ig}^*	V_p			
Mowrer, Williamson [39]	T_{ig}^*		Flammability parameter		
Opstad [85]	T_{ig}^*	V_p	HRR		
OSU [86–88]	T_{ig}^*	V_p	HRR	Smoke release	
Quintiere <i>et al.</i> [89]	T_{ig}^*	V_p			
Quintiere [90–93]	T_{ig}^*	V_p	HRR		
Saito <i>et al.</i> [37]	T_{ig}^*	V_p			
Steckler [94]	T_{ig}^*	V_p			
Thomas, Karlsson [38]	T_{ig}^*	V_p			
van Hees [36,95]	T_{ig}^*	V_p			
van Hees [36,95]	T_{ig}^*	V_p			
Wade [96]	T_{ig}^*	V_p	HRR		
Wang [97]	T_{ig}^*		T_{FO}		
Yan/Holmstedt model 1 [45]	T_{ig}^* , R_{flux}		HRR		
Yan, Holmstedt model 2 [45]	T_{ig}^* , R_{flux}		HRR		
Östman, Tsantaridis [98, 99]	T_{ig}^*		T_{FO}	Peak and total smoke rate	

From Table I it is clear that surface flame spread and HRR are commonly predicted for the models reviewed and that an ignition criterion is needed for all prediction methodologies. Less work has been focused on predicting smoke production and toxic species. This is explained by the fact that most of these models build on bench-scale HRR results.

In Table II, the reviewed models are divided into their given categories. The models are analysed regarding their inherent assumptions: The column *system predicted* explains what system the models have been validated against that represents a full-scale or large-scale scenario. The model designs and validations are results of what has been available test data for the modellers. Thus, not many models predict other systems than the SBI or the R/C. *Room environment/solution technique* is a description on how the environment has been taken into account. The environment may be modelled by CFD techniques or by one-zone or two-zone models. Analytical solutions are common amongst the simple models, where gas phase is treated by hand calculations. The column *thermal properties* displays whether the thermal properties are treated as temperature-dependent, invariant of temperature or lumped (as thermal inertia). The column *ignition* illustrates whether the ignition criterion is a critical time, temperature, heat flux or mass flux. The column *combustion* presents whether combustion is empirically calculated from a bench-scale HRR or MLR, or whether a combustion model such as mixture fraction or finite rate is used.

All full-scale prediction methodologies are based on empirically gathered data; however, some (thermal-limited and comprehensive) introduce more 'fundamental' properties. By increasing the quantity of properties, the area of applicability widens. Conversely, by an increased complexity, a higher level of uncertainty is also introduced as shown by Bal [100]. The different types of models are all appropriate depending on materials predicted and heating rates. Thus, an empirical model may be used for receiving a 'quick check' or for comparative studies. Thermal models are feasible for materials that do not release much volatile before ignition and for materials that burn at a steady rate. Polynomial models are of interest when the environmental and geometrical conditions lead to ventilation-controlled fires. Comprehensive studies are viable when vast experimental studies are possible to conduct, in order to use 'fundamental' properties.

The empirical methodologies provide quick and easy calculations with a minimal amount of parameters. The empirical approach is especially suitable for materials giving rise to complicated burning behaviour, such as melt flows, that may be hard to model comprehensively. However the arbitrary factors or functions used in the empirical models are based on the materials tested; hence, applicability outside the intended area, that is, non-validated area, may provide erroneous results. Moreover, models validated for well-ventilated standard fire tests cannot represent under-ventilated fire behaviour.

One common statement in empirical models is the use of surfacic parameters. The scalability of these parameters is not always physically sound in certain situations or for certain parameters. Incident heat flux per unit area for instance may initially be assumed uniform over the specimen in a Cone Calorimeter, whereas this is not the case in a real fire, where the product is heated by a flame and perhaps by several burning items with various view factors.

The thermal model assumption of a specific pyrolysis temperature as the starting point of decomposition is valid in cases where high external irradiance levels heat a solid with a thin region of pyrolysis. This implies that the methodology is feasible for high activation energies, where little pyrolysis occurs before ignition and where rate of pyrolysis increases rapidly when the material is ignited. However, thermal models are less viable for low heating rates and when in-depth heat entrainment is large.

Polynomial models are strictly mathematical descriptions of the fire phenomenon, although heat transfer properties and enthalpies are masked in the coefficients. Not many modellers have so far used the approach to predict full-scale fire behaviour, and thus, precision of the modelling remains to be validated. However, this type of model includes the change of both irradiance and oxygen concentration. A limitation related to polynomial models is the number of tests needed. To create matrices like the example in Figure 2, several small-scale tests are needed, which increases cost for the prediction of the large-scale fire. Another limitation is the test apparatus used and the boundary conditions that will be masked in the result of the small-scale test. By using the controlled atmosphere cone calorimeter (CCAC), both the common boundary conditions related to the cone

Table II. Modelling attempts of various phenomena.

Model	Category	System predicted	Room environment/ solution technique	Materials	Thermal properties	Ignition	Combustion	Model outputs
Östman, Tsantaris [98, 99]	Empirical, regression	R/C	—	28 building products	—	T_{ig}	THR input	T_{FO} and TSP
Hansen [67]	Empirical, regression	R/C	—	57 building products	—	T_{ig}	THR input	T_{FO}
Hansen, Hovde [68]	Empirical, regression	SBI	—	28 building products	—	T_{ig}	HRR input	TSP, SMOGRA
Hansen, Hovde [69]	Empirical, regression	R/C	—	28 building products	—	T_{ig}	HRR input	TSP, SMOGRA
Heskestad, Hovde [72]	Empirical, regression	R/C	—	—	—	T_{ig}	HRR input	δ_Q
Wang [97]	Empirical, regression	R/C	—	52 building products	—	T_{ig}	THR input	T_{FO}
Mowrer, Williamson [39]	Empirical, regression	R/C	—	Textile wall covering materials	Lumped	T_{ig}	HRR input	Flammability parameter
Dietenberger, Grexa [64]	Empirical, regression	R/C	—	6 wood products	—	T_{ig}	MLR input	SEA
Magnusson, Sundström [76, 81]	Empirical, fire growth	R/C	—	Wall linings	Lumped	q'_{ig}	HRR input	HRR
CONETOOLS [20, 21]	Empirical, fire growth	R/C, SBI	—	Wall linings	Lumped	T_s	HRR input	HRR
Dietenberger [62, 63]	Empirical, fire growth	R/C	—	Wall linings	Lumped	T_{ig}	HRR input	HRR, T_{FO}
Karlsson [30]	Empirical, fire growth	R/C	—	Wall linings	Lumped	T_{ig}	HRR input	V_p , HRR
Quintiere <i>et al.</i> [89]	Empirical, fire growth	Vertical slab/ wall	—	Wall linings	Lumped	T_{ig}	HRR input	V_p
Stecker [94]	Empirical, compartmental	R/C	Two-zone	Wall linings	Lumped	q'_{cr}	N.A.	V_p

(Continues)

Table 2: (Continued)

Model	Category	System predicted	Room environment/ solution technique	Materials	Thermal properties	Ignition	Combustion	Model outputs
OSU [86–88]	Empirical, compartmental	R/C	Two-zone	Wall and ceiling linings	Invariant	N.A.	N.A.	V_p , HRR and smoke release
Karlsson [30,75–77]	Empirical, compartmental	R/C	Two-zone	Wall and ceiling linings	lumped	T_{ig}	HRR input	V_p , HRR
Grant [66]	Empirical, compartmental	R/C	Two-zone	Corrugated fibreboard	Lumped	T_{ig}	HRR input	V_p , HRR
Mitler [83]	Empirical, compartmental	R/C	Two-zone	FRP composites	lumped	T_{ig}	HRR input	Ignition and V_p
Latimer [31, 32]	Empirical, compartmental	R/C	Two-zone	PMMA, plywood etc.	Lumped	T_{ig}	MLR input	HRR, gas temperature, smoke levels and species
Opstad [85]	Empirical, compartmental	R/C	CFD	Wall linings	Lumped	T_{ig}	HRR input	HRR, burned area
Yan/Holmstedt [45]	Empirical, compartmental	R/C*	CFD	Particle board, PMMA	Invariant	T_{ig}	HRR input	HRR, T_s , T_g , R_{flux}
Quintiere [90–93]	Thermal	R/C	One-zone	Wall and ceiling linings	Lumped	T_{ig}	Peak HR input	HRR, T_g , burned area
Janssens [63,74]	Thermal	R/C	One-zone	Wall linings	Lumped	T_{ig}	HRR input	HRR, T_g , burned area, smoke production rate
Wade [96]	Thermal	R/C	Two-zone	Wall linings	Lumped	T_{ig}	HRR input	V_p , HRR
van Hees [36,95]	Thermal	Room corridor scenario	Analytical	Floor coverings (PVC, carpet, linoleum, parquet, etc.)	Lumped	T_{ig}	HRR input	V_p
van Hees [36,95]	Thermal	Room corridor scenario	CFD	Floor coverings	Lumped	T_{ig}	HRR input	V_p
Saito <i>et al.</i> [37]	Thermal	Vertical slab/wall	Analytical	Particle board, PMMA	Lumped	T_p	HRR calculations	V_p
	Thermal	Vertical slab/wall	Analytical	PMMA	Lumped	T_p	HRR calculations	V_p

(Continues)

Table 2: (Continued)

Model	Category	System predicted	Room environment/ solution technique	Materials	Thermal properties	Ignition	Combustion	Model outputs
Hasemi <i>et al.</i> [70]	Thermal	Vertical slab/wall	Analytical	N.A.	Lumped	T_p	HRR calculations	V_p
Thomas, Karlsson [38]	Thermal	Vertical slab/wall	Analytical	PMMA	Invariant	T_p	HRR calculations	V_p
Delichatsios [43]	Thermal	Vertical slab/wall	Analytical	PMMA	Invariant	T_p	HRR calculations	Flame spread rate: V_p
Moghtaderi [44]	Thermal	R/C	CFD	Particleboard, PMMA	Invariant	T_p	Mixture fraction model	HRR, T_s , T_g , R_{flux}
Yan, Holmstedt [45]	Thermal	R/C	CFD	Plywood	Invariant	T_{ig}	Mixture fraction model	HRR
Moghaddam <i>et al.</i> [84]	Thermal	Warehouse rack	Analytical	Corrugated cardboard	Lumped	T_p	HRR calculations	V_p
Gollner [65]	Polynomial	CC	Analytical	ABS, PIR	Masked	—	—	MLR
Hermouet <i>et al.</i> [46, 47, 71]	Comprehensive	CC	CFD	PMMA	Invariant	T_{ig}	Mixture fraction model	HRR
Linteris <i>et al.</i> [80]	Comprehensive	R/C	CFD	Wood linings	Temperature-dependent	$.m_{cr}^*$	Mixture fraction model	HRR, q^* , T_s
Hostikka, McGrattan [73]	Comprehensive	R/C	CFD	Spruce linings	Temperature-dependent	$.m_{cr}^*$	Mixture fraction model	HRR, q^* , T_s
Carlsson [61]	Comprehensive	5 m wall	CFD	PMMA	Invariant	$.m_{cr}^*$	Mixture fraction model	HRR, q^*
Kwon [78]	Comprehensive	CC	CFD	(FR) plywood	Temperature-dependent	$.m_{cr}^*$	Finite rate model	MLR, T (front and back)
Fateh [59]	Comprehensive	CC	CFD		Temperature-dependent			
Bustamante [55]	Comprehensive	CC (only experimental)	CFD	PUR	Temperature-dependent	$.m_{cr}^*$	Mixture fraction model	HRR, MLR

(Continues)

Table 2: (Continued)

Model	Category	System predicted	Room environment/ solution technique	Materials	Thermal properties	Ignition	Combustion	Model outputs
Camillo [53]	Comprehensive	data for product scale) Train carriage	CFD	GRP composite and a seat	Temperature- dependent	\dot{m}''_{cr}	Mixture fraction model	T , heat flux, burned area, species
Marquis [9,57]	Comprehensive	'Demonstrator' room	CFD	FRP composite	Temperature- dependent	\dot{m}''_{cr}	Mixture fraction model	MLR, T

calorimeter and additional issues related to the CCAC will be visible in the experimental results. For instance, additional irradiance from the walls of the box will affect the burning behaviour of the test specimen. It is not yet validated if scaling is applicable for those tests.

Although polynomial models for mass loss rate are not common, the models resemble iterative methods for calculating a smoke layer temperature [101] (MQH correlation) and a smoke layer temperature in an adjacent room [102]. By recognizing the similarities it may be possible to comprehend an iterative hand-calculation methodology for mass loss rate based on empirical data, which in the future could be of use for fire safety engineers.

A critical limitation of comprehensive models is the number of parameters necessary to solve the equations and the uncertainty associated with determining these properties. As the number of parameters required in a model increase, so does also the number of degrees of freedom. The resulting uncertainty can accumulate up to a point for which the lack of confidence in the complex model overcome the sensitivity from errors found in simplistic models [100].

For comprehensive prediction models 'property calibration' is sometimes assessed, so that the model better fits with experimental data. Thus such models are still not truly predictive [9]. Greater understanding is needed for micro-scale phenomena, if comprehensive models shall be viewed as a way forward. Phenomenological considerations regarding properties are still lacking.

Recent authors have discussed the importance of taking effects of scaling into account in prediction models [34,103, 104]. By scaling up from micro-level, temperature gradients are no longer neglected, and the environment is harder to determine experimentally. Small-scale testing does not necessarily imply that fundamental material properties may be extracted as the retrieved properties may be apparatus-dependent. For example: pyrolysis pathways depend on heating rate. Heating rates in thermogravimetric studies are lower than that of a typical fire [34]. In the discussed prediction models, this consideration is often neglected. Multi-scale studies are a way forward as validation at intermediate steps is necessary with the methodologies of today. This due to the fact that assumptions made at each length scale level may affect the next level.

Methodologies need to couple environmental factors to solid material behaviour in order to be able to predict full-scale fire behaviour. Predictive methodologies encounter various challenges even after material properties have been derived. Such challenges may include, but are not limited to: boundary layer flows, radiation, turbulence, flame re-radiation, interaction between burning items and interaction with compartment [8]. A concrete example of one such challenge is that ignition source and position considerably alters whether/when ignition occurs as well as whether/when the spread of fire is self-propagating [103]. Another example is that oxygen content and smoke concentrations in a compartment may considerably affect rate of flame spread and type of smoke and species produced.

Most models use an ignition temperature as a criterion for ignition (refer Table II). Associating ignition to a material's surface temperature or to an ablative temperature is a prevailing way of experimentally determining ignitability. In most cases the practice is sufficiently precise, for example, for comparative ignitability studies. Despite this practicality, the traditional way is strictly not pertinent to other environments, scales or geometries [105]. Particularly for discontinuous heat fluxes, as the case is in real fires, an ignition temperature is not appropriate [106]. Thus, using an ignition temperature may lead to incorrect assumptions regarding material fire safety. There is also a lack of prediction models for smoke and toxicity, especially for comprehensive methodologies. Smoke production is seen as the most hazardous contribution in a fire [107], yet despite this, few models exist that predict smoke production. This may be explained by the postulation that HRR is the most important variable for depicting fire hazard [108].

Conclusively, a wide range of prediction models have been presented, which all predict large-scale fire behaviour from test results at small scale. A high degree of accuracy has been shown for the intended use of the models. As such, these predictive models may serve as a tool for product development or for product categorization based on material properties. However, the models cannot replace classifying tests, especially at large scale, where reaction-to-fire properties are affected by fixing arrangements or mounting of the products. In other words, a drawback for all presented models is that they do not theoretically explain, for example, thermomechanical failures and melt flows. With complex models using, for example, finite element discretization techniques, some of

those problems may be solved. One example is Onate *et al.* [109] that modelled melt flows in burning plastics. This type of complex model is not common in the fire safety field but states an example of a possible way forward for solving issues related to complex material behaviour in fire.

4. CONCLUSIONS

Fire models predicting reaction-to-fire parameters may serve as a tool for product development or for product categorization based on material properties. However, these models cannot replace classifying tests, especially at large scale, where reaction-to-fire properties are affected by fixing arrangements or mounting of the products. In this study models for building products have been divided into four categories – empirical, thermal, polynomial and comprehensive – depending on how pyrolysis is modelled. Empirical models are not pertinent to applications other than the validated. Thermal models are feasible for materials with high activation energies and where little pyrolysis occur before ignition. Polynomial models take the environment into account, but the validity of scaling is yet to be established. The comprehensive methodology has the prospect to be used for any application. However, not all solution techniques allow for modelling of thermomechanical failures, melt flows, etc.

The models mainly predict ignitability, flame spread and HRR. There is more research needed related to other ignition criteria than the commonly used ignition temperature, as an ignition temperature criterion is not valid for discontinuous heat fluxes. There is also more to be carried out on smoke production and toxicity, especially for models that build on a comprehensive methodology.

ACKNOWLEDGEMENTS

The authors acknowledge the European Union's Seventh Framework Programme, for the support under grant no. 316991. This study is part of FIRETOOLS, which is a collaborative project between Lund University and the Danish Institute of Fire and Security Technology. FIRETOOLS's overall goal is to model fire behaviour of building products, content and barriers from microlevel to system level. The authors wish to thank the fellow participants of the FIRETOOLS project, namely Blanca Andrés, Abhishek Bhargava, Karlis Livkiss and Konrad Wilkens, for input on the part of the first FIRETOOLS report, on which this manuscript is based. The authors are also indebted to the International FORUM of Fire Research Directors for collaboration and guidance on fire source modelling.

NOMENCLATURE

A	Pre-exponential factor
a_i	Coefficients
c	Specific heat capacity
E_a	Activation energy
ΔH_p	Heat of pyrolysis
h_T	Heat transfer coefficient
k	Thermal conductivity
\dot{m}''	Mass flux
N	Number of species
n	Order of reaction
\dot{q}''	Heat flux
\dot{Q}	Rate of heat release
R	Ideal gas constant
S_Q	Smoke to heat ratio
t	Time
T	Temperature
V_p	Flame spread rate
x_i	Factors
y	Selected parameter response

GREEK

α	Thermal diffusivity
ε_F	Reactive depth
ρ	Density
τ	Dimensionless time
$\dot{\omega}$	Reaction rate
χ	Permeability
Y	Mass fraction

SUBSCRIPTS AND SUPERSCRIPTS

bench	Bench-scale
c	Convection
co	Combustion
cr	Critical
δ	Reaction order
e	External
f	Flame
F	Fuel
FO	Flashover
full	Full-scale
g	Gas/Gasification
i	Condensed phase species i
ig	Ignition
k	Gaseous species k
n_i	Reaction order
O ₂	Oxygen
p	Pyrolysis
r	Radiation
s	Surface
\cdot	Per unit time
$'$	Per unit length
∞	Ambient

ACRONYMS

CC	Cone calorimeter
CCAC	Controlled atmosphere cone calorimeter
FDM	Finite Difference Method
HRR	Heat release rate
MLR	Mass loss rate
N.A.	Not available
R/C	Room/Corner test
SBI	Single Burning Item
SEA	Smoke extinction area
SMOGRA	Smoke growth rate index
THR	Total heat release
TSP	Total smoke production

REFERENCES

1. NFPA 550: Guide to the Fire Safety Concepts Tree. National Fire Protection Association: Quincy, MA, 2012.
2. Janssens ML. Fundamentals of fire tests and what tests measure. In *Fire Retardancy of Polymeric Materials* (2nd edn). CRC Press: Boca Raton, 2012; 352.

3. ISO 13943: Fire Safety – Vocabulary. International Organization for Standardization: Geneva, Switzerland, 2008.
4. ISO/TS 3814: Standard Tests for Measuring Reaction-to-Fire of Products and Materials – Their Development and Application. International Organization for Standardization: Geneva, Switzerland, 2014.
5. Stec A, Hull R. *Fire Toxicity*. Great Abington: Woodhead Publishing; CRC Press: Boca Raton, 2010; 3.
6. Lautenberger CW. A generalized pyrolysis model for combustible solids, PhD thesis, University of California, Berkeley, 2007.
7. Croce PA, Grosshandler WL, Bukowski RW, Gritzo LA. The International FORUM of Fire Research Directors: a position paper on performance-based design for fire code applications. *Fire Safety Journal* 2007; **43**(3):234–236.
8. Bill RG, Croce PA. The International FORUM of Fire Research Directors: a position paper on small-scale measurements for next generation standards. *Fire Safety Journal* 2006; **41**(7):536–538.
9. Marquis DM, Pavageau M, Guillaume É. Multi-scale simulations of fire growth on a sandwich composite structure. *Journal of Fire Science* 2012; **31**(1):3–34.
10. Lautenberger CW, Hostikka S. Full-scale fire modeling. In *Fire Retardancy of Polymeric Materials* (2nd edn). CRC Press: Boca Raton, 2012; 551–585.
11. EN 13823:2002. Reaction to fire tests for building products – building products excluding floorings exposed to the thermal attack by a single burning item. European Committee for Standardization (CEN): Brussels, 2002.
12. ISO 9705: Fire Tests – Reaction-to-Fire – Full Scale Room Test for Surface Products. International Organization for Standardization: Geneva, Switzerland, 1993.
13. Janssens ML. A survey of methods to predict performance of wall linings in the Room/Corner test. Proceedings of the 3rd Technical Symposium on Computer Applications in Fire Protection Engineering. September 12–13 2001, Baltimore, USA. 2–13, 2001
14. Janssens ML. Module 7: Surface Flame Spread Tests. In: *Fire Assessment Methods*. University of Maryland, Course Literature: Course ENFP652, 2013; 1–49.
15. Moghtaderi B. The state-of-the-art in pyrolysis modelling of lignocellulosic solid fuels. *Fire and Materials* 2006; **30**(1):1–34.
16. Mcgrattan K, McDermott R. *Fire Dynamics Simulator User's Guide* (6th edn). National Institute of Standards and Technology: Washington, 2013.
17. Guillaume É. Survey on Fire Source Modelling from the International FORUM of Fire Research Directors: Unfinished, 2015. Retrieved information, August 28 2014: <http://www.iafss.org/survey-on-fire-source-modelling-from-the-international-forum-of-fire-research-directors/>
18. Janssens ML. Challenges in predicting the pyrolysis rate of solid materials. Proceedings of Fire and Materials 2015 Conference, San Francisco, USA, February 2–4 2015; 271–284.
19. ISO 5660-1: Reaction-to-Fire Tests – Heat Release, Smoke Production and Mass Loss Rate. Part 1: Heat Release Rate (Cone Calorimeter Method). International Organization for Standardization: Geneva, Switzerland, 2002.
20. Wickström U, Göransson U. Full-scale/bench-scale correlations of wall and ceiling linings. *Fire and Materials* 1992; **16**(1):15–22.
21. Van Hees P, Hertzberg T, Hansen AS. Development of a screening method for the SBI and room corner using the cone calorimeter, Borås, SP Report 11, 2002.
22. Kim EM, Dembsey N. Engineering guide for estimating material pyrolysis properties for fire modeling, Worchester, 2012.
23. Karlsson B, Quintiere JG. *Enclosure Fire Dynamics*. CRC Press: Boca Raton, 2000; 251.
24. Quintiere JG. Smoke measurements: an assessment of correlations between laboratory and full-scale experiments. *Fire and Materials* 1982; **6**(3):145–160.
25. Christian WJ, Waterman TE. Ability of small-scale tests to predict full-scale smoke production. *Fire Technology* 1971; **7**(4):332–344.
26. Babrauskas V. The generation of CO in bench-scale fire tests and the prediction for real-scale fires. *Fire and Materials* 1995; **19**(5):205–213.
27. Gottuk DT, Lattimer BY. Effect of combustion conditions on species production. In *SFPE Handbook of Fire Protection Engineering* (5th edn). Springer: New York, 2015; 486–528.
28. Johnsson EL, Bundy MF, Hamins A. Reduced-Scale Ventilation-Limited Enclosure Fires – Heat and Combustion Product Measurements. Interflam Conference Proceedings, London, UK, September 3–5, 2007; 415–426.
29. Tsantaris LD, Östman B. Smoke, Gas and Heat Release Data for Building Products in the Cone Calorimeter: Report 8903013, Stockholm, 1989.
30. Karlsson B. Modeling Fire Growth on Combustible Lining Materials in Enclosures, Report TVBB-1009, Lund, 1992.
31. Lattimer BY, Beyler CL. Predicting Fire Growth Involving Interior Finish Materials Including the Effects of Lateral Flame Spread and Layer Heating, Report NIST SP 998, National Institute of Standards and Technology, Gaithersburg, USA, 1999.
32. Lattimer BY, Hunt SP, Wright M, Sorathia U. Modeling fire growth in a combustible corner. *Fire Safety Journal* 2003; **38**(8):771–796.
33. Jia F, Galea E, Patel M. The numerical simulation of noncharring thermal degradation and its application to the prediction of compartment fire development. *Fire Safety Science – Proceedings of the 6th International Symposium (IAFSS 1999)*, Poitiers, France, July 5–9, 1999; 953–964.
34. Torero JL. Flaming ignition of solid fuels. In *SFPE Handbook of Fire Protection Engineering* (4th edn). National Fire Protection Association: Quincy, 2008; 2–260.

35. Janssens ML, Kimble J, Murphy D. Computer tools to determine material properties for fire growth modelling from cone calorimeter data. *Proceedings of Fire and Materials 2003 Conference*, San Francisco, USA, 2003; 377–387.
36. van Hees P. Wind Aided Flame Spread of Floor Coverings – Meestroomvlamuitbreiding bij Vloerbekledingen – Ontwikkeling en Validatie van Grootchalige en Kleinschalige Meettechnieken. PhD thesis, University of Ghent, Ghent, 1995.
37. Saito K, Quintiere JG, Williams FA. Upward turbulent flame spread. *Fire Safety Science – Proceedings of the 1st International Symposium (IAFSS 1985)*, Berkeley, USA, 1985; 75–86.
38. Thomas PH, Karlsson B. On Upward Flame Spread on Thick Fuels. Report LUTVDGmVBB 3058, Lund, 1992.
39. Mowrer FW, Williamson RB. Flame spread evaluation for thin interior finish materials. *Fire Safety Science – Proceedings of the 3rd International Symposium (IAFSS 1991)*, Edinburgh, UK, 1991; 689–698.
40. Janssens ML. Prediction of LIFT data from cone calorimetry. In *Heat Release in Fires*. Interscience Communications Limited: London, 2009; 299.
41. Van Hees P, Vandevelde P. Mathematical models for wind-aided flame spread of floor coverings. *Fire Safety Science – Proceedings of the 5th International Symposium (IAFSS 1997)*, Edinburgh, UK, 1997; 321–332.
42. Babrauskas V, Grayson SJ. *Heat Release in Fires*. Elsevier Applied Science: London, 1992; 299.
43. Delichatsios MM, Mathews MK, Delichatsios MA. An upward fire spread and growth simulation. *Fire Safety Science – Proceedings of the 3rd International Symposium (IAFSS 1991)*, Edinburgh, UK, 1991; 207–216.
44. Moghtaderi B, Novozhilov V, Fletcher DF, Kent JH. An Integral Model for the Pyrolysis of Non-Charring Materials. *Asia-Oceania Fire Science and Technology – Proceedings of the 2nd International Symposium (AOFST 1995)*, Russia, 1991; 308–319.
45. Yan Z, Holmstedt G. CFD and experimental studies of room fire growth on wall lining materials. *Fire Safety Journal* 1997; **27**(3):201–238.
46. Hermouet F, Guillaume É, Rogaume T, Richard F, Ponticq X. Determination of the fire behaviour of an acrylonitrile butadiene styrene material using a controlled atmosphere cone calorimeter. *Proceedings of Fire and Materials 2015 Conference*, February 2–4 2015, San Francisco, USA, 2015; 776–787.
47. Hermouet F, Guillaume É, Rogaume T, Richard F, Ponticq X, Marquis DM. Evaluation of the thermal decomposition of solid materials in tunnel related conditions with a controlled atmosphere cone calorimeter. *Proceedings of 3rd International Conference on Fires in Vehicles (FIVE 2014)*, October 1–2 2014, Berlin, Germany, 2014; 99–110.
48. Rogers FE, Ohlemiller TJ. Pyrolysis kinetics of a polyurethane foam by thermogravimetry; a general kinetic method. *Journal of Macromolecular Science: Part A – Chemistry* 1981; **15**(1):169–185. doi:10.1080/00222338108066438.
49. Ohlemiller TJ. Modelling of smoldering combustion propagation. *Progress in Energy and Combustion Science* 1985; **11**(4):277–310. doi:10.1016/0360-1285(85)90004-8.
50. Marquis D, Guillaume É, Camillo A, Rogaume T, Richard F. Existence and uniqueness of solutions of a differential equation system modelling the thermal decomposition of polymer materials. *Combustion and Flame* 2012; **160**(4):818–829.
51. Lautenberger C. Gpyro3D: a three dimensional generalized pyrolysis model. *Fire Safety Science – Proceedings of the 11th International Symposium (IAFSS 2014)*, Christchurch, NZ, 2014; 193–207.
52. Kempel F, Scharfel B, Linteris GT, Stoliarov SI, Lyon RE, Walters RN, Hofmann A. Prediction of the mass loss rate of polymer materials: impact of residue formation. *Combustion and Flame* 2012; **159**(9):2974–2984.
53. Camillo A. Multi-scale investigation of fire behaviour of a seat and a wall panel from European Railway Transport System. PhD thesis, University of Poitiers, France, 2013.
54. Guillaume É, Camillo A, Rogaume T. Application and limitations of a method based on pyrolysis models to simulate railway rolling stock fire scenarios. *Fire Technology* 2014; **50**(2):317–348.
55. Bustamante Valencia L. Experimental and numerical investigation of the thermal decomposition of materials at three scales: application to polyether polyurethane foam used in upholstered furniture. PhD thesis, University of Poitiers, France, 2009.
56. Marquis DM, Pavageau M, Guillaume É. Multi-scale simulations of fire growth on a sandwich composite structure. *Journal of Fire Sciences* 2012; **31**(1):3–34.
57. Marquis DM, Pavageau M, Guillaume É, Chivas-Joly C. Modelling decomposition and fire behaviour of small samples of a glass-fibre-reinforced polyester/balsa-cored sandwich material. *Fire & Materials* 2013; **37**(6):413–439.
58. Marquis DM, Pavageau M, Guillaume É, Chivas-Joly C, Bustamante Valencia L, Gutierrez J. Multi-scale simulation of the fire behaviour of a FRP sandwich composite – comparison of model results with experimental data. *Interflam Conference Proceedings*, Nottingham, UK, 2010; 407–418.
59. Fateh T, Rogaume T, Richard F. Multi-scale modeling of the thermal decomposition of fire retardant plywood. *Fire Safety Journal* 2014; **64**(2):36–47.
60. Batiot B. Étude et Modélisation de la Cinétique de Décomposition Thermique des Matériaux Solides. Application à la Dégradation du Bois en Cas d’Incendie. PhD thesis, University of Poitiers, France, 2014.
61. Carlsson J. Computational strategies in flame-spread modelling involving wooden surfaces -an evaluation study. MS Thesis, Lund University, Sweden, 2003.
62. Grexa O, Dietenberger MA, White RH. Reaction-to-Fire of Wood Products and Other Building Materials: Part 1, Room/Corner Test Performance, USDA Forest Service, Forest Products Laboratory, Report FPL-RP-663, US, 2012.


63. Dietenberger MA, Grexa O, Janssens ML, White RH. Predictions of ISO 9705 room/corner test using a simple model. Proceedings of Fire and Materials 1995 Conference, London, UK, 1995; 73–83.
64. Dietenberger MA, Grexa O. Correlation of smoke development in room tests with cone calorimeter data for wood products. Wood and Fire Safety – Proceedings of the 4th International Conference, May 14–19 2000, Strbske Pleso, Slovak Republic, 2000; 45–56.
65. Gollner MJ. Studies on upward flame spread. PhD thesis, University of California, San Diego, USA, 2012.
66. Grant G, Drysdale D. Numerical modelling of early flame spread in warehouse fires. *Fire Safety Journal* 1995; **24**(3):247–278.
67. Hansen AS, Hovde PJ. Prediction of time to flashover in the ISO 9705 room corner test based on cone calorimeter test results. *Fire and Materials* 2002; **26**(2):77–86.
68. Hansen AS, Hovde PJ. Prediction of smoke production based on statistical analyses and mathematical modelling. Interflam Proceedings 2001. Edinburgh, UK, 2001; 113–124.
69. Hansen AS, Hovde PJ. Prediction of smoke production in large and intermediate scale tests based on bench scale test results. A multivariate statistical analysis. Proceedings of Fire and Materials 2001 Conference, San Francisco, USA, 2001; 363–374.
70. Hasemi Y, Yoshida M, Nohara A, Nakabayashi T. Unsteady-state upward flame spreading velocity along vertical combustible solid and influence of external radiation on the flame spread. *Fire Safety Science – Proceedings of the 3rd International Symposium (IAFSS 1991)*, Edinburgh, UK, 1991; 197–206.
71. Hermouet F, Guillaume É, Rogaume T, Ponticq X. Development of an experimental design methodology adapted to controlled atmosphere cone calorimeter in order to evaluate the thermal degradation of solid materials in tunnel fires. *Tunnel Safety and Security – Proceedings of the 6th International Symposium*, Marseille, France, 2013.
72. Heskestad AW, Hovde PJ. Empirical prediction of smoke production in the ISO room corner fire test by use of ISO cone calorimeter fire test data. *Fire and Materials* 1999; **23**(4):193–199.
73. Hostikka S, Mcgrattan K. Large eddy simulation of wood combustion. Interflam Proceedings, Edinburgh, UK, 2001; 755–762.
74. Janssens ML. A Simple Model of the ISO 9705 Ignition Source. In Abstracts of the Annual Conference on Fire Research, Report NISTIR 5904, National Institute of Standards and Technology, Gaithersburg, MD, 1996; 87–88.
75. Karlsson B. Calculating flame spread and heat release rate in the room/corner test, taking account of preheating by the hot gas layer. Interflam Proceedings, March 30–April 1 1993, London, UK; 1993; 25–37.
76. Karlsson B. A mathematical model for calculating heat release rate in the room corner test. *Fire Safety Journal* 1993; **20**(2):93–113.
77. Karlsson B. Models for calculating flame spread on wall lining materials and the resulting heat release rate in a room. *Fire Safety Journal* 1995; **23**(4):365–386.
78. Kwon JW, Dembsey N, Lautenberger C. Evaluation of FDS V.4: upward flame spread. *Fire Technology* 2007; **43**[4]: 255–284.
79. Beyler CL, Hunt SP, Iqbal N, Williams FW. A computer model of upward flame spread on vertical surfaces. *Fire Safety Science – Proceedings of the 5th International Symposium (IAFSS 1997)*, Edinburgh, UK, 1997; 297–308.
80. Linteris GT, Gewuerz L, McGrattan K, Forney G. Modeling solid sample burning. *Fire Safety Science – Proceedings of the 8th International Symposium (IAFSS 2005)*, Beijing, China, 2005; 625–636.
81. Magnusson SE, Sundström B. Combustible Linings and Room Fire Growth : A First Analysis, Report STP882, Lund, 1985.
82. Marquis DM, Pavageau M, Guillaume É, Chivas-Joly C. Modelling decomposition and fire behaviour of small samples of a glass-fibre-reinforced polyester/balsa-cored sandwich material. *Fire and Materials* 2013; **37**(6):413–439.
83. Mitler HE, Steckler KD. Spread: a model of flame spread on vertical surfaces, Report NISTIR 5619, National Institute of Standards and Technology, Gaithersburg, MD, 1997.
84. Moghaddam AZ, Moinuddin K, Thomas IR, Bennetts ID, Culton M. Fire behaviour studies of combustible wall linings applying fire dynamics simulator. 15th Australasian Fluid Mechanics Conference, December 13–17 2004 Sydney, Australia, 2004; 1–4.
85. Opstad K. Modelling of Thermal Flame Spread on Solid Surfaces in Large-Scale Fires, MTF Report 1995:114 (D), University of Trondheim, Trondheim, Norway, 1995.
86. Smith E, Satiya S. Release rate model for developing fires. *Journal of Heat Transfer* 1983; **105**(2):281–287.
87. Dickens ED, Smith GF. The use of computer fire models in corner burn tests. *Fire Technology* 1985; **21**(2):85–104.
88. Janssens ML. Critical analysis of the OSU room fire model for simulating corner fires. In Fire and Flammability of Furnishings and Contents, 169–185, ASTM Report STP1233, American Society for Testing Materials, Philadelphia, USA, 1994.
89. Quintiere JG, Harkleroad M, Hasemi Y. Wall flames and implications for upward flame spread. *Combustion Science and Technology* 1986; **48**(3–4):191–222.
90. Quintiere JG. A simulation model for fire growth on materials subject to a room-corner test. *Fire Safety Journal* 1993; **20**(4):313–339.
91. Quintiere JG. Estimating fire growth on compartment interior finish materials. Department of Fire Protection Engineering, University of Maryland, MD, 1995.
92. Quintiere JG, Haynes G, Rhodes BT. Applications of a model to predict flame spread over interior finish materials in a compartment. *Journal of Fire Protection Engineering* 1995; **7**(1):1–13.

93. Dillon S, Kim W, Quintiere JG. Determination of properties and the prediction of the energy release rate of materials in the ISO 9705 room-corner test. Report NIST-GCR-98-753, National Institute of Standards and Technology, Gaithersburg, USA, 1998.
94. Steckler K. Calculations of wall fire spread in an enclosure. Report LA-9911-C-VOL.2 National Bureau of Standards, Washington, USA, 1983.
95. van Hees P, Vandeveldel P. Wind aided flame spread of floor coverings – development and evaluation of small and large scale tests. *Interflam Proceedings*, London, UK, 1993; 57–68.
96. Wade C. Room-corner fire model including fire growth on linings and enclosure smoke-filling. *Journal of Fire Protection Engineering* 1996; **8**(4):183–193.
97. Wang Z, Hu X, Jia F, Galea ER. A Two-step method for predicting time to flashover in room corner test fires using cone calorimeter data. *Fire and Materials* 2013; **37**(6):457–473.
98. Östman BA, Nussbaum R. Correlation between small-scale rate of heat release and full-scale room flashover for surface linings. *Fire Safety Science – Proceedings of the 2nd International Symposium (IAFSS 1988)*, Beijing, China, 1988; 823–832.
99. Östman BA, Tsantaridis LD. Smoke production in the cone calorimeter and the room fire test. *Fire Safety Journal* 1991; **17**(1):27–43.
100. Bal N. Uncertainty and complexity in pyrolysis modelling. PhD thesis. University of Edinburgh, Edinburgh, UK, 2012.
101. McCaffrey BJ, Quintiere JG, Harkleroad MF. Estimating room temperatures and the likelihood of flashover using fire test data correlations. *Fire Technology* 1981; **17**(2):139–148.
102. Johansson N, van Hees P. A correlation for predicting smoke layer temperature in a room adjacent to a room involved in a pre-flashover fire. *Fire and Materials* 2012; **38**(2):182–193.
103. Janssens M. Reducing Uncertainty of Quantifying the Burning Rate of Upholstered Furniture. Report 01.15998, Southwest Research Institute, San Antonio, USA, 2012.
104. Ezinwa JU, Robson LD, Obach MR, Torvi DA, Weckman EJ. Evaluating models for predicting full-scale fire behaviour of polyurethane foam using cone calorimeter data. *Fire and Technology* 2011; **50**(3):693–719.
105. Rich D, Lautenberger C, Torero JL, Quintiere JG, Fernandez-Pello C. Mass flux of combustible solids at piloted ignition. *Proceedings of the Combustion Institute* 2007; **31**(2):2653–2660.
106. Drysdale D. *An Introduction to Fire Dynamics* (2nd edn). John Wiley & Sons: Chichester, UK, 1998; 222.
107. Drysdale D. The production and movement of smoke. In *An Introduction to Fire Dynamics* (2nd edn). John Wiley & Sons: Chichester, UK, 1998; 373.
108. Babrauskas V, Peacock RD. Heat Release Rate: The Single Most Important Variable in Fire Hazard. *Fire Safety Journal* 1992; **18**(3):255–272.
109. Onate E, Rossi R, Idelsohn SR, Butler KM. Melting and Spread of Polymers in Fire with the Particle Finite Element Method. *Numerical Methods in Engineering* 2009; **81**(8):1046–1072.

Paper II



Experimental assessment of bench-scale ignitability parameters

Frida Vermina Plathner^{1,2}  | Patrick van Hees¹

¹Division of Fire Safety Engineering, Lund University, PO Box 118, SE-221 00 Lund, Sweden

²RISE Research Institutes of Sweden, PO Box 857, SE-501 15 Borås, Sweden

Correspondence

Frida Vermina Plathner, RISE Research Institutes of Sweden, PO Box 857, SE-501 15, Borås, Sweden.

Email: frida.vermina.lundstrom@ri.se

Funding information

European Union's Seventh Framework Programme, Grant/Award Number: 316991

Summary

This work aims to explore possible ways of improving the precision of ignition measurements in the cone calorimeter. Both inherent repeatability of parts of the testing equipment and operator-dependent variations are considered. Inherent repeatability is indicated to be slightly improved if the test samples used are circular rather than square. Operator-dependent variation is discussed in terms of the method used for determining ignition. Four procedures are compared, namely, visual observation, usage of a light sensor, and looking at the peak of the second and first derivatives of the mass loss and heat release curves, respectively. Results indicate that the preferable operator-independent method depends on the test conditions; the derivative of the heat release rate is an alternative to the mass loss rate derivative when the scale is of standardised quality. A light sensor for ignition time observation is a good option when the surrounding light is not changed during the test.

KEYWORDS

critical energy flux, critical mass flux, plastics, sustained ignition

1 | INTRODUCTION

When selecting materials for any building application, it is necessary to consider their fire performance. For this purpose, bench-scale tests act as a tool for product development, screening of materials, and for property input in prediction models. The ISO 5660 cone calorimeter¹ is one of the common bench-scale tests that was primarily developed for measuring heat release rate (HRR) of solids.² But it has also been used for measurements of ignition properties such as time to ignition, ignition temperature, and critical radiant heat flux.³

Along with an increasing complexity of fire models where additional and more precise input properties are required, experimental work needs a contending progress.⁴ For instance, modellers now have the option to model ignition of condensed-phase fuels by the use of a critical mass loss or HRR.^{5,6} However, most experimental measures of these properties are approximate and dependent on test apparatus, operator, and possible differences in sample preparation. Just as with surface temperature, there is a rapid increase of the mass flow rate

just after ignition. The sharp increase may introduce a large error when determining the critical mass flow rate at ignition.⁷ Tewarson,⁸ for instance, reports an average critical heat release rate (CHRR) in the fire propagation apparatus (FPA) of 96 kW/m² ranging from 65 to 108 kW/m² for a number of polymers like polyethylene, polyurethane, and polystyrene. Quintiere⁹ mentions 50 kW/m² as the condition for sustained ignition in the cone calorimeter. However, these numbers are dependent on the convective heat transfer coefficient in the test apparatus.^{10–12} Different studies and experimental setups show heavy variation, as indicated in Table 1, where critical mass flow rates for sustained ignition have been measured under natural or mild convective conditions.¹³

Piloted ignition of a combustible material under heating is initiated with the build-up of pyrolysis gases in the vicinity of the solid surface. These decomposition products enter the air where they mix. When the fuel-gas mixture is approximately at the lower flammability limit close to the spark igniter, the gases may ignite, with a premixed flame propagating toward the fuel surface. This event is often referred to as the flash point, relating to the temperature of the fuel surface at the time of the flash.¹⁴ If the generation rate of pyrolysis gases is sufficient for a sustained flame, the flame anchors at the fuel surface. The flame then rapidly spreads out to involve burning of the full fuel

Nomenclature: CMLR, critical mass loss rate; dHRR, derivative of heat release rate (kW/m²/s); dMLR, derivative of mass loss rate (g/m²/s²); HRR, heat release rate (kW/m²); MLR, mass loss rate (g/m²/s); t, time

Subscripts: ig, ignition

TABLE 1 Variation in critical mass flux found in the literature

Material	Critical Mass Loss Rate, $\text{g}/\text{m}^2/\text{s}$
Polymethylmethacrylate	1.9-3.2
Polyoxymethylene	1.7-4.5
Polyethylene	1.3-2.5
Polypropylene	1.1-2.7
Polystyrene	0.8-4.0

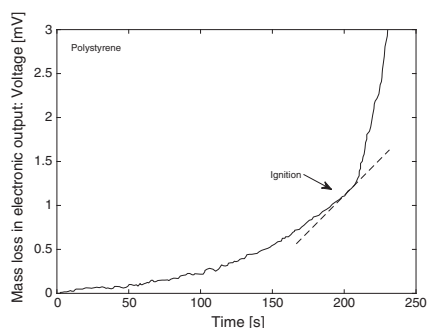
Reproduced from Lyon and Quintiere.¹³

surface. The moment of a nascent flame is the fire point. In a previous study,¹² full surface involvement of a sample is defined as the "anchor point." This moment in time is also the onset of quasi-steady burning.

Another way to describe sustained ignition is the transition from a nonreactive state to that where a reaction is self-sustained. This process is sometimes described by a thermochemical runaway in the system.¹⁵ In common experimental apparatuses for flammability of solids and liquids, this is seen by, eg, a rapid increase of heat produced in the HRR curve or by an increase in the mass loss rate. Previous studies have been using the definition of a thermochemical runaway to attain flammability parameters. For instance, Drysdale and Thomson fitted the mass loss curve to a cubic expression up to the point of ignition, then differentiating the curve to retrieve a critical mass loss rate (CMLR) at the measured time to ignition. In Figure 1 the increase in mass loss rate is reproduced from Drysdale and Thomson.¹⁰

Khan and de Ris¹⁶ showed that the time to ignition and CMLR could be determined independently of the operator by processing the mass loss data in the FPA. In this method ignition is proposed to occur when the second derivative of the time-dependent mass loss curve reaches its peak. In other words, it is the point at which the mass loss rate increases most rapidly.

Variation in results may stem not only from various operators but also from differences in test apparatuses, and even the sample preparation method may play a role. Differences between test apparatuses and sample sizes are mainly related to different flow conditions¹⁷ and are outside the scope of this study. Regarding the sample preparation method, it is common to follow the standard procedure of the specific

**FIGURE 1** Critical mass loss rate, reproduced from Drysdale and Thomson¹⁰

apparatus. The standard procedure in the cone calorimeter is testing a square shaped specimen. However, the corner areas of a square sample receive a lower heat flux from the irradiating cone.¹⁸ The effect of this nonuniform heat exposure is more pronounced in the burning of some materials, eg, shrinking flexible polyurethane foam¹⁹ or low-combustibility materials.¹⁸ Previous studies have therefore also elaborated with larger cones and samples¹⁸ or cylinder-shaped samples, in order to eliminate some of the effects of nonuniform exposure.^{20,21}

Many research studies have stated critical mass rates for various materials received in the cone calorimeter. Few studies have, however, examined the testing procedure itself. An experimental study was performed at Lund University to explore possibilities of improving the reproducibility of ignition measurements in the cone calorimeter.

2 | AIM AND OBJECTIVES

This work aims to explore possible ways of minimising the scatter of ignition measurements in the cone calorimeter by investigating different ignition criteria and by trying to improve sample preparation. The specific objectives of the study are the following:

- Compare repeatability of ignition measurements by the use of circular samples with nearly adiabatic boundaries vs square samples prepared according to the ISO standard.

It is hypothesised that testing repeatability may be improved by ensuring a uniform heat flux to the sample—and circular samples are assumed to remove some of the boundary problems generated by the heating of sample corners. Also, well-insulated sample sides are assumed to create nearly adiabatic boundaries.

- Develop and compare repeatability of operator-independent methods for determining ignition.

Some amount of the operator-induced error for ignition may be claimed to stem from the visual determination of ignition according to the ISO 5660 standard procedure; thus, alternatives are explored.

3 | EXPERIMENTAL

3.1 | Testing method and property definitions

The ISO 5660 cone calorimeter¹ is designed to study fire behaviour of small solid samples. Its name originates from the conical shape of the radiant heater, which is constructed to irradiate a nearly uniform heat flux over the sample surface. The ISO standard requires a uniform irradiance upon the sample within the central area of 50 by 50 mm.¹ In this study, samples were subjected to heat fluxes of 20, 30, 35, 40, and 50 kW/m^2 .

The tests included measurements and derivation of time to ignition, critical mass flow rate, and CHRR. Time to ignition consists of 3 components: (1) The pyrolysis time is characterised by the time required to heat up the solid from an ambient temperature to the temperature at which it starts releasing volatiles. (2) The flammable

mixture time is the time it takes for the increasing amounts of pyrolysis gases to leave the surface, mix with air, and build up a flammable mixture by the spark ignitor. This is dependent on geometry, flow, and fuel properties. (3) If the temperature of the gas mixture is increased and the gas-phase reactions are self-sustained, ignition occurs. This induction time corresponds to the time it takes to heat up the mixture to an ignition temperature. Component (1) is generally much larger than components (2) and (3); thus, ignition time is usually assumed equal to the pyrolysis time.

Critical mass flow rate is defined as the minimum mass flow rate from the fuel surface for a nascent flame. A related criterion—CHRR—was developed by Lyon and Quintiere¹³ because of its independence of fuel type, as opposed to the time to ignition and critical mass flow rate. The CHRR is the minimum rate of energy release produced in a nascent flame. It is *not* synonymous with critical (incident) heat flux, which is another ignitability property.

3.2 | Materials

Five plastics were tested, namely, polyamide (PA6), polyethylene (HD-PE), polyoxymethylene (POM-C), polypropylene (PP), and polyvinylchloride (PVC) (see Table 2). The motivation of material choice is 3-fold: (1) availability; (2) available studies using these plastics exist,^{8,10,13} which simplifies comparison of methods; and (3) the built environment contains plastic components at an increasing rate. The wide range of applications that the plastics exhibit can be seen in the publication by Martienssen and Warlimont.²³

3.3 | Samples

In order to see if the inherent repeatability of the equipment could be improved, 2 sets of experiments were conducted. One set used standard square samples (0.01 m²), and the other set involved circular samples ($d = 75$ mm). The reasoning behind using circular samples was that the cone-shaped heater provides a more uniform heat flux towards a circular specimen than towards a square. In addition, a circular specimen allows for simulating the heat transfer with a 1-dimensional model.²¹ The diameter was chosen to be 75 mm in order to be able to insulate the sides of the specimen properly. Circular specimens may, for instance, be cut with a water jet cutter, a laser cutter, or even with a drill using a circular cutter drill bit, a band saw, or a fly cutter. Well-insulated sample sides of the circular samples are assumed to create nearly adiabatic boundaries, causing a resemblance to one-dimensional heat transfer, which is not the case for the traditional samples in the cone calorimeter.

The square samples were prepared and tested according to the ISO 5660 standard¹; ie, each sample was wrapped in aluminium foil and placed onto a ceramic fibre blanket in a stainless steel retainer frame. The circular samples required an interim sample holder, seen in Figure 2. The specimens were wrapped with aluminium foil and insulated with several layers of 3 mm Kaowool ceramic paper in the bottom and on the sides of a sample holder. The ceramic insulation was finally enfolded with aluminium tape, as suggested by de Ris and Khan²⁰ and also in the ISO 5660 procedure where aluminium foil is being used.

To ensure that the ceramic paper did not affect mass and heat release recordings, eg, due to water release, a test was conducted containing only ceramic paper, in order to control the amount of mass released after one and after several tests. This test did not show any significant mass loss or heat release of the paper. After each test, the holder was left to dry in case the ceramic paper absorbed water. There was no desiccator at hand; therefore, the holder was also weighed before each test to control that water had not been absorbed. The sample holder with ceramic paper weighed approximately the same before every test, indicating that water interfering with material test results was not an issue.

3.4 | Reducing operator-dependent variations: 4 methods to determine ignition time

Both mass loss rate and HRR at ignition are commonly found by evaluating the mass loss rate or energy release rate at the instant of a sustained flame. Time to ignition was experimentally determined with 4 methods, which are presented below. The 2 first are commonly employed methods and the latter 2 were developed for this study.

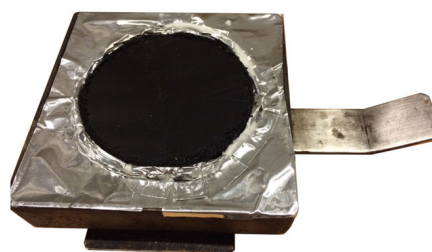


FIGURE 2 Insulated circular sample [Colour figure can be viewed at wileyonlinelibrary.com]

TABLE 2 Materials from Elfa Distrelec²²

Material	Measured Heat of Combustion, MJ/kg	Thickness, m	Density, kg/m ³
Polyamide (PA6)	31.4	0.010	1140
Polyethylene (HD-PE)	46.4	0.012	950
Polyoxymethylene (POM-C)	17.0	0.012	1410
Polypropylene (PP)	44.0	0.015	910
Polyvinylchloride (PVC)	18.0	0.012	1420

1. Visual observation

The ISO 5660 standard procedure to detect ignition in the cone calorimeter is by visual determination. The operator pushes a button on the recording instrumentation when a sustained flame is seen, and this is logged by the cone software as the time to ignition. The flame is supposed to exist on or over the test specimen surface for a duration of at least 10 seconds.¹

2. Peak of the second derivative of mass loss curve

As previously mentioned, Khan and de Ris¹⁶ showed that the time to ignition in the FPA could be determined independently of the operator by processing the mass loss data. In this method, ignition is proposed to occur when the second derivative of the time-dependent mass loss curve reaches its peak. In other words, it is the point in which the mass loss rate increases most rapidly. The mass loss data were analysed according to the Khan and de Ris method. Due to noise in the mass loss data and amplification of noise in the derivatives, it was necessary to smooth the data prior to evaluation of the peak. This was conducted using a fourth-order Savitski-Golay filtering method, also suggested by Khan and de Ris.¹⁶

3. Peak of the first derivative of HRR curve

Analogous to the method by Khan and de Ris, a mathematical model was developed based upon the first derivative of the HRR curve. That is, the time at which the HRR increases most rapidly, a peak is established in the derivative of the HRR curve. This peak (dHRR) was used for analysing time to ignition data and CHRR s.

4. Peak of the first derivative of light measurements

Another way of determining ignition is by light detection. A light sensor consisting of a fast response CdS photoconductive cell (Lida Optical and Electronic Co. Ltd., part no. GL5528) was enclosed in a metal housing and protected from heat with a glass shield (see Figure 3). The light sensor gave an analogue voltage output proportional to incoming light, which was received by a dataTaker, model no DT85. For this study, there was no need to convert the voltage output to units in Lux, as the 2 peaks concur. The ceiling lighting above the light sensor was slightly toned down.



FIGURE 3 Light sensor [Colour figure can be viewed at wileyonlinelibrary.com]

4 | DATA ANALYSIS

4.1 | Repeatability

The repeatability is the inherent precision of the test apparatus, ie, the closeness of successive test results under the same conditions, by the same operator in the same apparatus. In this work, 3 repeats were conducted for each test, as suggested by National Institute of Standards and Technology.²⁴ Average, standard deviations and coefficients of variation were calculated to compare repeatability between tests.

4.2 | Delay time

An important consideration is the delay time of the experimental readings. Measurements must be placed simultaneously in time with the physical event so that measurements are comparable. The delay time for mass loss and light readings consists only of the response time of the individual instruments; however, the delay time for the gas analysis upon which the HRR curve is based consists of both the transit time of gases from the sample to the analyser and the response time of the measuring instrument.

4.3 | Noise reduction

Khan and de Ris¹⁶ suggested a 19-point Savitski-Golay smoothing for the first derivative of mass loss data and a 25-point Savitski-Golay smoothing for the second derivative. This was used for filtering mass loss, heat release, and light sensor output.

5 | RESULTS AND DISCUSSION

5.1 | Inherent repeatability: Circular vs square samples

Table 3 shows an example of the repeatability for the 2 sets of circular and square samples at an irradiance of 35 kW/m² based on the peak of the first derivative of the HRR curve. The coefficient of variation, which is the normalised standard deviation, is generally somewhat smaller for the circular samples, indicating that the repeatability is higher using circular specimens.

Another result from Table 3 is that there is an observed difference between means for circular and square samples. From a statistical *t*-test analysis, it is seen that there is a significant effect for polypropylene ($t(4) = 3.14, P < .05$, where square samples have longer ignition time than circular. However, when correcting for multiple hypothesis testing using the Bonferroni method²⁵ for the 5 tested materials ($P = .05/5$), there is no significant difference. The other specimens did not show statistically significant differences.

There also seem to be high outliers for the square specimens in HD-PE and PVC measurements that skew the coefficient of variation to higher values than for the circular specimens. Although not statistically divergent, the trend of shorter ignition times for the circular samples raises awareness. Initially, it was thought that the observed difference was because of a thickening of the boundary layer (an increase of the convective heat transfer coefficient) with an increase

TABLE 3 Comparison of time to ignition of circular and square samples at 35 kW/m², based on dHRR measurements

		Time to Ignition, Based on the Peak of dHRR				
		PA6	HD-PE	POM-C	PP	PVC
Circular sample	Rep. 1	76	110	65	50	71
	Rep. 2	67	104	62	49	79
	Rep. 3	68	112	69	54	74
	Average	70	109	65	51	75
	Std	4	3	3	2	3
CV (%)	6	3	4	4	4	
Square sample	Rep. 1	68	127 (130) ^a	76	61 (62) ^a	69
	Rep. 2	73	108	85	59	80
	Rep. 3	77	113	68	55	72
	Average μ (s)	73	116	76	58	74
	Std σ (s)	4	8	7	2	5
CV (%)	5	8	9	5	6	

Abbreviations: CV, coefficient of variation; dHRR, derivative of heat release rate; HD-PE, polyethylene; PA6, polyamide; POM-C, polyoxymethylene; PP, polypropylene; PVC, polyvinylchloride.

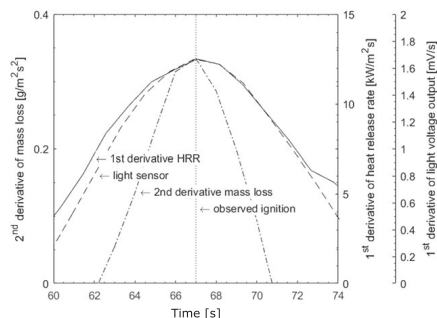
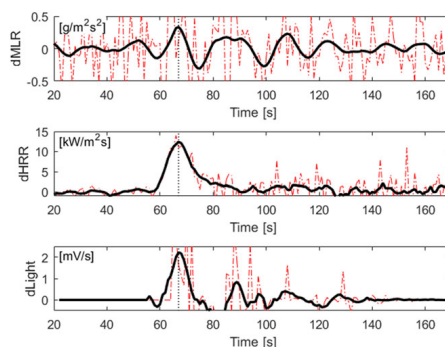
^aNumbers in brackets display observed time to ignition, where it differs from dHRR.

in sample size from circular to square. Buoyancy effects are dependent on sample size,¹⁷ although this dependency may be weak.²⁶ It seems reasonable to assume that the trend is more related to differences in sample design, with different amounts and type of insulation on the sides. In other words, the longer ignition times for the square samples are attributed to the heat-sink effect from the steel framed sample holder, where the circular specimens are well insulated. The well-insulated sides of the circular specimen create a resemblance to 1-dimensional heat transfer. This will consecutively simplify future pyrolysis modelling in the cone calorimeter. However, more data are needed in order to prove this hypothesis.

5.2 | Reducing operator-dependent variations: 4 methods to determine ignition time

The 4 proposed methods provide a relatively concurring view of the ignition times of the investigated materials; however, using the first derivative of mass loss measurements provided inaccurate results for some tests; the reason is explained below. In a few measurements (9%), the observed ignition time does not concur with the other methods. This indicates that a routine relying on the operator may not be as repeatable as methods based on fire behaviour data.

In Figures 4 and 5, an example is given for the peaks of PA6, showing a case where all methods give identical results for the time to ignition. It is also seen that the peaks vary in width. An initial evaluation of peak widths for similar peak heights would lead to a conclusion that a peak in the second derivative of the mass loss (dMLR) is sharper than one given by the first derivative of the HRR curve (dHRR)—and is therefore preferable. However, by zooming out to a larger time window (Figure 5), it is seen that the ignition peak is vague compared with other peaks that do not reflect “true” signals. The dMLR peaks at ignition are on average 50% larger than the second largest peak, while the dHRR peaks at ignition are 300% larger than the second largest peak. In some cases (~20% of the data), the largest dMLR peak is not found at ignition. On the other hand, dHRR

**FIGURE 4** Comparison of techniques for evaluating ignition time, for PA6, circular sample**FIGURE 5** Comparison of techniques for evaluating ignition time, large time window, for PA6, circular sample [Colour figure can be viewed at wileyonlinelibrary.com]

measurements give peaks that concur with ignition when looking at the larger time span, as seen in Figure 5.

Also, the second derivative of the mass loss curve includes a time history smothered by noise. The mass flux derivative in this example (Figure 5) cannot be used as an indication of ignition because the signal-to-noise ratio at 67 seconds is not significant and so it cannot be reliably detected. Although the program accurately read this as the time to ignition, it is probable that the ignition event could have been detected elsewhere on the x-axis in this example. The sample weight in Khan and de Ris' experiments was recorded each second by averaging 100 readings per second.¹⁶ A scale employed for standard cone calorimeter testing (as in this study) read sample weight data at a maximum speed of one time per second. Inevitably nonaveraged measurements do not have the same quality. Additional attempts of smoothing the dMLR curve have been conducted, but the “true” peak vanishes with a too strong filtering.

Table 4 provides a more complete view of the data for the circular samples. It supports the deduction in Figure 5 of dHRR being a more

TABLE 4 Comparison of average (μ), standard deviation (σ), and coefficient of variation (CV) for time to ignition between 3 of the methods (circular samples)

Polymer	Heat Flux (kW/m ²)	t_{obs}			t_{dMLR}			t_{dHRR}		
		μ	σ	CV, %	μ	σ	CV, %	μ	σ	CV, %
PA-6	20	603	20	3	613	6	1	608	6	1
	30	136	7	6	136	7	6	136	7	6
	35	70	4	6	70	4	6	70	4	6
	40	56	5	10	NP	NP	NP	56	5	10
	50	32	6	19	NP	NP	NP	32	6	19
HD-PE	20	NI	NI	NI	NI	NI	NI	NI	NI	NI
	30	202	25	12	202	25	12	202	25	12
	35	109	3	3	109	3	3	109	3	3
	40	44	4	9	44	4	9	44	4	9
	50	35	1	3	35	1	3	35	1	3
POM-C	20 ^a	341	ND	ND	NP	NP	NP	341	ND	ND
	30	116	6	5	116	6	5	116	6	5
	35	65	3	4	65	3	4	65	3	4
	40	44	3	7	44	3	7	44	3	7
	50	35	5	16	35	5	16	35	5	16
PP	20	215	41	20	NP	NP	NP	201	42	21
	30	74	3	4	74	3	4	74	3	4
	35	51	2	4	51	2	4	51	2	4
	40	ND	ND	ND	ND	ND	ND	ND	ND	ND
	50	34	5	14	34	5	14	34	5	14
PVC	20	NI	NI	NI	NI	NI	NI	NI	NI	NI
	30	109	5	4	109	5	4	109	5	4
	35	75	3	4	75	3	4	75	3	4
	40	ND	ND	ND	ND	ND	ND	ND	ND	ND
	50	41	3	7	42	3	7	42	3	7

Abbreviations: ND, not enough data available; NP, at least one of the maximum peaks does not occur at ignition; NI, no ignition.

^aOnly 2 out of 3 samples ignited.

robust method than dMLR for retrieving ignition measurements, because there are several peaks in the dMLR data that are larger than the ignition peak. These measurements are denoted NP in Table 4. It is also seen that observed ignition time and "calculated" ignition time via dHRR give similar results. In some cases, a low heat flux does not lead to an ignited sample (denoted NI in Table 4).

One of the benefits of dHRR and light measurements is that they could act as ways towards automating ignitability measurements for the cone calorimeter and for other bench-scale tests, independent of the operator. One drawback with both techniques is that there is no way to evaluate nonattached flames. The light sensor captures flashes; however, flashes or other disturbances of the signal give peaks that may be evaluated as sustained ignition.

As the diffusion flame anchors to the specimen sample, the flame is not covering the entire sample but grows rapidly out to the sample edges. The time it takes for the flame to spread to the sample edges depends on the material, and therefore, different HRR peak sizes are expected. For the investigated materials in this paper, this "flame spread time" is approximately in the order of ~1 to 2 seconds. Therefore, a small time lag could also be expected. However, the dHRR is considered a sufficient approximation, following Khan and de Ris.

Table 5 indicates physical evidence of combustion energy (critical HRR) as the correct criterion for ignition. Critical HRR (HRR*) in the table is retrieved from the oxygen consumption measurements. A second way to calculate critical HRR is from the mass loss measurements (MLR* Δh_c). It is seen that the 2 methods produce similar results and

that the method with oxygen consumption gives a slightly lower coefficient of variation.

5.3 | Summarising experimental data

To investigate if accuracy is improved by employing our preferred techniques (circular samples and evaluating ignition by the peak of the first derivative of the HRR curve), 2 data plots are drawn: Figure 6 shows an overview of the CHRRs obtained for the various materials, and Figure 7 is the critical mass flow rate plotted against the incident heat flux.

TABLE 5 Comparison of mass flux and heat release rate criteria for ignition of different materials

Polymer	HRR* (kW/m ²)	MLR* (g/m ² /s)	Δh_c (kJ/g)	MLR* Δh_c (kW/m ²)
POM-C	59 ± 8	3.3 ± 0.5	17.0	56 ± 8
PVC	48 ± 2	2.7 ± 0.1	18.0	48 ± 2
PA6	57 ± 8	1.8 ± 0.3	31.4	58 ± 9
HD-PE	59 ± 10	1.2 ± 0.2	46.4	58 ± 10
PP	60 ± 4	1.4 ± 0.1	44.0	59 ± 5
Average:	57 ± 8	2.1 ± 0.8		56 ± 8
CV (%)	14	41		15

Abbreviations: CV, coefficient of variation; HD-PE, polyethylene; PA6, polyamide; POM-C, polyoxymethylene; PP, polypropylene; PVC, polyvinylchloride.

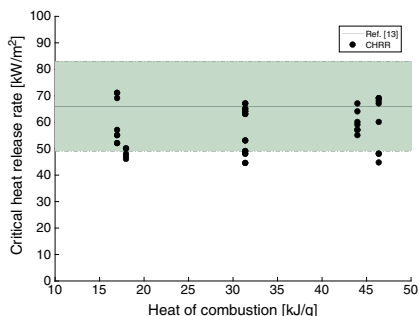


FIGURE 6 A constant trend: the critical heat release rate, circular samples [Colour figure can be viewed at wileyonlinelibrary.com]

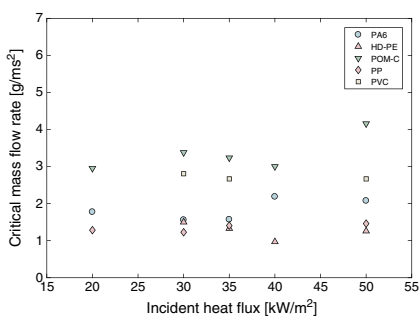


FIGURE 7 Influence of incident heat flux on the critical mass flow rate, circular samples [Colour figure can be viewed at wileyonlinelibrary.com]

There is a distinct scatter in Figure 6, but the data lie approximately within the range of what was measured by Lyon and Quintiere ($66 \pm 17 \text{ kWh/m}^2$).¹³ The reduced distribution ($58 \pm 9 \text{ kWh/m}^2$) in this work is likely more related to the fact that fewer materials were tested rather than the test method. Figure 6 and Table 5 also support the statement that a fixed CHRR is suitable for a variety of fuels. Therefore, it is reasonable to assume that this statement holds also for tests in other conditions. However, an important notion is that a fixed CHRR in other conditions is different because of the different boundary and environmental conditions. This consideration is not essential for the dHRR method.

As can be seen in Figure 7, the critical mass flow rate is scattered and any trend with incident heat flux is either weak or negligible. This result is in line with Thomson and Drysdale²⁷ and Panagiotou and Quintiere,²⁸ who showed that the critical mass flow rate for a number of plastics did not vary with incident heat flux, although there were exceptions, like ABS.

Piloted ignition is not bound to occur at the exact instant that the mass flow rate reaches its critical value. A more accurate description would be that sustained ignition occurs as a flammable mixture forms near the spark ignitor. In other words, the physical event of sustained ignition and the time it takes for the solid to release a critical mass

flow rate does not coincide. The spark energy and the gas transport time between the sample surface and the spark ignitor may introduce some error in the measurement. Also, by looking at the mass loss rate curve for different of incident heat fluxes, it is seen that the mass loss increases more rapidly at ignition at higher heat fluxes. Thus, larger errors in mass loss are hypothetically introduced for high heat fluxes than for low, while the uncertainty in time to ignition is apparently lower. This may be a possible reason for why our results differ from other studies claiming that the critical mass flow rate at sustained ignition is dependent on the incident radiant heat flux for both noncharring^{10,29,30} and charring^{7,31} polymers. This correlation is not found when ignition is evaluated with "operator-independent" methods.

6 | CONCLUSIONS

Five plastics have been tested at several incident heat fluxes in the cone calorimeter in order to investigate precision in ignitability measurements. Two sets of experiments have been conducted: one with standard square samples and one set with circular samples. Four different ways of determining ignition have been considered. The following concluding remarks are made from the study:

1. Circular samples show a slightly better repeatability of ignition results compared with square samples in the cone calorimeter.
2. Well-insulated sample sides create nearly adiabatic boundaries, which causes a resemblance to 1-dimensional heat transfer. This will simplify pyrolysis modelling in bench-scale.
3. A reliable method for determining when ignition occurs has been developed and validated, based on evaluation of the peak of the first derivative of the HRR curve. This method is a variant of Khan and de Ris's mass loss rate method and is beneficial in many standard cone calorimeters because oxygen consumption measurements are normally less noisy than mass loss data. Unlike a fixed CHRR, the method is not dependent on environmental- or boundary conditions.
4. A light sensor is proposed as another reliable method to determine ignition, giving sharp peaks for both flashing and sustained flames. The device is reliable if there are no changes in the surrounding light.
5. By using an operator-independent method, it is seen that (a) the CHRR is approximately independent of fuel type and (b) the CMLR for ignition does not show any clear trend with imposed radiant heat flux for the investigated materials.
6. Experimental data indicate physical evidence of a CHRR as ignition criterion

ACKNOWLEDGEMENTS AND FUNDING

The authors of this study would especially like to thank Konrad Wilkens for developing the light sensor used in this work. This study is part of FIRETOOLS, which is a collaborate project between Lund University and the Danish Institute of Fire and Security Technology,

funded by the European Union's Seventh Framework Programme under grant no. 316991.

ORCID

Frida Vermina Plathner  <http://orcid.org/0000-0001-5420-164X>

REFERENCES

- ISO 5660-1:2015 Reaction-to-fire tests—Heat release, smoke production and mass loss rate—Part 1: Heat release rate (cone calorimeter method) and smoke production rate (dynamic measurement), (2015).
- Babrauskas V, Parker WJ. Ignitability measurements with the cone calorimeter. *Fire Mater.* 1987;11(1):31-43.
- Mikkola E, Wickman IS. On the thermal ignition of combustible materials. *Fire Mater.* 1989;14(3):87-96. <https://doi.org/10.1002/fam.810140303>
- Lundstrom FV, van Hees P, Guillaume E. A review on prediction models for full-scale fire behaviour of building products. *Fire Mater.* 2017;41(3):225-244. <http://ludwig.lub.lu.se/login?url=http://search.ebscohost.com/login.aspx?direct=true&db=edswsc&AN=00039749300003&site=eds-live&scope=site>.
- Stoliarov SI, Leventon IT, Lyon RE. Two-dimensional model of burning for pyrolyzable solids. *Fire Mater.* 2014;38(3):391-408. <https://doi.org/10.1002/fam.2187>
- Lautenberger CW. *A Generalized Pyrolysis Model for Combustible Solids*. Berkeley, CA: University of California; 2007.
- Atreya A. Effect of environmental variables on piloted ignition. In: Cox G, Sangfried B, eds. *Fire Saf. Sci.* 3. Vol.3 Edinburgh, U.K.: Elsevier Applied Science; 1991:177-186. doi:10.3801/IAFSS.FSS.3-177
- Tewarson A. Generation of heat and chemical compounds in fire. In: DiNenno P, ed. *SFPE Handb. Fire Prot. Eng.* 3rd ed. National Fire Protection Association; 2002 3-82-3-161.
- Quintiere JG. A theoretical basis for flammability properties. *Fire Mater.* 2006;30(3):175-214. <https://doi.org/10.1002/fam.905>
- Drysdale DD, Thomson HE. Flammability of plastics II: critical mass flux at the Firepoint. *Fire Saf J.* 1989;14(3):179-188.
- Quintiere JG, Rangwala AS. A theory for flame extinction based on flame temperature. *Fire Mater.* 2004;28(5):387-402. <https://doi.org/10.1002/fam.835>
- Vermina Lundström F, Sunderland PB, Quintiere JG, van Hees P, de Ris JL. Study of ignition and extinction of small-scale fires in experiments with an emulating gas burner. *Fire Saf J.* 2017;87:18-24. <https://doi.org/10.1016/j.firesaf.2016.11.003>
- Lyon R, Quintiere J. Criteria for piloted ignition of combustible solids. *Combust Flame.* 2007;151(4):551-559. <https://doi.org/10.1016/j.combustflame.2007.07.020>
- ASTM D92, Standard test method for flash and fire points by Cleveland Open Cup Tester, (2010).
- Atreya A. Ignition of fires. *Philos Trans R Soc a Math Phys Eng Sci.* 1998;356(1748):2787-2813. <https://doi.org/10.1098/rsta.1998.0298>
- Khan MM, De Ris JL. Operator independent ignition measurements. In: *International Association for Fire Safety Science*. Vol.8 MD: Fire Saf. Sci., Baltimore; 2005:163-174. doi:10.3801/IAFSS.FSS.8-163.
- Delichatsios MA. *Critical Mass Pyrolysis Rates for Extinction in Fires Over Solid Materials NIST-GCR-98-746*, Norwood, 1998.
- Gregory S, Green A, Pasantes S, Grayson S, Kumar S. Use of the cone calorimeter for testing materials with low heat release rates, in: *Fire Mater.* 2013 13th Int. Conf. Exhib., Interscience Communications Ltd, San Francisco, USA, 2013; pp. 263-272.
- Vanspeybroeck R, Van Hees P, Vandevelde P. Combustion behaviour of polyurethane flexible foams under cone calorimetry test conditions. *Fire Mater.* 1993;17(4):155-166. <https://doi.org/10.1002/fam.810170403>
- de Ris J, Khan MM. A sample holder for determining material properties. *Fire Mater.* 2000;24(5):219-226. [https://doi.org/10.1002/1099-1018\(200009/10\)24:5<219::AID-FAM741>3.0.CO;2-7](https://doi.org/10.1002/1099-1018(200009/10)24:5<219::AID-FAM741>3.0.CO;2-7)
- Morgan AB, Bundy M. Cone calorimeter analysis of UL-94 V-rated plastics. *Fire Mater.* 2007;31(4):257-283. <https://doi.org/10.1002/fam.937>
- Distrelec E. (2018). https://www.elfa.se/?ext_cid=bpgooaqsesvna&kw=elfa+distrelec&gclid=EAlaQobChMlgJP38fXZ2QIV1ecbCh3PNQRDEAAAYASAAEGkIAfD_BwE&gsrc=aw.ds (accessed March 7, 2018).
- W. Martiensen, H. Warlimont, eds., *Polymers*, in: Springer Handb. Condens. Matter Mater. Data, Springer Science & Business Media 2006; pp. 480-522.
- Taylor BN, Kuyatt CE. *NIST Technical Note 1297: Guidelines for Evaluating and Expressing the Uncertainty of NIST Measurement Results*. MD: Gaithersburg; 1993.
- Armstrong RA. When to use the Bonferroni correction. *Ophthalmic Physiol Opt.* 2014;34(5):502-508. <https://doi.org/10.1111/opo.12131>
- Long RT, Torero JL, Quintiere JG, Fernandez-Pello AC. Scale and transport considerations on piloted ignition of PMMA. *Fire Saf Sci.* 2000;6:567-578. <https://doi.org/10.3801/IAFSS.FSS.6-567>
- Thomson H, Drysdale D. Critical mass flowrate at the firepoint of plastics. *Fire Saf. Sci.* 1989;2:67-76. <https://doi.org/10.3801/IAFSS.FSS.2-67>
- Panagiotou J, Quintiere JG. Generalizing flammability of materials. In: Grayson S, ed. *Interflam 10*. Greenwich, UK: Interscience Communications Limited; 2004:895-906.
- Rich D, Lautenberger C, Torero JL, Quintiere JG, Fernandez-Pello C. Mass flux of combustible solids at piloted ignition. *Proc Combust Inst.* 2007;31(2):2653-2660. <https://doi.org/10.1016/j.proci.2006.08.055>
- Rasbash DJ, Drysdale DD, Deepak D. Critical heat and mass transfer at pilot ignition and extinction of a material. *Fire Saf J.* 1986;10(1):1-10. [https://doi.org/10.1016/0379-7112\(86\)90026-3](https://doi.org/10.1016/0379-7112(86)90026-3)
- Staggs JEJ. Ignition of char-forming polymers at a critical mass flux. *Polym Degrad Stab.* 2001;74(3):433-439.

How to cite this article: Vermina Plathner F, van Hees P. Experimental assessment of bench-scale ignitability parameters. *Fire and Materials*. 2019;43:123-130. <https://doi.org/10.1002/fam.2675>

Paper III





Contents lists available at ScienceDirect

Fire Safety Journal

journal homepage: www.elsevier.com/locate/firesaf

Study of ignition and extinction of small-scale fires in experiments with an emulating gas burner



Frida Vermina Lundström^{a,b,*}, Peter B. Sunderland^c, James G. Quintiere^c, Patrick van Hees^a, John L. de Ris^{d,1}

^a Division of Fire Safety Engineering, Lund University, P.O. Box 118, SE-221 00 Lund, Sweden

^b Danish Institute of Fire and Security Technology (DBI), Jernholmen 12, Hvidovre 2650, Denmark

^c Department of Fire Protection Engineering, University of Maryland, 4356 Stadium Dr., College Park, MD 20742-3031, USA

^d FM Global, USA

ARTICLE INFO

Keywords:

Combustion
Laminar diffusion flame
Heat flux gage

ABSTRACT

The objective of this study is to explore mechanisms for ignition and extinction for condensed-phase fuels via the use of a gas-fueled burner. Flames were generated with a porous 25 mm circular burner using mixtures of methane and propane with nitrogen. The procedure was to specify a set of mass fluxes of nitrogen-fuel mixture that corresponded to the flash- fire- and extinction points and for the minimum mass flux where steady burning was achieved. The results show an increase in the critical mass flux with a decreased heat of combustion. The data fall into two regimes depending on the mixture flow rate; one buoyancy-driven ($Fr < 1$) and one induced by momentum jet forces. The buoyancy-driven regime is geometrically consistent with the definitions of flash and fire points under natural convection conditions. The results for the momentum regime align reasonably with existing stagnant layer theory. Extinction theory is also suggested to give approximate results for the fire point. This argument is based on similar flame geometries for fire point and extinction and theoretical reasoning. An anchor point is proposed as the end point of ignition. Produced anchor point data result in a flammability diagram, below which quasi-steady burning occurs.

1. Introduction

Ignition is often referred to as the initiation of fire growth and is therefore an important parameter in the context of fire safety [1]. Various criteria are used for identifying when ignition and extinction for condensed-phase fuels occur. The most common for ignition is a critical surface temperature. For most liquid fuels the criterion is the flash or fire point. But for solids the critical surface temperature will vary depending on the decomposition kinetics. Computational Fluid Dynamics (CFD) modellers using complex solid phase kinetics typically require a minimum mass flux for ignition, which avoids modelling gas phase ignition processes [2,3]. The work herein examines this minimum (critical) mass flux, and an associated critical energy flux, as criteria for ignition and extinction.

We will describe the ignition event by three terms: Firstly, a *flash point* is defined as the minimum mass flux for which a premixed flame propagates from the spark ignitor towards the burner surface. It occurs as a premixed fuel-oxidizer mixture approaches the lower flammability limit (LFL) at the surface. Secondly, a *fire point* is defined as the

minimum mass flux for which the flame is sustained for at least 5 s. A fire point occurs if the fuel-supply from the vaporizing liquid (or pyrolyzing solid) is enough for a diffusion flame to anchor at the fuel surface as the premixed flame approaches the surface of the fuel. The fire point begins at slightly above the LFL.

It is worth pointing out that the flash- and fire points are traditionally defined by critical temperatures of liquids and not by critical mass fluxes. A critical temperature of the fuel is often a satisfactory method for characterizing ignition in case of product screening [1], however a critical mass flux of volatiles was first proposed by Bamford et al.[4] as a more fundamental approach for modelling of ignition. This work takes the approach of using a critical mass flux and define ignition thereafter.

For a liquid the flash point and fire points are nearly the same compared to steady burning where the surface attains close to its boiling point which is much higher [5,6]. Thus, an *anchor point* is defined here as the minimum mass flux for which a flame is sustained over the entire burner surface. It is the condition of steady burning, and the state that a real fuel rapidly will approach after the fire point. In a

* Corresponding author at: Division of Fire Safety Engineering, Lund University, P.O. Box 118, SE-221 00 Lund, Sweden.

E-mail address: frida.vermina_lundstrom@brand.lth.se (F.V. Lundström).

¹ Retired.

<http://dx.doi.org/10.1016/j.firesaf.2016.11.003>

Received 30 March 2016; Received in revised form 3 October 2016; Accepted 20 November 2016

Available online 26 November 2016

0379-7112/ © 2016 Elsevier Ltd. All rights reserved.

Nomenclature			
α	Thermal Diffusivity	\dot{m}'_{cp}	Critical Mass Flux for Extinction
β	Thermal Expansion Coefficient	$\dot{m}'_{ig,LFL}$	Critical Mass Flux for a Flash
c_p	Heat Capacity at Constant Pressure	Nu_D	Nusselt Number
δ	Boundary Layer Thickness	\dot{q}'_{net}	Net Heat Flux
D	Diameter	ρ_{fuel}	Density of Fuel
Fr	Froude Number	r	Radius
g	Acceleration of Gravity	Ra_D	Rayleigh Number
h_c	Convective Heat Transfer Coefficient	T_f	Flame Temperature
Δh_c	Heat of Combustion	T_0	Initial Temperature
$\Delta h_{c,F}$	Heat of Combustion of Pure Fuel	T_s	Fuel Vaporization Temperature (Burner Surface Temperature)
Δh_{ox}	Heat of Combustion per Gram of Oxygen Consumed (13.1 kJ/g-O ₂)	T_∞	Ambient Temperature
k	Conductivity	ΔT	Characteristic Temperature Difference
L	Latent Heat of Vaporization	v	Velocity
\dot{m}'	Mass Flow Rate/Mass Flux	ν	Kinematic Viscosity
\dot{m}'_F	Mass Flow Rate of Pure Fuel	X_r	Flame Radiation Fraction
		Y_F	Fuel Mass Fraction in the Fuel Stream
		Y_{ox}	Ambient Oxygen Mass Fraction

condensed-phase fuel the transition from the fire point to the anchor point is caused by a continuous feedback from the flame that increases the mass flux [7]. Finally, a threshold for extinction is defined as the mass flux where the flame extinguishes before 5 s has passed. The point of extinction, although disputed [8], is often argued to coincide with the firepoint.

An experimental assessment of a critical mass flux for condensed-phase fuels by conventional methods has been difficult due to the transient nature of the ignition (and extinction) process. As condensed-phase materials ignite they experience a rapid increase in mass loss, which is challenging to capture. The opposite is true for extinction. Several studies have determined the critical mass flux of various materials. Although refined methods exist [9], there are large discrepancies between data. The difficulties stem primarily from interpretation of the rate of mass loss, noise in the measurements, and, in some cases, phenomena involving intermittent flames and non-attached flames. Hence there is a need for developing experimental methodologies that can measure small changes in mass flux.

Motivated by the lack of consistency in experimentally determined mass flux data this work started with determining fuel flow rates at ignition and extinction with a newly developed apparatus called the burning rate emulator (BRE). BRE is inspired from previous experimental apparatuses. Corlett [10] initiated the use of gas burners for the study of steady burning pool fires, followed by Orloff and de Ris [11,12], Kim et al.[13], and Rasbash and Drysdale [7]. These studies show that condensed-phase burning may be investigated by experimentally separating gaseous reactions from the mass and energy balance at the surface. In mentioned studies quasi-steady burning was of primary focus, but the emphasis here is instead on ignition and extinction.

Existing stagnant layer theory readily explains how to gain mass flux data for the flash- and extinction points [14,15], however the mechanisms leading to the fire point are different from those of extinction. Despite this, Roberts and Quince [16] successfully used stagnant layer theory for the prediction of fire point. Results showed that flame temperatures could be accurately predicted by the assumptions of (i) negligible heat flux from the premixed flame to the liquid surface and (ii) negligible radiative heat flux from the established flame. Following their study, this work evaluates the applicability of extinction theory to fire point data, through phenomenological similarities and differences and through theoretical reasoning, following the boundary layer analysis by Quintiere [14,17].

2. Experimental design and procedure

The burning rate emulator is shown in Fig. 1. It is fed with a fuel and diluent which are monitored with Alicat gas mass flow controllers, ranging between 0 and 2 SLPm, before entering a mixing pipe. Well-mixed gases flow into a plenum through two supply tubes. Internally a ceramic honeycomb enables flow uniformity. Finally the mixture passes through an upward-facing circular porous copper plate with a diameter of 25 mm, replicating a solid sample with high porosity. Two combined K-type thermocouples and 1/8" Medtherm heat flux gauges are mounted flush with the burner surface to measure surface temperature and heat flux close to the burner edge ($r=8.25$ mm) and centre ($r=0$ mm). The heat flux gauges have been calibrated by the supplier and then re-calibrated at the University of Maryland with the procedure detailed in NIST/BFRL Report of Test FR 4014 [18].

Initially different ignitors were used and the one giving the lowest mass flux at the flash and fire points was adopted. First, a vertical electrical arc gave a high temperature locally, but failed to cover the flammable zone. Secondly a pre-mixed fuel-air ignitor was used but the relatively high velocity blew away combustible gas. We found that the most robust ignitor for these experiments was a small propane diffusion flame ignitor. The ignitor was swept over the burner 2 mm above the burner surface, corresponding to the height of the Cleveland open cup test [19].

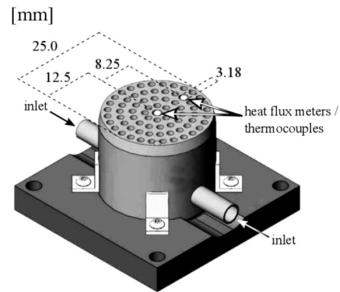


Fig. 1. Schematic of the BRE burner.

The experimental setup is located approximately one meter under a hood with low exhaust flow and the entire rig is protected from outer flow disturbances by a fine meshed net. Initial testing with incense streak lines proved this configuration satisfactory.

Fuels used are methane and propane which are diluted with nitrogen. An effective heat of combustion for each fuel/nitrogen mixture is found from

$$\Delta h_{c,e} = \frac{\dot{m}'_e}{\dot{m}'_f} \Delta h_{c,f} \tag{1}$$

where \dot{m}'_e and \dot{m}'_f are mass flux of pure fuel and mixture respectively and $\Delta h_{c,f}$ is the heat of combustion of pure fuel.

A series of experiments were conducted to achieve flash, fire, anchor and extinction point data. The procedure was to specify a set of mass flow rates of nitrogen within the limits of the gas mass flow controllers. For each mass flow rate of nitrogen a corresponding fuel flow rate was obtained, for which the flash, fire point, anchor point and extinction point were recorded. Firstly, a flash point was determined by increasing the fuel mass flow rate to the point where a propagating flash from the ignitor towards the burner surface was seen. Local flashes, i.e., flames that do not propagate, or just partially propagate, were discarded, in consistency with the Cleveland open cup test [19]. The fuel flow was then increased until a fire point was reached. For the anchor point the mass flow rate of fuel was then increased up until a point where the entire surface of the burner was covered by the flame. Before any readings, the surface temperature was allowed to stabilize. Surface temperatures and heat fluxes were recorded in addition to the mass flow rate of the gases. Finally, an extinction point was obtained by stepwise decreasing the fuel flow rate to the point at which the flame extinguished.

In order to show applicability of BRE data to condensed-phase fuels, a comparison was made between BRE mass fluxes and mass fluxes for a number of plastics, irradiated with 50 kW/m^2 in the Cone Calorimeter. Cone experiments was performed in the Federal Aviation Administration (FAA) lab and analysed by Lyon [20]. It is assumed here that the critical mass flux is not dependent on the level of irradiance, as a flame fed with a given fuel supply ignites or extinguishes without any ‘knowledge’ of where the fuel came from. This is supported by the findings of Panagiotou and Quintiere, showing that the critical mass flux for ignition of four plastics is nearly constant for heat fluxes ranging between 20 and 50 kW/m^2 [21].

A few experimental matters are noted with the use of the gas burner. Firstly, the BRE is not water cooled. Therefore the burner

surface temperature was monitored to remain at ambient temperature ($<30^\circ\text{C}$) for both flash and fire points. However, for an anchor or extinction point this was not possible; instead stabilized surface temperatures for those measurements were recorded. Secondly, propane, which is heavier than air, can gather at the burner surface when it is not diluted by nitrogen. Thus the first flash and fire point measurements are disregarded for propane; instead the second ignition is viewed as valid. Another point of apprehension is the velocity distribution over the burner surface. The BRE maintains a uniform velocity over the surface. On radiative ignition and on heating a liquid to determine its flash point, the condensed-phase has a fairly uniform velocity distribution. This is also true at the fire point before the impact of the premixed flame. But when a flame is established over a condensed-phase material, the burning achieves a heat flux distribution, and thus also a variable velocity over the surface. This is the case for the fire point after the impact of the premixed flame, and also for the anchor and extinction points. The velocity is greatest at the edge where the flame is closest to the surface. In this case, the BRE burner is imperfect. However, agreement between flame shapes in BRE to that of real materials, suggests that the initial burning velocity quickly adjusts to the diffusional flows of the flame [22].

3. Flow regime results

Lyon and Quintiere [20] have shown that the critical energy flux (the fuel flow rate multiplied by its heat of combustion) is constant over a range of materials (heat of combustions) at the flash and fire points, showing values of 21 ± 6 and $66 \pm 17 \text{ kW/m}^2$ for the flash and fire point in the cone calorimeter. This is also partly true for BRE results, shown in Fig. 2(a), where the critical energy fluxes for flash, fire and extinction points are plotted.

Fig. 2(a) also shows that there is a regime where the statement of a constant critical energy flux doesn't hold. At low heats of combustion the critical energy flux increases rapidly with a decreasing heat of combustion. Experimental observations imply that burning is buoyancy-driven at low flow rates, whereas burning at high flow rates depend on momentum jet forces. This is supported by the flame not being attached to the burner surface at high mass fluxes. Theoretically the transition between the two regimes is explained by the Froude number ($Fr = v/\sqrt{gD}$; $v = \dot{m}'/\rho_{fuel}$) where $Fr < 1$ indicates buoyant flow and $Fr > 1$ is momentum-driven. At, and close to, $Fr=1$ there is a transitional behavior, where the flame is both buoyancy and momentum-driven.

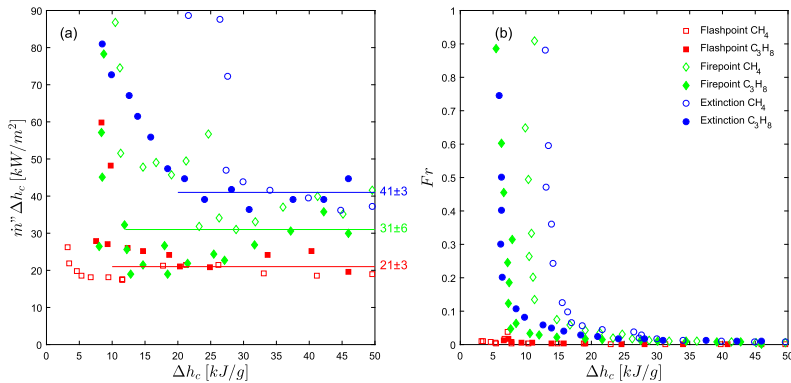


Fig. 2. Comparison of flash, fire and extinction points: (a) Critical energy flux, and; (b) Froude number.

Returning to Fig. 2(b), a rise in calculated Fr is initiated at $\Delta h_c=5-10$ kJ/g for the flash point and at $\Delta h_c=5-15$ kJ/g and $\Delta h_c=5-20$ kJ/g for the fire point and extinction respectively, where Fr approaches (flash point) or equals (fire point and extinction) unity. This approximately concurs with the visual determination of flame lift-off, occurring at $\Delta h_c=10, 12,$ and 20 kJ/g for the flash, fire and extinction points respectively.

In the transient region, a flame with a methane/nitrogen mixture is sometimes extinguished due to a flame instability introduced when the supply velocity approaches the burning velocity of methane. Methane is also easily affected by outer disturbances. Because of this a few unrealistic methane results in the transient region have been discarded. After this consideration, averaged critical energy fluxes in the buoyant region are $21 \pm 3, 31 \pm 6,$ and 41 ± 3 kW/m² for flash- fire and extinction points respectively ($0r 21 \pm 3, 35 \pm 10,$ and 49 ± 17 kW/m² with transient methane results included). In other words, the BRE suggests that fire point and extinction are not identical and that a higher critical mass- or energy flux is seen when a flame is extinguished than at the fire point. The averages are shown for the buoyant regions as solid lines in Fig. 2(a).

4. Flash point

4.1. Flame appearance

In the BRE, as the ignitor flame reaches the burner rim, a blue flash propagates over the entire burner surface. The flame moves rapidly close to the surface before it extinguishes upon reaching the opposite side of the burner. With increasing flow velocity the flash no longer propagates along the burner surface. The premixed flame instead propagates through the flow field above the burner where the supply velocity of fuel matches the flame velocity. This produces a lifted flame.

4.2. Flash point theory

A stagnant layer one-dimensional model, previously developed by Quintiere [17] is used for evaluating experimental data. At the flash point, the mole fraction of vaporized fuel at the fuel surface is close to its LFL. The liquid fuel vapours are released at a constant rate and then diffuse and convect upwards. The highest fuel concentration is at the surface. A low burning rate is assumed, leading to following expression

$$\dot{m}'_{lg,LFL} \approx \frac{h_c}{\Delta h_c} (T_f - T_0) \tag{2}$$

In Eq. (2) h_c is the convective heat transfer coefficient, and Δh_c the effective heat of combustion for the fuel/nitrogen mixture. T_f and T_0 denote flame and initial temperatures. By assuming constant values for h_c, T_0 and T_f it is seen that $\dot{m}'_{lg,LFL}$ is a function of Δh_c . The reader is referred to Ref. [17] for a thorough derivation of the equation.

In stagnant layer analysis the convective heat transfer coefficient is approximated by $h_c=k/\delta$, where k is the thermal conductivity and δ is the thickness of the thermal boundary layer. Our approach is to utilize heat transfer correlations from literature to find the convective heat transfer coefficient. Gebhart derived a correlation for a hot plate facing up [23]

$$Nu_D=0.43 + 0.60Ra_D^{1/4} \tag{3}$$

where Nu is the Nusselt number ($Nu_D=h_c D/k$) and Ra is the Rayleigh number ($Ra_D=g\beta\Delta T D^3/\nu\alpha$), evaluated at a film temperature. A complete list of terms is found in the nomenclature. For the calculation of the heat transfer coefficient we use gas properties from the SFPE Handbook [24], which results in $h_c=6W/m^2K$ for the flash point. In the evaluation, T_0 is 298 K. The flame temperature T_f is taken as 1600 K for both the flash point and extinction, in line with the results of Maček and Williams amongst others [25,26]. The flame temperature is independent of fuel dilution since the mass stoichiometric air to fuel

ratio is large.

4.3. Burning rate emulator results

In Fig. 3 flash point BRE results are presented along with experimental results for plastics in the Cone Calorimeter [20] and a theoretical solid line based on Eq. (2). The critical mass flux increases as the effective heat of combustion decreases. In other words, liquids and plastics (with relatively high Δh_c) exhibit lower mass flux values than charring materials (with relatively low Δh_c) at the flash point [20]. The minimum mass flux for flashing increases for materials with heats of combustion lower than 4–8 kJ/g, as is seen by both the theoretical solid trace and the experimental dots in Fig. 2. Below these values flashing is less likely.

Although Fig. 3 shows that BRE results match the magnitude and scatter for real plastics well, the theoretical description underestimates the results. Property assumptions is one reason for this discrepancy, especially the convective heat transfer coefficient has an impact on the critical mass flux, as seen in Eq. (2). A theoretical h_c of $12 W/m^2K$ would hit the experimental data. Another reason for the discrepancy is that the theory assumes a flash at the LFL. It is likely that this limit is not captured experimentally. At high mass flow rates the theory deviates from the experimental data. This is attributed to a theoretical assumption of a low burning rate assumed in Eq. (2).

5. Extinction

5.1. Flame appearance

Fig. 4 shows variations in flame shape with mass flow rate for extinction. The appearance is discussed below in terms of flame height, width and shape as well as colour, flame location and oscillating behavior.

Firstly, for all fuels, the flame height increases with increasing mass flux. At high mass fluxes the flame lifts off and the flame stand-off distance may be several mm. The lift-off is caused by the flame losing its stability close to the rim as a large excess of air is entrained at the flame base.

The width of the flame also increases with increasing mass flux up to the point where the flame lifts off from the burner surface. In the low mass flux zone ($0-1.5$ g/m²s), indicative of a buoyancy dominated flow field, the flame is centred at a small portion of the burner. It is attached to the burner surface but not to the rim. The buoyant flame has a conical shape and a blue luminosity. It is anchored to the centre of the burner and flickers only at the last instant before it goes out. The buoyancy-driven flame is very close to the burner surface, which means that the flame loses much heat to the surface via conduction. If there is

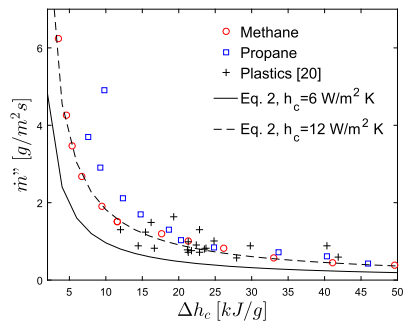


Fig. 3. Mass loss rate at the flash point.

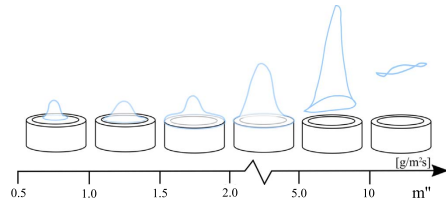


Fig. 4. Extinction behavior: Sketches of flame appearance at different mass fluxes. (For interpretation of the references to color in this figure, the reader is referred to the web version of this article).

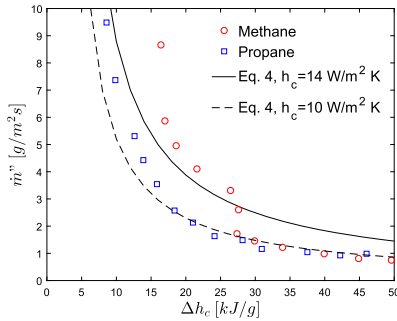


Fig. 5. Extinction behavior: critical mass flux.

not sufficient supply of fuel the flame is quenched by those heat losses. The flame at 1.5–2.0 g/m² s is attached to the burner rim. As the mass flux is slightly increased (2–5 g/m² s) the flame gets more robust against thermal quenching and a wider flame is visible. The flames are attached to the entire burner surface and oscillate in an axisymmetric fashion. The lifted flame, where the mass flux is 5–15 g/m² s, has moved inwards from the edge, just slightly. This may have to do with the flame compelling to stoichiometric conditions. The flame is cavernous with a non-luminous core and the flame stand-off distance may be several mm.

5.2. Extinction theory

Using stagnant layer theory, Quintiere and Rangwala [15] derived following equation for the critical mass flux at extinction

$$\dot{m}_{c,r} = \frac{\frac{h_c}{c_p} [Y_{O_2}(1-X_r)\Delta h_{O_2} - c_p(T_r - T_\infty)]}{Y_f \Delta h_c + c_p(T_r - T_\infty) - c_p(T_f - T_\infty) \left(1 + \frac{\Delta h_c}{\Delta h_{O_2}} \frac{Y_f}{Y_{O_2}}\right)} \quad (4)$$

where Y_{O_2} is the oxygen mass fraction, X_r is the radiative fraction, Δh_{O_2} is the heat of combustion per unit gram of oxygen consumed, c_p is the specific heat capacity, T_∞ is the ambient temperature, and Y_f is the fuel mass fraction. This equation is used for analysing extinction experiments. The theory will not be explained in this work. Eq. (4) is assumed to have the following values: $Y_{O_2}=0.233$ because the test setup was well-ventilated, $X_r=0$ as the flames were blue, indicating low radiation, $\Delta h_{O_2}=13.1$ kJ/g-O₂ [27], $c_p=1$ kJ/kgK [14], $T_f=1600$ K [25,26], and an assumed $T_\infty=298$ K. The average surface temperature was measured to 400 K for both propane and methane at the point of extinction in a buoyant region and that is also the temperature that has been chosen as surface temperature for the theoretical line.

5.3. Burning rate emulator results

Extinction measurements are presented in Fig. 5 along with a solid line based on Eq. (4). The Froude number is plotted against the right-hand side y-axis, indicating a buoyant flow field when $\Delta h_c > 20$ kJ/g.

The theoretical description overestimates the results. This is likely due to sensitivity of the heat transfer coefficient. A heat transfer coefficient of $h_c=14$ W/m²K is calculated from Eq. (3). Re-calculating with $h_c=10$ W/m²K fits the experimental data in the buoyant region better. It should be noted that the approximate model used in this study relies on an accurate convective heat transfer correlation. Our approach has been to find the best correlation from literature that can deal with low Rayleigh numbers. Ra is associated with the boundary layer flow and when $Ra \rightarrow 0$ there is pure diffusion. Small adjustments of constants are common in heat transfer and may have a large impact on the end result.

6. Considerations of applying extinction theory to fire point data

6.1. Flame appearance

The appearance of a flame is an important characteristic when studying laminar diffusion flames, as it may give indications of the fundamental behavior depicting the appearance, e.g. the effects of air and gas movement. Flame colour, for instance, indicates radiative influence, but the colour also reveals where a fuel-rich core exists and where combustion takes place [10]. Another example is flame height which has been shown to correlate with mass flux at different burner geometries [28]. With this in mind, we propose consideration of extinction theory for fire point data. The BRE results namely suggest that the flame appearance for fire point is identical to that of extinction (refer Fig. 4). Flame heights and width are similar for similar mass fluxes. Also oscillating behavior, colour and flame location match the flame at extinction. In Fig. 6 example flames at fire point and extinction are presented to show the similarity. Analogous to extinction: At low mass fluxes the flame takes a conical shape and the flame does not necessarily cover the entire burner surface. At high mass fluxes the flame lifts off and the flame stand-off distance may be several mm; these measurements are not regarded to establish attached flames (i.e. not ‘true’ fire points) and are therefore mainly reported for completeness.

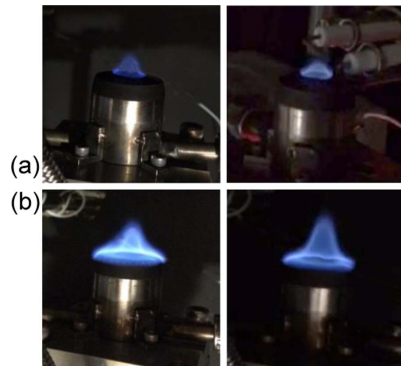


Fig. 6. Flame appearance: (a) fire point (LHS) and extinction flame (RHS) at $\dot{m}'=0.70$ g/m² s and (b) fire point (LHS) and extinction flame (RHS) at $\dot{m}'=1.5$ g/m² s. (For interpretation of the references to color in this figure, the reader is referred to the web version of this article).

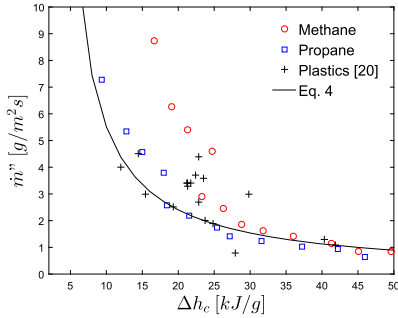


Fig. 7. Fire point behavior: Critical mass flux.

6.2. Burning rate emulator results

Fig. 7 presents the critical mass flux at the fire point based on various heats of combustion. Experimentally retrieved data for plastics matches the trend and the scattering for BRE results. Again, the transition from a buoyant to momentum driven regime is evaluated by the Froude number, shown by a right-hand side y-axis in Fig. 7. At, and close to, $Fr=1$ there is a transitional behavior, where the flame is both buoyancy and momentum-driven. This occurs at a heat of combustion of ~ 12 kJ/g. For $Fr < 1$ the flame is buoyant.

It seems reasonable to assume that a theoretical flame temperature of 1600 K may also be used for approximating fire point data. This has previously been verified by Roberts and Quince, who related the surface temperature at the fire point to that of the flame, finding limiting flame temperatures of 1530–1710 K [16]. Commonly the fire point is experimentally determined in terms of a surface temperature; however Spalding’s theory does not suggest a critical surface temperature below which a flame cannot be sustained.

Despite similar flame appearances the validity of the theoretical application to fire point experiments is uncertain, due to the fact that the heat flow mechanisms determining extinction and fire point are different. Here we take use of an engineering approach, where a heat transfer coefficient for the fire point is estimated. The direction and magnitude of convective heat transfer can be discussed in terms of a characteristic temperature difference incorporated into the Rayleigh number. For example, the convective heat flow at the flash point goes from a hot burner surface to a colder ambient surrounding. For extinction, a characteristic temperature difference is instead found between a hot flame and the colder burner surface. We assume an intermediate value between these two cases for the fire point. This is because the fire point may be regarded as the transition between a hot surface (heated by a premixed flame) losing heat to the surrounding and an established flame losing heat to the burner surface. In other words, there is a change of both direction and magnitude of the convective flow at the fire point. An approximate value for the heat transfer coefficient of $h_c=9$ W/m²K is obtained from Eq. (3). Data for real plastics [20], as well as BRE results, show encouraging agreement to the theory, when this approximation is applied.

It is worth noting that there is a larger heat loss from the flame to the burner surface at the fire point than at extinction, as the surface temperature at the fire point is lower ($> 30^\circ\text{C}$). In future testing a water cooled burner will ensure a better comparison of the two phenomena.

7. Steady burning: anchor point

When ignition occurs for a material in a test apparatus with a pilot flame, the process begins with the flash point (premixed flame), then

evolves to the fire point. However, for a liquid or solid fuel the feedback from the flame will increase the mass flux and drive the system from the fire point to full surface involvement. In this process the mass flux is increasing. We measure this end point as the “anchor point.” For a liquid or non-charring solid the fuel can then attain steady burning.

The flame shape of the steady burning flame is similar to that of extinction for 2–5 g/m²s (refer Fig. 4). The BRE allows us to define the anchor point where steady burning is initiated (i.e., the entire burner surface is fully involved in burning and the mass flux is fixed). The anchor point is determined by considering the average flame diameter vs. burner diameter. It is evident that the anchor point is not as easily obtained as the mixture flow rate is increased (jet regime). This is because the flame for high nitrogen flow rates initially is wide but is lifted from the burner. An anchor point is defined by flame attachment to the burner. Thus, for results in the jet regime the flame does not increase in diameter with increasing fuel rate, however the distance to the burner surface decreases.

The heat flux over the burner is estimated by using the two heat flux meters. Akita and Yumoto [29] have shown that the heat flux distribution over similar pool radii takes an exponential form, where the heat flux to the edge is higher than that to the centre. An accurate description of the heat flux would place the measurements into such a distribution. Here the heat flux is approximated with a weighted average of an exponential distribution including the two heat flux meters

$$\ln(q''_{net}) = \int_0^{12.5} 2\pi r \left[\frac{\ln(q''_{r=8.25mm}) - \ln(q''_{r=0mm})}{8.25} r + \ln(q''_{r=0mm}) \right] dr \quad \leftrightarrow \quad q''_{net} = \frac{q''_{r=8.25mm} \cdot 1.01}{q''_{r=0mm} \cdot 0.01} \quad (5)$$

where q''_{net} is the net heat flux, r is radius and q''_{r} is the heat flux at the locations of the heat flux meters. With this a heat of gasification ($L = q''_{net}/\dot{m}''_c$) is calculated. This data was determined as the flow rate of diluent was gradually increased from the fire point to the maximum capacity of the flow meter. The convective heat transfer coefficient is taken as $h_c=14$ W/m²K as measured by Kim [30].

The gas burner is intended to emulate approximate generalized flammability results of liquids and solids. Fig. 8 presents a “flammability diagram”, in terms of heat of gasification L and heat of combustion Δh_c . Below the regression line is a regime of steady burning. Above the line transient burning behavior may occur, such as ignition and extinction.

The slope of the line $L/\Delta h_c$ represents the fraction of energy released needed for continuation of steady burning. The inverted slope has previously been referred to as the combustibility ratio by Rasbath [31], or the heat release parameter (HRP) by Tewarson [32]. The

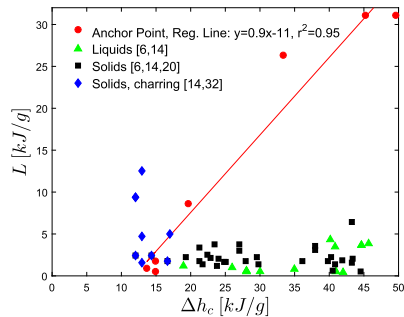


Fig. 8. Anchor point behavior: flammability diagram based on methane/nitrogen flow rates.

results show an approximate trend for liquids [6,14] and solids [6,14,20], whereas charring solids [14,32] (with low Δh_c) lie outside the domain of “steady burning”. This could be expected as char-forming materials do not burn without the support of external heating.

8. Conclusions

The BRE offers a simple and accurate way to emulate ignition and extinction conditions compared to standard tests for condensed-phase materials. While liquids and solids show rapid transitions at the moment of ignition, the BRE has the advantage of loading the fuel gas at a specific rate irrespective of the heat flux exposed onto the surface. As such, it has an additional degree of freedom to examine the mechanisms leading to ignition/extinction. By slowly increasing the fuel flow rate the BRE readily demonstrates the flame appearance, first at the flash point that with increasing fuel flow rate is followed by a fire point. At the fire point it is shown that a flame does not necessarily cover the entire fuel surface area in order to sustain. By increasing the fuel flow rate even further, an anchor point is proposed as the end point of the ignition phenomenon (or starting point of steady burning).

The critical mass flux criterion used for ignition and extinction is not a constant, but changes with the effective heat of combustion of the fuel. The data fall into two regimes depending on the flow rate of the mixture: one buoyancy-driven ($Fr < 1$) and one induced by momentum jet forces. The former is geometrically consistent with the stated definitions of flash- and fire points at natural convection, while the latter, although aligning with the theory presented, is driven by momentum forces. Lyon and Quintiere [20] has shown that the critical energy flux (the fuel flow rate multiplied by its heat of combustion) is constant over a range of materials (heats of combustion) at the flash and fire point. BRE results show that this is true in a buoyant region, but in the momentum jet region the critical energy flux varies with the heat of combustion.

Stagnant layer theory is suggested to approximately predict fire point data. The fore laid argument is based on the similar flame geometries exhibited at the fire point and point of extinction. However, the heat flow mechanisms leading up to the occurrence of a fire point are different from the heat transfer at extinction. Unlike extinction, there is a change of both direction and magnitude of the convective flow at the fire point. It is proposed that this may be accounted for through modification of the convective heat transfer coefficient.

Conclusively, BRE results match those of real condensed-phase fuels. The BRE's main advantage is that the gas flow (emulating pyrolysates or vapours) is independent of the heating source. As such it may be a support to better define the limiting conditions at ignition and extinction.

Conflict of interest

There are no, to the authors known, conflicts of interest in the completion of this work.

Acknowledgements and funding

The authors are truly grateful to dr. Haiqing Guo for discussions and assistance in the lab. The authors are also grateful to NASA for funding the development of the burner, under Grant no. NNX10AD98G. This study is part of FIRETOOLS which is a collaborate project between Lund University and the Danish Institute

of Fire and Security Technology, funded by the European Union's Seventh Framework Programme under Grant no. 316991.

References

- [1] D.D. Drysdale, *An Introduction to Fire Dynamics*, 2nd ed., John Wiley & Sons, Chichester, 1999, p. 193.
- [2] S.I. Stolarov, L.T. Leventon, R.E. Lyon, Two-dimensional model of burning for pyrolyzable solids, *Fire Mater.* 38 (3) (2014) 391–408.
- [3] C.W. Lautenberger, *A Generalized Pyrolysis Model for Combustible Solids* (Ph.D. Dissertation), University of California, Berkeley, 2007.
- [4] CH. Bamford, J. Crank, DH. Malan, H. Wilson, *The Combustion of Wood. Part I, in: Mathematical Proceedings of the Cambridge Philosophical Society*, vol. 42(2), 1946, pp. 166–182.
- [5] D.D. Drysdale, Ignition of liquids, in: M.J. Hurley (Ed.) *SFPE Handbook Fire Protection Engineering* 5th ed., Springer, New York, 2015, p. 568.
- [6] F.W. Mowrer, *Fundamentals of the fire hazards of materials*, in: C.A. Harper (Ed.) *Handbook of Building Materials for Fire Protection*, McGraw-Hill Book Co, New York, 2004, p. 1.25.
- [7] D.D. Rashbash, D.D. Drysdale, Theory of fire and fire processes, *Fire Mater.* 7 (2) (1983) 79–88.
- [8] J. Dai, M.A. Delichatsios, L. Yang, et al., Piloted ignition and extinction for solid fuels, *Proc. Combust. Inst.* 34 (2014) 2487–2495.
- [9] M.M. Khan, J.L. de Ris, Operator independent ignition measurements, *Fire Saf. Sci.* 8 (2005) 163–174.
- [10] R.C. Corlett, Gas fires with pool-Like boundary conditions, *Combust. Flame* 12 (3) (1968) 19–32.
- [11] J.L. De Ris, L. Orloff, A dimensionless correlation of pool burning data, *Combust. Flame* 18 (3) (1972) 381–388.
- [12] J.L. De Ris, L. Orloff, The role of buoyancy direction and radiation in turbulent diffusion flames on surfaces, *Symp. (Int.) Combust.* 15 (1975) 175–182.
- [13] J.S. Kim, J.L. De Ris, F.W. Kroesser, Laminar free-convective burning of fuel surfaces, *Symp. (Int.) Combust.* 13 (1971) 949–961.
- [14] J.G. Quintiere, *Fundamentals of Fire Phenomena*, John Wiley & Sons, Chichester, 2006, pp. 227–296.
- [15] J.G. Quintiere, A.S. Rangwala, A theory for flame extinction based on flame temperature, *Fire Mater.* 28 (5) (2004) 387–402.
- [16] A.F. Roberts, B.W. Quince, A limiting condition for the burning of flammable liquids, *Combust. Flame* 251 (2) (1973) 245–251.
- [17] J.G. Quintiere, A theoretical basis for flammability properties, *Fire Mater.* 30 (3) (2006) 175–214.
- [18] WM. Pitts, JR. Lawson, JR. Shields, Report of Test FR 4014: NIST/BFRL Calibration System for Heat-Flux Gages, NIST, Gaithersburg, 2001.
- [19] American Society for Testing Materials, *Standard Test Method for Flash and Fire Points by Cleveland Open Cup Tester*. ASTM D92-12b, ASTM, Philadelphia, 2010.
- [20] R. Lyon, J.G. Quintiere, Criteria for piloted ignition of combustible solids, *Combust. Flame* 151 (4) (2007) 551–559.
- [21] J. Panagiotou, J.G. Quintiere, Generalizing Flammability of Materials, in: *Proceeding of the Interflam 2004, 10th International Fire Science and Engineering Conference*, Greenwich, 2004, pp. 895–905.
- [22] Y. Zhang, M. Kim, P.B. Sunderland, J.G. Quintiere, J.L. de Ris, A burner to emulate condensed phase fuels, *Exp. Therm. Fluid Sci.* 73 (5) (2016) 87–93.
- [23] B. Gebhart, *Heat Transfer*, 2nd ed., McGraw-Hill Book Co, New York, 1971, pp. 371–372.
- [24] Appendix 2: Thermophysical property data, in: M.J. Hurley et al. (Ed.), *SFPE Handbook Fire Protection Engineering*, 5th ed. New York: Springer, 2015, p. 3427.
- [25] A. Maćek, *Flammability Limits: Thermodynamics and Kinetics*, National Bureau of Standards, Center for Fire Research, Washington DC, 1976 (Final report no. PB-254180; NBSIR-76-1076).
- [26] F.A. Williams, A review on flame extinction, *Fire Saf. J.* 3 (3) (1981) 163–175.
- [27] M.L. Janssens, Measuring rate of heat release by oxygen consumption, *Fire Technol.* 27 (3) (1991) 234–249.
- [28] F.G. Roper, The prediction of laminar jet diffusion flame sizes: Part I. Theoretical model, *Combust. Flame* 29 (1977) 219–226.
- [29] K. Akita, T. Yumoto, Heat transfer in small pools and rates of burning of liquid methanol, *Proc. Combust. Inst.* 10 (1) (1965) 943–948.
- [30] H. Kim, *Procedures to Obtain Accurate Measurement from a Gas Fuelled Burner* (Ms. Thesis), University of Maryland, College Park, 2014.
- [31] DJ. Rashbash, Theory in the evaluation of fire properties of combustible materials, in: *Proceedings of the 5th International Fire Protection Seminarium, Karlsruhepp*, 1976, pp. 113–130.
- [32] A. Tesarova, Generation of heat and chemical compounds in fire, in: P. DiNenno (Ed.) *3th ed., SFPE Handbook Fire Protection Engineering* 3–161, Springer, New York, 2002, pp. 3–82.

Paper IV





Contents lists available at ScienceDirect

Fire Safety Journal

journal homepage: www.elsevier.com/locate/firesaf

Analysis of extinction and sustained ignition

Frida Vermina Plathner^{a,b,*}, James G. Quintiere^c, Patrick van Hees^a^a Division of Fire Safety Engineering, Lund University, P.O. Box 118, SE-221 00, Lund, Sweden^b Research Institutes of Sweden (RISE), Box 857, 501 15, Borås, Sweden^c Department of Fire Protection Engineering, University of Maryland, College Park, MD, 20742, USA

ARTICLE INFO

Keywords:

Burner

Combustion

Diffusion flames

Limits

Pool

ABSTRACT

The limiting conditions for sustained burning of materials are studied experimentally using gas burners. Small pool fire configurations are examined to determine the mass flux for a sustained surface diffusion flame (fire point) and the subsequent extinction limit of that flame. The burner results are compared to material data for sustained ignition, and are found to be lower. Material reported values of a critical mass flux are disparate, and burner data show that the critical mass flux can range from about 1 to 50 g/m²s. Previous studies have indicated the results depend on the convective heat transfer coefficient and the heat of combustion of the gases, but until this work no study has been presented to systematically show these dependencies. Three porous gas burners of diameters 25, 50 and 100 mm were used with fuel gases including methane, propane, isobutene, and ethylene mixed with nitrogen to precisely change the mixture heat of combustion. Diffusion flame theory based on a critical flame temperature at extinction is used to explain and correlate data for both limits. It was found that there is no statistical difference between the sustained ignition and extinction limits. A correlation for the critical mass flux is produced with heat of combustion and fuel diameter as sole dependent variables for all the fuels except methane. The results show that no burning is possible below a heat of combustion of 3–4 kJ/g. This is consistent with the European classification system for non-combustibility where the corresponding limit is set at 2 kJ/g.

1. Introduction

The conditions for materials burning are important in flammability performance, modeling, and basic research. For example, the Cleveland Cup [1] test is a standard test that rates the flammability of liquids by the flash and fire points. The former being the temperature of the liquid to cause the flashing of a premixed flame with a pilot, and the latter the temperature (slightly higher) to cause a sustained flame on the liquid. Staggs [2] illustrates the use of a critical mass flux property to avoid modeling the gas phase in predicting the ignition of char forming polymers. Fundamentally ignition and extinction of a diffusion flame is controlled by the Damköhler number, Da [3], which can be defined as the ratio of the diffusion time to chemical reaction time. A large Da (> 1) might imply the existence of a flame. In fire there is little knowledge of the composition of the pyrolyzates and therefore approaching ignition/extinction from gas phase kinetics is problematic. That is why the use of a simplified criterion of a critical mass flow rate of volatiles below which a flame cannot sustain [4] could be useful. This paper examines data from burners of different sizes and variations in the fuel stream in an attempt to generalize this criterion.

Past studies on the ignition and extinction of fires have offered various empirical criteria for these phenomena. Early on Rasbash et al. [5] proposed a critical heat flux at the *fire point* as a distinct fraction of the energy flux in steady burning (mass flux x heat of combustion). Lyon et al. [6] show data for polymers ignited by radiant heating that indicate there might be a critical energy flux at the flashpoint and at the fire point. Their reasoning was based on the well-known empirical energy density value of 2050 kJ/m³ at the lower flammability limit in air [7]. Roberts and Quince [8] show that a critical flame temperature can explain the critical mass (or energy) flux at extinction of liquids, and Quintiere et al. [9] extend this idea to solids. Additionally Delichatsios et al. [10,11] have indicated that there is a critical value for the ratio of mass flux with the convective mass transfer coefficient at extinction.

Simple arguments can show these criteria to be related. First assume the fire point (sustained ignition) and the extinction point (cessation of sustained ignition) are the same. Ignore radiation effects and say that convective heat transfer is dominant. The convective heat flux can be approximately given by $\dot{q}'_{f,c} \approx h_c(T_f - T_\infty)$ where h_c is the convective heat transfer coefficient, T_f is the flame temperature and T_∞ is the initial

* Corresponding author. Division of Fire Safety Engineering, Lund University, P.O. Box 118, SE-221 00, Lund, Sweden.

E-mail address: frida.vermina.plathner@brand.lth.se (F. Vermina Plathner).<https://doi.org/10.1016/j.firesaf.2019.02.003>

Received 9 June 2018; Received in revised form 8 January 2019; Accepted 4 February 2019

Available online 15 February 2019

0379-7112/ © 2019 Elsevier Ltd. All rights reserved.

temperature. Consider $Y_{F,L}$ to be the fuel mass fraction at the lower limit, then by convective mass transfer theory, the corresponding mass flux is $\dot{m}''_{c,F} \approx (h_c/c_p)Y_{F,L}$ and $Y_{F,L} \approx c_p(T_f - T_\infty)/\Delta h_c$ where Δh_c is the heat of combustion. Furthermore, approximate the limit burning as quasi-steady in the condensed phase so that $\dot{q}''_{f,c} = \dot{m}''_{c,F}L$ where L is the heat of gasification. Combining accordingly, the criteria for sustained ignition or extinction might be expressed as indicated by the various researchers as:

1. Rasbash: $\dot{m}''_{c,F}\Delta h_c = \dot{q}''_{f,c}\Delta h_c/L$, (or $\dot{q}''_{f,c}/\dot{m}''_{c,F}\Delta h_c = L/\Delta h_c$ as the heat flux – energy fraction of Rasbash [5])
2. Lyon-Roberts-Quintiere-Delichatsios: $\dot{m}''_{c,F}\Delta h_c \approx h_c(T_f - T_\infty)$

where a fixed critical flame temperature is universally invoked. It is clear that all previous investigators recognized the importance of the heat of combustion and the convective mass and heat transfer processes. It is recognized that in general, the critical flame temperature is a function of strain rate [12] and weak diffusion flames in fire have relatively low strain rates.

Let us see how these criteria might be affirmed by using data taken from gas burners. The advantage is that the flow rate can be measured with precision compared to trying to identify the burning rate of a solid or liquid during the unsteady process of ignition or extinction. Gas burners have been used to represent the burning conditions in small pool fires effectively before [13,14] with good predictability. However, the burner fuel compositions might not be representative of evolved gases from solids and liquids. This will be addressed in this paper.

Lundström et al. [15] examined the ignition and extinction process using a 25 mm diameter burner with nitrogen diluted flow rates of methane and propane. The heat of combustion of the fuel – nitrogen mixture is given as $\Delta h_c = (\dot{m}_F/\dot{m}_{mix})\Delta h_{c,F}$ where $\Delta h_{c,F}$ is that for the pure fuel adjusted by the fuel to mixture mass flow rates. From here on Δh_c will represent the heat of combustion of the fuel stream emulated as the evaporative or pyrolysis gases for the burner. The results from Ref. [15] are shown in Fig. 1 for the ignition and extinction processes. For Δh_c sufficiently high, the conditions of flashpoint, fire point, anchor point and extinction suggest distinct critical energy fluxes. In comparison to the critical values shown in Fig. 1, Lyon et al. [6] reported for

polymers the flashpoint value of $21 \pm 6 \text{ kW/m}^2$ and $66 \pm 17 \text{ kW/m}^2$ for the fire point. The burner value is consistent with the polymers for the flashpoint but lower for the fire point.

All observations show the limiting flames to be blue. It was noticed that the fire point and extinction flames did not cover the surface of the burner, and a much higher mass flux was needed to “anchor” the flame to the edge of the burner.

While these experiments gave insight into the processes and distinct values for the critical conditions, they raised some questions: Why is methane so different from propane? Do the burner gases represent real solid and liquid fuels? What about the effect of diameter as the convective heat transfer coefficient should play a role? Why does the critical energy flux increase as the heat of combustion decreases?

The results in Fig. 1 shows that the process of ignition is indeed transient, where a small mass flux of pyrolyzates is needed for the flash point, a slightly higher value is needed to establish a nascent diffusion flame (fire point) and a much higher mass flux is needed for the flame to cover the full fuel surface (anchor point). This anchor point is the end of the ignition process and initiation of quasi-steady burning. For a solid fuel the ignition process is rapid and the transition from flash to ultimately anchor point occurs over seconds. The recognition of the time for the fire point is operationally difficult for a solid.

Fig. 1 also indicates similar critical energy fluxes for fire point and extinction. Furthermore, visual interpretation of the experiments indicated that flame shape appeared identical between the two phenomena, with similar flame heights, flame widths, colour and oscillating behavior [15]. May fire point and extinction be treated as the natural on-off point for diffusion-controlled burning?

2. Experiments

Gas burners were used to attempt to emulate extinction and sustained ignition for liquid pools or horizontal solids. As ignition might be interpreted in several ways an operational definition is needed. For example, ignition could be defined by the event of a premixed flame induced by a pilot (flashpoint), or perhaps the event when flame covers the entire surface (“anchor” point). This study deals with ignition relevant to fire inception that is commonly recognized in flammability as the fire point. The operational definition for sustained ignition (fire point) is specified as the minimum mass flux of fuel gases for which the flame is sustained for at least 5 s. Extinction is similarly defined as the mass flux for which the flame extinguishes within 5 s, when the fuel flow rate to the burner is stepwise decreased. These definitions are based on the fire point definition in the Cleveland open cup test [1]. Extinction was obtained by step-wise decreasing the fuel flow rate until the flame went out.

Since a flame is present before extinction and after ignition, combustion kinetic properties are key to governing these phenomena. The burners emulate these gas phase combustion effects.

Three burners of diameters of 25, 50 and 100 mm were used. The heat of combustion of the fuel stream gases expresses the variation of the critical mass and energy fluxes for ignition and extinction. Pure fuel gases were mixed with various levels of nitrogen to change the heat of combustion of the fuel stream. Two Alicat gas mass flow controllers measured their flow rates. The mixture arrived in a plenum at the bottom of the burner and continued through a layer of glass beads for a uniform flow. A thin brass mesh was used to replicate a porous solid surface. Temperature was measured at two points: one in the center of the burner top and one close to the burner edge. Temperature readings were conducted with K-type thermocouples. As the burners were not water-cooled, the surface temperature was allowed to stabilize at 30 °C before each attempt of ignition, and surface temperature was measured at the critical points of sustained ignition and extinction.

The choice of igniter for ignition results was based on a preliminary study to examine what type of igniter gave the lowest mass flux at the fire point. A pre-mixed fuel-air igniter was found to blow away the

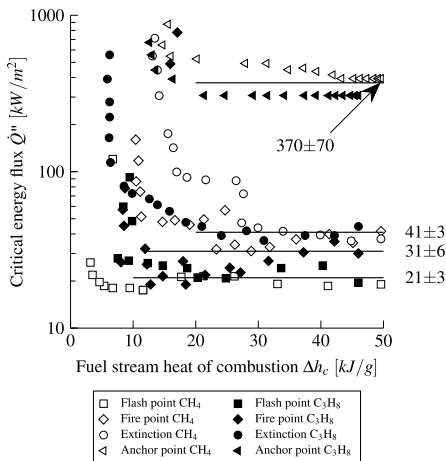


Fig. 1. Ignition and extinction critical energy flux for a 25 mm diameter burner using propane (filled) and methane (open) fuel mixtures [15].



Fig. 2. 50 mm burner and flame igniter.

combustible gases at the burner surface. A vertical electrical spark igniter was also ruled out, as it failed to satisfactorily cover the flammable zone. Ignition of the mixture was instead made by a small propane diffusion flame igniter as seen in Fig. 2, which was swept 2 mm above the burner surface, similar to that in the Cleveland open cup test.

Different fuel gases were used to represent a variety of flame behavior effects. The fuel gases chosen were methane, propane, ethylene and iso-butane. Table 1 lists some of the fuel gas properties. The smoke point l_{sp} displays some variation and is likely most significant in these laminar flames over the turbulent flame radiation fraction X_r . It is assumed that thermal-oxidation products of these hydrocarbon gases are representative of the thermal-oxidation products of solid pyrolyzates having the similar chemical composition (heat of combustion).

Global combustion kinetics for these and other gases are listed in Table 2 (note: Table 2 is for combustion, *not* for decomposition of the solid polymer). Most of them are normal hydrocarbons (alkanes), two liquid fuels, and a few polymers. The data on the polymers is limited, but the data on various pure gases from Turns [16] (taken from Dryer and Westbrook) should be indicative. It could be reasoned that the fire point and extinction limit are controlled by the same kinetics.

The pre-exponential factor, A , and the activation energy, E , in the Arrhenius expression for the global, single-step oxidation rate of the fuel, represent the reactivity potential of the various gases. The combustion reaction rate increases with A and decreases with E . It is clear from Table 2 that nearly all of the hydrocarbons shown there and more [16] have similar reaction rates. Methane however, is a well-known exception, and its kinetic data seem to span the limited polymer pyrolyzate data. It might appear that methane represents the uncertainty of solid pyrolyzate gases. Hence the gases included in this study have a broad representation.

3. Experimental results

3.1. Extinction

Fig. 3 plots the critical mass flux at extinction and sustained ignition for a wide range of heats of combustion representative of a wide variety of solids and liquids. The larger diameter has the smallest critical mass

Table 1
Fuel properties with data from Ref. [17], except * by Ref. [18].

Fuel	Formula	Δh_c [kJ/g]	l_{sp} [mm]	X_r [-]
Methane	CH_4	49.6	290*	0.14
Propane	C_3H_8	46.0	162	0.27
Isobutane	C_4H_{10}	45.4	160	0.29
Ethylene	C_2H_4	48.0	106	0.25

flux. The data appear to have an asymptote at a heat of combustion of about 5–10 kJ/g implying that combustion may not be possible below this value. There is no significant distinction among the fuel gases except for the distinct higher mass flux values for the methane-nitrogen mixture in the 25 and 50 mm diameter burners.

At low heats of combustion, the critical mass flux is high, and the higher gas velocity might affect buoyancy and the flame configuration at extinction. The inlet Froude number ($Fr = v/\sqrt{gD}$; $v = \dot{m}'/\rho_{fuel}$) was investigated to assess this effect, where v is the gas flow velocity at the outlet, g is the acceleration of gravity, D is the burner diameter and ρ_{fuel} is the density of fuel gases. Fig. 4 shows the corresponding Fr number range for the extinction data. When nitrogen flow rate is increased one step, a higher gas flow velocity is given at the burner outlet. At the same time, a slightly higher mass flow of fuel gas is needed. This increase is however generally smaller than the increase of nitrogen. Therefore, a high velocity at the outlet indicates a low heat of combustion of the mixture. In Fig. 4 we see that $Fr \ll 1$ for the extinction results of both the 50 and 100 mm burners, suggest a buoyancy dominated region. For the 25 mm burner the Fr number is higher and at $\Delta h_c < 20$ kJ/g the flame is visually observed to take a higher elevation at extinction. No elevated flame effect was observed for the 100 mm burner. In conclusion, a buoyancy dominated field with a near-surface flame at extinction can be expected for all diameters and fuel gases when $\Delta h_c > 20$ kJ/g.

3.2. Sustained ignition (fire point)

The fire point data for this study along with available data for horizontal solids of 10 cm square under radiative piloted-ignition are displayed in Fig. 5. The surface temperature of the burner (and combustible solid) can influence the heat losses at the critical points of ignition and extinction, but not sustained burning which is a stationary point where fuel gases are produced at a steady (constant) rate. For information purposes, typical values of burner surface temperatures for various burner sizes and fuels are found in Table 3. A cursory comparison of the corresponding extinction and ignition limits of Figs. 3 and 5 respectively shows no significant differences for the data trends. Indeed, the methane data in Fig. 5 for 25 mm diameter is higher than for the other fuels, as was noted for extinction. The rest of the fuels and the effect of surface temperature appear to have marginal effect on the results. Clearly diameter and the heat of combustion are the key variables controlling the critical mass fluxes at both extinction and ignition.

The plastic data in Fig. 5 are taken for a square 100 mm sample from Lyon et al. [6] and range from 0.8 to 8 g/m²s with heats of combustion from about 10 to 42 kJ/g. They are above the main trend of the burner fuels.

For the burners, low heats of combustion are associated with a higher supply velocity of gas and the same Fr number behavior is exhibited for these ignition data as shown in Fig. 4 for the extinction data. In both cases the Froude is below 1.

4. Model

It follows from previous theories [5,6,8–11] that heat of combustion and the heat transfer coefficient are important variables for controlling sustained burning. But fundamentally, the Damköhler number (Da) governs the sustained ignition and extinction processes. The Da can be expressed as the ratio of the diffusion time and the time for the chemical reaction. The operating parameter for the diffusion time is the local gas velocity of fuel and oxygen at the flame, where an increase in the local gas velocity reduces the diffusion time. The diffusion time is represented in terms of a convective heat transfer coefficient. Expressing these characteristic times in terms of fluid properties, reaction variables, length scale and the heat transfer coefficient gives

Table 2
Kinetic data for gases and polymer pyrolyzates in combustion.

Fuel	Formula	A s ⁻¹ (see note)	E kJ/mol	n	m	Reference
Methane	CH ₄	1.3 × 10 ⁸	203	1.3	-0.3	Turns [16]
"	"	8.3 × 10 ⁵	126	1.3	-0.3	"
"	"	10 ¹²	241	1	0	Lyon [19]
Propane	C ₃ H ₈	8.6 × 10 ¹¹	126	1.65	0.1	Turns [16]
Isobutane	C ₄ H ₁₀	7.4 × 10 ¹¹	126	1.6	0.15	"
Octane	C ₈ H ₁₈	4.6 × 10 ¹¹	126	1.5	0.25	"
Ethylene	C ₂ H ₄	2.0 × 10 ¹²	126	1.65	0.1	"
Methanol	CH ₃ OH	3.2 × 10 ¹²	126	1.5	0.25	"
Ethanol	C ₂ H ₅ OH	1.5 × 10 ¹²	126	1.6	0.15	"
Polymethylmethacrylate	PMMA	10 ⁷	130	1	0	Lyon [19]
Polypropylene	PP	10 ⁵	94	1	0	"
Polystyrene	PS	10 ¹³	245	1.0	0.3	Stoliarov [20]

$$\frac{d[F]}{dt} = k[F]^n[O_2]^m, k = Ae^{-E/RT}$$

Note: units of A: Turns, s⁻¹(mol/cm³)^{1-n-m}; Stoliarov, s⁻¹(kg/m³)^{1-n-m}.

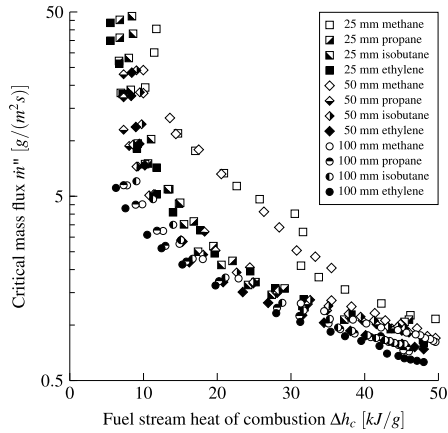


Fig. 3. Critical mass flux at extinction.

$$Da = \frac{t_{diff}}{t_{chem}} = \frac{(\rho c_p D)/h_c}{(\rho c_p T)/(E/RT)\Delta h_c Ae^{-(E/RT)}} = \frac{(E/RT)D\Delta h_c Ae^{-(E/RT)}}{h_c T} \quad (1)$$

A model to predict the critical mass flux in sustained ignition and extinction from the *Da* alone is not simple or obvious, instead it must include a reaction rate model. However, it is clear from Eq. (1) that temperature controls the value of *Da*. A sustained chemical reaction requires the *Da* be large enough to ensure that the chemical time is faster than the diffusion time. Ideally this would suggest *Da* > 1 might be a critical value for burning. It can be shown that, of the gases used in this study, methane would stand out as requiring a higher gas temperature to achieve this critical condition. The other gases used in this study, according to their kinetics of Table 2, would have similar critical flame temperatures. Therefore, this critical flame temperature will be used as an alternative to the *Da* or a full kinetic model for defining the limits of combustion at the onset and at extinction. This approach of a critical temperature has proven productive in correlating data at extinction before [3,9].

Without a loss in generalization, a stagnant combustion boundary layer model is considered to derive a result for the critical mass flux based on a critical flame temperature. It is assumed here, that these results apply to both the extinction data and the sustained ignition data,

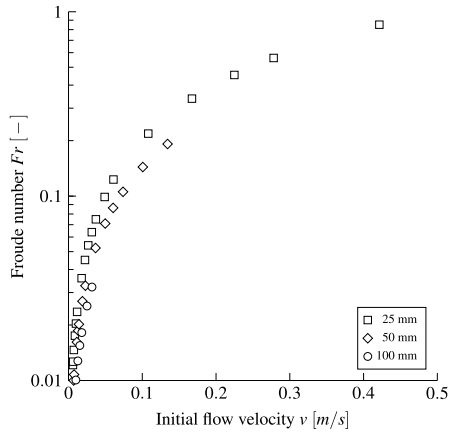


Fig. 4. Froude number for gas mixtures at extinction: all fuel gases.

as there is a flame present in both.

4.1. Burning of evaporating condensed phase fuel

The burning of an evaporating liquid or solid, with effective heat of gasification *L_m* can be described in terms of the convective flame heat flux as

$$\dot{m}'L_m = \dot{q}'_{f,c} \quad (2)$$

where *L_m* includes all of the flame, surface and external radiation heat fluxes and all of the heating terms (transient) in the condensed phase [9].

$$L_m = L - \left(\dot{q}'_{f,r} + \dot{q}'_{ext,r} - \dot{q}'_{rr} - \dot{q}'_{condensed} \right) / \dot{m}' \quad (3)$$

where

- $\dot{q}'_{ext,r}$ denotes the external radiant heat flux,
- $\dot{q}'_{f,c}$ convective flame heat flux to fuel,
- $\dot{q}'_{f,r}$ the radiative flame heat flux to fuel,
- \dot{q}'_{rr} is the re-radiation from fuel surface,

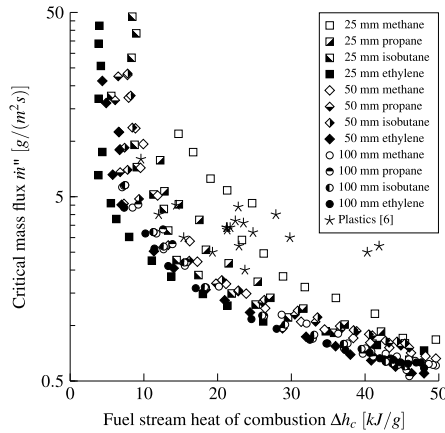


Fig. 5. Mass flow rate at the fire point.

$\dot{q}'_{condensed}$ contains all of the transient condensed phase terms, such that L is the heat of gasification.

Framed in this way, the purely convective processes in the gas phase with combustion can be computed in the stagnant diffusive layer (or boundary layer). The condensed phase may be transient, but the gas phase is assumed to be quasi-steady responding instantaneously for a given mass flux.

The parameter L_m is a mathematical generalization of the well-defined heat of gasification L , so that not only vaporization, but also complex decomposition processes are approximated. The condensed phase in Eq. (3) may therefore for instance include charring effects or additional phase changes. The effect of char reduces the effective L so that burning rate reduces as more char is produced. Rangwala and Quintiere [9] have described these transient terms well, where they also include the effect of water interacting with the flame and surface in the unsteady term. L for steady burning of non-charring polymers is composed of the melting and pyrolysis heats along with the sensible enthalpies ($c_p \Delta T$) associated with each solid and liquid phase. It is a thermodynamic quantity. The unsteady and charring terms are lumped into $q''_{condensed}$ and are given explicitly in Rangwala and Quintiere [9]. Whatever these terms are, they are eliminated from the governing equation for the burning limit as later given by Eq. (7) with only gas phase properties remaining.

The analytical solution for the mass flux in this case has been developed by Spalding, e.g. Ref. [21]. The mass flux in combustion follows where the purely convective heat transfer coefficient is introduced to generalize diffusion in the convective boundary layer for many flow and geometry conditions.

Table 3
Burner surface temperatures for pure fuels (no nitrogen).

Fuel	25 mm		50 mm		100 mm	
	$T_{s, fire\ point}[^\circ\text{C}]$	$T_{s, extinction}[^\circ\text{C}]$	$T_{s, fire\ point}[^\circ\text{C}]$	$T_{s, extinction}[^\circ\text{C}]$	$T_{s, fire\ point}[^\circ\text{C}]$	$T_{s, extinction}[^\circ\text{C}]$
Methane	140	180	160	160	170	200
Propane	150	210	160	230	200	220
Isobutane	220	230	210	260	240	260
Ethylene	190	210	210	250	220	220

$$\dot{m}' = \frac{h_c}{c_p} \ln(1 + B) \tag{4}$$

where h_c is the convective heat transfer coefficient without blowing, c_p is the specific heat capacity and B is the mass transfer number based on L_m .

$$B = \frac{Y_{ox}(1 - X_r)\Delta h_{ox} - c_p(T_s - T_\infty)}{L_m} \tag{5}$$

A radiative fraction (X_r) is added to account for radiation loss overall from the flame and the heat of combustion per unit mass of oxygen Δh_{ox} (generally taken as a constant, 13.1 kJ/g) has been substituted for the heat of combustion of the pure fuel divided by its stoichiometric fuel to oxygen mass ratio. In Eq. (5) Y_{ox} is the ambient oxygen mass concentration and T_s and T_∞ denotes surface and ambient temperatures respectively.

The key to formulating the critical mass flux is to use the solution given in the stagnant layer problem for the flame temperature. This depends on L_m and the flame temperature T_f can be calculated from

$$c_p(T_f - T_\infty) = \frac{(1 - X_r)\Delta h_c - L_m - c_p(T_s - T_\infty)}{1 + \Delta h_c/(\Delta h_{ox} Y_{ox})} \tag{6}$$

where again the heat of combustion per unit mass of oxygen Δh_{ox} and the heat of combustion of the fuel (mixture) stream Δh_c is used. Eliminating L_m from Equations (4) and (6) gives in dimensionless parameters:

$$(e^\lambda - 1) = \frac{1 - \beta}{\alpha + \beta - \gamma(1 + \alpha)} \tag{7}$$

where

$$\alpha = \frac{\Delta h_c}{Y_{ox}\Delta h_{ox}}$$

$$\beta = \frac{c_p(T_s - T_\infty)}{Y_{ox}\Delta h_{ox}(1 - X_r)}$$

with $\lambda \equiv \frac{m'_{sp}}{h_c}$ as the dimensionless mass flux.

Approximations can be made but for now all terms will be retained. λ may be small, β is always small, and X_r can be considered negligible. That is, at sustained ignition and extinction, radiation losses are considered small based on the small flames and lack of dominant soot. Note that radiant heating, which is important in the ignition of solids, is contained in the L_m term which cancels out in Eq. (7).

4.2. A critical flame temperature

The concept of using a critical flame temperature is steeped in the literature. Burgess and Wheeler [7] showed that the adiabatic flame temperature at the lower flammability limit is ~1600 K for most common hydrocarbons and later also Zabetakis et al. [22] amongst others [23,24] extended the generality of the concept. Williams [3], Simmons and Wolfhard [25] and others [26] proved the concept viable for extinction of diffusion flames, and Rasbash et al. [5] proved the applicability of the flame temperature concept through his fire point theory. In the following analysis a critical flame temperature of 1600 K

will universally be used, even though this value is affected by the combustion kinetics. Hence methane is likely to be represented by a higher temperature due to its higher activation energy.

4.3. Correlation for the convective heat transfer coefficient

Natural convection controls the diffusion process for the burners. A general heat transfer correlation for natural convection with laminar flow conditions applicable to the burner sizes here can be given in the form as [27]:

$$Nu_D = \frac{h_c D}{k} = (C_0 + C Ra_D^{1/4}) \tag{8}$$

In Eq. (8) Nu_D is the Nusselt number, D the fuel bed diameter, k gas conductivity, and Ra_D is the Rayleigh number, with a constant C that depends on application but has been empirically determined to $0.54 < C < 0.60$ [27]. The value C_p is taken from an exact pure conduction solution as $8/\pi$ [28]. Fluid properties in the dimensionless groups in the above expression are evaluated at the film temperature [29] ($T_{film} = (T_f + T_\infty)/2$) where $Ra_D = (g(T_f - T_\infty)D^3)/(T_{film}\alpha\nu)$.

Taking the flame temperature at 1600 K, the ambient temperature at 298 K, and the film temperature at approximately 950 K appropriate use of air properties gives $Ra_D = 8.1 \times 10^8 D(m)^3$ and $c_p = 1.13$ kJ/kgK, $k = 0.0652$ W/mK.

4.4. Correlation form for the critical mass flux

Let us write the heat transfer coefficient in terms of Eq. (8) but with the C term unspecified so that the dimensionless mass flux λ is given by

$$\lambda = \frac{m' c_p D}{k \left(\frac{8}{\pi} + C Ra_D^{1/4} \right)} \tag{9}$$

The parameters in Eq. (7) can be written for normal ambient air and negligible radiation as

$$\alpha = \frac{\Delta h_c \text{ (kJ/g)}}{3.052 \text{ (kJ/g)}}$$

$\beta = 0.04 - 0.07$ for ignition and $0.06 - 0.08$ for extinction, using measured surface temperatures from Table 3.

$$\gamma = 0.482$$

As a consequence, it is clear that λ is a primarily function of Δh_c by Eqs. (7) and (8). Plotting the data in this way should show if the theory guides us to a general correlation independent of fuel and diameter.

5. Correlation results

5.1. Correlations for extinction

Theory suggests that there are two important variables for predicting if extinction and ignition will occur. The first is Δh_c , a property of the material. The second is λ that includes the critical mass flux along with diameter through the heat transfer coefficient and basically air properties. Then all burner data should collapse in a plot of λ versus Δh_c -plot, independent of burner diameter. Theory also proposes that there should be no significant scatter between different fuels, since there are no specific fuel properties in Eq. (7). However, the unusual reaction rate kinetics of methane will make it an outlier.

A correlating strategy was based on a linearization of Eq. (7) for small λ and in which β is neglected. Then theoretically $1/\lambda = (1 - \gamma)\alpha - \gamma$. Recall γ relates to the critical flame temperature in Eq. (7), and in this formulation γ controls a minimum heat of combustion below which there can be no burning. Properties used to compute λ , α and γ can be found in Table 4. All the data produced in the burner experiments is plotted in Fig. 6. It is seen that the propane/isobutene/ethylene data

Table 4
Values used in calculations.

α	0.000168	m^2/s
c_p	1.17	J/(gK)
g	9.81	m/s^2
h_{air}	13.1	kJ/gO ₂
k	0.066	W/(mK)
T_∞	298	K
T_f	1600	K
T_{film}	1025	K
T_s	450	K
ν	0.000122	m^2/s
X_r	0	-
$Y_{f,o}$	1	-
Y_{ox}	0.233	-

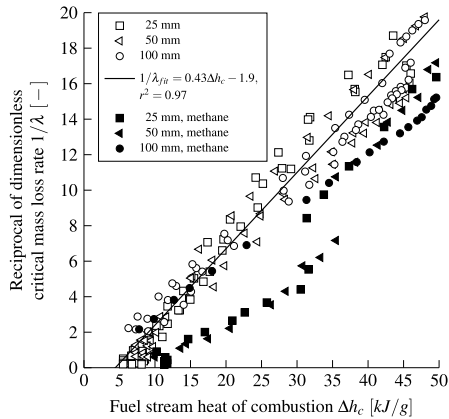


Fig. 6. Reciprocal of dimensionless mass loss rate at extinction: mixtures of nitrogen with propane, isobutane, ethylene and methane ($C = 0.57$ for linear fit).

falls into the same regime, and a best fit is rendered with $C = 0.57$ appropriate for the natural convection formula (recall $0.54 < C < 0.60$), as evaluated by King [27]). Methane results (solid markers) are ignored in the fit, because its behavior is very different from the other gases as expected.

A linear fit to the data gives $\lambda = 1/[0.43\Delta h_c - 1.9]$, ($r^2 = 0.97$). The corresponding theoretical result for small λ (and for $\gamma = 0.48$ and β neglected) from Eq. (7) is $\lambda = 1/[0.17\Delta h_c - 0.48]$. Both give a similar minimum heat of combustion of 4.4 and 2.8 kJ/g, accordingly. This minimum relates to “non-combustibility” of materials in general. A criterion in the European classification system to qualify a building material as non-combustible (A1) is a maximum heat of combustion of 2.0 kJ/g¹ [30,31]. This value comes from 2.5 kJ/g in the disused French regulation (NFP 92–510), which was experimentally found in the seventies [32]. It is in some agreement with the burner results here.

The methane data was not fitted in Fig. 6. From previous discussion it is expected that methane would have a higher critical flame temperature. Therefore, methane would have a higher value for γ than the other fuels in this study due to a higher T_f . By fitting the methane data

¹ 2.0 kJ/g is the limit for “homogeneous products and substantial components of non-homogeneous products and for products as a whole”. For “any internal non-substantial component of non-homogeneous products” the limit is 1.4 kJ/g.

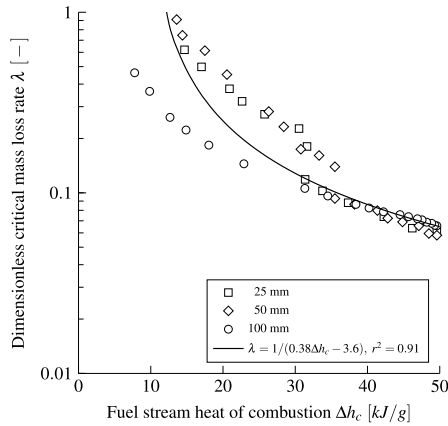


Fig. 7. Extinction, methane, with $C = 0.57$ in the fit.

only in Fig. 6, the x-axis interception is $\Delta h_c = 9.6$ kJ/g, and the linear regression gives $\lambda = 1/[0.38\Delta h_c - 3.6]$, ($r^2 = 0.91$). Here γ is higher (3.6) than the γ of 1.9 for of the correlated gases in Fig. 6. Fig. 7 shows the methane data alone with this fit. In analogy with real condensed-phase fuels, methane might represent the behavior of flame-retarded fuels having a higher E , but this is speculation.

Extinction, dimensional correlations

Neglecting β and studying Figs. 6 and 7 it is possible to develop a correlation for small λ so that the critical mass flux is

$$\dot{m}'_{cr} = \left(\frac{0.14}{D} + \frac{5}{\sqrt[3]{D}} \right) \left(\frac{1}{0.43\Delta h_c - 1.9} \right) \quad (10)$$

The corresponding theoretical results for Eq. (7) is given as

$$\dot{m}'_{cr} = \left(\frac{0.14}{D} + \frac{5}{\sqrt[3]{D}} \right) \left(\frac{1}{0.17\Delta h_c - 0.48} \right). \quad (11)$$

Fig. 8 show how these results compare to all the data for each diameter. For the 100 mm diameter, the data from all the gases including methane follow the empirical fit.

5.2. Fire point

It could be expected that the critical mass flux for sustained ignition is higher than for extinction because (1) for ignition an igniter is needed, and this may not cover the entire flammable zone, and (2) burner surface is originally cooler in ignition tests than during extinction. Instead, although there is some variance in both experiments, ignition data is approximately superimposed with extinction data for ethylene at 100 mm in Fig. 9. There appears to be no significant differences.

In a similar correlating process as in extinction, a dimensionless form of the critical mass flux at sustained ignition is presented in Fig. 10. A linear fit to the data gives $\lambda = 1/[0.49\Delta h_c - 1.4]$, ($r^2 = 0.95$), with methane neglected. The minimum heat of combustion to all sustained ignition is 3.1 kJ/g.

In dimensional form, sustained ignition is described by

$$\dot{m}'_{cr} = \left(\frac{0.14}{D} + \frac{5}{\sqrt[3]{D}} \right) \left(\frac{1}{0.49\Delta h_c - 1.4} \right) \quad (12)$$

A statistical analysis shows that there is no significant difference

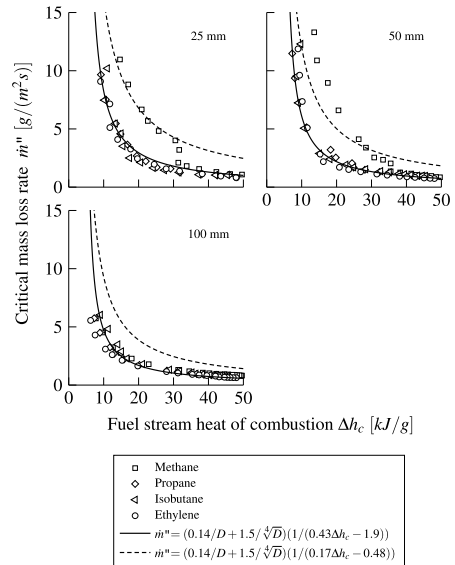


Fig. 8. Critical mass loss rate at extinction for fit and theory.

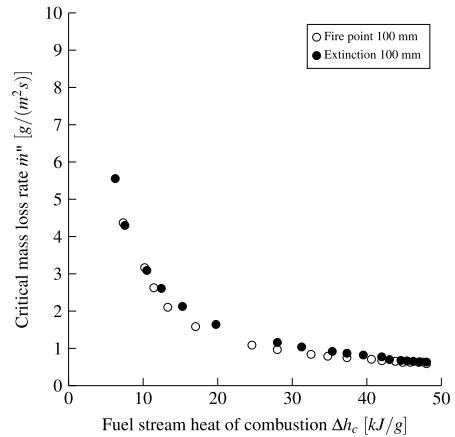


Fig. 9. Critical mass flux for ethylene: fire point and extinction.

between ignition and extinction regressions. Differences in regression lines are usually tested based on their slopes and intercepts. The slopes can be compared with a two-tailed Student's t -test, with a chosen probability $p < 0.05$ of receiving coincident significance. Such a test gives the significance level $t(327) = 1.26$, compared to the critical absolute value for statistical significance $t_{crit} = 1.97$. In other words, the extinction slope also fit approximately to ignition data. The other statistical hypothesis regards the intercepts. The calculated t -value t

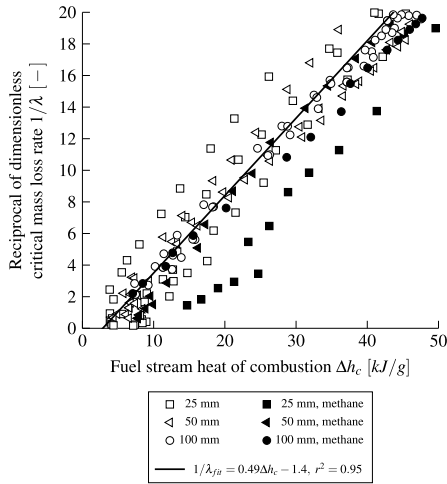


Fig. 10. Reciprocal of dimensionless mass loss rate at the firepoint

(328) = 0.60 is lower than $t_{crit} = 1.97$, hence no statistical difference in intercepts is found, and the correlation for extinction can be used to approximate ignition data.

Fig. 11 shows critical mass flux for the three burners at sustained ignition as well as for solid materials in the cone calorimeter and the

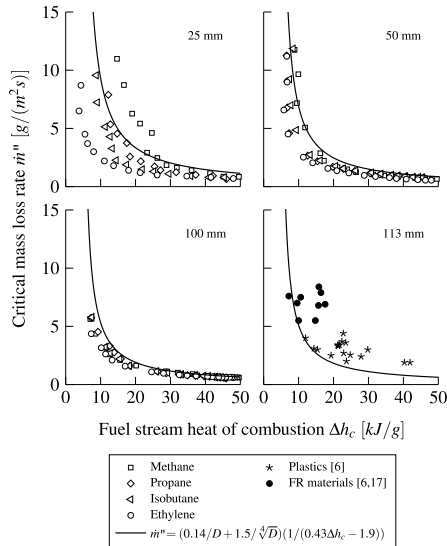


Fig. 11. Critical mass loss rate at the fire point for the burners and common plastics.

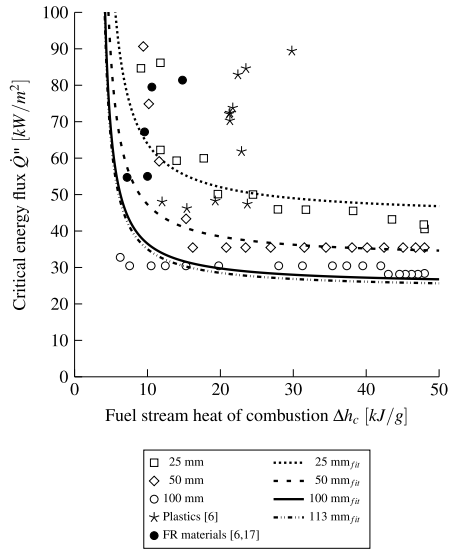


Fig. 12. Critical energy flux at the fire point for common plastics and ethylene.

FPA. Taking differences in h_c into account from Eq. (7), a comparison between burner data and experimental data for plastics [6] ignited in the cone calorimeter [33]/fire propagation apparatus (FPA) [34] can be conducted. Both cone calorimeter and the FPA square samples have an equivalent diameter of 113 mm, i.e. $h_c = 12 \text{ W/m}^2\text{K}$. This is in line with an experimentally retrieved heat transfer coefficient of $h_c = 10 \text{ W/m}^2\text{K}$ [6]. The solid line is the experimental fit for extinction. The burner data for ignition fall slightly below the correlation for extinction. The plastic data all fall above the recommended correlation from the gas burner data (excluding methane).

Initially it was suggested that there might be a critical energy flux for the fire point (see Fig. 1). In Fig. 12 the critical energy release rate is plotted for sustained ignition. Ethylene data for the three burners are also included in the plot, to represent burner results. As expected from the correlation the results depend on the burner diameter. At heats of combustion above about 10 kJ/g the fit suggests a constant asymptotic value of energy flux for a given diameter. These asymptotic results can be discerned as about 48 kW/m² for the 25 mm, 35 kW/m² for the 50 mm and 27 kW/m² for the 100 mm burners. But the burner correlation indicates an asymptote for the plastic data of Lyon and Quintiere as about 26 kW/m² compared to their finding of $66 \pm 17 \text{ kW/m}^2$ [6]. Perhaps an explanation for this discrepancy can be offered by the rapid process occurring at ignition of condensed-phase fuels. When a solid is ignited it should follow the phenomena shown in Fig. 1. First there is a flashpoint, a premixed flame. This is then followed by the fire point that is the onset of a diffusion flame. Then the increased heating of the diffusion flame causes an increase in mass flux which makes it difficult to measure the mass flux at the fire point. The increased mass flux will then eventually lead to a flame over the entire surface, the anchor point. According to the gas burner data of Fig. 1 there is a significant difference in the asymptotic value for the critical energy flux at the anchor point and fire point – a factor of ten.

6. Summary

In the introduction, five questions were raised that this study has sought to answer. This section summarises the findings of the study and state limitations.

1. Why is the burning behavior for methane so different than for propane?

Methane is known to be less reactive than other hydrocarbons, as a result of the high thermal stability imparted by the exclusive carbon-hydrogen bond structure, as evidenced by its lower burning velocity. Also, Table 2 indicates significantly much smaller values for A than other pure gaseous fuels. For the existence of a stable diffusion flame the Damköhler number has to be larger than a specific value. Moreover, from Eq. (1), for a given environmental condition for a flame, a critical Da suggests a critical E/RT . This implies that methane would have a higher critical flame temperature than 1600 K as selected in the theory. Figs. 3 and 5 show that over

2. Do the burner gases represent real solid and liquid fuels?

The gases used here are pure compounds with N_2 instead of an assortment of hetero-atom containing (N, O, S) solid fuel fragments with lower heats of combustion. However, as these pure gases diffuse into the flame they all are broken down into CH_4 , CO , H_2 , etc. as are hydrocarbon solids and liquids. Gas phase combustion inhibitors (halogens) are excluded from consideration in the burner data. Burner gases introduced here do not have exactly the same mixture of compounds as a vaporized gas from a liquid or as the pyrolyzates from a solid. However, by changing the gaseous fuel–inert mixture in the burners, the heat of combustion and the radiation character (i.e. laminar smoke point) is varied over a wide range representative of liquid and solid fuel gases. This representation has previously been shown valid for quasi-steady burning of PMMA and POM [35]. Here we extend it to the burning limits of sustained ignition and extinction. Others have shown at these limits the significance of the heat of combustion of the fuel stream [5–11]. The value of this study is to accurately and completely show how heat of combustion and fuel supply rate can be used to determine gas phase extinction and ignition. In CFD modeling of the solid phase, it is common to use a “critical mass flux” estimate for ignition or extinction. Here we show that the critical mass flux at ignition and extinction varies inversely with the heat of combustion. By inference with liquid or solid fuels experiencing similar cracking compounds before the flame, this wide range of gaseous fuels is expected to represent their overall characteristics.

As it is the gas phase that controls ignition and extinction, transients in the solid and the advent of charring do not change the results presented here. Indeed, materials that produce char upon heating have relatively high critical mass flow rates due to their low heats of combustion for their pyrolyzates.

We show in Figs. 11 and 12 that the critical results for solids is higher than the gas burner data. Also there is significant scatter among the solid data, but their trend is similar to the gases. We believe the solid data are overestimates of correct values because of the transient nature of the solid moving through ignition and extinction. It must be realized that the solid mass loss data is taken from a load cell in which its time derivative must be found at the moment of ignition or extinction. These solid data are for ignition, and it must be realized that there is a considerable change in mass loss rate from the flashpoint to the anchor point. The consistency in observing ignition, and the accuracy of the derived derivative suggest that the solid data are overestimated. Hence we believe the burner data are more accurate and representative of solids and liquids.

3. What is the effect of burner diameter?

Looking at Eqns. (8) and (9) the critical mass flux is expected to reduce accordingly at higher diameters, as approximately $\dot{m}'_{cr} \propto (D^{-1} + D^{-1/4})$. The decrease in critical mass flux with increasing diameter is explained by a change in the Ra number. This result is restricted to laminar burning of horizontal pool fires. For larger fires or other configurations, existing heat transfer coefficient data could be applied. Theory indicates that only convective heat transfer applies to the burning limits.

The dominant heat transfer to the surface passes from convective (or conductive in microgravity) to radiative as the scale of a fire is increased. Turbulence enhances mixing of fuel and air. In turn, mixing cause diffusion and increase the convection heat transfer rate [36].

Therefore, the results in this study are applicable (and restricted) to laminar diffusion flames above fuel beds between 25 and 100 mm diameter. The theory can be extended to other configurations by use of the appropriate heat transfer coefficient. Radiation is nearly negligible by the elimination of L_m (Eq. (3) in Eq. (7)) except for the radiative fraction still appearing.

4. Why does the critical energy flux increase as the heat of combustion decreases?

The critical energy flux is essentially independent of the heat of combustion. This is in line with the Lyon and Quintiere findings [6]. However, there is a minimum heat of combustion that limits this constancy. Below 15 kJ/g the trendline in Fig. 12 is no longer horizontal. This basically means that for materials with a low effective heat of combustion the statement of a constant critical energy flux is not applicable.

The asymptote indicates non-combustibility at heats of combustion of about 3–4 kJ/g. This is consistent with standard tests [30,31]. Others suggest that a critical heat release rate should be the basis for non-combustibility [32,37]. The constancy of 15 kJ/g is consistent with a critical heat release rate for heats of combustion below this value.

5. May fire point and extinction be treated as the natural on-off point for diffusive burning?

The fire point is dependent on an ignition source which is obviously not the case for extinction. In this study, it is however seen that ignition with a carefully chosen igniter gives critical mass flux results which are not statistically different from extinction.

7. Conclusions

Liquids and solids show rapid transition processes at the moment of ignition and extinction which makes it difficult to measure the mass flux and indeed previous studies show a distinct scatter of measured mass fluxes for solids at the observed ignition point. We believe that the results of using a gas burner with a variety of fuels has more accurately produced these limit conditions of burning (excluding gas phase combustion inhibitors/halogens).

The burner results clearly show that the critical conditions depended primarily on the fuel heat of combustion and the diameter of the fuel source. The observations of fire point and extinction show that both occur with diffusion flames partially over the surface. Fuel kinetics of combustion can influence the results as shown particularly for the case of methane.

Experiments with gas burners also show that there is no significant difference in carefully measured mass fluxes for extinction and fire points. The experiments were taken over conditions where buoyancy dominates over momentum in the burner flow rates. Except for the kinetic peculiarities of methane, most hydrocarbon gases yield similar data for the fire point and extinction.

Based on these findings, a general formula for the mass flux at sustained ignition and at extinction is given, for horizontal burning

with diameters of 25–100 mm, as $\dot{m}'_c = (0.14/D + 5/\sqrt{D})(1/(0.43\Delta h_c - 1.9))$. The formula is offered to represent the conditions for condensed phase fuels. It could be extended to other convective conditions with appropriate use of the theory, but without verification.

Non-combustibility is illustrated by the correlation with a heat of combustion of $\Delta h_c \sim 3\text{--}4\text{ kJ/g}$, related to an infinite critical mass flux. This finding supports the European classification system for non-combustibility, where the corresponding limit is set at 2 kJ/g.

Acknowledgements and funding

The authors are grateful to dr. Peter Sunderland and dr. John de Ris for stimulating discussions. The work herein is funded by the European Union's Seventh Framework Programme under grant n° 316991 and by RISE, Research Institutes of Sweden.

Nomenclature

<i>A</i>	Pre-exponential factor
<i>B</i>	Spalding B number
<i>C</i>	Empirical constant
<i>c</i>	Heat capacity
<i>D</i>	Diameter
<i>Da</i>	Damköhler number
<i>E</i>	Activation energy
<i>Fr</i>	Froude number
<i>g</i>	Acceleration of gravity
<i>h</i>	Heat transfer coefficient
Δh_c	Heat of combustion
$\Delta h_{c,ox}$	Heat of combustion per gram of oxygen consumed (13.1 kJ/g-O ₂)
<i>k</i>	Gas conductivity/Rate constant
<i>l_{sp}</i>	Laminar smoke point
<i>L</i>	Heat of gasification
<i>m</i>	Mass
<i>Nu</i>	Nusselt number
<i>Q</i>	Energy
<i>q</i>	Heat
<i>R</i>	Universal gas constant
<i>Ra</i>	Rayleigh number
<i>T</i>	Temperature
<i>v</i>	Velocity
<i>X_r</i>	Flame radiation fraction
<i>Y</i>	Mass fraction
α	Thermal diffusivity/Dimensionless group
β	Thermal expansion coefficient/Dimensionless group
γ	Dimensionless group
ρ	Density
λ	Dimensionless mass loss rate
<i>v</i>	Kinematic viscosity
Subscripts	
<i>c</i>	Convection
<i>c, F</i>	Combustion of pure fuel
<i>chem</i>	Chemical
<i>cr</i>	Critical
<i>D</i>	Diameter
<i>diff</i>	Diffusion
<i>ext, r</i>	External radiation
<i>F</i>	Pure fuel
<i>f</i>	Flame/Pure fuel
<i>film</i>	Film
<i>F, L</i>	Fraction at lower limit
<i>f, c</i>	Flame convection
<i>f, r</i>	Flame radiation

<i>x</i>	Conduction
<i>m</i>	Modified
<i>mix</i>	Fuel-diluent mixture
<i>net</i>	Net
<i>ox</i>	Oxygen
<i>p</i>	Pressure
<i>r</i>	Radiation
<i>rr</i>	Re-radiation from fuel surface
<i>s</i>	Surface
∞	Ambient
Superscripts	
'	Per unit length
•	Per unit time

References

- [1] ASTM D92, Standard Test Method for Flash and Fire Points by Cleveland Open Cup Tester, (2010).
- [2] J.E.J. Staggs, Ignition of char-forming polymers at a critical mass flux, *Polym. Degrad. Stabil.* 74 (2001) 433–439.
- [3] F.A. Williams, A review of flame extinction, *Fire Saf. J.* 3 (1981) 163–175, [https://doi.org/10.1016/0379-7112\(81\)90041-2](https://doi.org/10.1016/0379-7112(81)90041-2).
- [4] J.L. Torero, Flaming ignition of solid fuels, in: M.J. Hurley (Ed.), *SPFE Handb. Fire Prot. Eng. fifth ed.*, Springer, New York, 2016, p. 650, <https://doi.org/10.1007/978-1-4939-2565-0>.
- [5] D.J. Rasbash, D.D. Drysdale, D. Deepak, Critical heat and mass transfer at pilot ignition and extinction of a material, *Fire Saf. J.* 10 (1986) 1–10, [https://doi.org/10.1016/0379-7112\(86\)90026-3](https://doi.org/10.1016/0379-7112(86)90026-3).
- [6] R. Lyon, J. Quintiere, Criteria for piloted ignition of combustible solids, *Combust. Flame* 151 (2007) 551–559, <https://doi.org/10.1016/j.combustflame.2007.07.020>.
- [7] M.J. Burgess, R.V. Wheeler, The lower limit of inflammation of mixtures of the paraffin hydrocarbons with air, *J. Chem. Soc.* 99 (1911) 2013–2030.
- [8] A.F. Roberts, B.W. Quince, A limiting condition for the burning of flammable liquids, *Combust. Flame* 251 (1973) 245–251.
- [9] J.G. Quintiere, A.S. Rangwala, A theory for flame extinction based on flame temperature, *Fire Mater.* 28 (2004) 387–402, <https://doi.org/10.1002/fam.835>.
- [10] M. Delichatsios, M. Gummala, D.G. Vlachos, Extinction of surface stabilized gaseous diffusion flames: Part I Simplified numerical model and implications for solid fuels in fires, *Fire Saf. J.* 55 (2013) 152–159.
- [11] M.A. Delichatsios, M.M. Delichatsios, Critical Mass Pyrolysis Rates for Extinction in Fires over Solid Materials NIST-CCR-98-746, Norwood, 1998.
- [12] V.R. Lecoustre, P. Narayanan, H.R. Baum, A. Trounev, Local extinction of diffusion flames in fires, *Fire Saf. Sci.* (2010) 583–596.
- [13] R.C. Corlett, Gas Fires with Pool-Like Boundary Conditions, (1968).
- [14] J. De Ris, L. Orloff, A dimensionless correlation of pool burning data, *Combust. Flame* 18 (1972) 381–388, [https://doi.org/10.1016/S0010-2180\(72\)80189-5](https://doi.org/10.1016/S0010-2180(72)80189-5).
- [15] F. Vermina Lundström, P.B. Sunderland, J.G. Quintiere, P. van Hees, J.L. de Ris, Study of ignition and extinction of small-scale fires in experiments with an emulating gas burner, *Fire Saf. J.* 87 (2017) 18–24, <https://doi.org/10.1016/j.fire saf.2016.11.003>.
- [16] S.R. Turns, *An Introduction to Combustion*, second ed., McGraw Hill, 2000.
- [17] A. Tewarson, Generation of heat and chemical compounds in fire, in: P. DiNenno (Ed.), *SPFE Handb. Fire Prot. Eng. third ed.*, National Fire Protection Association, 2002pp. 3–82, 3–161.
- [18] C.W. Lautenberger, CFD Simulation of Soot Formation and Flame Radiation, Worcester Polytechnic Institute, 2002.
- [19] R. Lyon, R. Walters, S. Stoliarov, A thermal analysis method for measuring polymer flammability, *J. ASTM Int. (JAI)* 3 (2006) 13895, <https://doi.org/10.1520/JAI13895>.
- [20] S.I. Stoliarov, F. Raffan-Montoya, R.N. Walters, R. Lyon, Measurement of the global kinetics of combustion for gaseous pyrolyzates of polymeric solids containing flame retardants, *Combust. Flame* 173 (2016) 65–76.
- [21] D.B. Spalding, *Convective Mass Transfer*, McGraw-Hill Book Co., New York, 1963.
- [22] M.G. Zabetakis, S. Lambiris, G.S. Scott, Flame temperatures of limit mixtures, Seventh Symp. Combust. 7 (1959) 484–487.
- [23] A.G. White, Limits for propagation of flame in inflammable gas-air mixtures. Part III. The effect of temperature on the limits, *J. Chem. Soc.* 127 (1925) 672–684, <https://doi.org/10.1039/CT9252700672>.
- [24] F.J. Weinberg, Combustion temperatures: the future? *Nature* 233 (1971) 239–241, <https://doi.org/10.1038/233239a0>.
- [25] R.F. Simmons, H.G. Wolfhard, Some limiting oxygen concentrations for diffusion flames in air diluted with nitrogen, *Combust. Flame* 1 (1957) 155–161, [https://doi.org/10.1016/0010-2180\(57\)90042-1](https://doi.org/10.1016/0010-2180(57)90042-1).
- [26] A. Maćek, *Flammability Limits: Thermodynamics and Kinetics*, (1976) Gaithersburg, MD.
- [27] B. Gebhart, *Heat Transfer*, second ed., McGraw-Hill Book Co., New York, 1971.
- [28] Y. Zhang, M. Kim, H. Guo, P.B. Sunderland, J.G. Quintiere, J.L. de Ris, D.P. Stocker, Emulation of condensed fuel flames with gases in microgravity, *Combust. Flame* 162 (2015) 3449–3455.

- [29] J.P. Holman, Heat Transfer, McGraw-Hill Book Co., New York, 1990.
- [30] EN 13501-1, Fire Classification of Construction Products and Building Elements—Part 1: Classification Using Test Data from Reaction to Fire Tests, (2007) 2007.
- [31] EN ISO 1182, Reaction to Fire of Building Materials - Non-combustibility Test, (2010) 2010.
- [32] R.L. Alpert, M.M. Khan, A new test method for rating materials as noncombustible, *Fire Saf. Sci.* (2003) 791–802, <https://doi.org/10.3801/IAFSS.FSS.7-791>.
- [33] ISO 5650-1:2015 Reaction-to-fire tests, Heat Release, Smoke Production and Mass Loss Rate — Part 1: Heat Release Rate (Cone Calorimeter Method) and Smoke Production Rate (Dynamic Measurement), (2015).
- [34] ASTM E2058, 13a Standard Test Methods for Measurement of Material Flammability Using a Fire Propagation Apparatus, FPA), 2013.
- [35] Y. Zhang, M. Kim, P.B. Sunderland, J.G. Quintiere, J. De Ris, A burner to emulate condensed phase fuels, *Exp. Therm. Fluid Sci.* 73 (2016) 87–93, <https://doi.org/10.1016/j.expthermflusci.2015.09.025>.
- [36] R.F. Simmons, Premixed burning, in: D.D. P.J. DiNenno (Eds.), SFPE Handb. Fire Prot. Eng. National Fire Protection Association, Quincy, MA, 2002p. 1,144-1,154.
- [37] K. Carpenter, M. Janssens, Using heat release rate to assess combustibility of building products in the Cone Calorimeter, *Fire Technol.* 41 (2005) 79–92, <https://doi.org/10.1007/s10694-005-6390-z>.



LUND
UNIVERSITY

ISBN 978-91-7895-412-4
ISSN 1402-3504
ISRN LUTVDG/TVBB-1062-SE
Report 1062

Fire Safety Engineering
Lund University

